Schwinger–Dyson Equations In QED and QCD

The calculation of fermion–antifermion condensates

A thesis presented for the degree of

Doctor of Philosophy

by

Richard Williams

Institute for Particle Physics Phenomenology

University of Durham

June 2007

Durham University

Abstract

We present non-perturbative solutions for the fermion and boson propagators of QED in both three- and four-dimensions, and QCD. In doing so, we solve the coupled system of Schwinger-Dyson equations numerically in Euclidean space, investigating criticality, gauge dependence and phenomenology of the solutions. We do so by exploiting a new and novel three-point ansatz, the Kızılersü–Pennington vertex, designed to satisfy multiplicative renormalisability in unquenched QED.

The efficacy of this is demonstrated numerically for QED_4, where we find a marked improvement in the gauge-invarance of the photon wave-function. The critical coupling associated with dynamical mass generation is investigated for a variety of gauges; remarkably a lessening of this dependence is seen, despite the ansatz's origins from a massless theory, which is improved further by constructing a hybrid system.

As with many studies in the past, we apply this ansatz to the three-dimensional non-compact formulation of QED, checking gauge covariance of the propagators through a momentum-space formulation of the Landau-Khalatnikov-Fradkin transformations. The critical dependence on the number of active fermions was investigated, with the gauge dependence of the condensate unresolved. As an aside, we found numerically that LKF transforming the propagators gave rise to a constant condensate; a fact supported analytically through an explicit proof.

We turn our attention towards QCD, where we explore a variety of phenomenological models, including the full ghost-gluon system, in which we make comparisons between traditional vertices and the new KP-vertex. These models are used in a determination of the physical quark condensate for massive quarks, through the exploitation of a class of non-positive definite solutions accessible for small quark masses.

Finally, we examine Generalised Ward-Takahashi identities, which hold promise to further constrain the tranvserse part of the vertex. The identity is shown to hold true at one-loop through an explicit calculation, and a constraint on one of the basis coefficients is given as an example of its use.

Acknowledgements

First and foremost, my thanks go to my supervisor, Mike Pennington, for providing me with the opportunity to work with him. I am eternally grateful for his continued help and guidance throughout my PhD, the enlightening discussions, and the plethora of anecdotes that truly gave context and insight into the world of particle physics.

My gratefulness goes also to Christian Fischer, for his advice in solving the ghost-gluon system, and for his input in the work of Chapter 5.

Special thanks must go to office mates old and new: Gareth, Simon, Steve; Aiofe, Cobos and David – without whom the IPPP would have been much less colourful, and for whose useful discussions, particularly Gareth's, I am indebted to. My gratitude goes to all my fellow PhD students and staff of the Ogden centre, for providing a lively and friendly atmosphere in which to work. I must also mention Cesario Almeida, for the many problem solving sessions over coffee.

My thanks must also go to my parents for their encouragement and support throughout all my studies. I must also thank all my friends accumulated during my time in Durham: to Eldor, Samir, and Natasha for Russian card-games; to my decadent friends Kostas and Matthew; to Francisca for telling me what to do; Luciane and Yoon-joung for telling me what not to do; former housemates Chris and Michelle; and especially to Anna, for being such a close and supportive friend.

This work was supported by a PPARC studentship which is gratefully acknowledged.

Declaration

I declare that no material presented in this thesis has previously been submitted for a degree at this or any other university.

The research described in this thesis has been carried out in collaboration with M.R.Pennington.

The research described in Chapter 2 was carried out with Prof. M. R. Pennington and will be contained within the paper:

- M. R. Pennington and R. Williams. *Systematic numerical study of the fermion propagator in strong coupling QED_4.*

The contents of Chapter 3 and 4 are the result of work with Prof. M. R. Pennington.

Chapter 5 is derived from:

- R. Williams, C. S. Fischer, M. R. Pennington. *$\bar{q}q$ condensate for light quarks beyond the chiral limit. Phys. Lett.* **B645** (2007) 167–172 [hep-ph/0612061]
- R. Williams, C. S. Fischer, M. R. Pennington. *Quark Condensates: Flavour Dependence* [hep-ph/0703255]
- R. Williams, C. S. Fischer, M. R. Pennington. *Extracting the $\bar{q}q$ condensate for light quarks beyond the chiral limit in models of QCD.* [hep-ph/0704.2296]

Chapter 6 is derived from:

- M. R. Pennington and R. Williams, 2005. *Checking the Transverse Ward Takahashi Identity at One-Loop. J. Phys. G: Nucl. Part. Phys.* **32** 2219-2233 [hep-ph/0511254].

Contents

List of Figures

List of Tables

Introduction

Quantum Field Theory (QFT) is arguably one of the most significant developments of the last one-hundred years. Combining the equally influential ideas of special relativity and quantum mechanics, and considering the fundamental particles dual to *fields*, we have a tool that provides a highly successful description of elementary processes. However, QFT is lacking with its inability to describe gravity, due to its non-renormalisability; and in this respect we may regard it as an *effective theory* of some broader, more fundamental theory (string theory, for example). Ignoring gravity, valid at the scales we are interested in, we have a more pressing problem – that of giving mass to the particles of our theory. The Standard Model (SM) is given by the $SU(3) \times SU(2) \times U(1)_Y$ gauge group with $SU(3)$ describing the quark sector, coupled to the electroweak $SU(2) \times U(1)_Y$ group. In principle the masses are input parameters – arising from Yukawa couplings between the *hypothetical* Higgs field and the fermions – and require significant fine-tuning to keep their scale with added loop corrections. This tuning process is an unsatisfactory byproduct of the Higgs mechanism, and one feels this should be unnecessary. The Higgs sector is of great interest to particle physicists, and its exploration together with searches for other new physics, is the primary focus of the Large Hadron Collider (LHC) at CERN, to come online Summer 2007. While the already running Tevatron reaches collisions at 2 TeV, the LHC will reach 14 TeV. These high energies are achieved by colliding these massive particles, at the cost of significantly reduced signals and far more complicated background.

At hadron-hadron colliders, we in fact observe interactions between composite particles at very high energies. Because QCD exhibits the property of asymptotic freedom, whereby the coupling strength tends to zero as energy increases, perturbation theory may be used to describe these short range effects. We have not, however, observed these coloured quarks and gluons in our detectors, owing to the phenomenon of confinement. We must separate the short range effects from the long range by introducing a factorisation scale. Linking the two regions together

is a difficult task, with the resulting parton shower and hadronisation modeled by Monte-Carlo event generators. A thorough understanding of these background processes is necessary to have any hope of detecting the Higgs, let alone measure its quantum numbers or those of other new particles.

A more interesting possibility would be if a scalar Higgs was found to be absent, or replaced by a composite field. Several such propositions have been made, for example Technicolour [1, 2], and the Top quark condensate [3], which both draw influence from the dynamics observed in Quantum Chromodynamics (QCD): confinement; and dynamical breaking of chiral symmetry. While the current mass of light quarks is of the order of a few MeV, their constituent mass significantly exceeds the scale as set by the Lagrangian. This generation of a mass gap has its origins with chiral symmetry breaking and the vacuum structure of QCD. Whereas the vacuum of quantum electrodynamics (QED) is considered to be nearly empty, the opposite is true for QCD owing to the strong coupling at low energies. Here, the vacuum is highly non-trivial, and is polarised due to long range correlations between quarks and antiquarks. These objects are called *condensates*, whose scale determines the mass generated. Much of QCD phenomenology is related to the scale of these chiral condensates: a scale determined by a multitude of calculational techniques such as the Operator Product Expansion (OPE) and QCD sum-rules. In perturbation theory, all corrections to the mass are proportional to the mass appearing in the Lagrangian, and so dynamical mass generation is entirely non-perturbative in nature – as is the process of confinement.

In order to study non-perturbative processes, we must resort to tools other than perturbation theory. While there exist many useful models of QCD, such as the Nambu–Jona-Lasinio (NJL) model which shares the same symmetries, we are interested in a representation stemming from the Lagrangian of QCD. Our choices here are Lattice gauge theory and the Schwinger-Dyson equations, both of which have their own advantages and drawbacks. Working on the lattice involves discretising space-time, but to be computationally tractible we must confine ourselves to small volumes and unphysically large values for the quark masses. With the Schwinger-Dyson equations, we can work in either Minkowski or Euclidean space, for any value of the quark mass – but we must deal with an infinite number of coupled integral equations. This forces the introduction of a truncation, which in turn produces a model dependence that is difficult to quantify. However, these two methods are entirely complementary in their strengths and weaknesses.

In this thesis we will be concerned with the Schwinger-Dyson approach to non-perturbative physics. Chapter 1 introduces the central concepts for both Abelian

and non-Abelian field theories, with a review of some basic principles and the introduction of the Schwinger-Dyson equations.

Chapter 2 concerns strongly coupled QED in four dimensions, which we use as a prototype field theory in the development of truncation schemes for the Schwinger-Dyson equations, at the level of vertex ansätze. We show how the Ward-Green-Takahashi identities constrain the longitudinal part of the vertex, and demonstrate how multiplcative renormalisability offers constraints on the transverse components. Chapter 3 applies what is learnt to the three dimensional variant of QED, employing the Landau-Khalatnikov-Fradkin (LKF) transformation to study the gauge covariance of the truncation scheme.

In Chapter 4 we move towards non-Abelian models, i.e. QCD, and investigate the ensuing phenomenology. This brings us to Chapter 5, in which we study the dependence of the chiral condensate, the order parameter governing the breaking of chiral symmetry, on the the current quark mass in a variety of phenomenologically inspired models.

We end with Chapter 6, which suggests how an additional class of Ward identities may be used to constrain the transverse part of vertex ansätze further. Further investigation of this may lead to improved models of the three point vertices in both QED and QCD.

Chapter 1

Background

High-energy particle physics is the study of the fundamental building blocks of nature. These particles interact with one another according to a set of rules, whose form and structure is determined and hinted at empirically through experiment. The observed physics obey conservation laws, and so the underlying symmetries may be described by constructing a Lagrangian that too exhibits these characteristics. The Lagrangian approach to QFT is standard, and may be found in any text book on Quantum Field Theory [4–8]. In reality we may take advantage of approximate symmetries in nature, which are then broken explicitly, spontaneously or dynamically – a discussion of the latter may be found in [9]. We will introduce the gauge principle for both Abelian and non-Abelian field theories. This follows with the functional integral formalism, from which our main tools of this thesis, the Schwinger-Dyson equations are most naturally derived.

1.1 The Gauge Principle

Both quantum electrodynamics (QED) and quantum chromodynamics (QCD) are derived from the principle of gauge invariance. We write down an interaction for matter fields, in which our Lagrangian is (usually) trivially invariant under global gauge transformations. Vector fields and gauge interactions are introduced naturally by the generalisation of this global gauge transformation to one that depends upon the local space-time coordinate, while still requiring that the Lagrangian remains invariant. It is this idea that leads to QED and QCD, which we now present.

1.1.1 Abelian Gauge Theories

The simplest non-trivial gauge theory we can construct is one obeying an Abelian transformation. If we take the free Dirac field ψ and write down its Lagrangian we have:

$$\mathcal{L} = \bar{\psi}\,(i\gamma^{\mu}\partial_{\mu}\psi - m)\,\psi\,, \tag{1.1}$$

where m is the unrenormalised bare mass, ψ a fermionic field and γ^{μ} the Dirac gamma matrices. We first note that this Lagrangian describing the free Dirac field is invariant under the global transformation:

$$\psi \rightarrow \psi' \equiv e^{i\,e\,\lambda}\psi\,, \qquad\qquad \bar{\psi} \rightarrow \bar{\psi}' \equiv \bar{\psi}e^{-i\,e\,\lambda}\,, \tag{1.2}$$

where λ is a constant that parametrises the change of phase. In order to obtain a gauge theory, and hence QED, we generalise this to a local gauge transformation; that is, we make the change $\lambda \rightarrow \lambda(x)$. On employing this local transformation we find that the Lagrangian changes according to:

$$\mathcal{L}' = \mathcal{L} \;-\; e\,\bar{\psi}\,\gamma^{\mu}\,\psi\,\partial_{\mu}\,\lambda(x)\,, \tag{1.3}$$

and is thus *not* invariant under this local transformation. Invariance of the Lagrangian may be restored by replacing the usual derivative ∂_{μ} with the covariant one:

$$\partial_{\mu} \rightarrow D_{\mu} \;=\; \partial_{\mu} \;+ i\,e\,A_{\mu}\,. \tag{1.4}$$

This introduces a new vector field A_{μ}, that must also transform in a particular way to preserve gauge invariance of the Lagrangian:

$$A'_{\mu} \;=\; A_{\mu} \;+\; \partial_{\mu}\,\lambda(x)\,. \tag{1.5}$$

We now have a new Lagrangian that is invariant under local gauge transformations:

$$\mathcal{L} = \bar{\psi}\,(i\not{D}_{\mu} - m_0)\,\psi\,. \tag{1.6}$$

To finally obtain QED, our vector field must have a corresponding kinetic term in the Lagrangian. A term simply of the form $A_{\mu}A^{\mu}$ would not be gauge invariant, and so we construct:

$$\mathcal{L}_{QED} = \bar{\psi}\,(i\not{D} - m_0)\,\psi \;-\; \frac{1}{4}F_{\mu\nu}F^{\mu\nu}\,, \tag{1.7}$$

where we have introduced the field strength tensor $F_{\mu\nu}$, a quantity invariant under local gauge transformations. Its definition is:

$$F_{\mu\nu} = \partial_\mu A_\nu - \partial_\nu A_\mu \ . \tag{1.8}$$

We will see later that this gauge should be fixed during calculations by imposing a constraint on A^μ; in covariant gauges this would be $\partial^\mu A_\mu = 0$. The method of introducing a Lagrange multiplier to achieve this is the most useful for dynamical systems, and so we obtain:

$$\mathcal{L}_{QED} = \bar{\psi}\,(i\,\not{D} - m)\,\psi \ - \ \frac{1}{4}F_{\mu\nu}F^{\mu\nu} \ - \ \frac{1}{2\xi}\,(\partial_\mu A^\mu)^2 \ , \tag{1.9}$$

where ξ is the so-called covariant gauge parameter, with $\xi = 0, 1$ corresponding to Landau and Feynman gauges respectively.

We note that the gauge principle is to construct the most general Lagrangian that obeys the transformations laid down by local gauge invariance. However, requirements such as renormalisability, and the neglection of topological terms, restrict the choices significantly – leaving just those terms presented in Eq. (1.9). In the next section we generalise the Abelian gauge principle to the non-Abelian gauge group, and so obtain the Lagrangian of Yang-Mills and hence QCD.

1.1.2 Non-Abelian Gauge Theories

For an Abelian gauge theory, we found that the Lagrangian of Eq. (1.1) was invariant under the global gauge transformation of Eq. (1.2). Promoting this to a local transformation, by forming the covariant derivative and imposing appropriate transformation rules on the gauge field we arrived at QED. This may be extended to non-Abelian gauge theories by generalising the algebra embodying the transformation to be *non-commutative* in nature. Since we will ultimately be dealing with the SU(3) colour group, we shall concentrate upon semi-simple Lie algebras. The transformation for our fermion fields is given by:

$$\psi_i(x) \rightarrow \psi_i'(x) = U_{ij}\psi_j \ , \qquad U = \exp(-it^a\lambda^a) \ , \tag{1.10}$$

where the t^a are the usual generators of the underlying Lie algebra, and we shall consider all gauge transformations to be infinitesimal. For QCD we have the SU(3) group and so $t^a = \bar{\lambda}^a/2$, where $\bar{\lambda}^a$ is the standard Gell-Mann choice of basis [10]. In order to satisfy the requirements of group theory, the commutator algebra of the t^a

must close and so:

$$\left[t^a, t^b\right] = i f^{abc} t^c \,, \tag{1.11}$$

where the f^{abc} are the totally antisymmetric structure constants characterising the group algebra.

The fermionic fields are in the fundamental representation, and so the covariant derivative D_μ is defined:

$$D_\mu = \partial_\mu - i\, g A^a_\mu(x) t^a \,, \tag{1.12}$$

The gauge field $A^a_\mu(x)$, later corresponding to the gluons of the theory, transforms according to the adjoint representation:

$$\begin{aligned} A^a_\mu(x) \to A^{a\prime}_\mu(x) &\equiv A^a_\mu(x) - \frac{1}{g}\partial_\mu \lambda^a(x) + f^{abc}\lambda^b(x) A^c_\mu(x) \\ &\equiv A^a_\mu(x) - \frac{1}{g} D^{ab}_\mu \lambda^b(x) \,, \end{aligned} \tag{1.13}$$

with D^{ab}_μ the covariant derivative in the adjoint representation:

$$D^{ab}_\mu = \partial_\mu \delta^{ab} - g\, f^{abc} A^c_\mu(x) \,. \tag{1.14}$$

The equivalent of the Abelian field strength tensor for non-Abelian gauge theories is:

$$F^a_{\mu\nu}(x) = \partial_\mu A^a_\nu(x) - \partial_\nu A^a_\mu(x) - g\, f^{abc} A^b_\mu(x) A^c_\nu(x) \,. \tag{1.15}$$

where $F^a_{\mu\nu}(x)$ does not transform covariantly. With this we find the covariant derivative satisfies the commutation relation $[D_\mu, D_\nu] = -igt^a F^a_{\mu\nu}$.
With these transformation rules in place, our Lagrangian for fermionic fields ψ^q is given by:

$$\mathcal{L} = \sum_q \bar{\psi}^q \left(i\gamma^\mu D_\mu - m_q\right) \psi^q - \frac{1}{4} F^a_{\mu\nu} F^{a\mu\nu} \,, \tag{1.16}$$

and yields QCD for the $SU(3)$ colour group.

This machinery leaves the Lagrangian of Eq. (1.16) invariant under local gauge transformations. However, we are now left with the task of quantizing the gauge theory. This is the process of identifying the physical degrees of freedom of the soon-to-be quantum field theory, and is traditionally done by employing canonical quantization when treating QED. For QCD however, one prefers the functional integral approach for this and hence one employs the Faddeev-Popov method to perform the gauge fixing. As alluded to earlier in the context of QED, this is a necessary step since we must pick out one representative gauge orbit of the theory to

avoid integrating over an infinite and equivalent gauge volume. This is also necessary for performing the matrix inversion when we derive the photon propagator.

1.2 Functional Integral Methods

So far we have introduced the classical Lagrangian for both QED and QCD. We have not, however, yet arrived at a quantum field theory. In order to proceed, we must quantize the theory. The traditional approach is to promote the classical fields $\varphi(x)$ to operators $\hat{\varphi}(x)$ via canonical commutation relations [11,12]. Difficulties with the canonical method arise when applied to QED due to the gauge freedom, which are circumventing by a gauge-fixing procedure. However, this is not sufficient in QCD and the canonical method remained inapplicable until the work of Kugo and Ojima [13–15]. Before this, Feynman introduced the functional integral approach [16] which we will introduce below. Here the Lagrangian is regarded as classical with c-numbered fields, thus preserving the same classical symmetries. One final method for quantization is achieved via the stochastic formalism [17] which treats the fields as stochastic variables. This draws analogy between the expressions of the path-integral method in Euclidean space with statistical physics and thermodynamics.

Since the path-integral approach will prove to be the most direct method for deriving the Schwinger-Dyson equations, we shall concentrate on this formalism. A quantum field theory is completely characterised by its Green's functions, which written as a functional integral over fields are:

$$\langle 0|\, T\left[\hat{\varphi}(x_1)\cdots\hat{\varphi}(x_n)\right]|0\rangle = \frac{\int \mathcal{D}[\varphi]\;\varphi(x_1)\cdots\varphi(x_n)\exp(i\mathrm{S})}{\int \mathcal{D}[\varphi]\exp(i\mathrm{S})}\,. \tag{1.17}$$

Here, $\varphi(x)$ is the classical scalar field at space-time point x, and T indicates the operators are time-ordered. The quantity S is the classical action:

$$S = \int d^d x \mathcal{L}(x)\,. \tag{1.18}$$

We may write Eq. (1.17) with a more compact notation [18,19] by the introduction of an external source J. The Green's functions of Eq. (1.17) are then obtained by taking functional derivatives with respect to these external sources:

$$\langle 0|\, T\left[\hat{\varphi}(x_1)\cdots\hat{\varphi}(x_n)\right]|0\rangle = \frac{(-i)^n}{\mathcal{Z}\left[0\right]}\frac{\delta^n \mathcal{Z}\left[J\right]}{\delta J(x_1)\cdots\delta J(x_n)}\bigg|_{J=0}\,, \tag{1.19}$$

where $\mathcal{Z}$ is the generating functional for the bosonic field, φ, given by:

$$\mathcal{Z}[J] = \int \mathcal{D}[\varphi] \exp\left[i \int d^4x \left(\mathcal{L} + J\,\varphi\right)\right] . \tag{1.20}$$

The two-point Green's function, or propagator for a free bosonic field is thus:

$$\langle 0|\, T\left[\hat{\varphi}(x_1)\hat{\varphi}(x_2)\right]|0\rangle = -\left.\frac{\delta^2 \mathcal{Z}[J]}{\delta J(x_1)\delta J(x_2)}\right|_{J=0} = i\Delta_F(x_1 - x_2) . \tag{1.21}$$

In the case of fermionic fields, the generating functional would be:

$$\mathcal{Z}[\eta, \bar{\eta}, J] = \int \mathcal{D}[\bar{\psi}\psi A] \exp\left[i \int d^4x \left(\mathcal{L} + \bar{\psi}\eta + \bar{\eta}\psi + J^\mu A_\mu\right)\right] , \tag{1.22}$$

where we have employed the shorthand $\mathcal{D}[\bar{\psi}\psi A] = \mathcal{D}[\bar{\psi}]\mathcal{D}[\psi]\mathcal{D}[A]$. The A_μ corresponds to the gauge field, with an associated external source J^μ. The fermionic fields ψ and $\bar{\psi}$ come with Grassmann-valued source terms $\bar{\eta}$ and η. The two point fermionic propagator is given by:

$$\langle 0|\, T\left[\hat{\psi}(x_1)\bar{\hat{\psi}}(x_2)\right]|0\rangle = \frac{(-i)^2}{\mathcal{Z}[0,0,0]} \left.\frac{\delta^2 \mathcal{Z}[\eta, \bar{\eta}]}{\delta\bar{\eta}(x_1)\delta\left(-\eta(x_2)\right)}\right|_{J=\eta=\bar{\eta}=0} = iS_F(x_1 - x_2) , \tag{1.23}$$

where the rightmost equality is in the free-field case. Note the functional derivative with respect to $-\eta$ to account for the Grassmannian algebra.

In the forthcoming sections, it will be useful to define some more quantities in connection with functional integrals. The first is the concept of the *connected* Green's function; that is, the class of diagrams that contribute towards the S-matrix. The generating functional for connected Green's functions, $\mathcal{W}$, is defined by:

$$\mathcal{Z}[\bar{\eta}, \eta, J] = \exp\left(\mathcal{W}[\bar{\eta}, \eta, J]\right) , \tag{1.24}$$

and is related to another quantity, the proper vertex or effective action $\Gamma\left[\bar{\psi}, \psi, A\right]$:

$$\mathcal{W}[\bar{\eta}, \eta, J] \equiv i\Gamma\left[\bar{\psi}, \psi, A\right] + i \int d^4x \left[\bar{\psi}\eta + \bar{\eta}\psi + A_\mu J^\mu\right] , \tag{1.25}$$

from which we can obtain one-particle irreducible Green's functions. We thus need

to define:

$$\begin{aligned} -i\frac{\delta \mathcal{W}[J]}{\delta J^\mu} = A_\mu \ , \qquad -i\frac{\delta \mathcal{W}[\eta]}{\delta \bar{\eta}} = \psi \ , \qquad i\frac{\delta \mathcal{W}[\bar{\eta}]}{\delta \eta} = \bar{\psi} \ , \\ i\frac{\delta \Gamma[A]}{\delta A^\mu} = J_\mu \ , \qquad i\frac{\delta \Gamma[\bar{\psi}]}{\delta \psi} = \eta \ , \qquad -i\frac{\delta \Gamma[\psi]}{\delta \bar{\psi}} = \bar{\eta} \ , \end{aligned} \tag{1.26}$$

which we must remember are functionals. We refer to these as the classical fields.

1.2.1 Quantization of Gauge Theories

If we ignore fermionic fields, the generating functional for a general gauge field A^a_μ is given by:

$$\mathcal{Z}[J] = \int \mathcal{D}[A] \exp\left[i \int d^4x \left(\mathcal{L} + J^{a\mu} \, A^a_\mu \right) \right] \ . \tag{1.27}$$

As it stands, the Lagrangian $\mathcal{L}$ and the measure $\mathcal{D}[A]$ are both gauge invariant, but the source term is not. Thus our generating functional does not respect gauge invariance, and hence our Green's functions are gauge dependent quantities. If we ignore fermionic fields and concentrate on the gauge part, our Lagrangian is given by:

$$\mathcal{L} = -\frac{1}{4} F^a_{\mu\nu} F^{a\mu\nu} \ . \tag{1.28}$$

On attempting to quantize the gauge field, we encounter a difficulty associated with the freedom of gauge. On performing the integral over gauge configurations, we have an overcounting due to equivalent field configurations. In order for the generating functional to yield physically meaningful results, we must restrict the functional to pick out only one representative gauge-orbit. This is achieved by placing a restriction upon the gauge field A^a_μ, which may be written in generality as:

$$G^\mu A^a_\mu = B^a \ . \tag{1.29}$$

This condition must be satisfied by all A^a_μ as a function of the gauge parameter, λ^a. To introduce this constraint in the functional integral, we insert unity in the form of a functional integral:

$$\Delta_G[A] \int \mathcal{D}[\prod_a \lambda^a] \delta \left(G^\mu A^{(\lambda)a}_\mu - B^a \right) = 1 \ , \tag{1.30}$$

which is directly evaluated to give:

$$\Delta_G[A] = \det M_G \ , \qquad \text{with } (M_G(x_1,x_2))^{ab} = \frac{\delta(G^\mu \ A_\mu^{(\lambda)a}(x_1))}{\delta\lambda^b(x_2)} \ . \tag{1.31}$$

Thus putting Eq. (1.30) in our expression for the generating functional, we find:

$$\mathcal{Z}[J] = \int \mathcal{D}[A] \det M_G \prod_{a,x} \delta\left(G^\mu A_\mu^{(\lambda)a} - B^a\right) \exp\left[i \int d^4x \left(\mathcal{L} + J^{a\mu} \ A_\mu^a\right)\right] \ . \tag{1.32}$$

The delta function may be removed, thus imposing the gauge fixing condition of Eq. (1.29), by introducing a Gaussian integral centered on B^a and integrating over the auxiliary field functionally:

$$\mathcal{Z}[J] = \int \mathcal{D}[AB] \det M_G \exp\left[i \int d^4x \left(\mathcal{L} + B^a G_\mu A_\mu^a + \frac{\xi}{2}(B^a)^2 + J^{a\mu} \ A_\mu^a\right)\right] \ . \tag{1.33}$$

This only affects the overall normalisation of the functional and is hence unimportant. We thus obtain, for arbitrary constant ξ, the following form for the generating functional:

$$\mathcal{Z}[J] = \int \mathcal{D}[A] \det M_G \exp\left[i \int d^4x \left(\mathcal{L} - \frac{1}{2\xi}\left(G^\mu A_\mu^a\right)^2 + J^{a\mu} \ A_\mu^a\right)\right] \ . \tag{1.34}$$

If we employ the covariant gauge $G^\mu = \partial^\mu$ we see that this gauge fixing condition is equivalent to adding:

$$\mathcal{L}_{GF} = -\frac{1}{2\xi}\left(\partial_\mu A^\mu(x)\right)^2 \tag{1.35}$$

to the Lagrangian. In this same gauge, the matrix M_G of Eq. (1.31) is given by:

$$(M_G(x,y))^{ab} = -\frac{1}{g}\left(\delta^{ab}\partial^2 - g f^{abc}\partial^\mu A_\mu^c\right)\delta^4(x-y) \ . \tag{1.36}$$

It is here that the famous Faddeev–Popov procedure [20] is employed. For an Abelian theory, $f^{abc} = 0$ and so the determinant $\det M_G$ is a constant. This is similarly true in both Coulomb and Axial gauges. However, in the covariant gauge, the determinant depends upon the gauge parameter A^μ and hence is no longer a constant. It must be considered carefully for it will contribute towards the physical predictions. The method of Faddeev and Popov is to exponentiate this determinant by introducing an additional field, called the Faddeev–Popov ghost, and so obtain an effective Lagrangian.

1.2.2 Faddeev–Popov Ghosts

The dependence of the Faddeev-Popov determinant on the gauge field, together with the gauge coupling constant g, gives rise to an added complication when dealing with non-Abelian gauge theories. To deal with this, we write the determinant in terms of a fictitious complex field $\chi^a(x)$ that belongs to the adjoint representation of the gauge group SU(3), is Grassmannian but whose propagator turns out to be bosonic:

$$\det M_G = \int \mathcal{D}[\chi\chi^*] \exp\left\{-i \int d^4x_1 d^4x_2 \chi^{a*}(x_1) \left(M_G(x_1, x_2)\right)^{ab} \chi^b(x_2)\right\} . \quad (1.37)$$

Simple integration by parts allows us to rewrite the exponent, so:

$$\det M_G = \int \mathcal{D}[\chi\ \chi^*] \exp\left\{i \int d^4x \left(\partial^\mu \chi^{a*}(x)\right) D_\mu^{ab} \chi^b(x)\right\} , \quad (1.38)$$

where we have relabelled x_1 to x. In the next section we put this machinery together in the context of QCD. We will find that the ghosts cannot appear in physical final states because they have the wrong spin statistics.

On putting in the terms corresponding to the quark fields together with their sources we obtain the generating functional of QCD:

$$\begin{aligned} \mathcal{Z}[J, \sigma, \sigma^*, \eta, \bar{\eta}] = \int \mathcal{D}[A\chi\chi^*\psi\bar{\psi}] \exp\Big\{i \int d^4x \Big(\mathcal{L}_F + \mathcal{L}_G + \mathcal{L}_{GF} + \mathcal{L}_{FP} \\ + A_\mu^a J^{a\mu} + \chi^*\sigma + \sigma^*\chi + \bar{\psi}\eta + \bar{\eta}\psi\Big)\Big\} . \end{aligned} \quad (1.39)$$

Where the Lagrangian has been decomposed into its constituent parts:

$$\begin{aligned} \mathcal{L}_F &= \bar{\psi}\left(i\gamma^\mu D_\mu - m\right)\psi \quad , & \mathcal{L}_G &= -\frac{1}{4}(F_{\mu\nu}^a)^2 \quad , \\ \mathcal{L}_{GF} &= -\frac{1}{2\xi}\left(\partial A\right)^2 \quad , & \mathcal{L}_{FP} &= \left(\partial^\mu \chi^{a*}\right) D_\mu^{ab} \chi^b \quad . \end{aligned}$$

1.2.3 BRST invariance

Instead of employing the fictitious complexified ghost field χ^a, we can instead introduce two real fields c and $\bar{c}$, related to χ^a by:

$$\chi^a = \left(c^a + i\bar{c}^a\right)/\sqrt{2} . \quad (1.40)$$

The functional of Eq. (1.39) is minimally changed to:

$$\mathcal{Z}[J,\sigma,\bar{\sigma},\eta,\bar{\eta}] = \int \mathcal{D}[Ac\bar{c}\psi\bar{\psi}] \exp\left\{ i \int d^4x \Big(\mathcal{L}_F + \mathcal{L}_G + \mathcal{L}_{GF} + \mathcal{L}_{FP} + A^a_\mu J^{a\mu} + \bar{c}\sigma + \bar{\sigma}c + \bar{\psi}\eta + \bar{\eta}\psi \Big) \right\} , \quad (1.41)$$

and the Faddeev–Popov part of the Lagrangian changes from $(\partial^\mu \chi^{a*})\, D^{ab}_\mu \chi^b$ to:

$$\mathcal{L}_{FP} = i\,(\partial_\mu \bar{c}^a)\, D^{ab}_\mu c^b \, , \quad (1.42)$$

taking into account the Grassmann property that $c^2 = \bar{c}^2 = 0$.

Starting with the Lagrangian of QCD, keeping this time the auxiliary field B^a (and remembering the condition of Eq. (1.29)), we have:

$$\mathcal{L} = \underbrace{\bar{\psi}\,(i\gamma^\mu D_\mu - m)\,\psi - \frac{1}{4}(F^a_{\mu\nu})^2}_{\mathcal{L}_F+\mathcal{L}_G} + \underbrace{\frac{\xi}{2}\,(B^a)^2 + B^a \partial_\mu A^a_\mu + i\,(\partial_\mu \bar{c}^a)\, D^{ab}_\mu c^b}_{\mathcal{L}_{GF}+\mathcal{L}_{FP}} , \quad (1.43)$$

with the fermion and gauge part of the Lagrangian invariant under the local gauge transformation. However, the gauge-fixing and Faddeev–Popov part of the Lagrangian are not invariant. The possibility that this invariance may be restored by exploiting the simultaneous transform of the ghost fields was explored by Becchi, Rouet, Stora [21] and independently by Tyutin [22].

We already found that the $\mathcal{L}_F + \mathcal{L}_G$ part of the Lagrangian was invariant under the local gauge transformations:

$$A^a_\mu \to A'^a_\mu = A^a_\mu - \frac{1}{g} D^{ab}_\mu \lambda^b \ , \qquad \psi \to \psi' = \psi - i t^a \lambda^a \psi \, . \quad (1.44)$$

As an ansatz, Becchi *et al.* proposed the following connection between the ghost fields c, $\bar{c}$ and the gauge parameter $\lambda^a(x)$

$$-\frac{1}{g}\lambda^a(x) = \delta\lambda c^a(x) \, , \quad (1.45)$$

where $\delta\lambda(x)$ is an infinitesimal Grassmannian number and anti-commutes with c. Our gauge transformations of Eq. (1.44) become:

$$A^a_\mu \to A'^a_\mu = A^a_\mu + \delta\lambda D^{ab}_\mu c^b \ , \qquad \psi \to \psi' = \psi + i\delta\lambda g t^a c^a \psi \, . \quad (1.46)$$

The $\mathcal{L}_F + \mathcal{L}_G$ part of the Lagrangian remains invariant under this new transfor-

mation. We can make the remaining $\mathcal{L}_{GF} + \mathcal{L}_{FP}$ part invariant by introducing the following transformation laws for the ghost fields:

$$\bar{c}^a \to \bar{c}'^a = \bar{c}^a + \frac{i}{\xi}\delta\lambda\partial^{a\mu}_{\mu} \quad , \qquad c^a \to c'^a = c^a - \frac{g}{2}\delta\lambda f^{abc}c^b c^c \; . \tag{1.47}$$

This auxiliary field B^a simply transforms as $B^a \to B'^a = B^a$. The most general QCD Lagrangian that may be constructed by recourse to BRS and anti-BRS invariance, neglecting topological terms is [23]:

$$\begin{aligned} \mathcal{L} \;\; = \;\; & \bar{\psi}\left(i\gamma^\mu D_\mu - m\right)\psi - \frac{1}{4}\left(F^a_{\mu\nu}\right)^2 - \frac{1}{2\xi}\left(\partial_\mu A^{a\mu}\right)^2 \\ & + \frac{\alpha}{2}\left(1 - \frac{\alpha}{2}\right)\frac{\xi}{2}\left(g f^{abc}\bar{c}^b c^c\right)^2 + i\frac{\alpha}{2}D^{ab}_\mu \bar{c}^a \partial^\mu c^b + i\left(1 - \frac{\alpha}{2}\right)\partial^\mu \bar{c}^a D^{ab}_\mu c^b \; . \end{aligned} \tag{1.48}$$

Any gauge choice $\alpha \neq 0, 2$ will result in a four-ghost interaction, with $\alpha = 1$ providing the hermitian case where $\bar{c}$ can be viewed as the antiparticle of c. We choose here to work with linear covariant gauges, employing the usual Faddeev–Popov Lagrangian with real ghosts, by setting $\alpha = 0$:

$$\mathcal{L} \;\; = \;\; \bar{\psi}\left(i\gamma^\mu D_\mu - m\right)\psi - \frac{1}{4}\left(F^a_{\mu\nu}\right)^2 - \frac{1}{2\xi}\left(\partial_\mu A^{a\mu}\right)^2 + i\partial^\mu \bar{c}^a D^{ab}_\mu c^b \; . \tag{1.49}$$

Furthermore, our studies of QCD will be restricted to the Landau gauge, $\xi = 0$ due to the simplifications that occur.

1.3 Ward–Green–Takahashi Identities

The Ward-Green-Takahashi [24–26] identities are most readily obtained using the path integral formalism just presented. Here, we start with the generating functional, Eq. (1.22), with the QED Lagrangian of Eq. (1.9):

$$\mathcal{Z}\left[\eta, \bar{\eta}, J\right] = \int \mathcal{D}[A\psi\bar{\psi}]\left\{ \exp\left[i\int dx \mathcal{L}(A_\mu, \psi, \bar{\psi}) + A_\mu J^\mu + \bar{\eta}\psi + \eta\bar{\psi}\right]\right\} . \tag{1.50}$$

We wish to make an infinitesimal gauge transformation of this functional, which should be left invariant under such changes. This is because a gauge transformation amounts to nothing more than a shift in the variables, that leave an integral unchanged. By varying the functional, we need only worry about the gauge fixing term and the coupling to the external sources for these are not gauge invariant. With

$\lambda(x)$ parameterising the gauge transformation, we have:

$$\begin{aligned}\mathcal{Z}+\delta\mathcal{Z} &= \int \mathcal{D}[A\psi\bar{\psi}]\Bigg\{ \exp\left[i\int dx\left(\mathcal{L}(A_\mu,\psi,\bar{\psi})+A_\mu J^\mu+\bar{\eta}\psi+\eta\bar{\psi}\right)\right.\\ &+ \left.\left(-\frac{1}{\xi}\left(\partial_\mu A^\mu\right)\partial^2\lambda(x)+J^\mu\left(\partial_\mu\lambda(x)\right)+ie\lambda(x)\left(\bar{\psi}\eta-\bar{\eta}\psi\right)\right)\right]\Bigg\}\,.\end{aligned} \tag{1.51}$$

We may use integration by parts on the variation terms to eliminate the derivatives acting upon the λ, and expand the exponential to $\mathcal{O}(\lambda)$ exploiting the infinitesimal transformation:

$$\begin{aligned}\delta\mathcal{Z} &= \int \mathcal{D}[A\psi\bar{\psi}]\Bigg\{ \exp\left[i\int dx\left(\mathcal{L}(A_\mu,\psi,\bar{\psi})+A_\mu J^\mu+\bar{\eta}\psi+\eta\bar{\psi}\right)\right]\\ &\times \left(-\frac{\partial^2}{\xi}\left(\partial_\mu A^\mu\right)-\partial_\mu J^\mu+ie\left(\bar{\psi}\eta-\bar{\eta}\psi\right)\right)i\lambda(x)\Bigg\}\,.\end{aligned} \tag{1.52}$$

The condition $\delta\mathcal{Z}=0$ is written as a functional differential equation acting upon the generating functional $\mathcal{Z}$:

$$\left[-\partial_\mu J^\mu+e\left(\eta\frac{\delta}{\delta\eta(x)}-\bar{\eta}\frac{\delta}{\delta\bar{\eta}(x)}\right)+i\frac{\partial^2}{\xi}\partial_\mu\frac{\delta}{\delta J_\mu}\right]\mathcal{Z}\left[J,\eta,\bar{\eta}\right]=0\,, \tag{1.53}$$

We may trivially rewrite this in terms of connected Green's functions, Eq. (1.24), by use of the proper vertex, Eq. (1.25):

$$\left[\partial_\mu\frac{\delta\Gamma}{\delta A_\mu(x)}+ie\left(\bar{\psi}\frac{\delta\Gamma}{\delta\bar{\psi}(x)}-\psi\frac{\delta\Gamma}{\delta\psi(x)}\right)-\frac{\partial^2}{\xi}\partial_\mu A^\mu(x)\right]\mathcal{Z}\left[J,\eta,\bar{\eta}\right]=0\,. \tag{1.54}$$

The Ward-Green-Takahashi for QED in coordinate space is then obtained by taking functional derivatives with respect to ψ and $\bar{\psi}$, and setting the fields A, ψ and $\bar{\psi}$ equal to zero:

$$\begin{aligned}\delta^\mu_x\frac{\delta^3\Gamma}{\delta\bar{\psi}(z)\delta\psi(y)\delta A^\mu(x)} &= ie\frac{\delta^2}{\delta\bar{\psi}(z)\delta\psi(y)}\left(\bar{\psi}\frac{\delta\Gamma}{\delta\bar{\psi}(x)}-\psi\frac{\delta\Gamma}{\delta\psi(x)}\right) \qquad (1.55)\\ &= ie\left[\delta^4(x-y)\frac{\delta^2\Gamma}{\delta\bar{\psi}(z)\delta\psi(x)}-\delta^4(x-z)\frac{\delta^2\Gamma}{\delta\bar{\psi}(x)\delta\psi(y)}\right]\,.\end{aligned}$$

Fourier transforming to momentum space, we find:

$$q_\mu\Gamma^\mu(p,q,p+q)=S_F^{-1}(p+q)-S_F^{-1}(p)\,, \tag{1.56}$$

which is the well-known Ward-Green-Takahashi identity (WGTI) in momentum space, with $q = k - p$. On taking the $q \to 0$ limit of this, we obtain the first Ward identity:

$$\Gamma^{\mu}_{V}(p,p) = \frac{\partial S_F^{-1}(p)}{\partial p_\mu} \quad . \tag{1.57}$$

We may obtain a further Ward-identity for the photon by taking Eq. (1.54), but this time we differentiate with respect to the field A^μ. On setting the fields to zero we find:

$$\partial^{\mu}_{x} \frac{\delta^2 \Gamma}{\delta A_\nu(y) \delta A_\mu(x)} = \frac{\delta^2}{\xi} \partial^{\nu}_{x} \delta^4(x-y) \; , \tag{1.58}$$

whose Fourier transform yields:

$$q^\mu \left[\Delta_{\mu\nu}\right]^{-1} = \frac{1}{\xi} q_\nu q^2 \; . \tag{1.59}$$

This tells us the transverse part of the photon receives no higher order corrections, at least in linear covariant gauges.

1.4 Schwinger–Dyson Equations

The starting point for the derivation of the Schwinger-Dyson equations is the fact that the functional integral of a total derivative is zero:

$$\int \mathcal{D}[\varphi] \frac{\delta}{\delta \varphi} \equiv 0 \; . \tag{1.60}$$

If we use Eq. (1.60) in the context of a simple scalar theory, we can write:

$$0 = \int \mathcal{D}\left[\varphi\right] \frac{\delta}{\delta \varphi} \exp\left\{ i \left(S(\varphi) + \int dx J \varphi \right) \right\} \tag{1.61}$$

$$= \int \mathcal{D}\left[\varphi\right] i \left[\frac{\delta S}{\delta \varphi} + J \right] \exp\left\{ i \left(S(\varphi) + \int dx J \varphi \right) \right\} \; . \tag{1.62}$$

In terms of the generating functional $\mathcal{Z}$ this can be written as a differential equation:

$$\left[\frac{\delta S}{\delta \varphi} \left(-i \frac{\delta}{\delta J} \right) + J \right] \mathcal{Z}[J] = 0 \; . \tag{1.63}$$

We will now derive the Schwinger-Dyson equations for the fermion propagator and gauge boson propagator of QED. Following this we present the equations for QCD, whose derivations are contained within [27, 28].

1.4.1 Fermion SDE

To derive the Schwinger-Dyson equation for the fermion equation of QED, we take the derivative with respect to $\bar{\psi}(x)$:

$$\begin{aligned} 0 &= \int \mathcal{D}\left[A\psi\bar{\psi}\right] \frac{\delta}{\delta\bar{\psi}} \exp\left\{iS\left(A_\mu,\psi,\bar{\psi}\right) + A_\mu J^\mu + \bar{\psi}\eta + \bar{\eta}\psi\right\} \\ &= \left[\frac{\delta S}{\delta\bar{\psi}(x)}\left(-i\frac{\delta}{\delta J}, -i\frac{\delta}{\delta\bar{\eta}}, i\frac{\delta}{\delta\eta}\right) + \eta(x)\right] \mathcal{Z}\left[\bar{\eta},\eta,J\right] . \end{aligned} \tag{1.64}$$

The action S is given by:

$$S = \int d^4x \left(\bar{\psi}\left(i\not{D} - m\right)\psi - \frac{1}{4}F_{\mu\nu}F^{\mu\nu} - \frac{1}{2\xi}\left(\partial_\mu A^\mu\right)^2\right) . \tag{1.65}$$

Performing the functional derivative we have:

$$0 = \left[\eta(x) + \left(i\not{\partial} - m + e\gamma^\mu\left(-i\right)\frac{\delta}{\delta J^\mu(x)}\right)\left(-i\right)\frac{\delta}{\delta\bar{\eta}(x)}\right] \mathcal{Z}\left[\bar{\eta},\eta,J\right] . \tag{1.66}$$

Since we are interested in the two point Green's function, we take one more functional derivative with respect to $\psi(y)$:

$$\delta\left(x-y\right)\mathcal{Z}\left[\bar{\eta},\eta,J\right] - \left(i\not{\partial} - m + e\gamma^\mu\left(-i\right)\frac{\delta}{\delta J^\mu(x)}\right)\mathcal{Z}\left[\bar{\eta},\eta,J\right]S_F\left(x-y\right) . \tag{1.67}$$

We use the definition of the connected Green's functions to remove $\mathcal{Z}$, via Eq. (1.24) and apply the chain rule to obtain:

$$\mathrm{e}^{\mathcal{W}[\bar{\eta},\eta,J]}\left[\delta\left(x-y\right) - \left(i\not{\partial} - m + e\gamma^\mu\frac{\left(-i\right)\delta\mathcal{W}}{\delta J^\mu(x)} + e\gamma^\mu\frac{\left(-i\right)\delta}{\delta J^\mu(x)}\right)S_F\left(x-y\right)\right] . \tag{1.68}$$

We can now divide out this extra factor $\mathcal{Z} = \exp\left(\mathcal{W}\left[\bar{\eta},\eta,J\right]\right)$ and rewrite in terms of the classical fields, Eq. (1.26), to arrive at:

$$\delta\left(x-y\right) - \left(i\not{\partial} - m + e\gamma^\mu A_\mu(x) + e\gamma^\mu\frac{\left(-i\right)\delta}{\delta J^\mu(x)}\right)S_F\left(x-y\right) = 0 . \tag{1.69}$$

The inverse propagator is given brewrite in terms of the :

$$S_F^{-1}(x-y) = \left.\frac{\delta^2\Gamma}{\delta\psi(x)\delta\bar{\psi}(y)}\right|_{\bar{\psi}=\psi=0} , \tag{1.70}$$

and so we have:

$$\begin{aligned}\frac{(-i)\,\delta}{\delta J^{\mu}(x)}S_F(x-y) &= -i\int d^4z\frac{\delta A_\nu(z)}{\delta J^{\mu}(x)}\frac{\delta}{\delta A_\nu(z)}\left(\frac{\delta^2\Gamma}{\delta\psi(x)\delta\bar{\psi}(y)}\Big|_{\bar{\psi}=\psi=0}\right)^{-1}\\ &= -e\int d^4zd^4ud^4w\,(-i)\,\frac{\delta A_\nu(z)}{\delta J^{\mu}(x)}S_F(x-w)\Gamma_\nu\,(u,w,z)\,S_F(w,y)\\ &= -ie\int d^4zd^4ud^4wD_{\mu\nu}(x,z)S_F(x-w)\Gamma_\nu\,(u,w;z)\,S_F(w,y)\,.\end{aligned} \tag{1.71}$$

We now take Eq. (1.69) with external fields set to zero, multiply through by $S_F^{-1}(y,y')$, integrate with respect to y' and relabel to find:

$$\begin{aligned}S_F^{-1}(x,y) &= -(i\partial\!\!\!/ - m)\delta(x-y)\\ &\quad -ie^2\int d^4z\;d^4uD^{\mu\nu}(x,z)\gamma_\mu S_F(x,u)\Gamma_\nu(u,y;z)\,.\end{aligned} \tag{1.72}$$

This is the SDE for the fermion propagator of QED in coordinate space. Performing the Fourier transform gives the usual momentum space equation:

$$S_F^{-1}(p) = p\!\!\!/ - m_0 - \frac{ie^2}{(2\pi)^4}\int d^4k\gamma^\mu S(k)\Gamma^\nu(k,p;k-p)D_{\nu\mu}(k-p)\,, \tag{1.73}$$

and is represented diagrammatically in Fig. 1.1.

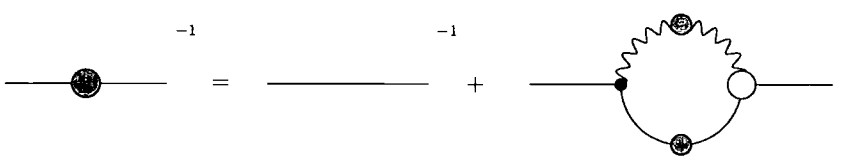

Figure 1.1: The unquenched fermion SDE. Filled dots indicate full propagators and vertices.

1.4.2 Photon SDE

The derivation for the photon proceeds similarly to that of the fermion. We vary the action with respect to the external photon field:

$$0 = \left[\frac{\delta S}{\delta\bar{A}_\mu(x)}\left(-i\frac{\delta}{\delta J},-i\frac{\delta}{\delta\bar{\eta}},i\frac{\delta}{\delta\eta}\right)+\eta)\right]\mathcal{Z}\left[\bar{\eta},\eta,J\right]\,. \tag{1.74}$$

Performing the derivative with respect to the action yields:

$$0 = \left[J_\mu(x) + \left(\partial^2 g_{\mu\nu} - \left(1 - \frac{1}{\xi}\right) \partial_\mu \partial_\nu \right) \left(-i \frac{\delta}{\delta J_\nu} \right) - e \left(\frac{i\delta}{\delta \eta} \right) \gamma_\mu \left(\frac{-i\delta}{\delta \bar{\eta}} \right) \right] \mathrm{e}^{\mathcal{W}[\bar{\eta},\eta,J]} \,. \tag{1.75}$$

We have already substituted in the generating functional for connected Green's functions. We now use Eq. (1.25) to replace this $\mathcal{W}$ with the proper vertex function Γ through the Legendre transformation:

$$\left. \frac{\delta \Gamma}{\delta A_\mu(x)} \right|_{\psi=\bar{\psi}=0} = \left(\partial^2 g_{\mu\nu} - \left(1 - \frac{1}{\xi}\right) \partial_\mu \partial_\nu \right) A^\nu(x) - ie\gamma_\mu \left(\left. \frac{\delta^2 \Gamma}{\delta \bar{\psi}(x) \psi(x)} \right|_{\psi=\bar{\psi}=0} \right)^{-1} . \tag{1.76}$$

We want the photon propagator, so we take a further derivative with respect to A_μ at a different space-time point, y:

$$\begin{aligned} \left. \frac{\delta^2 \Gamma}{\delta A_\nu(y) \delta A_\mu(x)} \right|_{A=\psi=\bar{\psi}=0} &= \left(\partial^2 g_{\mu\nu} - \left(1 - \frac{1}{\xi}\right) \partial_\mu \partial_\nu \right) \delta(x-y) \\ &- ie\gamma_\mu \frac{\delta}{\delta A_\nu(y)} \left(\left. \frac{\delta^2 \Gamma}{\delta \bar{\psi}(x) \psi(x)} \right|_{\psi=\bar{\psi}=0} \right)^{-1} . \end{aligned} \tag{1.77}$$

To perform the functional derivative of an inverse matrix one uses:

$$\frac{\delta M^{-1}}{\delta A_\mu} = -M^{-1} \frac{\delta}{\delta A_\mu} M \; M^{-1} \,, \tag{1.78}$$

with

$$M = \frac{\delta^2 \Gamma}{\delta \psi(x_1) \delta \bar{\psi}(x_2)} \,, \tag{1.79}$$

and the appropriate integrals in the relation implied. This reduces Eq. (1.77) to:

$$\left. \frac{\delta^2 \Gamma}{\delta A_\nu(y) \delta A_\mu(x)} \right|_{A=\psi=\bar{\psi}=0} = \left(\partial^2 g_{\mu\nu} - \left(1 - \frac{1}{\xi}\right) \partial_\mu \partial_\nu \right) \delta(x-y) + \Pi_{\mu\nu}(x_1, x_2) \,, \tag{1.80}$$

with the photon polarisation tensor given by the expression:

$$\Pi_{\mu\nu} = ie \int dx_1 dx_2 \gamma_\mu \left(\frac{\delta^2 \Gamma}{\delta \bar{\psi}(x) \psi(x_1)} \right)^{-1} \frac{\delta^3 \Gamma}{\delta A_\nu(y) \delta \bar{\psi}(x_1) \psi(x_2)} \left(\frac{\delta^2 \Gamma}{\delta \psi(x_2) \delta \bar{\psi}(x)} \right)^{-1} . \tag{1.81}$$

The derivatives with respect to these proper vertices can be idenfified with the connected two and three point Green's functions of the theory, and so we arrive at

the photon SDE in coordinate space:

$$[D_{\mu\nu}]^{-1}(x,y) = \left[\partial^2 g_{\mu\nu} + \left(\frac{1}{\xi} - 1\right)\partial_\mu\partial_\nu\right]\delta(x-y) + iN_f e^2 \int d^4x_1 d^4x_2 \mathrm{Tr}_D\left[\gamma_\mu S_F(x,x_1)\Gamma_\nu(x_1,x_2;y)S_F(x_2,x)\right] . \quad (1.82)$$

This can then be Fourier transformed to momentum space, yielding the usual form of the SDE for the photon propagator:

$$iD^{-1}_{\mu\nu}(q) = -q^2\left[g_{\mu\nu} + \left(\frac{1}{\xi} - 1\right)\frac{q_\mu q_\nu}{q^2}\right] + \Pi^{\mu\nu}(q) , \quad (1.83)$$

with the photon polarisation vector:

$$\Pi_{\mu\nu}(q) \equiv \frac{iN_f e^2}{(2\pi)^4}\int d^4k \mathrm{Tr}_D\left[\gamma^\mu S_F(k)\Gamma^\nu(k,k-q)S_F(k-q)\right] . \quad (1.84)$$

This is represented diagrammatically in Fig. 1.2, where we have generalised the partitioning of the loop momenta by the parameter η.

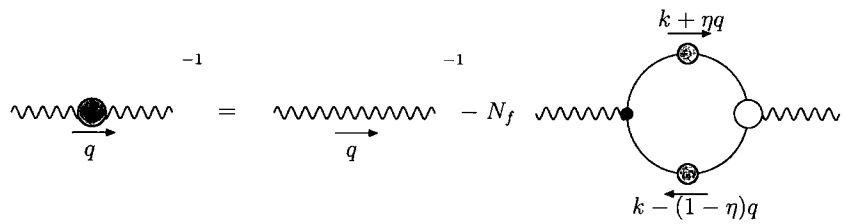

Figure 1.2: The unquenched photon SDE. Filled dots indicate full propagators and vertices.

1.4.3 Schwinger–Dyson Equations for QCD

We have derived the Schwinger-Dyson equations for quantum electrodynamics which involve just one three-point Green's function, the fermion-boson vertex, and two corresponding to the propagators for the fermion and photon. QCD, however, is a much more complicated animal as a result of its non-Abelian structure, and so we have SDEs for the ghost, gluon and quarks. These in turn require knowledge of the quark-gluon vertex, 3- and 4-gluon vertices and the ghost-gluon vertex. The Schwinger-Dyson equations are necessarily more complicated than for Abelian theories, with the Yang-Mills sector involving diagrams that are two-loop in nature in addition to one-loop forms. Of particular importance here are the diagrams proving

self-interactions.

We will employ the Lagrangian of Eq. (1.49), which must still be renormalised. This is done according to the following field renormalisation prescription:

$$\begin{aligned} g = Z_g g_R \,, \qquad \xi = Z_\xi \xi_R \,, \qquad \bar{\psi}\psi = Z_2 \bar{\psi}_R \psi_R \,, \\ \bar{c}^a c^b = \widetilde{Z}_3 \bar{c}^a_R c^b_R \,, \qquad A^a_\mu = Z_3^{1/2} A^a_{\mu R} \,, \end{aligned} \tag{1.85}$$

with the subscript R indicating the renormalised quantity. In addition to this, the vertices for the ghost-gluon (Γ_μ), three-gluon ($\Gamma_{\mu\nu\rho}$), four-gluon ($\Gamma_{\mu\nu\rho\lambda}$), and quark-gluon ($\Gamma^q_\mu$) interactions are renormalised via:

$$\begin{aligned} \Gamma^R_\mu = \widetilde{Z}_1 \Gamma_\mu \,, \qquad \Gamma^R_{\mu\nu\rho} = Z_1 \Gamma_{\mu\nu\rho} \,, \\ \Gamma^R_{\mu\nu\rho\lambda} = Z_4 \Gamma_{\mu\nu\rho\lambda} \,, \qquad \Gamma^{q,R}_\mu = Z_{1F} \Gamma^q_\mu \,. \end{aligned} \tag{1.86}$$

These factors are related through the Slavnov-Taylor identities, for which:

$$Z_1 = Z_g Z_3^{3/2}, \qquad \widetilde{Z}_1 = Z_g \widetilde{Z}_3 Z_3^{1/2}, \qquad Z_{1F} = Z_g Z_3^{1/2} Z_2, \qquad Z_4 = Z_g^2 Z_3^2 \,. \tag{1.87}$$

The prescription of Eq. (1.85) leads to the following renormalisation for the propagators of the theory:

$$\begin{aligned} D^R_G(k) &= \widetilde{Z}_3^{-1} D_G(k) \,, && \text{(Ghost)} \\ D^R_{\mu\nu}(k) &= Z_3^{-1} D_{\mu\nu}(k) \,, && \text{(Gluon)} \\ S^R_F(k) &= Z_2^{-1} S_F(k) \,, && \text{(Quark)} \end{aligned} \tag{1.88}$$

where again the superscript R indicates the renormalised quantity.

Putting these together, and dropping the R from now on, the ghost Schwinger-Dyson equations presented directly in Euclidean space, following the notation of [27], is:

$$\begin{aligned} [D_G(p)]^{-1} &= \widetilde{Z}_3 \left[D^{(0)}_G(p) \right]^{-1} \\ &+ \widetilde{Z}_1 (-N_c) \frac{g^2}{(2\pi)^4} \int d^4k \Gamma^{(0)}_\mu(p,k) D_{\mu\nu}(p-k) \Gamma_\nu(k,p) D_G(k) \,, \end{aligned} \tag{1.89}$$

where the superscript (0) indicates the quantity is *bare*. This SDE we show diagrammatically in Fig. 1.3.

The Schwinger-Dyson equation for the gluon propagator has been similarly de-

rived [28], in which we neglect the contribution from quark loops:

$$
\begin{aligned}
[D(p)]^{-1}_{\mu\nu} &= Z_3\left[D^{(0)}(p)\right]^{-1}_{\mu\nu} + \tilde{Z}_1\frac{g^2N_c}{(2\pi)^4}\int d^4k\Gamma^{(0)}_{\mu}(p,k)D_G(p-k)\Gamma_{\nu}(k,p)D_G(p) \\
&- Z_1\frac{1}{2}\frac{g^2N_c}{(2\pi)^4}\int d^4k\Gamma^{(0)}_{\mu\rho\sigma}(p,k)D_{\rho\rho'}(p-k)\Gamma_{\rho'\nu\sigma'}(k,p)D_{\sigma\sigma'}(k) \\
&- Z_4\frac{1}{2}\frac{g^2N_c}{(2\pi)^4}\int d^4k\Gamma^{(0)}_{\mu\nu\rho\sigma}D_{\rho\sigma}(k) \\
&- Z_4\frac{1}{6}\frac{g^4N_c^2}{(2\pi)^8}\int d^4k_1d^4k_2\Gamma^{(0)}_{\mu\rho\sigma\lambda}D_{\rho\rho'}(k_2)D_{\sigma\sigma'}(p-k_1-k_2) \\
&\qquad\qquad \times\Gamma_{\rho'\nu\lambda'\sigma'}(p,k_1,k_2)D_{\lambda\lambda'}(k_1) \\
&- Z_4\frac{1}{2}\frac{g^4N_c^2}{(2\pi)^8}\int d^4k_1d^4k_2\Gamma^{(0)}_{\mu\rho\sigma\lambda}D_{\rho\rho'}(p-k_1-k_2)D_{\sigma\sigma'}(k_2) \\
&\quad \times\Gamma_{\rho'\zeta\sigma'}(p-k_1-k_2,k_2)D_{\zeta\zeta'}(p-k_1)\Gamma_{\zeta'\nu\lambda'}(p-k_1,k_1)D_{\lambda\lambda'}(k_1)\,.
\end{aligned}
\tag{1.90}
$$

Whose diagrammatic form we again see in Fig. 1.3.

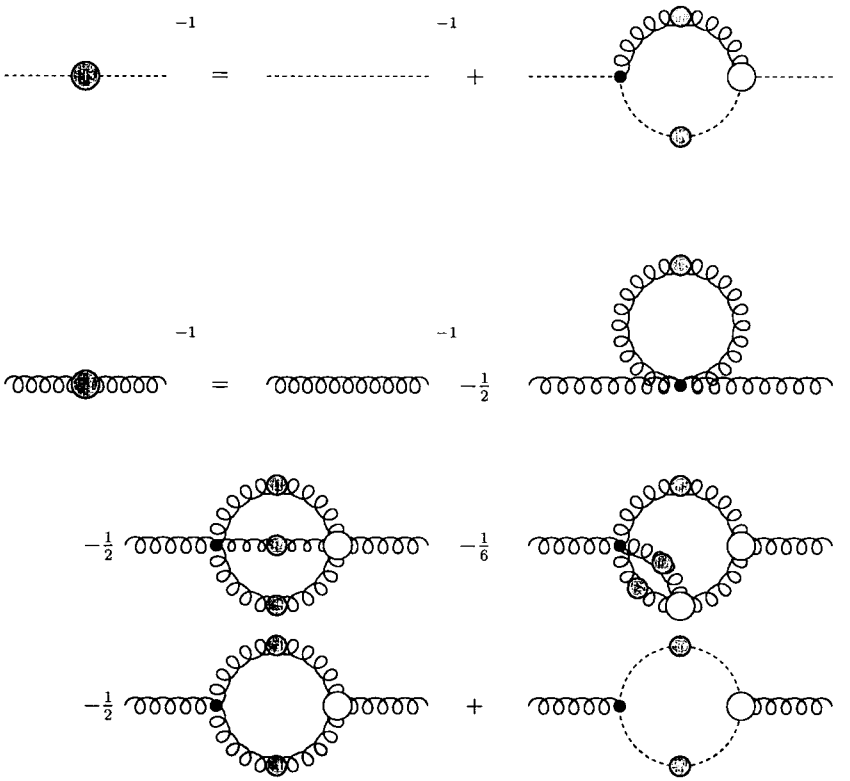

Figure 1.3: The quenched ghost and gluon Schwinger-Dyson equations for the Faddeev–Popov Lagrangian. Filled dots indicate full propagators and vertices. Dashed lines represent ghosts and springs show gluons.

Finally, we have at this level of Green's functions the Schwinger-Dyson equation for the quarks, Fig. 1.4. Their derivation is similar to that for QED, with the addition of the appropriate colour group factors:

$$[S(p)]^{-1} = \left[S^{(0)}(p)\right]^{-1} - Z_{1F}\frac{g^2 C_F}{(2\pi)^4}\int d^4k \Gamma^{(0)q}_{\mu}(p,k) D_{\mu\nu}(p-k) S(k) \Gamma^{q}_{\mu}(p,k) \ . \quad (1.91)$$

A common method of solving the SDE, Eqs. (1.90, 1.89, 1.91), is to expand each Green's function to a given order in the coupling α. Here we wish to undertake studies in which this coupling is not small, and so perturbation theory is inapplicable. By introducing ansätze for the higher order Green's functions (vertices), we can collapse the infinite tower that is the Schwinger-Dyson equations and so solve for the propagators of the theory. It is this approach that we take throughout this thesis.

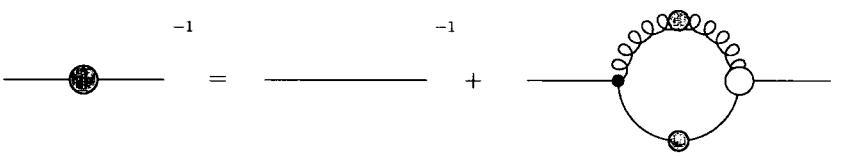

Figure 1.4: The quark Schwinger-Dyson equation for the Faddeev–Popov Lagrangian. Filled dots indicate full propagators and vertices. Springs show gluons and unbroken lines are for quarks.

1.5 Landau–Khalatnikov–Fradkin Transformation

The Landau-Khalatnikov-Fradkin (LKF) transformations [29,30] are a set of rules for relating Greens functions in one gauge to that of another. They are most easily derived and presented in coordinate space [31] where we have for the photon propagator:

$$D_{\mu\nu}(x,\Delta) = D_{\mu\nu}(x,0) + \partial_\mu\partial_\nu\Delta(x) \ , \quad (1.92)$$

and for the fermion propagator:

$$S(x,\Delta) = S(x,0)e^{(\Delta(x)-\Delta(0))e^2} \ , \quad (1.93)$$

where $\Delta(x)$ is some function corresponding to the particular gauge fixing choice. In linear covariant gauges, such as those employed throughout this thesis we have the

explicit form in d-dimensions:

$$\Delta(x) = -\xi \int \frac{d^d k}{(2\pi)^d} \frac{e^{-ik\cdot x}}{k^4} \,. \tag{1.94}$$

If we insert Eq. (1.94) into Eq. (1.92) and perform a Fourier transform, we obtain the familiar result:

$$D_{\mu\nu}(p,\xi) = \left(g_{\mu\nu} - \frac{p_\mu p_\nu}{p^2}\right) \frac{\mathcal{G}(p^2)}{p^2} + \xi \frac{p_\mu p_\nu}{p^4} \,. \tag{1.95}$$

The gauge dependent part is separate from the wave-function renormalisation, $\mathcal{G}(p^2)$, which is a gauge-invariant object.

The transformation for the fermion propagator requires direct evaluation of the function Δ. Employing dimensional regularisation we have:

$$\Delta(x) = -\frac{i\xi}{16\pi^{d/2}} (\mu x)^{4-d} \Gamma\left(\frac{d-4}{2}\right) \,, \tag{1.96}$$

a quantity that is divergent in 4-dimensions, creating additional complexity in performing the transformation. However, if we work in just three space-time dimensions:

$$\Delta(x) = -\frac{i\xi x}{8\pi} \,. \tag{1.97}$$

The corresponding transformation for the Fermion propagator is then easily written in coordinate space:

$$S\,(x,\xi) = S\,(x,0)\, e^{-x\,a} \,, \tag{1.98}$$

where the parameter a is equal to $e^2\xi/(8\pi)$.

One may similarly write down the LKF transformation for the three-point vertex of QED, from Landau gauge to arbitrary gauge ξ. If we define the non-amputated vertex (in momentum space) as:

$$B_\mu(k,p) = S_F(k)\Gamma_\nu(k,p;q)S_F(p)D_{\mu\nu}\,(k-p) \,, \tag{1.99}$$

where Γ_μ is the amputated vertex, then the corresponding LKF transformation, in position space, is:

$$\begin{aligned} B_\mu(x,y,z;\Delta) &= B_\mu(x,y,z;0) e^{e^2[\Delta(0)-\Delta(x-y)]} \\ &+ S_F(x-y;0) e^{e^2[\Delta(0)-\Delta(x-y)]} \frac{\partial}{\partial z_\mu} \left[\Delta(x-z) - \Delta(z-y)\right] \,. \end{aligned} \tag{1.100}$$

Writing the partially amputated vertex as:

$$\Lambda_\mu(k,p) = S_F(k)\Gamma_\mu(k,p;q)S_F(p) \ , \tag{1.101}$$

its LKF transformation is just given by [31]:

$$\Lambda_\mu(x,y,z;\Delta) = \Lambda_\mu(x,y,z;0)e^{e^2[\Delta(0)-\Delta(x-y)]} \ . \tag{1.102}$$

We must of course include the appropriate Fourier transformations between coordinate space and momentum space (and *vice-versa*), which complicates the application of the LKF transform. Regularisation of the integrals, necessary in renormalisable quantum field theories, brings further difficulties in applying LKF to propagators and vertices.

Chapter 2

QED in Four Dimensions

Strongly coupled QED has been extensively studied in the literature, for it promises to give us insight into the non-perturbative treatment of quantum field theories. Its gauge transformation is governed by the Abelian $U(1)$ group; there are thus no self-interactions between the gauge fields that complicate the studies of QCD. However, since we choose to work with a coupling of $\mathcal{O}(1)$ – much like in QCD – we are prohibited from a direct application of perturbation theory, and so non-perturbative methods must be employed.

The Schwinger-Dyson equations for the two-point Green's functions of QED were derived and presented in Sect. 1.4. It is from these that our non-perturbative treatment begins. However, all is not so straightforward for these two-point correlation functions involve three-point Green's functions – the fermion-boson vertex – which in turn obeys its own SDE, involving Green's functions of progressively higher order. Thus our Schwinger-Dyson equations form an infinite tower of non-linear integral equations, giving rise to a system so complicated it would be impossible to solve as a whole. It is at this point that we are forced to introduce some form of truncation. Perturbation theory, applicable only if the coupling were small, would simply generate all of the one-particle irreducible Feynman diagrams we are all so familiar with. Instead, we introduce an ansatz for one of the higher-order Green's functions – in principle the three-point function – so as to collapse our tower of Schwinger-Dyson equations to the basic building blocks, the propagators of the theory. This necessitates the belief that the inclusion of even higher order Green's functions should not drastically change those of lowest order. Put another way: do we *really* need to know the 100-point Green's function to describe the propagators?

It is hoped that what we learn with regards to four-dimensional QED may be applicable, or at least serve as a guide, to truncating and solving other strongly

coupled field theories. We refer, of course, to quantum chromodynamics, whose features of asymptotic freedom and confinement give rise to regions that may or may not be probed by perturbation theory respectively. We will explore this in forthcoming chapters, but for now focus on Abelian theories in the hope of developing appropriate techniques and tools applicable to the non-Abelian field theory that is QCD.

In this chapter we demonstrate how consideration of the symmetries of the gauge theory gives rise to constraints on the form of the non-perturbative vertex. The WGTI and Ward identities form the basis of the well-known Ball–Chiu vertex that constrains the longitudinal part, while imposing multiplicative renormalisability (MR) yields the largely successful Curtis–Pennington vertex for quenched QED. We proceed to discuss the novel ansatz of Kızılersü and Pennington that respects MR for the massless unquenched theory. This follows with a detailed numerical investigation of these vertices in different gauges, so determining the critical coupling and quantifying the residual gauge dependence.

2.1 The General Fermion-Boson Vertex

The non-perturbative fermion-boson vertex of QED, $\Gamma^\mu(k,p;q)$, must satisfy several key constraints [31]. Not only does it obey its own Schwinger-Dyson equation, Fig. 2.1, in which is hidden twelve coupled integral equations, but it must satisfy the Ward-Green-Takahashi identity (WGTI) of Eq. (1.56), and be free of kinematic singularities by satisfying its differential form, the Ward identity, Eq. (1.57). In the weak-coupling limit, the vertex $\Gamma^\mu(k,p;q)$ must reduce to the bare-vertex, γ^μ; they must also share the same transformation under charge conjugation, C, and the Lorentz transformations P and T. The full vertex is required to satisfy gauge covariance, as exhibited through the LKF transformations [29,30]. Note that satisfying the WGTI is not sufficient for this constraint, for it acts only upon the longitudinal part of the vertex. Finally, our vertex Γ^μ must ensure that multiplicative renormalisability is preserved in the SDEs, a requirement that is not trivially satisfied.

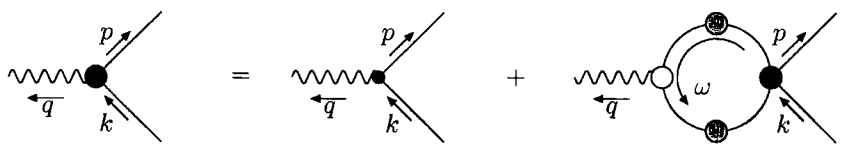

Figure 2.1: The Schwinger-Dyson equation for fermion-boson vertex in QED. Note the four-fermion scattering kernel in the loop.

2.1.1 The Ward-Green-Takahashi Identity

In gauge theories, it is necessary to pick out a representative orbit out of infinitely many, thereby removing (in QED at least) an infinite constant in the path integral. This is achieved using the traditional method of introducing a Lagrange multiplier. Doing so breaks the gauge invariance of the Lagrangian, though this symmetry is still manifest in the action leaving physical quantities independent of the gauge parameter. This principle of gauge invariance leads to the Ward-Green-Takahashi identities, whose satisfaction is required to all orders in perturbation theory, and indeed non-perturbatively. Whilst these identities exist for Green's functions of all orders, it is those that concern the three-point functions that we focus upon here. For the fermion-boson vertex of quantum electrodynamics we have:

$$q_\mu \Gamma^\mu(k,p;q) = S_F^{-1}(k) - S_F^{-1}(p) \; . \tag{2.1}$$

From here, we make our first attempt to satisfy condition one of the vertex as given above. We know that the vertex may be written in terms of longitudinal and transverse components:

$$\Gamma^\mu(k,p;q) = \Gamma_L^\mu(k,p;q) + \Gamma_T^\mu(k,p;q) \, , \tag{2.2}$$

where the transverse part satisfies the transversality condition $q_\mu \Gamma_T^\mu(k,p;q) = 0$, with q_μ the outgoing photon momentum, Fig. 2.2. This means that the transverse part is blind to the WGTI, so it is solely the longitudinal part that must satisfy Eq. (2.1):

$$q_\mu \Gamma^\mu(k,p) = q_\mu \Gamma_L^\mu(k,p) = S_F^{-1}(k) - S_F^{-1}(p) \; . \tag{2.3}$$

We can clearly see a trivial way of satisfying the WGTI from the longitudinal part by writing:

$$\Gamma_L^\mu(k,p) = \frac{q^\mu}{q^2} \left(S_F^{-1}(k) - S_F^{-1}(p) \right) \; , \tag{2.4}$$

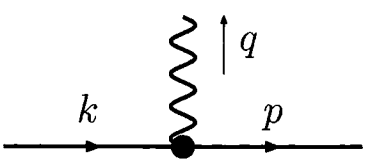

Figure 2.2: Fermion-vector boson vertex and its momenta.

and using this in an attempt to specify the full vertex:

$$\Gamma^{\mu}(k,p) = \frac{q^{\mu}}{q^2}\left(S_F^{-1}(k) - S_F^{-1}(p)\right) + \left(g^{\mu\nu} - \frac{q^{\mu}q^{\nu}}{q^2}\right) T_{\nu}(k,p) \;, \tag{2.5}$$

where the second term is the as yet unconstrained transverse part $\Gamma_T^{\mu}(k,p)$. It is clear that this satisfies the WGTI independently of the choice of the transverse part. However, we must also satisfy the Ward identity – that is to say we must have a unique limit when $k \longrightarrow p$:

$$\Gamma^{\mu}(p,p) = \lim_{k\to p} \Gamma^{\mu}(k,p;q) = \frac{\partial S_F^{-1}(p)}{\partial p_{\mu}} \;. \tag{2.6}$$

Taking this same limit in Eq. (2.5) we find:

$$\Gamma^{\mu}(p,p) = \left(g^{\mu\nu} - \frac{q^{\mu}q^{\nu}}{q^2}\right) T_{\nu}(p,p) + \frac{q^{\mu}q^{\nu}}{q^2}\frac{\partial S_F^{-1}(p)}{\partial p^{\nu}} \;, \tag{2.7}$$

which can only satisfy the Ward identity if the transverse part also has the following limit:

$$T_{\nu}(p,p) = \frac{\partial S_F^{-1}(p)}{\partial p^{\nu}} \;. \tag{2.8}$$

Though the WGTI is satisfied for any function T_{ν}, the Ward identity requires a very specific form of T_{ν} in the $q \longrightarrow 0$ limit. This connection arises because the Ward identity is only the limit of the WGTI if Γ^{μ} is free of kinematic singularities at $q^2 = 0$, whereas our construction, Eq. (2.4), has such a singularity.

Instead of starting with the Ward-Green-Takahashi identity, as we attempted previously, we begin with the Ward identity of Eq. (1.57). In general we can write the inverse fermion propagator in terms of it's Dirac-odd and Dirac-even components:

$$S_F^{-1}(p) = A(p^2)\not{p} + B(p^2) \;, \tag{2.9}$$

and so the Ward identity gives:

$$\Gamma^{\mu}(p,p) = \frac{\partial S_F^{-1}}{\partial p_{\mu}} = A(p^2)\gamma^{\mu} + 2A'(p^2)p^{\mu}\not{p} + 2B'(p^2)p^{\mu} \;. \tag{2.10}$$

If we now write this in a (k,p)-symmetric fashion we find:

$$\Gamma^\mu(p,p) = \lim_{k\to p}\left[\frac{1}{2}\left(A(k^2)+A(p^2)\right)\gamma^\mu + \frac{1}{2}\frac{A(k^2)-A(p^2)}{k^2-p^2}(k+p)^\mu\left(\not{k}+\not{p}\right) + \frac{B(k^2)-B(p^2)}{k^2-p^2}(k+p)^\mu\right] . \tag{2.11}$$

Making the identification $\Gamma^\mu(p,p) = \Gamma^\mu_L(p,p) + \Gamma^\mu_T(p,p)$ and noting that Eq. (2.11) also satisfies the WGTI, we find that we can specify the longitudinal part to be:

$$\Gamma^\mu_{BC}(k,p) \equiv \Gamma^\mu_L(k,p) = \frac{1}{2}\left(A(k^2)+A(p^2)\right)\gamma^\mu + \frac{1}{2}\frac{A(k^2)-A(p^2)}{k^2-p^2}(k+p)^\mu\left(\not{k}+\not{p}\right) + \frac{B(k^2)-B(p^2)}{k^2-p^2}(k+p)^\mu . \tag{2.12}$$

There are some additional constraints found with this construction. Not only is the transverse part of the vertex perpendicular to the photon momentum, $q_\mu\,\Gamma^\nu = 0$, but:

$$\Gamma^\mu_T(p,p) = 0 , \tag{2.13}$$

i.e., the transverse part of the vertex is zero in the limit of vanishing photon momentum. The full vertex is thus decomposed into two pieces, the longitudinal piece and the transverse piece:

$$\Gamma^\mu(k,p) = \Gamma^\mu_L(k,p) + \Gamma^\mu_T(k,p) , \tag{2.14}$$

with the longitudinal part of the vertex given by Eq. (2.12), and $\Gamma^\mu_T(k,p)$ as yet unspecified.

2.1.2 Decomposing the Vertex

Although we have succeeded in writing down an explicit form for the longitudinal part of the vertex, we have not yet elucidated its transverse part. According to Bernstein [32], the full vertex consists of twelve spin amplitudes comprised of $\mathbf{1}$, γ^μ and two independent four-momenta, k^μ and p^μ. Thus the full vertex may be written as:

$$\Gamma^\mu = \sum_{i=1}^{12} P^i V_i^\mu , \tag{2.15}$$

where the vectors V_i^μ are as follows:

$$\begin{aligned} V_1^\mu &= k^\mu \not{k} \;, \quad V_2^\mu = p^\mu \not{p} \;, \quad V_3^\mu = k^\mu \not{p}, \quad V_4^\mu = p^\mu \not{k} \\ V_5^\mu &= \gamma^\mu \not{k}\not{p}, \quad V_6^\mu = \gamma^\mu \;, \quad V_7^\mu = k^\mu \mathbf{1} \;, \; V_8^\mu = p^\mu \mathbf{1} \\ V_9^\mu &= p^\mu \not{k}\not{p}, \quad V_{10}^\mu = k^\mu \not{k}\not{p}, \quad V_{11}^\mu = \gamma^\mu \not{k}, \quad V_{12}^\mu = \gamma^\mu \not{p} \,. \end{aligned} \tag{2.16}$$

We are free to choose any basis of twelve vectors from these, and do so in the manner laid out by Ball and Chiu [33]. These will yield four longitudinal vectors and eight transverse. The full vertex is then written:

$$\Gamma^\mu(k,p;q) = \sum_{i=1}^{4} \lambda_i(k,p;q)\, L_i^\mu(k,p;q) + \sum_{i=1}^{8} \tau_i(k,p;q)\, T_i^\mu(k,p;q) \,. \tag{2.17}$$

Three suitable basis vectors for the longitudinal part have been identified in Eq. (2.12), *viz.*

$$\begin{aligned} L_1^\mu(k,p;q) &= \gamma^\mu \,, \\ L_2^\mu(k,p;q) &= (k+p)^\mu \,(\not{k}+\not{p}) \;, \\ L_3^\mu(k,p;q) &= (k+p)^\mu \;, \end{aligned} \tag{2.18}$$

where the fourth component, $\sigma_{\mu\nu}\,(k+p)^\nu$, has a coefficient of zero owing to gauge invariance and the WGTI.

By recourse to perturbation theory, Ball and Chiu constructed a set of basis vectors for the transverse components free of kinematic singularities in Feynman gauge [33]. A calculation in arbitrary covariant gauges by Kızılersü *et al.* showed that a modification to one of the components was necessary [34]. The same calculation has been performed for QCD by Davydychev *et al.* [35] correcting some minor

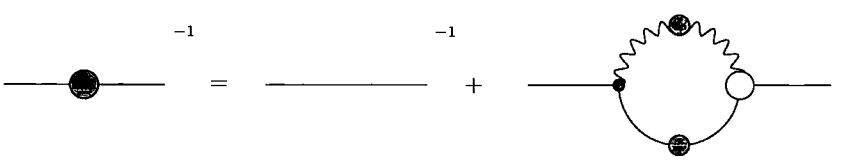

Figure 2.3: The unquenched fermion SDE. Filled dots indicate full propagators and vertices.

typographic errors in the text. We present the final basis here:

$$\begin{aligned}
T_1^\mu(k,p;q) &= p^\mu(k\cdot q) - k^\mu(p\cdot q) \\
T_2^\mu(k,p;q) &= (p^\mu k\cdot q - k^\mu p\cdot q)\,(\not{k}+\not{p}) \\
T_3^\mu(k,p;q) &= -q^2\gamma^\mu + q^\mu \not{q} \\
T_4^\mu(k,p;q) &= q^2\left(\gamma^\mu(\not{p}+\not{k}) - p^\mu - k^\mu\right) - 2(k-p)^\mu k^\lambda p^\nu \sigma_{\lambda\nu} \\
T_5^\mu(k,p;q) &= q_\nu \sigma^{\nu\mu} \\
T_6^\mu(k,p;q) &= \gamma^\mu\left(k^2-p^2\right) - (k+p)^\mu \not{q} \\
T_7^\mu(k,p;q) &= \frac{1}{2}(p^2-k^2)\left(\gamma^\mu(\not{p}+\not{k}) - p^\mu - k^\mu\right) + (k+p)^\mu\, k^\lambda p^\nu \sigma_{\lambda\nu} \\
T_8^\mu(k,p;q) &= \gamma^\mu \sigma^{\alpha\beta} k_\alpha p_\beta - k^\mu \not{p} + p^\mu \not{k}
\end{aligned} \tag{2.19}$$

In this thesis we will concern ourselves with the longitudinal vectors, but restrict our attention to those T_i with $i = 2,3,6,8$, for these latter are the only ones that appear in the massless fermion case.

In principle, we have the choice as to how to partition the momentum travelling in the loops of our Schwinger-Dyson equations. This impacts upon how we write down this basis, and in terms of which momenta. This will be discussed in context in the next two sections, giving reasons as to the pros and cons of the available choices of momentum partition in the loops.

Our task is now to write out our Schwinger-Dyson equations for the fermion and gauge-boson propagators in terms of this general basis. This will be done in d-dimensions, for we later intend to study the three-dimensional variant of QED. We first note that these propagators conform to a certain structure, allowing us to parameterise their behaviour in terms of scalar functions: two for the fermion propagator; and one for the photon. Thus we have:

$$S_F^{-1}(p) = \mathcal{A}(p^2)\not{p} + \mathcal{B}(p^2)\,, \tag{2.20}$$

for the inverse fermion propagator, which is often written as:

$$S_F(p) = \frac{\mathcal{F}(p^2)}{\not{p} - \mathcal{M}(p^2)} = \frac{\mathcal{F}(p^2)}{p^2 - \mathcal{M}^2(p^2)}\left(\not{p} + \mathcal{M}(p^2)\right)\,. \tag{2.21}$$

using $\mathcal{A}(p^2) = 1/\mathcal{F}(p^2)$ and $\mathcal{M}(p^2) = \mathcal{B}(p^2)/\mathcal{A}(p^2)$.

Similarly, the photon propagator may be decomposed into its representative

	Basis Vector	Dimension
$\boldsymbol{L_1}$	γ^μ	1
$\boldsymbol{L_2}$	$(k+p)^\mu\,(\not{k}+\not{p})$	d
$\boldsymbol{L_3}$	$(k+p)^\mu$	$d^{1/2}$
$\boldsymbol{T_2}$	$(p^\mu k\cdot q - k^\mu p\cdot q)\,(\not{k}+\not{p})$	d^2
$\boldsymbol{T_3}$	$-q^2\gamma^\mu + q^\mu \not{q}$	d
$\boldsymbol{T_6}$	$\gamma^\mu\,(k^2-p^2) - (k+p)^\mu\,\not{q}$	d
$\boldsymbol{T_8}$	$\gamma^\mu\sigma^{\alpha\beta}k_\alpha p_\beta - k^\mu\not{p} + p^\mu\not{k}$	d

Table 2.1: Basis vectors with an asymmetric momentum partition.

Lorentz structure:

$$D_{\mu\nu} = -\frac{1}{q^2}\left[\mathcal{G}(q^2)\left(g_{\mu\nu} - \frac{q_\mu q_\nu}{q^2}\right) + \xi\frac{q_\mu q_\nu}{q^2}\right] , \tag{2.22}$$

with the photon renormalisation function $\mathcal{G}(q^2)$ related to the scalar polarisation tensor by:

$$\mathcal{G}(q^2) \equiv \frac{1}{1+\Pi(q^2)} , \tag{2.23}$$

and $\alpha(q^2) = \alpha\,(\kappa^2)\,\mathcal{G}\,(q^2,\kappa^2)$ is the running coupling. It is the Ward identity for the photon, Eq. (1.59), that tells us in covariant gauges the ξ-piece does not receive corrections due to loops.

We can reduce these full propagators to their bare form, denoted by $S_F^{(0)}$ and $D_{\mu\nu}^{(0)}$, by setting the scalar functions $\mathcal{A} = \mathcal{G} = 1$, while $\mathcal{B} = m_0$, the bare mass of the fermion entering the Lagrangian. Recall that this means in perturbation theory, if the bare mass is zero then $\mathcal{B} = 0$.

2.1.3 Fermion Schwinger-Dyson Equation

The derivation for the fermion SDE of QED was presented in the introduction, culminating in its momentum-space form, Eq. (1.73), which we write in d-dimensions:

$$S_F^{-1}(p) = \not{p} - m_0 - \frac{ie^2}{(2\pi)^d}\int d^dk\gamma^\mu S(k)\Gamma^\nu(k,p;k-p)D_{\nu\mu}(k-p) . \tag{2.24}$$

We have chosen an asymmetric choice for the momentum partition, which is appropriate since the loop is over two different propagators. The appropriate vectors for the decomposition of the vertex are given in Table 2.1. The incoming momentum is denoted p, with loop momenta k through the internal fermion line. The photon carries momentum $q = k - p$, in keeping with conservation of momentum.

Basis Vector	Dirac Trace
$\boldsymbol{L_1}$:	$-4\mathcal{A}(k^2)\mathcal{G}(q^2)\left((2-d)\,q^4+(d-3)\,(k^2+p^2)\,q^2+(k^2-p^2)^2\right)/2q^2$
$\boldsymbol{L_2}$:	$-8\mathcal{A}(k^2)\mathcal{G}(q^2)\,(k^2+p^2)\,\Delta^2/q^2$
$\boldsymbol{L_3}$:	$-8\mathcal{B}(k^2)\mathcal{G}(q^2)\Delta^2/q^2$
$\boldsymbol{T_2}$	$-4\mathcal{A}(k^2)\mathcal{G}(q^2)\,(k^2+p^2)\,\Delta^2$
$\boldsymbol{T_3}$	$2\mathcal{A}(k^2)\mathcal{G}(q^2)\left(-(d-2)\,q^4+(d-3)\,(k^2+p^2)\,q^2+(k^2-p^2)^2\right)$
$\boldsymbol{T_6}$	$4(d-1)\mathcal{A}(k^2)\mathcal{G}(q^2)k\cdot p\,(p^2-k^2)$
$\boldsymbol{T_8}$	$4(d-2)\mathcal{A}(k^2)\mathcal{G}(q^2)\Delta^2$

Table 2.2: The trace factor of Eq. (2.27) evaluated with an asymmetric momentum partition.

From Eq. (2.20) we see the fermion propagator consists of a Dirac odd part, with scalar function $\mathcal{A}(p^2)$, and an even part, described by $\mathcal{B}(p^2)$. We may project out these two functions by taking appropriate Dirac traces of Eq. (2.24).

Dirac-Odd Projection

The scalar function $\mathcal{A}(p^2)$ is projected out from the SDE by taking the Dirac trace with the inclusion of an extra factor of $\not{p}$. We have:

$$\mathcal{A}(p^2) = 1 - \frac{ie^2}{4p^2\,(2\pi)^d}\int d^dk \mathrm{Tr}_D\left[\not{p}\gamma^\mu S(k)\Gamma^\nu(k,p)\right] D_{\nu\mu}\,(k-p)\ . \tag{2.25}$$

The full vertex here $\Gamma^\nu(k,p)$ is replaced by the decomposition given in Eq. (2.17), save for the part proportional to ξq_ν in $D_{\nu\mu}$. This latter piece may be replaced by the WGTI in Eq. (1.56) directly, and can hence be exactly specified in the SDE irrespective of our ansatz. We must be careful to exploit translational invariance here, by directly evaluating the integral:

$$\int d^dk \frac{\not{q}}{q^4} = \int d^dq \frac{\not{q}}{q^4}\ , \tag{2.26}$$

to be zero, thus avoiding a potentially spurious term due to the imposition of a finite cut-off.

We concern ourselves only with those basis coefficients λ_i for $i = 1\ldots3$ and τ_i for $i = 2,3,6,8$. It is necessary to evaluate the Dirac trace contained in the integrand of Eq. (2.25):

$$\mathrm{Tr}_D\left[\not{p}\gamma^\mu S(k)\Gamma^\nu(k,p)\right]\ . \tag{2.27}$$

The results of this trace are given in Table 2.2, in which d is the number of space-

time dimensions, and $\Delta^2 = (k \cdot p)^2 - k^2 p^2$ is the triangle function. These traces are substituted into Eq. (2.25), upon which we perform a Wick rotation to Euclidean space. We replace the integration measure $d^d k_E$ by introducing hyper-spherical coordinates:

$$\begin{aligned} d^d k &= \frac{1}{2} k^{d-2} dk^2 d\phi \prod_{k=1}^{d-2} \sin^k \theta_k d\theta_k \\ &= \Omega_d k^{d-2} \sin^{d-2} \psi dk^2 d\psi \ , \end{aligned} \tag{2.28}$$

with the trivial angular integrals performed. The angular measure yields $\Omega_{d=3} = \pi$ for three dimensions, $\Omega_{d=4} = 2\pi$ for four. The final form of the projected $\mathcal{A}$-equation in Euclidean space is thus:

$$\begin{aligned} \mathcal{A}(p^2) &= 1 + \frac{e^2}{(2\pi)^d p^2} \int dk^2 \frac{\Omega_d k^{d-2} \mathcal{A}(k^2)}{\mathcal{A}^2(k^2)k^2 + \mathcal{B}^2(k^2)} \int d\psi \frac{\sin^{d-2}\psi}{q^2} \mathcal{G}(q^2) \\ &\times \Bigg\{ \lambda_1(k,p) \left((2-d)\frac{q^2}{2} + (d-3)\frac{(k^2+p^2)}{2} + \frac{(k^2-p^2)^2}{2q^2} \right) \\ &+ \lambda_2(k,p) \frac{2\,(k^2+p^2)\,\Delta^2}{q^2} - 2\,\lambda_3(k,p) \frac{\mathcal{B}(k^2)}{\mathcal{A}(k^2)} \frac{\Delta^2}{q^2} \\ &+ \tau_2(k,p;q) \left(k^2+p^2\right) \Delta^2 \\ &- \tau_3(k,p;q) \left(-(d-2)\frac{q^4}{2} + (d-3)\left(k^2+p^2\right)\frac{q^2}{2} + \left(k^2-p^2\right)^2/2 \right) \\ &+ \tau_6(k,p;q)\,(d-1))\,k \cdot p \left(k^2-p^2\right) - \tau_8(k,p;q)\,(d-2)\,\Delta^2 \Bigg\} \\ &+ \mathcal{A}_\xi(p^2) \ . \end{aligned} \tag{2.29}$$

The last piece $\mathcal{A}_\xi(p^2)$ is proportional to ξ and can be projected either by exploiting the WGTI through $q_\mu \Gamma^\mu$, or by direct use of the full longitudinal part of the vertex as specified by Ball and Chiu, where the λ_i may reflect the ansatz being employed. The former gives:

$$\begin{aligned} A_\xi(p^2) &= \frac{e^2 \xi}{(2\pi)^d p^2} \int dk^2 \frac{\Omega_d k^{d-2}}{\mathcal{A}^2(k^2)k^2 + \mathcal{B}^2(k^2)} \int d\psi \frac{\sin^{d-2}\psi}{q^2} \frac{p^2}{q^2} \\ &\times \left\{ \mathcal{A}(k^2)\mathcal{A}(p^2) \left(k^2 - k \cdot p\right) - \frac{\mathcal{B}(k^2)\mathcal{B}(p^2)}{p^2} \left(p^2 - k \cdot p\right) \right\} , \end{aligned} \tag{2.30}$$

while the latter provides:

$$\begin{aligned}\mathcal{A}_\xi(p^2) &= \frac{e^2\xi}{(2\pi)^d p^2}\int dk^2 \frac{\Omega_d k^{d-2}\mathcal{A}(k^2)}{\mathcal{A}^2(k^2)k^2+\mathcal{B}^2(k^2)}\int d\psi \frac{\sin^{d-2}\psi}{q^2} \\ &\times\Bigg\{\lambda_1(k,p)\left[\frac{1}{2}\left(k^2+p^2\right)-\frac{\left(k^2-p^2\right)^2}{2q^2}\right] \\ &+\lambda_2(k,p)\left(p^2-k^2\right)\left[\frac{p^2-k^2}{2}+\frac{k^4-p^4}{2q^2}\right] \\ &+\lambda_3(k,p)\frac{\mathcal{B}(k^2)}{\mathcal{A}(k^2)}\left[\frac{p^2-k^2}{2}+\frac{\left(k^2-p^2\right)^2}{2q^2}\right]\Bigg\}\,. \end{aligned} \tag{2.31}$$

It is understood that in Eqs. (2.29–2.31) we have Wick rotated the coefficient functions λ_i and the τ_i according to their dimension. We note that on employing a cut-off in the integration range, the two forms of the ξ-part, Eq. (2.30) and Eq. (2.31) will differ by terms spoilt by the violation of translational invariance. Additionally, the angular integrals relating to these ξ pieces may be evaluated analytically, as given in Appendix B.2.

Dirac-Even Projection

The scalar function $\mathcal{B}(p^2)$, corresponding to the mass function $\mathcal{M}(p^2)$ through the ratio $\mathcal{B}/\mathcal{A}$, is projected out from the SDE by taking the Dirac trace of Eq. (2.24) as it stands. Hence we have:

$$\mathcal{B}(p^2) = m_0 + \frac{ie^2}{4\,(2\pi)^d}\int d^dk\ \mathrm{Tr}_D\left[\gamma^\mu S(k)\Gamma^\nu(k,p)\right]D_{\nu\mu}\left(k-p\right)\,. \tag{2.32}$$

We split this into two pieces, one of which is proportional to $\xi\ q_\mu$, and exploit the WGTI to arrive at:

$$\begin{aligned}\mathcal{B}(p^2) &= m_0 - \frac{i\,e^2}{4\,(2\pi)^d}\int_M \frac{d^dk}{q^2}\frac{1}{\mathcal{A}^2(k^2)k^2-\mathcal{B}^2(k^2)} \\ &\mathrm{Tr}_D\Bigg[\gamma^\nu\left(\mathcal{A}(k^2)\not{k}+\mathcal{B}(k^2)\right)\Gamma^\mu(k,p;q)\mathcal{G}(q^2)\left(g_{\mu\nu}-\frac{q_\mu q_\nu}{q^2}\right) \\ &-\xi\frac{\not{q}}{q^2}\left(\mathcal{A}(k^2)\not{k}+\mathcal{B}(k^2)\right)\left(\mathcal{A}(p^2)\not{p}-\mathcal{B}(p^2)\right)\Bigg]\,. \end{aligned} \tag{2.33}$$

The full vertex Γ^μ is decomposed into its set of basis vectors. We perform traces on these in Minkowski space in d-dimensions, with the results listed in Table 2.3. We

Basis Vector	Dirac Trace
$\boldsymbol{L_1}$:	$4(d-1)\mathcal{B}(k^2)\mathcal{G}(q^2)$
$\boldsymbol{L_2}$:	$-16\mathcal{B}(k^2)\mathcal{G}(q^2)\Delta^2/q^2$
$\boldsymbol{L_3}$:	$-8\mathcal{A}(k^2)\mathcal{G}(q^2)\Delta^2/q^2$
$\boldsymbol{T_2}$	$-8\mathcal{B}(k^2)\mathcal{G}(q^2)\Delta^2$
$\boldsymbol{T_3}$	$-4(d-1)\mathcal{B}(k^2)\mathcal{G}(q^2)q^2$
$\boldsymbol{T_6}$	$4(d-1)\mathcal{B}(k^2)\mathcal{G}(q^2)\,(k^2-p^2)$
$\boldsymbol{T_8}$	0

Table 2.3: The Dirac trace part of the even projection of the fermion SDE with an asymmetric momentum partition.

insert this basis into Eq. (2.33) and Wick rotate:

$$\begin{aligned}
\mathcal{B}(p^2) &= m_0 + \frac{e^2}{(2\pi)^d}\int dk^2 \frac{\Omega_d k^{d-2}}{\mathcal{A}^2(k^2)k^2+\mathcal{B}^2(k^2)}\int d\psi \frac{\sin^{d-2}\psi}{q^2}\mathcal{G}(q^2) \\
&\quad\times\Big\{ (d-1)\,\lambda_1(k,p)\mathcal{B}(k^2) - 4\lambda_2(k,p)\mathcal{B}(k^2)\frac{\Delta^2}{q^2} - 2\lambda_3(k,p)\mathcal{A}(k^2)\frac{\Delta^2}{q^2} \\
&\quad -2\tau_2(k,p;q)\mathcal{B}(k^2)\Delta^2 - \tau_3(k,p;q)\,(d-1)\,\mathcal{B}(k^2)q^2 \\
&\quad +\tau_6(k,p;q)\,(d-1)\,\mathcal{B}(k^2)\,\big(k^2-p^2\big)\Big\} \\
&\quad + \frac{e^2\xi}{(2\pi)^d}\int dk^2 \frac{\Omega_d k^{d-2}}{\mathcal{A}^2(k^2)k^2+\mathcal{B}^2(k^2)}\int d\psi \frac{\sin^{d-2}\psi}{q^2}\frac{1}{q^2} \\
&\quad\times\Big\{ \big(k^2-k\cdot p\big)\,\mathcal{B}(p^2)\mathcal{A}(k^2) + \big(p^2-k\cdot p\big)\,\mathcal{B}(k^2)\mathcal{A}(p^2)\Big\}\,. \qquad (2.34)
\end{aligned}$$

Here, we do not exploit the Ball–Chiu vertex directly in the ξ-part for it gives the same result. Analytic results for the integrals may be found in Appendix B.2.

2.1.4 Photon Schwinger-Dyson Equation

The SDE for the photon was given in Eq. (1.83), and can be written explicitly in d-dimensions:

$$D^{-1}_{\mu\nu}(q) = \left[D^{(0)}_{\mu\nu}(q)\right]^{-1} + \frac{iN_f e^2}{(2\pi)^d}\int d^dk \mathrm{Tr}_D\left[\gamma^\mu S_F(k)\Gamma^\nu(k,k-q)S_F(k-q)\right]. \qquad (2.35)$$

The loop consists of two fermions, one with momentum k and the other carrying $k-q$. This is, of course, not a problem for any theory satisfying translational invariance – a necessary requirement for our physical world – but what if this invariance is

broken? We clearly see that this equation involves an integral over all space-time; an impossible calculation for any computer to undertake numerically. Bearing in mind that very large scales are irrelevent since we enter the realms of new physics, the easiest way to tackle the calculation is to impose an upper limit κ in the integration – a scale that should disappear on renormalisation. It is this hard cut-off that breaks translational invariance, giving rise to spurious terms that should have integrated to zero. We choose our two loop momenta to be $k + \eta\, q$ and $k - (1 - \eta)\, q$, where the parameter η determines the momentum partition. The asymmetric choice often employed takes $\eta = 0, 1$, whose benefit is a simpler numerical treatment. However, if we choose $\eta = 1/2$, the two fermions, and indeed the vertex, are put on a more equal footing. It is hoped that this will eliminate or reduce spurious contributions arising from the breaking of translational invariance. This entails the symmetric basis choice, as given in Table 2.4 with q the incoming photon momentum and

	Basis Vector	Dimension
$\boldsymbol{L_1}$	γ^μ	1
$\boldsymbol{L_2}$	$l^\mu \not{l}$	d
$\boldsymbol{L_3}$	l^μ	$d^{1/2}$
$\boldsymbol{T_2}$	$2\left(l^\mu q^2 - q^\mu l\cdot q\right)\not{l}$	d^2
$\boldsymbol{T_3}$	$-q^2\gamma^\mu + q^\mu \not{q}$	d
$\boldsymbol{T_6}$	$2\gamma^\mu l\cdot q - 2l^\mu \not{q}$	d
$\boldsymbol{T_8}$	$\frac{1}{2}\gamma^\mu\left(\not{q}\not{l} - \not{l}\not{q}\right) - q^\mu \not{l} + l^\mu \not{q}$	d

Table 2.4: Basis vectors of the full-vertex with a symmetric momentum partition.

$l = k + p$ the loop momentum. We use the following:

$$l^\mu = k^\mu + p^\mu \quad , \quad l_+^\mu = l^\mu + q^\mu/2 \quad , \quad l_-^\mu = l^\mu - q^\mu/2\,, \tag{2.36}$$

upon which our basis coefficients depend through $\lambda_i = \lambda_i(l_+, l_-; q)$, $\tau_i = \tau_i(l_+, l_-; q)$, in which we have introduced the convenient shorthand $\mathcal{A}_\pm \equiv \mathcal{A}(l_\pm)$, $\mathcal{B}_\pm \equiv \mathcal{B}(l_\pm)$.

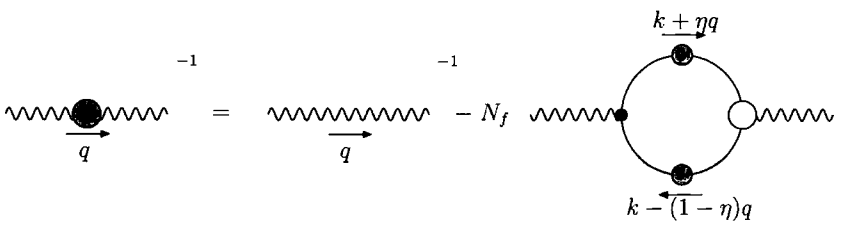

Figure 2.4: The unquenched photon SDE. Filled dots indicate full propagators and vertices.

To project out the scalar function $\mathcal{G}(q^2)$ of Eq. (2.22) we employ the Brown–Pennington projector [36]:

$$\mathcal{P}_{\mu\nu} = \left(d\frac{q_\mu q_\nu}{q^2} - g_{\mu\nu} \right) , \tag{2.37}$$

eliminating quadratically divergent pieces in the integrand, thus yielding:

$$\begin{aligned} \frac{1}{\mathcal{G}(q^2)} &= 1 + \frac{i\,e^2 N_f}{(2\pi)^d} \int d^d l \frac{1}{(\mathcal{A}_+^2 l_+^2 - \mathcal{B}_+^2)\,(\mathcal{A}_-^2 l_-^2 - \mathcal{B}_-^2)} \\ &\quad \times \frac{1}{(d-1)\,q^2} \mathcal{P}_{\mu\nu} \mathrm{Tr}_D \left[\gamma^\mu \left(\mathcal{A}_+ \not{l}_+ + \mathcal{B}_+ \right) \Gamma^\nu \left(l_+, l_-; q \right) \left(\mathcal{A}_- \not{l}_- + \mathcal{B}_- \right) \right] . \end{aligned} \tag{2.38}$$

The d-dimensional traces are evaluated according to the basis decomposition of the full vertex, Table 2.4, with the results given in Table 2.5. We finally have in Euclidean space:

$$\begin{aligned} \frac{1}{\mathcal{G}(q^2)} &= 1 + \frac{e^2 N_f}{(2\pi)^d\,(d-1)\,q^2} \int dl^2 d\psi \frac{\Omega_d l^{d-2} \sin^{d-2}\psi \mathcal{A}_+ \mathcal{A}_-}{(\mathcal{A}_+^2 l_+^2 + \mathcal{B}_+^2)\,(\mathcal{A}_-^2 l_-^2 + \mathcal{B}_-^2)} \Bigg\{ \\ &\quad 2\lambda_1 \left(4l^2 + (d-1)\,q^2 - 4d\frac{(l\cdot q)^2}{q^2} \right) \\ &\quad + \lambda_2 \left[4\frac{\mathcal{B}_+\mathcal{B}_-}{\mathcal{A}_+\mathcal{A}_-} \left(d\frac{(l\cdot q)^2}{q^2} - l^2 \right) - \left(4d\frac{l^2}{q^2} - (d-2) \right) (l\cdot q)^2 + 4l^4 + l^2 q^2 \right] \\ &\quad + 2\lambda_3 \left[-(d-1) \left(\frac{\mathcal{B}_+}{\mathcal{A}_+} - \frac{\mathcal{B}_-}{\mathcal{A}_-} \right) l\cdot q + \left(\frac{\mathcal{B}_+}{\mathcal{A}_+} + \frac{\mathcal{B}_-}{\mathcal{A}_-} \right) \left(2d\frac{(l\cdot q)^2}{q^2} - 2l^2 \right) \right] \\ &\quad + 2\tau_2 \left(4\frac{\mathcal{B}_+\mathcal{B}_-}{\mathcal{A}_+\mathcal{A}_-} - 4l^2 - q^2 \right) \Delta^2 \\ &\quad + \tau_3 \left(4\,(d-1)\,\frac{\mathcal{B}_+\mathcal{B}_-}{\mathcal{A}_+\mathcal{A}_-} q^2 + 8\,(l\cdot q)^2 + \left(4\,(d-3)\,l^2 - (d-1)\,q^2 \right) q^2 \right) \\ &\quad - 2\,(d-1)\,\tau_6 \left(\left(4l^2 - q^2 \right) + 4\frac{\mathcal{B}_+\mathcal{B}_-}{\mathcal{A}_+\mathcal{A}_-} \right) (l\cdot q) + 4\,(d-2)\,\tau_8 \Delta^2 \Bigg\} , \end{aligned} \tag{2.39}$$

which should be a gauge-independent object. One can see that this requirement is non-trivial since the integrand is a complicated function of gauge-dependent quantities. The triangle function here is given by $\Delta^2 = (l\cdot q)^2 - l^2 q^2$ and the angular measure Ω_d is π in three dimensions and 2π in four.

The choice of momentum partition is only of real importance in renormalisable theories, when we eliminate the cut-off κ in favour of the renormalisation point, μ.

Basis Vector	Projected Dirac Trace
$\boldsymbol{L_1}$:	$2\mathcal{A}_+\mathcal{A}_-\left[4d\frac{(l\cdot q)^2}{q^2}-4l^2-(d-1)q^2\right]$
$\boldsymbol{L_2}$:	$\mathcal{A}_+\mathcal{A}_-\left[\left(4d\frac{l^2}{q^2}-(d-2)\right)(l\cdot q)^2-4l^4-l^2q^2\right]+4\mathcal{B}_+\mathcal{B}_-\left(d\frac{(l\cdot q)^2}{q^2}-l^2\right)$
$\boldsymbol{L_3}$:	$4\left(\mathcal{A}_-\mathcal{B}_++\mathcal{A}_+\mathcal{B}_-\right)\left(d\frac{(l\cdot q)^2}{q^2}-l^2\right)-2(d-1)\left(\mathcal{A}_-\mathcal{B}_+-\mathcal{A}_+\mathcal{B}_-\right)(l\cdot q)$
$\boldsymbol{T_2}$	$2\left[4\mathcal{B}_-\mathcal{B}_++\mathcal{A}_-\mathcal{A}_+\left(4l^2+q^2\right)\right]\Delta^2$
$\boldsymbol{T_3}$	$4(d-1)\mathcal{B}_+\mathcal{B}_-q^2-2\mathcal{A}_-\mathcal{A}_+\left(8\left(l\cdot q\right)^2+\left(4(d-3)l^2-(d-1)q^2\right)q^2\right)$
$\boldsymbol{T_6}$	$2\left(d-1\right)\left(l\cdot q\right)\left(\mathcal{A}_+\mathcal{A}_-\left(4l^2-q^2\right)-4\mathcal{B}_+\mathcal{B}_-\right)$
$\boldsymbol{T_8}$	$-4\left(d-2\right)\mathcal{A}_+\mathcal{A}_-\Delta^2$

Table 2.5: The contraction $\mathcal{P}_{\mu\nu}\mathrm{Tr}_D\left[\cdots\right]$ of Eq. (2.38) evaluated for a symmetric momentum partition.

Thus, in three-dimensional QED it does not matter how we choose η. For numerical comparison, we also use the photon equation for an asymmetric partition choice in four-dimensions. Without giving the explicit traces, the projected SDE is:

$$\begin{aligned}
\frac{1}{\mathcal{G}(p^2)} \;=\; & 1+\frac{N_f e^2}{6\pi^3 p^2}\int dk^2 d\psi \frac{k^2\sin^2\psi\mathcal{A}(k^2)\mathcal{A}(q^2)}{\left(\mathcal{A}^2(k^2)k^2+\mathcal{B}^2(k^2)\right)\left(\mathcal{A}(q^2)q^2+\mathcal{B}^2(q^2)\right)} \\
& \times\Big\{2\lambda_1(k^2,q^2)\left[k^2(1-4\cos^2\psi)+3k\cdot p\right] \\
& +\lambda_2(k^2,q^2)\left[\left(k^2+q^2-2\frac{\mathcal{B}(k^2)\mathcal{B}(q^2)}{\mathcal{A}(k^2)\mathcal{A}(q^2)}\right)\left(2k^2(1-4\cos^2\psi)+3k\cdot p\right)\right. \\
& \qquad \left.+3(k^2-q^2)\left(k^2-\frac{\mathcal{B}(k^2)\mathcal{B}(q^2)}{\mathcal{A}(k^2)\mathcal{A}(q^2)}\right)\right] \\
& -\lambda_3(k^2,q^2)\left[\left(\frac{\mathcal{B}(k^2)}{\mathcal{A}(k^2)}+\frac{\mathcal{B}(q^2)}{\mathcal{A}(q^2)}\right)\left(2k^2(1-4\cos^2\psi)+3k\cdot p\right)\right. \\
& \qquad \left.+3(k^2-q^2)\frac{\mathcal{B}(k^2)}{\mathcal{A}(k^2)}\right] \\
& +\tau_2\cdot p^2k^2\left(\left(k^2+q^2\right)-2\frac{\mathcal{B}(k^2)\mathcal{B}(q^2)}{\mathcal{A}(k^2)\mathcal{A}(q^2)}\right)\sin^2\psi \\
& -\tau_3\cdot p^2\left(k^2(1+2\cos^2\psi)-3k\cdot p+3\frac{\mathcal{B}(k^2)\mathcal{B}(q^2)}{\mathcal{A}(k^2)\mathcal{A}(q^2)}\right) \\
& -\tau_6\cdot 3(k^2-q^2)(k^2-k\cdot p+\frac{\mathcal{B}(k^2)\mathcal{B}(q^2)}{\mathcal{A}(k^2)\mathcal{A}(q^2)}) \\
& +\tau_8\cdot 4k^2(k^2-q^2)\sin^2\psi\Big\}\,. \qquad (2.40)
\end{aligned}$$

2.2 Multiplicative Renormalisability

In the previous section, we satisfied two key constraints of the vertex through the Ward-Green-Takahashi identity and its differential counterpart, the Ward identity. This allowed us to write an explicit non-perturbative form for the longitudinal part of the basis. Perturbative investigations of the structure of the vertex gave rise to a general basis decomposition for the transverse part that was also free of kinematic singularities. In order to constrain the as yet unknown transverse part, we turn our attention to a further constraint on the vertex: *multiplicative renormalisability.*

When one performs calculations in quantum field theory we are confronted with integrals that are divergent. If we think of our QFT as an effective theory, this breakdown at high energies is attributed to our poor understanding of physics at these scales. However, any satisfactory field theory must be able to make predictions independently of this unknown high energy (or short distance) behaviour. This is accomplished by the theory being renormalisable.

The usual procedure of regulating the divergences such that the expressions become mathematically meaningful is to employ dimensional regularisation. Instead of working in, say, four dimensions, we shift to $d = 4 + \varepsilon$ dimensions for some small parameter ε. The UV (and IR) divergences are identified in this formalism as poles in ε, which we remove through a renormalisation prescription. This procedure, however, is difficult to implement numerically [37, 38], and moreover breaks chiral symmetry for all values of α. In these studies we resort to a more crude cut-off κ in the ultraviolet, whose breaking of translational invariance we have already touched upon. As a result of the regulating procedure, our Green's functions are dependent upon the regularisation parameter, κ. The process of renormalisation should remove the dependence of our theory on this cut-off, trading it in favour of another scale μ at which we may define our physical constants.

The renormalisation procedure is achieved by introducing a finite number of multiplicative factors, $Z_i(\mu, \kappa)$, for each Green's function. Following the prescription for QCD, Eqs (1.85–1.88), we have for the fermion-boson vertex of QED:

$$\Gamma^{\mu}_{R}(k, p; \mu) = Z_1(\mu, \kappa)\Gamma^{\mu}(k, p; \kappa) \,, \tag{2.41}$$

whilst for the fermion and boson propagators:

$$S^{R}_{F}(p; \mu) = Z_2^{-1}(\mu, \kappa)S_F(p; \kappa) \,, \tag{2.42}$$

$$D^{R}_{\mu\nu}(q; \mu) = Z_3^{-1}(\mu, \kappa)D_{\mu\nu}(q; \kappa) \,. \tag{2.43}$$

From these we can define a renormalised coupling, related to the bare one that appears in the Lagrangian:

$$\alpha_R(\mu) = \left(\frac{Z_2(\mu,\kappa)}{Z_1(\mu,\kappa)}\right)^2 Z_3(\mu,\kappa)\,\alpha(\kappa)\;, \tag{2.44}$$

with $\alpha = e^2/4\pi$. We also renormalise the gauge parameter via $\xi = Z_\xi \xi_R$, which from the invariant $\alpha\xi$ implies $Z_\xi = Z_3$. In terms of the photon wave-function renormalisation, $\mathcal{G}$, the running coupling is defined as:

$$\alpha_R(p^2) = \alpha(\mu)\mathcal{G}(p^2,\mu)\;. \tag{2.45}$$

From now on we drop R from subscripts and superscripts as it will be obvious from the context whether or not we are working with renormalised quantities.

At this stage we find relations between the renormalisation constants Z_i of QED by looking at the Ward-Green-Takahashi identity of Eq. (2.1), which holds for both bare and renormalised quantities. This implies:

$$Z_1^{-1}(\mu,\kappa) q_\mu \Gamma^\mu(k,p,\mu) = Z_2^{-1}(\mu,\kappa)\left(S_F^{-1}(k,\mu) - S_F^{-1}(p,\mu)\right)\;, \tag{2.46}$$

which can only be satisfied if we make the identification:

$$Z_1(\mu,\kappa) = Z_2(\mu,\kappa)\;. \tag{2.47}$$

This simplifies Eq. (2.44) to $\alpha_R(\mu) = Z_3(\mu,\kappa)\,\alpha(\kappa)$. We now have all the necessary tools at hand to renormalise the Schwinger-Dyson equations of QED.

Introducing the appropriate renormalisation constants, the fermion SDE is written:

$$S_F^{-1}(p;\mu) = Z_2(\mu,\kappa)\left(\left[S_F^{(0)}(p)\right]^{-1} - \bar{\Sigma}(p;\mu)\right)\;, \tag{2.48}$$

with $\bar{\Sigma}$ representing the integral of Eq. (2.24). This may be projected out in terms of its scalar functions $\mathcal{A}$ and $\mathcal{B}$:

$$\begin{aligned} \mathcal{A}(p;\mu) &= Z_2(\mu,\kappa)(1 - \bar{\Sigma}_d(p;\mu))\;, \\ \mathcal{B}(p;\mu) &= Z_2(\mu,\kappa)\left(Z_m(\mu,\kappa) m_R(\mu) + \bar{\Sigma}_s(p^2;\mu)\right)\;. \end{aligned} \tag{2.49}$$

Here, the bare mass is related to the renormalised mass by $m_0 = Z_m m_R$, with the additional definition $Z_4 = Z_2 Z_m$. Note that we have $\mathcal{M}(p) = \mathcal{B}(p;\mu)/\mathcal{A}(p;\mu)$ with

the mass-function $\mathcal{M}(p)$ independent of the renormalisation point, as seen from Eq. (2.48):

$$\mathcal{A}(p;\mu)\Big(\not{p} - \mathcal{M}(p;\mu)\Big) = Z_2\mathcal{A}(p;\kappa)\Big(\not{p} - \mathcal{M}(p;\kappa)\Big) \ . \tag{2.50}$$

We eliminate the renormalisation constant $Z_2(\mu,\kappa)$ by setting $\mathcal{A}(p;\mu)$ equal to some number at renormalisation point $p=\mu$. This will give:

$$\mathcal{A}(p;\mu) = Z_2(\mu,\kappa)\left(1 - \bar{\Sigma}_d(p;\mu)\right) \ , \tag{2.51}$$

with

$$Z_2(\mu,\kappa) = \frac{\mathcal{A}(\mu;\mu)}{1-\bar{\Sigma}_d(\mu;\mu)} \ , \tag{2.52}$$

and a common choice being $\mathcal{A}(\mu;\mu)=1$. If we have no mass in the Lagrangian, i.e. $m_0 = m_R = 0$, the renormalised equation for $\mathcal{B}$ is:

$$\mathcal{M}(p)\mathcal{A}(p;\mu) = Z_2(\mu,\kappa)\ \bar{\Sigma}_s(p;\mu) \ , \tag{2.53}$$

with Z_2 given by Eq. (2.52). When an explicit mass term is present, we must undertake an additional subtraction. Defining $\mathcal{M}(\mu) = m_R$, through $\mathcal{B}(p;\mu)/\mathcal{A}(p;\mu) = \mathcal{M}(p)$ at $p=\mu$ we find:

$$\mathcal{M}(p)\mathcal{A}(p;\mu) = M(\mu)\mathcal{A}(\mu;\mu) + Z_2(\mu,\kappa)\left(\bar{\Sigma}_s(p;\mu) - \bar{\Sigma}_s(\mu;\mu)\right) \ , \tag{2.54}$$

where again Z_2 is as Eq. (2.52), and Z_m can be determined by an appropriate rearrangement of Eq. (2.49) with renormalisation conditions at $p=\mu$.

Lastly, we must renormalise the photon SDE. Its projected form, in terms of photon scalar $\mathcal{G}(p;\mu)$ is given by:

$$\frac{1}{\mathcal{G}(q;\mu)} = Z_3(\mu,\kappa) + Z_2(\mu,\kappa)\bar{\Pi}(q;\mu) \ , \tag{2.55}$$

with the integral term represented by Π. The Z_2 is readily determined from the fermion SDE, and so we subtract this equation at $q=\mu$, specifying $\mathcal{G}(\mu;\mu)$:

$$\frac{1}{\mathcal{G}(p;\mu)} = \frac{1}{\mathcal{G}(\mu;\mu)} + Z_2(\mu,\kappa)\left(\bar{\Pi}(p;\mu) - \bar{\Pi}(\mu;\mu)\right) \ . \tag{2.56}$$

Typically we choose the condition $\mathcal{G}(\mu;\mu)=1$ for simplicity.

2.2.1 The Curtis–Pennington Vertex

The first attempt to restrict the transverse part of the vertex using multiplicative renormalisability was made by Curtis and Pennington [39]. Since multiplcative renormalisability is related to the ultraviolet divergences of loop-diagrams, we can concentrate on the form of the vertex $\Gamma^\mu(k,p)$ for momenta $|k| \gg |p|$.

Resorting to perturbation theory, and working in the quenched approximation, the fermion-boson vertex at one-loop in the leading logarithm approximation is given by:

$$\Gamma^\mu(k,p) = \gamma^\mu \left(1 - \frac{\alpha\xi}{4\pi} \log\frac{k^2}{\kappa^2}\right) - \frac{\alpha}{4\pi} \left(\not{p}\gamma^\mu \not{k} + (\xi - 1)\, k^\mu \not{p}\right) \frac{1}{k^2} \log\frac{k^2}{p^2} + \cdots . \quad (2.57)$$

In the same leading logarithm approximation to one-loop, the massless fermion propagator $\not{p}\mathcal{A}(p^2)$ is:

$$\mathcal{A}(p^2) = 1 + \frac{\alpha\xi}{4\pi} \log\frac{p^2}{\kappa^2} + \cdots . \quad (2.58)$$

Inserting this into the BC piece of Eq. (2.12), and subtracting from Eq. (2.57) we get the transverse part in the leading logarithm approximation:

$$\Gamma^\mu_T = \frac{\alpha\xi}{8\pi} \left(-\gamma^\mu - \frac{2k^\mu \not{p}}{k^2} + \frac{(k+p)^\mu (\not{k} + \not{p})}{k^2 - p^2}\right) \log\frac{k^2}{p^2} + \cdots . \quad (2.59)$$

Notice that the transverse part is subleading being as it is of $\mathcal{O}(\alpha)$. Taking the limit for $|k| \gg |p|$:

$$\Gamma^\mu_T \simeq -\frac{\alpha\xi}{8\pi} T_6^\mu \frac{1}{k^2} \log\frac{k^2}{p^2} , \quad (2.60)$$

and using Eq. (2.58) to eliminate α gives the following form of the transverse part of the vertex in the limit of large k:

$$\Gamma^\mu_T(k,p;q) = \frac{1}{2} \left(\mathcal{A}(k^2) - \mathcal{A}(p^2)\right) \frac{T_6^\mu}{k^2} . \quad (2.61)$$

This is in the limit $k^2 \gg p^2$, so Curtis and Pennington chose to write this in a way that is symmetric in k and p by replacing the k^2 in the denominator by a symmetric function $d(k,p)$ free of singularities:

$$\Gamma^\mu_T(k,p;q) = \frac{1}{2} \left(\mathcal{A}(k^2) - \mathcal{A}(p^2)\right) \frac{T_6^\mu}{d(k,p)} . \quad (2.62)$$

Massive fermions were then considered. It was found that no further transverse basis vectors were required to maintain multiplicative renormalisability. The coefficient

τ_6 required regulating, and so they proposed that:

$$d(k,p) = \frac{\left(k^2-p^2\right)^2 + \left(M^2(k^2)+M^2(p^2)\right)^2}{k^2+p^2}\,, \tag{2.63}$$

was a suitable choice for the unknown symmetric function $d(k,p)$. This gives the Curtis–Pennington ansatz:

$$\Gamma^\mu_{CP}(k,p;q) = \Gamma^\mu_{BC}(k,p;q) + \tau_6(k,p;q)\underbrace{\left(\gamma^\mu\left(k^2-p^2\right) - (k+p)^\mu \not{q}\right)}_{T^\mu_6(k,p)}\,, \tag{2.64}$$

with

$$\tau_6(k,p;q) = \frac{1}{2}\left(\frac{\mathcal{A}(k^2)-\mathcal{A}(p^2)}{k^2-p^2}\right)\frac{\left(k^2+p^2\right)\left(k^2-p^2\right)}{\left(k^2-p^2\right)^2+\left(\mathcal{M}^2(k^2)+\mathcal{M}^2(p^2)\right)^2}\,. \tag{2.65}$$

2.2.2 MR and Vertex Ansätze

The provision of a vertex ansatz is not the only method in which we may truncate the Schwinger-Dyson equations. The procedure most often employed is that of perturbation theory, and so the SDEs simply generate all of the one-particle irreducible diagrams corresponding to a particular Green's function.

If we expand our fermion wave-function renormalisation as a series of logs, with κ the ultraviolet cutoff, we obtain:

$$\begin{aligned}\mathcal{F}(p^2,\kappa^2) = 1 \;&+\; \alpha\left(A_{1,1}\ln\frac{p^2}{\kappa^2} + A_{1,0}\right) + \alpha^2\left(A_{2,2}\ln^2\frac{p^2}{\kappa^2} + A_{2,1}\ln\frac{p^2}{\kappa^2}\right)\\ &+\; \alpha^3\left(A_{3,3}\ln^3\frac{p^2}{\kappa^2} + A_{3,2}\ln^2\frac{p^2}{\kappa^2}\right) + \cdots\,.\end{aligned} \tag{2.66}$$

The coefficients of these leading order and next-to-leading order logarithms are not independent. The $A_{i,j}$ are related through:

$$\begin{aligned} A_{n,n} &= A^n_{1,1}/n!\,,\\ A_{n,n-1} &= A_{n-2,n-2}A_{2,1} - A_{n-1,n-1}A_{1,0}\,.\end{aligned} \tag{2.67}$$

If we consider the bare-vertex approximation in the quenched massless case we have:

$$\frac{1}{\mathcal{F}(p^2)} = 1 + \frac{\alpha\xi}{4\pi p^2}\left[\int_0^{p^2} dk^2\mathcal{F}(k^2)\frac{k^2}{p^2} + \int_{p^2}^{\kappa^2} dk^2\mathcal{F}(k^2)\frac{p^2}{k^2}\right]\,. \tag{2.68}$$

This can be solved iteratively for $\mathcal{F}(p^2)$, starting with $\mathcal{F}(p^2) = 1$. Expanding in powers of α and displaying only the leading order terms we have:

$$\mathcal{F}\left(p^2,\kappa^2\right) = 1 + \frac{\alpha\xi}{4\pi}\ln\frac{p^2}{\kappa^2} + \frac{3}{2}\left(\frac{\alpha\xi}{4\pi}\right)^2\ln^2\frac{p^2}{\kappa^2} + \frac{5}{2}\left(\frac{\alpha\xi}{4\pi}\right)^3\ln^3\frac{p^2}{\kappa^2} + \mathcal{O}(\alpha^4)\,. \quad (2.69)$$

Looking at the coefficients, we find:

$$A_{1,1} = \frac{\alpha\xi}{4\pi} \quad , \quad A_{2,2} = \frac{3}{2}A_{1,1}^2 \quad , \quad A_{3,3} = \frac{5}{2}A_{1,1}^3\,. \quad (2.70)$$

Clearly, the $A_{n,n}$ do not obey the relation of Eq. (2.67) for arbitrary covariant gauge ξ. Indeed, with this vertex the Ward-Green-Takahashi identity is violated for $\xi \neq 0$.

We see that the bare vertex is insufficient to ensure that multiplicative renormalisability be preserved. Can this situation be changed by preserving the WGTI in the vertex ansatz? If we look at the Ball–Chiu vertex in the quenched massless case, and integrate over the angular measure using Eq. B.9 of Appendix B.2, we have:

$$\begin{aligned}\frac{1}{\mathcal{F}(p^2)} &= 1 - \frac{\alpha}{2\pi p^2} \\ &\times \left\{\int_0^{p^2} dk^2\mathcal{F}(k^2)\left[-\xi\lambda_1\frac{k^2}{2p^2} + \lambda_2\frac{k^2}{p^2}\left(\frac{3}{4}\left(k^2+p^2\right) - \xi\left(k^2-p^2\right)\right)\right]\right. \\ &\left. + \int_{p^2}^{\kappa^2} dk^2\mathcal{F}(k^2)\left[-\xi\lambda_1\frac{p^2}{2k^2} + \lambda_2\frac{p^2}{k^2}\left(\frac{3}{4}\left(k^2+p^2\right) + \xi\left(k^2-p^2\right)\right)\right]\right\}.\end{aligned} \quad (2.71)$$

We once again solve for this iteratively with starting condition $\mathcal{F}(p^2) = 1$, and perform a perturbative expansion in α at each step. We need only consider the upper part of the integral, $\int_{p^2}^{\kappa^2}$, for the leading pieces to be apparent, obtaining:

$$\begin{aligned}\mathcal{F}\left(p^2,\kappa^2\right) &= 1 + \left(\frac{\alpha\xi}{4\pi}\right)\left(\frac{\xi^2}{8} - \frac{3\xi}{8}\right)\ln\frac{p^2}{\kappa^2} + \left(\frac{\alpha\xi}{4\pi}\right)^2\ln^2\frac{p^2}{\kappa^2} \\ &+ \left(\frac{\alpha\xi}{4\pi}\right)^3\left(\frac{\xi^3}{6} - \frac{3\xi^2}{8} + \frac{3\xi}{16}\right)\ln^3\frac{p^2}{\kappa^2} + \mathcal{O}(\alpha^4)\,.\end{aligned} \quad (2.72)$$

The fully specified longitudinal piece is again not sufficient to satisfy the requirements of multiplicative renormalisability. Thus the inclusion of the transverse piece is essential, and so we look at the Curtis–Pennington vertex in the same approxi-

mation scheme:

$$\frac{1}{\mathcal{F}(p^2)} = 1 - \frac{\alpha\xi}{4\pi p^2}\left\{\int_0^{p^2} dk^2 \left(3 - \frac{\mathcal{F}(k^2)}{\mathcal{F}(p^2)}\right)\frac{k^2}{p^2} - \int_{p^2}^{\kappa^2} dk^2 \left(1 - \frac{\mathcal{F}(k^2)}{\mathcal{F}(p^2)}\right)\frac{p^2}{k^2}\right\}. \tag{2.73}$$

This can be solved via the same iterative procedure employed for the bare vertex and Ball–Chiu vertex, yielding the series:

$$\mathcal{F}(p^2) = 1 + \frac{\alpha\xi}{4\pi}\ln\frac{p^2}{\kappa^2} + \frac{1}{2!}\left(\frac{\alpha\xi}{4\pi}\right)^2 \ln^2\frac{p^2}{\kappa^2} + \frac{1}{3!}\left(\frac{\alpha\xi}{4\pi}\right)^3 \ln^3\frac{p^2}{\kappa^2} + \mathcal{O}(\alpha^4)\,. \tag{2.74}$$

We now see that the relation of Eq. (2.67) is upheld and multiplicative renormalisability preserved for the quenched massless case.

Curtis and Pennington [39] performed a similar leading log expansion for the mass function using:

$$\mathcal{M}(p^2) = m_0\left(1 + \alpha\left(C_{1,1}\ln\frac{p^2}{\kappa^2} + C_{1,0}\right) + \alpha^2\left(C_{2,2}\ln^2\frac{p^2}{\kappa^2} + C_{2,1}\ln\frac{p^2}{\kappa^2}\right) + \alpha^3\left(C_{3,3}\ln^3\frac{p^2}{\kappa^2} + C_{3,2}\ln^2\frac{p^2}{\kappa^2}\right) + \cdots\right). \tag{2.75}$$

Their generalisation of the massless CP ansatz to include a mass, Eq. (2.65), turns out to satisfy the same requirements of multiplicative renormalisability for leading and next-to-leading logarithms. The $C_{n,n}$ obey the same relations as the $A_{n,n}$ of Eq. (2.67). We will give numerical solutions to these ansätze in the forthcoming sections.

2.2.3 The Kızılersü–Pennington Vertex

Although the Curtis–Pennington construction is successful in ensuring multiplicative renormalisability in quenched QED for the $\mathcal{F}$ and $\mathcal{M}$ functions, and as a result has improved the situation regarding gauge invariance, it has had limited success in the realms of the fully unquenched theory. The introduction of this ansatz into the transverse part of the vertex in the photon equation leads to unresolvable quadratic divergences, although one may make some modifications to avoid this. This does not lead us to a vertex ansatz that preserves multiplicative renormalisability in the photon equation because of the different momentum regions probed by the two Schwinger-Dyson equations; the vertex is found in the limit $k \gg p$ for the fermion

equation, but in the photon propagator we must consider $k \sim p \gg q$.

The most recent innovation in the construction of vertex ansätze is that due to Kızılersü and Pennington [40]. They attempt to construct a vertex that satisfies the notion of multiplicative renormalisability for unquenched QED. This they achieve by considering a selection of forms for the transverse coefficients τ_2, τ_3, τ_6 and τ_8, embodying the appropriate charge conjugation symmetries. This was first attempted by considering effective τ_i's independent of the momenta q^2, and choosing those that led to analytically solvable integrals [41]. From this analysis, it was hinted that to achieve the correct resummation of logarithmic pieces, they needed to include logarithms of $\mathcal{F}$. Since this component is fixed in very particular limits, the generalisation of this piece does contain some ambiguity. The form we present below is therefore not unique. As with the Curtis–Pennington vertex, the longitudinal part of the vertex is specified by Ball and Chiu, Eq. (2.12):

$$\begin{aligned}
\lambda_1(k,p) &= \frac{1}{2}\left(\mathcal{A}(k^2)+\mathcal{A}(p^2)\right) , \\
\lambda_2(k,p) &= \frac{1}{2}\frac{1}{k^2-p^2}\left(\mathcal{A}(k^2)-\mathcal{A}(p^2)\right) , \\
\lambda_3(k,p) &= -\frac{1}{k^2-p^2}\left(\mathcal{B}(k^2)-\mathcal{A}(B^2)\right) ,
\end{aligned}$$

with Kızılersü and Pennington [40] proposing the following form for the transverse part:

$$\begin{aligned}
\tau_2\left(p,k,q\right) &= -\frac{4}{3}\frac{2}{\left(k^2+p^2\right)}\lambda_2\left(k,p\right) - \frac{1}{3}\frac{2}{\left(k^2+p^2\right)^2}\lambda_1\left(k,p\right)\log\left(\frac{\mathcal{A}(k^2)\mathcal{A}(p^2)}{\mathcal{A}^2(q^2)}\right) , \\
\tau_3\left(p,k,q\right) &= -\frac{5}{12}2\,\lambda_2\left(k,p\right) - \frac{1}{6}\frac{2}{\left(k^2+p^2\right)}\lambda_1\left(k,p\right)\log\left(\frac{\mathcal{A}(k^2)\mathcal{A}(p^2)}{\mathcal{A}^2(q^2)}\right) , \\
\tau_6\left(p,k,q\right) &= \frac{1}{4}\frac{\left(k^2-p^2\right)}{\left(k^2+p^2\right)}2\,\lambda_2\left(k,p\right) , \\
\tau_8\left(p,k,q\right) &= 0 .
\end{aligned} \tag{2.76}$$

The full set of transverse vectors are of course required when we have a dynamically generated mass. We know, however, that the transverse part of the vertex is suppressed by one power of α in perturbation theory, compared to the longitudinal part, and that the mass-function in the chiral limit is renormalisation point independent. These tell us that the contribution from the mass-function – specifically that with regards to the consistent renormalisation of the SDEs – is sub-leading to that of the fermion and photon wave-function renormalisations. It thus seems to be a good first approximation to neglect those τ_i proportional to the bare mass in perturbation

theory.

To demonstrate the efficacy of this ansatz, we first introduce it into the massless Schwinger-Dyson equations for the fermion and photon propagators. We then examine the solutions in a perturbative expansion of α in the limit of vanishing photon momenta. This will be sufficient to show that the leading logarithms are correctly summed to all orders. A more detailed analysis is needed to demonstrate the same process for sub-leading logarithms. To show how these transverse pieces combine together to satisfy multiplicative renormalisability, we replace the numerical coefficients 4/3, 1/3, 5/12, 1/6 and 1/4 by c_i for $i = 1..5$.

We work directly with the wave-function renormalisation of the fermion propagator, $\mathcal{F}$, and the photon renormalisation function $\mathcal{G}$. In terms of an expansion in leading and sub-leading logarithms these are:

$$\begin{aligned}\mathcal{F}(p^2) = 1 \;&+\; \alpha\left(A_{1,1}\ln\frac{p^2}{\kappa^2} + A_{1,0}\right) + \alpha^2\left(A_{2,2}\ln^2\frac{p^2}{\kappa^2} + A_{2,1}\ln\frac{p^2}{\kappa^2}\right) \\ &+\; \alpha^3\left(A_{3,3}\ln^3\frac{p^2}{\kappa^2} + A_{3,2}\ln^2\frac{p^2}{\kappa^2}\right) + \cdots ,\end{aligned} \tag{2.77}$$

and

$$\begin{aligned}\mathcal{G}(p^2) = 1 \;&+\; \alpha\left(B_{1,1}\ln\frac{p^2}{\kappa^2} + B_{1,0}\right) + \alpha^2\left(B_{2,2}\ln^2\frac{p^2}{\kappa^2} + B_{2,1}\ln\frac{p^2}{\kappa^2}\right) \\ &+\; \alpha^3\left(B_{3,3}\ln^3\frac{p^2}{\kappa^2} + B_{3,2}\ln^2\frac{p^2}{\kappa^2}\right) + \cdots .\end{aligned} \tag{2.78}$$

The idea is to substitute this into the SDE, with ansätze for the τ_i that permit the integrals to be performed analytically. The resulting solution must exhibit the correct relationship between the coefficients $A_{i,j}$ and $B_{i,j}$ in the leading-log expansion.

Fermion Propagator

We first start with Eq. (2.29) with the mass set to zero, and insert the Kızılersü–Pennington vertex:

$$\begin{aligned}
\frac{1}{\mathcal{F}(p^2)} = 1 \;+\; & \frac{\alpha}{2\pi^2 p^2}\int dk^2 \mathcal{F}(k^2)\int d\psi \frac{\sin^2\psi}{q^2}\mathcal{G}(q^2) \\
\times\; & \left\{ \frac{1}{2}\left(\frac{1}{\mathcal{F}(k^2)}+\frac{1}{\mathcal{F}(p^2)}\right)\left[3k\cdot p + 2\frac{\Delta^2}{q^2}\right] \right. \\
& + \frac{1}{2}\left(\frac{1}{\mathcal{F}(k^2)}-\frac{1}{\mathcal{F}(p^2)}\right)\frac{1}{k^2-p^2}\frac{2\left(k^2+p^2\right)}{q^2}\Delta^2 \\
& + \left(k^2+p^2\right)\Delta^2\left[-c_1 \frac{1}{k^2+p^2}\frac{1}{k^2-p^2}\left(\frac{1}{\mathcal{F}(k^2)}-\frac{1}{\mathcal{F}(p^2)}\right)\right. \\
& \qquad \left. -c_2\frac{1}{\left(k^2+p^2\right)^2}\left(\frac{1}{\mathcal{F}(k^2)}+\frac{1}{\mathcal{F}(p^2)}\right)\ln\left(\frac{\mathcal{F}^2(q^2)}{\mathcal{F}(k^2)\mathcal{F}(p^2)}\right)\right] \\
& - \left(3k\cdot p\, q^2 + 2\Delta^2\right)\left[-c_3\frac{1}{k^2-p^2}\left(\frac{1}{\mathcal{F}(k^2)}-\frac{1}{\mathcal{F}(p^2)}\right)\right. \\
& \qquad \left. -c_4\frac{1}{k^2+p^2}\left(\frac{1}{\mathcal{F}(k^2)}+\frac{1}{\mathcal{F}(p^2)}\right)\ln\left(\frac{\mathcal{F}^2(q^2)}{\mathcal{F}(k^2)\mathcal{F}(p^2)}\right)\right] \\
& \left. + 3k\cdot p\left(k^2-p^2\right)\left[c_5\frac{1}{k^2+p^2}\left(\frac{1}{\mathcal{F}(k^2)}-\frac{1}{\mathcal{F}(p^2)}\right)\right]\right\} \\
& + \frac{\alpha\xi}{2\pi^2 p^2\mathcal{F}(p^2)}\int dk^2\mathcal{F}(k^2)\int d\psi\frac{\sin^2\psi}{q^2}\frac{p^2}{q^2}\left(k^2-k\cdot p\right) . \qquad (2.79)
\end{aligned}$$

To tackle this equation in one go would be unpresentable, so we break it down into its basis components and deal with each separately.

In order to considerably simplify the calculation and yet still obtain the leading log behaviour, we will work under two approximations. The first is to expand in powers of the coupling α, considered here to be a small parameter. The second approximation is to work in the limit of vanishing photon momentum, that is $k \to p$. This final step considerably reduces the work involved in calculating the angular integrals, at the cost of rendering the sub-leading logarithms inaccessible. Thus we

write the photon renormalisation as a Taylor series about $q^2 = k^2$:

$$\begin{aligned}\mathcal{G}(q^2) &= \mathcal{G}(k^2) + \left(p^2 - 2\,k\cdot p\right)\mathcal{G}'(k^2) + \frac{1}{2!}\left(p^2 - 2\,k\cdot p\right)^2\mathcal{G}''(k^2) + \cdots \\ &= \left(\mathcal{G}(k^2) + p^2\mathcal{G}'(k^2) + \mathcal{O}(p^4)\right) \\ &\quad + \left(-2\mathcal{G}'(k^2) - 4p^2\mathcal{G}''(k^2) + \mathcal{O}(p^4)\right)(k\cdot p) \\ &\quad + \left(4\mathcal{G}''(k^2) + 12p^2\mathcal{G}'''(k^2) + \mathcal{O}(p^4)\right)(k\cdot p)^2 \\ &\quad + \mathcal{O}\left((k\cdot p)^3\right)\ . \end{aligned} \tag{2.80}$$

All of the necessary angular integrals are given in Appendix B.2.

The λ_1-piece

The first piece to evaluate is that associated with $\lambda_1(k,p)$ from Eq. (2.29). Employing Eqs. (2.77, 2.78), keeping only those terms to $\mathcal{O}(\alpha^3)$ we have:

$$\begin{aligned} L_1 &= \frac{\alpha}{2\pi^2 p^2}\int_{p^2}^{\kappa^2} dk^2 d\psi \frac{\sin^2\psi}{q^4}\mathcal{G}(q^2)\mathcal{F}(k^2)\lambda_1(k,p)\left[3\,k\cdot p\,q^2 + 2\Delta^2\right] \\ &= \frac{\alpha}{2\pi^2 p^2}\int_{p^2}^{\kappa^2} dk^2\mathcal{F}(k^2)\lambda_1(k,p)\Bigg[\\ &\qquad \left(\mathcal{G}(k^2) + p^2\mathcal{G}'(k^2)\right)\left(-2\,k^2p^2I_{0,2} + 3I_{1,1} + 2I_{2,2}\right) \\ &\qquad + \left(-2\mathcal{G}'(k^2) - 4p^2\mathcal{G}''(k^2)\right)\left(-2\,k^2p^2I_{1,2} + 3I_{2,1} + 2I_{3,2}\right) + \cdots\Bigg]\ , \end{aligned} \tag{2.81}$$

with the $I_{k,m}$ defined in the Appendix. For the angular integrals we are interested in the region $k^2 > p^2$ to $\mathcal{O}(p^2)$:

$$L_1 = \frac{\alpha}{2\pi^2 p^2}\int_{p^2}^{\kappa^2} dk^2\mathcal{F}(k^2)\lambda_1(k,p)\left[-\frac{3\pi}{4}p^2\mathcal{G}'(k^2)\right]\ . \tag{2.82}$$

Expanding the product $\mathcal{F}(k^2)\lambda_1(k,p)$ in logarithms, together with $\mathcal{G}'(k^2)$ we can easily perform the radial integral:

$$L_1 = \frac{3}{8\pi}\left[\alpha^2\left(B_{1,1}\right)\ln\frac{p^2}{\kappa^2} + \alpha^3\left(B_{2,2} - \frac{1}{4}A_{1,1}B_{1,1}\right)\ln^2\frac{p^2}{\kappa^2}\right]\ . \tag{2.83}$$

The λ_2-piece

The coefficient of this piece does not have any additional angular dependence, simplifying the calculation. Thus:

$$\begin{aligned} L_2 &= \frac{\alpha}{2\pi^2 p^2}\int_{p^2}^{\kappa^2} dk^2 d\psi \frac{\sin^2\psi}{q^4}\mathcal{G}(q^2)\mathcal{F}(k^2)\left(k^2-p^2\right)\lambda_2\left(k,p\right)\left[\frac{2}{q^2}\frac{(k^2+p^2)}{(k^2-p^2)}\Delta^2\right] \\ &= \frac{\alpha}{2\pi^2 p^2}\int_{p^2}^{\kappa^2} dk^2 \mathcal{F}(k^2)\left(k^2-p^2\right)\lambda_2\left(k,p\right) \\ &\qquad \times\Bigg[\left(\mathcal{G}(k^2)+p^2\mathcal{G}'(k^2)\right)\left(-k^2p^2I_{0,2}+I_{2,2}\right) \\ &\qquad\quad +\left(-2\mathcal{G}'(k^2)-4p^2\mathcal{G}''(k^2)\right)\left(-k^2p^2I_{1,2}+I_{3,2}\right)+\cdots\Bigg]. \end{aligned} \tag{2.84}$$

Performing the angular integrals to $\mathcal{O}(p^2)$ for the appropriate region gives:

$$L_2 = \frac{\alpha}{2\pi^2 p^2}\int_{p^2}^{\kappa^2} dk^2\mathcal{F}(k^2)\lambda_2(k,p)\left(k^2-p^2\right)\left[-\frac{3\pi}{4}\frac{p^2}{k^2}\mathcal{G}(k^2)\right]. \tag{2.85}$$

We expand the remaining functions in terms of logarithms and perform the radial integral:

$$L_2 = \frac{3}{8\pi}\left[\alpha^2\left(\frac{1}{4}A_{1,1}\right)\ln^2\frac{p^2}{\kappa^2}+\alpha^3\left(-\frac{1}{4}A_{1,1}^2+\frac{1}{3}A_{2,2}+\frac{1}{12}A_{1,1}B_{1,1}\right)\ln^3\frac{p^2}{\kappa^2}\right]. \tag{2.86}$$

The τ_2-piece

The τ_2 piece brings an added complication due to the angular dependence on the photon momentum q^2. We need to evaluate the expression:

$$\begin{aligned} T_2 &= \frac{\alpha}{2\pi^2 p^2}\int dk^2\mathcal{F}(k^2)\int d\psi\frac{\sin^2\psi}{q^2}\mathcal{G}(q^2)\left((k\cdot p)^2-k^2p^2\right) \\ &\qquad \times\left[-c_1 2\lambda_2(k,p)-c_2\frac{1}{(k^2+p^2)}2\lambda_1(k,p)\ln\left(\frac{\mathcal{F}^2(q^2)}{\mathcal{F}(k^2)\mathcal{F}(p^2)}\right)\right]. \end{aligned} \tag{2.87}$$

We thus expand the q^2-dependent part in powers of alpha:

$$\begin{aligned}\ln\left(\frac{\mathcal{F}^2(q^2)}{\mathcal{F}(k^2)\mathcal{F}(p^2)}\right) &= -A_{1,1}\left(\ln\frac{p^2}{\kappa^2}+\ln\frac{k^2}{\kappa^2}-2\ln\frac{q^2}{\kappa^2}\right)\alpha \\ &+ \frac{1}{2}\left(A_{1,1}^2-2A_{2,2}\right)\left(\ln^2\frac{p^2}{\kappa^2}+\ln^2\frac{k^2}{\kappa^2}-2\ln^2\frac{q^2}{\kappa^2}\right)\alpha^2 \\ &+ \mathcal{O}\left(\alpha^3\right), \end{aligned} \tag{2.88}$$

followed by an expansion about $q^2 \to 0$ using the substitution:

$$\ln\frac{q^2}{\kappa^2} \to \ln\frac{k^2}{\kappa^2}+\left(p^2-2k\cdot p\right)\frac{1}{k^2}+\left(p^2-2k\cdot p\right)^2\frac{1}{2\left(k^2\right)^2}+\cdots . \tag{2.89}$$

This yields:

$$\begin{aligned} T_2 &= \frac{\alpha}{2\pi^2p^2}\int dk^2\mathcal{F}(k^2) \\ &\times\Bigg\{-c_1\,2\lambda_2(k,p)\Bigg[\left(\mathcal{G}(k^2)+p^2\mathcal{G}'(k^2)\right)\left(I_{2,1}-k^2p^2I_{0,1}\right)+\cdots\Bigg] \\ &-c_2\,2\lambda_1(k,p)\frac{1}{(k^2+p^2)}\Bigg[\left(\mathcal{G}(k^2)+p^2\mathcal{G}'(k^2)\right)\Bigg\{ \\ &\alpha A_{1,1}\left[\ln\frac{k^2}{p^2}\left(I_{2,1}-k^2p^2I_{0,1}\right)-\frac{4}{k^2}\left(I_{3,1}-k^2p^2I_{1,1}\right)\right] \\ &+\alpha^2\frac{1}{2}\left(A_{1,1}^2-2A_{2,2}\right)\Bigg[\ln^2\frac{k^2}{p^2}\left(k^2p^2I_{0,1}-I_{2,1}\right) \\ &\qquad+\frac{8}{k^2}\ln\frac{k^2}{\kappa^2}\left(I_{3,1}-k^2p^2I_{1,1}\right) \\ &\qquad+\frac{8}{k^4}\left(\ln\frac{k^2}{\kappa^2}-1\right)\left(I_{4,1}-k^2p^2I_{2,1}\right)\Bigg]+\cdots\Bigg\}\Bigg]\Bigg\}. \end{aligned} \tag{2.90}$$

The angular integrals are substituted in, keeping only terms to order p^2. The radial integrals are then trivially performed, giving:

$$\begin{aligned} T_2 &= \frac{3}{8\pi}\Bigg[-\frac{\alpha^2}{4}A_{1,1}\left(c_1-2c_2\right)\ln^2\frac{p^2}{\kappa^2} \\ &\quad+\frac{\alpha^3}{12}\left(3A_{1,1}^2-B_{1,1}A_{1,1}-4A_{2,2}\right)\left(c_1-2c_2\right)\ln^3\frac{p^2}{\kappa^2}+\cdots\Bigg]. \end{aligned} \tag{2.91}$$

The τ_3-piece

Like the τ_2 coefficient, this piece has a dependence upon the photon momentum q^2:

$$T_3 = \frac{\alpha}{2\pi^2 p^2}\int dk^2 \mathcal{F}(k^2)\int d\psi \frac{\sin^2\psi}{q^2}\mathcal{G}(q^2)\left(3k\cdot p\, q^2 + 2\Delta^2\right) \times\left[c_3 2\lambda_2(k,p) + c_4\frac{1}{(k^2+p^2)}2\lambda_1(k,p)\ln\left(\frac{\mathcal{F}^2(q^2)}{\mathcal{F}(k^2)\mathcal{F}(p^2)}\right)\right]. \tag{2.92}$$

The function $\mathcal{G}$ is expanded using Eq. (2.80), with the logarithmic piece replaced via Eqs. (2.88, 2.89).

$$\begin{aligned} T_3 = \frac{\alpha}{2\pi^2 p^2}\int dk^2\mathcal{F}(k^2) & \\ \times\Bigg\{ c_3\, 2\lambda_2(k,p)\Bigg[& \left(\mathcal{G}(k^2)+p^2\mathcal{G}'(k^2)\right)\left(3I_{1,0}+2I_{2,1}-2k^2p^2I_{0,1}\right) \\ & +\left(-2\mathcal{G}'(k^2)-4p^2\mathcal{G}''(k^2)\right)\left(3I_{2,0}+2I_{3,1}-2k^2p^2I_{1,1}\right)+\cdots\Bigg] \\ +c_4\, 2\lambda_1(k,p)\frac{1}{(k^2+p^2)}\Bigg[& \left(\mathcal{G}(k^2)+p^2\mathcal{G}'(k^2)\right)\Bigg\{ \\ & \alpha A_{1,1}\left[\ln\frac{k^2}{p^2}\left(3I_{1,0}+2I_{2,1}-2k^2p^2I_{0,1}\right)-\frac{4}{k^2}\left(3I_{2,0}+2I_{3,1}-2k^2p^2I_{1,1}\right)\right] \\ & +\alpha^2\frac{1}{2}\left(A_{1,1}^2-2A_{2,2}\right)\Bigg[-\ln^2\frac{k^2}{p^2}\left(3I_{1,0}+2I_{2,1}-2k^2p^2I_{0,1}\right) \\ & \quad +\frac{8}{k^2}\ln\frac{k^2}{\kappa^2}\left(3I_{2,0}+2I_{3,1}-2k^2p^2I_{1,1}\right)\Bigg\} \\ & +\left(-2\mathcal{G}'(k^2)-4p^2\mathcal{G}''(k^2)\right)\Bigg\{\alpha A_{1,1}\left[\ln\frac{k^2}{p^2}\left(3I_{2,0}+2I_{3,1}-2k^2p^2I_{1,1}\right)\right] \\ & +\alpha^2\frac{1}{2}\left(A_{1,1}^2-2A_{2,2}\right)\left[-\ln^2\frac{k^2}{p^2}\left(3I_{1,0}+2I_{2,1}-2k^2p^2I_{0,1}\right)\right]\Bigg\}\Bigg]\Bigg\}. \end{aligned} \tag{2.93}$$

We substitute in these angular integrals for $k^2 > p^2$ and employ the leading log expansion for $\mathcal{F}$ and $\mathcal{G}$. On performing the radial integrals we have:

$$\begin{aligned} T_3 = \frac{3}{8\pi}\Bigg[& \alpha^2\left(\frac{A_{1,1}}{2}\left(c_3-2c_4\right)\right)\ln^2\frac{p^2}{\kappa^2} \\ - & \alpha^3\left(3A_{1,1}^2-B_{1,1}A_{1,1}-4A_{2,2}\right)\left(c_3-2c_4\right)\ln^3\frac{p^2}{\kappa^2}+\cdots\Bigg]. \end{aligned} \tag{2.94}$$

The τ_6-piece

This coefficient function does not have any dependence upon the angle and is hence simple to compute. We are concerned with:

$$\begin{aligned} T_6 &= \frac{\alpha}{2\pi^2 p^2}\int dk^2\mathcal{F}(k^2)\int d\psi\frac{\sin^2\psi}{q^2}\mathcal{G}(q^2)\tau_6(k,p;q)\left[3\,k\cdot p\left(k^2-p^2\right)\right] \\ &= \frac{\alpha}{2\pi^2 p^2}\int_{p^2}^{\kappa^2} dk^2\mathcal{F}(k^2)\,c_5\,\frac{(k^2-p^2)}{(k^2+p^2)}2\,\lambda_2\,(k,p)\Bigg[\left(\mathcal{G}(k^2)+p^2\mathcal{G}'(k^2)\right)3\,I_{1,1} \\ &\qquad + \left(-2\mathcal{G}'(k^2)-4p^2\mathcal{G}''(k^2)\right)3\,I_{2,1} \\ &\qquad +\cdots\Bigg]\,. \end{aligned} \tag{2.95}$$

We perform the angular integrals to $\mathcal{O}(p^2)$ for the region $k^2 > p^2$gives:

$$T_6 = \frac{\alpha}{2\pi^2 p^2}\int_{p^2}^{\kappa^2} dk^2\mathcal{F}(k^2)c_5\,2\,\lambda_2(k,p)\frac{(k^2-p^2)}{(k^2+p^2)}\left[\frac{3\pi p^2}{4k^2}\mathcal{G}(k^2)-2\mathcal{G}'(k^2)\frac{3\pi p^2}{8}\right]\,. \tag{2.96}$$

Expanding the remaining functions in terms of leading logarithms and performing the radial integral we have:

$$\begin{aligned} T_6 &= \frac{3}{8\pi}c_5\Bigg[\alpha^2\left(-\frac{1}{2}A_{1,1}\right)\ln^2\frac{p^2}{\kappa^2}+\alpha^3\left(\frac{1}{2}A_{1,1}^2-\frac{1}{6}B_{1,1}A_{1,1}-\frac{2}{3}A_{2,2}\right)\ln^3\frac{p^2}{\kappa^2} \\ &\qquad +\cdots\Bigg]\,. \end{aligned} \tag{2.97}$$

The ξ-piece

The final piece to compute is the most trivial.

$$\begin{aligned} L_\xi &= \frac{\alpha\xi}{2\pi^2 p^2\mathcal{F}(p^2)}\int dk^2\mathcal{F}(k^2)\int d\psi\frac{\sin^2\psi}{q^2}\frac{p^2}{q^2}\left(k^2-k\cdot p\right) \\ &= \frac{\alpha\xi}{2\pi^2}\int dk^2\frac{\mathcal{F}(k^2)}{\mathcal{F}(p^2)}\left(k^2 I_{0,2}-I_{1,2}\right)\,. \end{aligned} \tag{2.98}$$

On expanding the fermion wavefunction renormalisation in leadings logs and integrating we find:

$$L_\xi = \frac{3}{8\pi}\left[-\frac{2}{3}\alpha\xi\ln\frac{p^2}{\kappa^2}+\frac{1}{3}A_{1,1}\alpha^2\xi\ln^2\frac{p^2}{\kappa^2}-\frac{1}{9}\left(3A_{1,1}^2-4A_{2,2}\right)\alpha^3\xi\ln^3\frac{p^2}{\kappa^2}\right]\,. \tag{2.99}$$

Combining Terms

Combining Eqs. (2.83, 2.86, 2.91, 2.94, 2.97, 2.99) and exploiting the relationship between the coefficients $A_{i,j}$ we have:

$$\begin{aligned}\frac{1}{\mathcal{F}(p^2)} &= 1+\frac{3}{8\pi}\Bigg[-\frac{2}{3}\alpha\xi\ln\frac{p^2}{\kappa^2} \\ &- \alpha^2\ln^2\frac{p^2}{\kappa^2}\frac{A_{1,1}}{12}\left(3c_1-6c_2-6c_3+12c_4+6c_5-4\xi-3\right) \\ &+ \alpha^3\ln^3\frac{p^2}{\kappa^2}\Bigg(\frac{1}{12}\left(A_{1,1}^2-B_{1,1}A_{1,1}\right)\left(c_1-2c_2-2c_3+4c_4+2c_5-1\right) \\ &\qquad -\frac{1}{9}A_{1,1}^2\xi\Bigg)\Bigg]+\cdots . \end{aligned} \tag{2.100}$$

The Kızılersü–Pennington vertex requires, via comparison with perturbation theory [40], that the coefficients c_i take the values:

$$c_1=\frac{4}{3}\,,\qquad c_2=\frac{1}{3}\,,\qquad c_3=\frac{5}{12}\,,\qquad c_4=\frac{1}{6}\,,\qquad c_5=\frac{1}{4}\,, \tag{2.101}$$

resulting in:

$$\frac{1}{\mathcal{F}(p^2)} = 1-\frac{\alpha\xi}{4\pi}\ln\frac{p^2}{\kappa^2}+\frac{\alpha^2\xi}{8\pi}A_{1,1}\ln^2\frac{p^2}{\kappa^2}-\frac{\alpha^3\xi}{24\pi}A_{1,1}^2\ln^3\frac{p^2}{\kappa^2}+\cdots . \tag{2.102}$$

Comparing this with the leading log expansion Eq. (2.77):

$$\frac{1}{\mathcal{F}(p^2)}=1-\alpha A_{1,1}\ln\frac{p^2}{\kappa^2}+\alpha^2\frac{A_{1,1}^2}{2!}\ln^2\frac{p^2}{\kappa^2}-\alpha^3\frac{A_{1,1}^3}{3!}\ln^3\frac{p^2}{\kappa^2}+\cdots\,, \tag{2.103}$$

and setting $A_{1,1}=\xi/4\pi$ we find agreement between Eq. (2.102) and Eq. (2.103). This demonstrates that the Kızılersü–Pennington ansatz satisfies multiplicative renormalisability in terms of leading logarithms in the SDE for the unquenched fermion propagator.

Photon Propagator

The investigation of leading logarithms in the photon propagator proceeds in a similar fashion to that of the fermion. We work in the massless limit with no dynamical symmetry breaking, and so are to consider the projected Schwinger-Dyson equation of Eq. (2.39) in four dimensions with symmetric momentum partition.

Inserting the Kızılersü–Pennington vertex here explicitly yields:

$$\begin{aligned}\frac{1}{\mathcal{G}(q^2)} = 1 \;-\; & \frac{\alpha N_f}{6\pi^2 q^2}\int dl^2 d\psi \frac{l^2\sin^2\psi}{(l^2+q^2/4)^2-(l\cdot q)^2} \\ \times\; & \left\{(\mathcal{F}_- + \mathcal{F}_+)\left(16\frac{(l\cdot q)^2}{q^2} - 4l^2 - 3q^2\right)\right. \\ & + \frac{\mathcal{F}_- - \mathcal{F}_+}{(l\cdot q)}\left(\left(16\frac{l^2}{q^2}-2\right)(l\cdot q)^2 - 4l^4 - l^2q^2\right) \\ & + 2\left((l\cdot q)^2 - l^2q^2\right)\left(4l^2+q^2\right)\left[-\frac{c_1}{4}\frac{1}{l^2+q^2/4}\frac{(\mathcal{F}_- - \mathcal{F}_+)}{(l\cdot q)}\right. \\ & \qquad \left.-\frac{c_2}{4}\frac{1}{(l^2+q^2/4)^2}(\mathcal{F}_- + \mathcal{F}_+)\ln\left(\frac{\mathcal{F}^2(q^2)}{\mathcal{F}_-\mathcal{F}_+}\right)\right] \\ & + \left(3q^4 - 8(l\cdot q)^2 - 4l^2q^2\right)\left[-\frac{c_3}{2}\frac{(\mathcal{F}_- - \mathcal{F}_+)}{(l\cdot q)}\right. \\ & \qquad \left.-\frac{c_4}{2}\frac{1}{l^2+q^2/4}(\mathcal{F}_- + \mathcal{F}_+)\ln\left(\frac{\mathcal{F}^2(q^2)}{\mathcal{F}_-\mathcal{F}_+}\right)\right] \\ & \left. + 6(l\cdot q)^2\left(4l^2-q^2\right)\left(\frac{c_5}{2}\frac{1}{l^2+q^2/4}\frac{(\mathcal{F}_- - \mathcal{F}_+)}{(l\cdot q)}\right)\right\}, \end{aligned} \tag{2.104}$$

where we have employed the shorthand $\mathcal{F}_\pm = \mathcal{F}(l_\pm)$, with $l_\pm^\mu = l^\mu \pm q^\mu/2$. It is apposite to expand these functions $\mathcal{F}(l_\pm)$ in the limit $q^2 \to 0$ using the Taylor expansion:

$$\begin{aligned}\mathcal{F}(l_+) &= F(l) + \left(l\cdot q - q^2/4\right)\mathcal{F}'(l) + \frac{1}{2}\left(l\cdot q - q^2/4\right)^2\mathcal{F}''(l) + \cdots, \\ \mathcal{F}(l_-) &= F(l) + \left(-l\cdot q - q^2/4\right)\mathcal{F}'(l) + \frac{1}{2}\left(-l\cdot q - q^2/4\right)^2\mathcal{F}''(l) + \cdots,\end{aligned} \tag{2.105}$$

which allows us to expand terms of the form:

$$\begin{aligned}\frac{\mathcal{F}_- - \mathcal{F}_+}{l\cdot q} &\simeq -2\mathcal{F}'(l) - \frac{q^2}{2}\mathcal{F}''(l) + \cdots, \\ \mathcal{F}_- + \mathcal{F}_+ &\simeq 2\mathcal{F}(l) + \frac{q^2}{2}\mathcal{F}'(l) + \left((l\cdot q)^2 + q^4/16\right)\mathcal{F}''(l) + \cdots.\end{aligned} \tag{2.106}$$

The expansion of Eq. (2.104) will be broken up into its component basis pieces and calculated individually in the following sections. The necessary angular pieces are given in Appendix B.2.

λ_1-piece

To begin the calculation we look at the leading piece in the UV; that belonging to the L_1 basis vector:

$$L_1 = -\frac{\alpha N_f}{6\pi^2 q^2}\int dl^2 d\psi \frac{l^2\sin^2\psi\left(\mathcal{F}_- + \mathcal{F}_+\right)}{\left(l^2+q^2/4\right)^2-(l\cdot q)^2}\left(16\frac{(l\cdot q)^2}{q^2}-4l^2-3q^2\right) . \quad (2.107)$$

Taylor expanding the functions for small q using Eq. (2.105) gives:

$$\begin{aligned} L_1 = & -\frac{\alpha N_f}{6\pi^2 q^2}\int dl^2 l^2 \Bigg\{ K_{0,1}\left[\left(-4l^2-3q^2\right)\left(2\mathcal{F}(l)+\frac{q^2}{2}\mathcal{F}'(l)+\cdots\right)\right] \\ & +K_{2,1}\left[\frac{16}{q^2}\left(2\mathcal{F}[l]+\frac{q^2}{2}F'(l)+\cdots\right)+\left(-4l^2-3q^2\right)\left(\mathcal{F}''(l)+\cdots\right)\right] \\ & +K_{4,1}\left[\frac{16}{q^2}\left(\mathcal{F}''(l)+\cdots\right)\right]\Bigg\} . \end{aligned} \quad (2.108)$$

For the angular integrals we are interested in the region $l^2 \gg q^2$ to $\mathcal{O}(q^2)$, and so find:

$$L_1 = -\frac{\alpha N_f}{12\pi}\int dl^2\left(-4\frac{\mathcal{F}(l)}{l^2}+\mathcal{F}''(l)l^2+\cdots\right) . \quad (2.109)$$

Finally, we substitute in the leading log expansion for $\mathcal{F}(l)$ via Eq. (2.66) and perform the radial integral:

$$\begin{aligned} L_1 = & -\frac{\alpha N_f}{12\pi}\Bigg[4\ln\frac{q^2}{\kappa^2}+\alpha A_{1,1}\left(2\ln^2\frac{q^2}{\kappa^2}+\ln\frac{q^2}{\kappa^2}\right) \\ & + \frac{1}{3}\alpha^2 A_{2,2}\left(4\ln^3\frac{q^2}{\kappa^2}+3\ln^2\frac{q^2}{\kappa^2}-6\ln\frac{q^2}{\kappa^2}\right)+\cdots\Bigg] . \end{aligned} \quad (2.110)$$

λ_2-piece

For this basis vector we wish to evaluate:

$$\begin{aligned} L_2 = & -\frac{\alpha N_f}{6\pi^2 q^2}\int dl^2 d\psi \frac{l^2\sin^2\psi}{\left(l^2+q^2/4\right)^2-(l\cdot q)^2} \\ & \times \Bigg\{\left(\left(16\frac{l^2}{q^2}-2\right)(l\cdot q)^2-4l^4-l^2q^2\right) \\ & \left(-2\mathcal{F}'(l)-\frac{q^2}{2}\mathcal{F}''(l)-\left(\frac{q^4}{16}+\frac{(l\cdot q)^2}{3}\right)\mathcal{F}'''(l)+\cdots\right)\Bigg\} , \end{aligned} \quad (2.111)$$

which on writing out the angular integrals symbolically becomes:

$$\begin{aligned} L_2 &= -\frac{\alpha N_f}{6\pi^2 q^2}\int dl^2 l^2 \Bigg\{ K_{0,1}\left[(-4l^4 - l^2q^2)\left(-2\mathcal{F}'(l) - \frac{q^2}{2}\mathcal{F}''(l) + \cdots\right)\right] \\ &\quad + K_{2,1}\Bigg[(-4l^4 - l^2q^2)\left(\frac{-\mathcal{F}'''(l)}{3} + \cdots\right) \\ &\qquad + \left(16\frac{l^2}{q^2} - 2\right)\left(-2\mathcal{F}'(l) - \frac{q^2}{2}\mathcal{F}''(l) + \cdots\right)\Bigg] \\ &\quad + K_{4,1}\left[\left(16\frac{l^2}{q^2} - 2\right)\left(-\frac{\mathcal{F}'''(l)}{3} + \cdots\right)\right] + \cdots \Bigg\} . \end{aligned} \tag{2.112}$$

Using the Appendix to evaluate this angular integrals explicitly to the required order gives:

$$L_2 = -\frac{\alpha N_f}{12\pi}\int dl^2 \left(\mathcal{F}'(l) - \frac{l^4}{3}\mathcal{F}'''(l)\right) , \tag{2.113}$$

which one may trivially integrate on inserting the logarithmic expansion of the remaining functions:

$$L_2 = -\frac{\alpha N_f}{12\pi}\left[-\frac{1}{3}\alpha A_{1,1}\ln\frac{q^2}{\kappa^2} - \frac{1}{3}\alpha^2 A_{2,2}\left(\ln^2\frac{q^2}{\kappa^2} + 6\ln\frac{q^2}{\kappa^2}\right) + \cdots\right] . \tag{2.114}$$

τ_2-piece

The first transverse piece to be calculated, exhibiting a non-trivial angular dependence through its logarithmic term is:

$$\begin{aligned} T_2 &= -\frac{\alpha N_f}{6\pi^2 q^2}\int dl^2 d\psi \frac{l^2\sin^2\psi}{\left(l^2 + q^2/4\right)^2 - (l\cdot q)^2} 8\left((l\cdot q)^2 - l^2q^2\right) \\ &\quad \times \Bigg\{ \left(-\frac{c_1}{4}\right)\left(-2\mathcal{F}'(l) + \cdots\right) \\ &\qquad + \left(-\frac{c_2}{4}\right)\frac{1}{l^2}\left(1 - \frac{q^2}{4l^2} + \cdots\right)\left(2\mathcal{F}(l) + \cdots\right)\ln\frac{\mathcal{F}(q^2)}{\mathcal{F}_+\mathcal{F}_-}\Bigg\} . \end{aligned} \tag{2.115}$$

This gives a lengthy expansion and so we only present those pieces that contribute to our final answer at the order we are working. To evaluate the angular dependence,

we must expand $\ln \frac{\mathcal{F}(q^2)}{\mathcal{F}_+\mathcal{F}_-}$ with the aid of Eqs. (2.66, 2.105):

$$\ln \frac{\mathcal{F}(q^2)}{\mathcal{F}_+\mathcal{F}_-} \simeq \alpha A_{1,1}\Bigg[-2\left(\ln\frac{l^2}{\kappa^2}-\ln\frac{q^2}{\kappa^2}\right)+\frac{q^2}{l^2}+\left(1-\frac{q^2}{2l^2}\right)\frac{(l\cdot q)^2}{l^4} + \left(1-\frac{q^2}{l^2}\right)\frac{(l\cdot q)^4}{l^8}+\cdots\Bigg], \tag{2.116}$$

in which we have already exploited the expected relationship between the expansion coefficients of the leading log expansion, Eq. (2.67)[1]. Terms higher than $\mathcal{O}(\alpha)$ vanish in this limit. Identifying the relevant angular integrals gives:

$$\begin{aligned} T_2 &= -\frac{\alpha N_f}{6\pi^2 q^2}\int dl^2 l^2 \\ &\times \Bigg\{\left(-\frac{c_1}{4}\right)\Big[8K_{0,1}\left(-l^2q^2\right)\left(-2\mathcal{F}'(l)+\cdots\right) \\ &\qquad +8K_{2,1}\left(-2\mathcal{F}'(l)+\cdots\right)+\cdots\Big] \\ &\quad +\left(-\frac{c_2}{4}\right)\frac{1}{l^2}\Big[8K_{0,1}\left(-l^2q^2\right)\left(2\mathcal{F}(l)+\cdots\right) \\ &\qquad \times\left(-2A_{1,1}\alpha\left(\ln\frac{l^2}{\kappa^2}-\ln\frac{q^2}{\kappa^2}\right)+\cdots\right) \\ &\qquad +8K_{2,1}\left(2\mathcal{F}(l)+\cdots\right)\left(-2A_{1,1}\alpha\left(\ln\frac{l^2}{\kappa^2}-\ln\frac{q^2}{\kappa^2}\right)+\cdots\right) \\ &\qquad\qquad +\cdots\Big]\Bigg\}, \end{aligned} \tag{2.117}$$

which are evaluated according to the appendix for the region $l^2 > q^2$:

$$\begin{aligned} T_2 &= -\frac{\alpha N_f}{12\pi}\int dl^2\Bigg\{\left(-\frac{c_1}{4}\right)\left[12\mathcal{F}'(l)+\cdots\right] \\ &\quad +\left(-\frac{c_2}{4}\right)\frac{1}{l^2}\left[-12\mathcal{F}(l)+\cdots\right]\left(-2A_{1,1}\alpha\left(\ln\frac{l^2}{\kappa^2}-\ln\frac{q^2}{\kappa^2}\right)+\cdots\right) \\ &\qquad\qquad +\cdots\Big]\Bigg\}. \end{aligned} \tag{2.118}$$

[1] If this relationship was not preserved, we would later find inconsistency in the equations

We obtain our final result here by introducing the leading log expansion for the function $\mathcal{F}$ and its derivatives, and perform the radial integral to give:

$$\begin{aligned} T_2 &= -\frac{\alpha N_f}{12\pi}\Bigg[c_1\left(3A_{1,1}\alpha\ln\frac{q^2}{\kappa^2}+3A_{2,2}a^2\ln^2\frac{q^2}{\kappa^2}+\cdots\right) \\ &\quad +c_2\left(-3A_{1,1}\alpha\ln^2\frac{q^2}{\kappa^2}-A_{1,1}^2\alpha^2\ln^3\frac{q^2}{\kappa^2}+\cdots\right)\Bigg]. \end{aligned} \tag{2.119}$$

τ_3-piece

The second non-trivial transverse piece to be calculated is that owing to the T_3 basis vector:

$$\begin{aligned} T_3 &= -\frac{\alpha N_f}{6\pi^2q^2}\int dl^2d\psi\frac{l^2\sin^2\psi}{\left(l^2+q^2/4\right)^2-\left(l\cdot q\right)^2}\left(3q^4-8\left(l\cdot q\right)-4l^2q^2\right) \\ &\times \Bigg\{\left(-\frac{c_3}{2}\right)\left(-2\mathcal{F}'(l)+\cdots\right) \\ &\quad +\left(-\frac{c_4}{2}\right)\frac{1}{l^2}\left(1-\frac{q^2}{4l^2}+\cdots\right)\left(2\mathcal{F}(l)+\cdots\right)\ln\frac{\mathcal{F}(q^2)}{\mathcal{F}_+\mathcal{F}_-}\Bigg\}. \end{aligned} \tag{2.120}$$

The procedure is the same as for T_2, whereby we expand the logarithmic term:

$$\ln\frac{\mathcal{F}(q^2)}{\mathcal{F}_+\mathcal{F}_-} \simeq \alpha A_{1,1}\left[-2\left(\ln\frac{l^2}{\kappa^2}-\ln\frac{q^2}{\kappa^2}\right)+\cdots\right], \tag{2.121}$$

and identify the angular integrals. Substituting these in from the appendix gives:

$$\begin{aligned} T_3 &= -\frac{\alpha N_f}{12\pi}\int dl^2\Bigg\{\left(-\frac{c_3}{2}\right)\left[12F'(l)+\cdots\right] \\ &\quad +\left(-\frac{c_4}{2}\right)\frac{1}{l^2}\left[-12\mathcal{F}(l)+\cdots\right]\left(-2A_{1,1}\alpha\left(\ln\frac{l^2}{\kappa^2}-\ln\frac{q^2}{\kappa^2}\right)+\cdots\right) \\ &\qquad +\cdots\Bigg]\Bigg\}. \end{aligned} \tag{2.122}$$

The last step is a leading log expansion of the remaining functions, followed by the evaluation of the radial integral:

$$T_3 = -\frac{\alpha N_f}{12\pi}\left[c_3\left(6A_{1,1}\alpha\ln\frac{q^2}{\kappa^2}+6A_{2,2}\alpha^2\ln^2\frac{q^2}{\kappa^2}+\cdots\right)\right.$$
$$\left.+c_4\left(-6A_{1,1}\alpha\ln^2\frac{q^2}{\kappa^2}-2A_{1,1}^2\alpha^2\ln^3\frac{q^2}{\kappa^2}+\cdots\right)\right]. \qquad (2.123)$$

τ_6-piece

The last transverse piece of the Kızılersü–Pennington vertex is described by:

$$T_6 = -\frac{\alpha N_f}{6\pi^2q^2}\int dl^2d\psi\frac{l^2\sin^2\psi}{(l^2+q^2/4)^2-(l\cdot q)^2}6\,(l\cdot q)\left(4-\frac{q^2}{l^2}\right)$$
$$\times\left\{\left(\frac{c_5}{2}\right)\left(1-\frac{q^2}{4l^2}+\cdots\right)(-2F'(l)+\cdots)\right\}. \qquad (2.124)$$

The angular integrals are identified:

$$T_6 = -\frac{\alpha N_f}{6\pi^2q^2}\int dl^2l^2\left(\frac{c_5}{2}\right)[6K_{2,1}\,(-8F'(l)+\cdots)]+\cdots, \qquad (2.125)$$

and are easily evaluated, giving:

$$T_6 = -\frac{\alpha N_f}{6\pi^2q^2}\int dl^2\left(\frac{c_5}{2}\right)(-12F'(l)+\cdots). \qquad (2.126)$$

Introducing the leading logarithm expansion and performing the radial integral gives:

$$T_6 = -\frac{\alpha N_f}{12\pi}c_5\left[6A_{1,1}\alpha\ln\frac{q^2}{\kappa^2}+6A_{2,2}\alpha^2\ln^2\frac{q^2}{\kappa^2}+\cdots\right]. \qquad (2.127)$$

Combining Terms

The leading log expansion of the photon functions is given by the sum:

$$\frac{1}{\mathcal{G}(q^2)} = 1+L_1+L_2+T_2+T_3+T_6+T_8\,. \qquad (2.128)$$

Exploiting the relationship between coefficients of the log expansion, Eq. (2.67) and simplifying we obtain:

$$\begin{aligned}\frac{1}{\mathcal{G}(q^2)} &= 1+\frac{N_f}{3\pi}\Bigg[-\alpha\ln\frac{q^2}{\kappa^2} \\ &+ \frac{1}{4}A_{1,1}\alpha^2\ln\frac{q^2}{\kappa^2}\left((2-3c_2-6c_4)\ln\frac{q^2}{\kappa^2}+\frac{1}{3}(9c_1+18c_3+18c_5+2)\right) \\ &+ \frac{1}{4}\frac{A_{11}^2}{3}\alpha^2\ln^2\frac{q^2}{\kappa^2}\left((2-3c_2-6c_4)\ln\frac{q^2}{\kappa^2}-\frac{1}{2}(9c_1+18c_3+18c_5+2)\right) \\ &\qquad +\cdots\Bigg]. \end{aligned} \tag{2.129}$$

This is to be compared with Eq. (2.78):

$$\frac{1}{\mathcal{G}(p^2)} = 1-\alpha B_{1,1}\ln\frac{p^2}{\kappa^2}+\alpha^2\frac{B_{1,1}}{2!}\ln^2\frac{p^2}{\kappa^2}-\alpha^3\frac{B_{1,1}^3}{3!}\ln^3\frac{p^2}{\kappa^2}\,, \tag{2.130}$$

on substitution of the Kızılersü–Pennington choice for the coefficients c_i:

$$c_1=\frac{4}{3}\,,\qquad c_2=\frac{1}{3}\,,\qquad c_3=\frac{5}{12}\,,\qquad c_4=\frac{1}{6}\,,\qquad c_5=\frac{1}{4}\,. \tag{2.131}$$

All but the $\mathcal{O}(\alpha)$ leading logarithms cancel with this choice, and so Eq. (2.129) becomes:

$$\frac{1}{\mathcal{G}(p^2)} = 1+\frac{N_f}{3\pi}\left[-\alpha\ln\frac{q^2}{\kappa^2}\right], \tag{2.132}$$

which is the expected result.

2.3 Quenched QED

In the course of studying coupled non-linear integral equations, one finds it appropriate to introduce a further series of approximations in order to make the problem numerically tractable. The first of such simplifications, and one that leads to an interesting theory in its own right, is that of quenching the model, i.e. setting $\mathcal{G} = 1$, leading to the SDE of Fig. 2.5. The coupling now no longer runs, with the result that angular integrals may (usually) be calculated analytically rather than numerically. Despite this, when not concerned with analytic results, we in fact choose to perform these integrations numerically thus demonstrating the robustness of our numerical method.

There have been many numerical studies of strongly coupled quenched QED, both with the Schwinger-Dyson equations and on the lattice. The aim of these has been to determine the phase-structure of the theory, an indication of which is given by scaling laws close to critical points. The anomalous dimensions of the mass function of the fermion propagator are related to those associated with operators such as $\overline{\psi}(x)\psi(x)$. While renormalisability prevents us from including terms such as $G\left\langle\bar{\psi}\psi\right\rangle^2/\kappa^2$ in the Lagrangian – due to its canonical dimensions – the *anomalous dimensions* can modify this significantly, thus rendering them renormalisable [42,43] and hence relevant [9,44]. It is thus believed that the study of the phase structure of QED is incomplete without the inclusion of such terms. Early lattice studies [45–47] were found to be contaminated with these four-fermion interactions, i.e. $G \neq 0$, and hence exhibited a different phase structure to *pure* QED. It was hoped in a later reformulation of the lattice in momentum space [48] that the contribution from the four-fermion interaction could be controlled, thus allowing comparisons of the two approaches to be made.

Our goal is not to investigate the full phase structure of the theory. Instead, we are solely interested in dynamical mass generation and its critical point in the coupling constant for pure QED. This critical point should, in principle be a physical observable and hence be gauge independent. We first explore the residual gauge dependence of the critical coupling in quenched QED for a selection of vertex ansätze, including that of Kızılersü and Pennington [40].

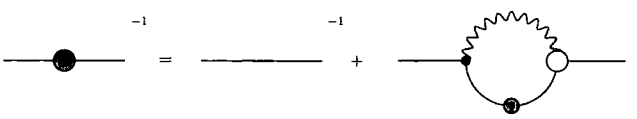

Figure 2.5: The quenched fermion SDE. Filled dots indicate full propagators and vertices.

2.3.1 The Rainbow approximation

The rainbow approximation is the name attributed to the simultaneous use of both the bare vertex and quenched approximations. This is due to the rainbow-like structure appearing in the pictorial expansion of the SDEs, as illustrated in Fig. 2.6. Our SDE for the fermion propagator in this case is given by:

$$-i\,S_F^{-1}(p) = -i\,S_F^{0\,-1} - \int_M \frac{d^4k}{(2\pi)^4}\,(-i\,e\,\gamma^\mu)\;i\,S_F(k)\;(-i\,e\,\gamma^\nu)\;i\Delta^0_{\mu\nu}(q)\;, \qquad (2.133)$$

where we have replaced the full vertex appearing in Eq. (1.73) by γ^μ and the photon propagator remains undressed.

This equation has been investigated extensively in the literature [49–52] where it has been determined when dynamically generated mass is supported. If we project out the Dirac-odd and even parts of the fermion propagator, by substitution of the general forms given in Eq. (2.20) and Eq. (2.22) we have:

$$\mathcal{A}(p^2) = 1+\frac{\alpha\xi}{4\pi p^2}\left[\int_0^{p^2} dk^2 \frac{\mathcal{A}(k^2)k^2}{\mathcal{A}^2(k^2)k^2+\mathcal{B}^2(k^2)}\frac{k^2}{p^2} + \int_{p^2}^{\kappa^2} dk^2 \frac{\mathcal{A}(k^2)k^2}{\mathcal{A}^2(k^2)k^2+\mathcal{B}^2(k^2)}\frac{p^2}{k^2}\right], \qquad (2.134)$$

and

$$\mathcal{B}(p^2) = m+\frac{\alpha(3+\xi)}{4\pi}\left[\int_0^{p^2} \frac{\mathcal{B}(k^2)}{\mathcal{A}^2(k^2)k^2+\mathcal{B}^2(k^2)}\frac{k^2}{p^2} + \int_{p^2}^{\kappa^2} \frac{\mathcal{B}(k^2)}{\mathcal{A}^2(k^2)k^2+\mathcal{B}^2(k^2)}\right], \qquad (2.135)$$

where we have analytically performed the angular integrals according to Appendix B.2, and presented the equations in Euclidean space. In Landau gauge the wave-function renormalisation is trivially 1, and for general gauge is $1+\mathcal{O}(\alpha)$ in perturbation theory – leading to another oft-employed approximation, $A(p^2)=1$. In Landau gauge, the mass function $\mathcal{M}=\mathcal{B}/\mathcal{A}$ is:

$$\mathcal{M}(p^2) = \frac{3\alpha}{4\pi}\left[\int_0^{p^2} dk^2 \frac{k^2}{p^2}\frac{\mathcal{M}(k^2)}{k^2+\mathcal{M}^2(k^2)} + \int_{p^2}^{\kappa^2} dk^2 \frac{\mathcal{M}(k^2)}{k^2+\mathcal{M}^2(k^2)}\right], \qquad (2.136)$$

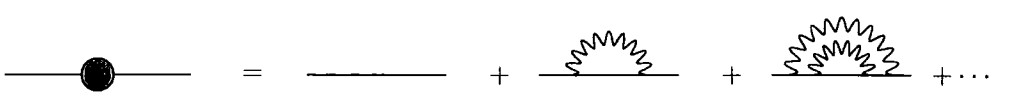

Figure 2.6: The quenched fermion SDE in the rainbow approximation.

which can be recast as a differential equation:

$$\frac{d}{dx}\left(x^2\frac{d\mathcal{M}(x)}{dx}\right) = -\frac{3\alpha}{4\pi}\frac{x\mathcal{M}(x)}{x+\mathcal{M}^2(x)} \,. \tag{2.137}$$

Rewriting this with $x = p^2$ and for $x \gg \mathcal{M}^2$ we may explore the asymptotics of Eq. (2.136):

$$x^2\mathcal{M}''(x) + 2x\mathcal{M}'(x) + \frac{3\alpha}{4\pi}\mathcal{M}(x) = 0 \,, \tag{2.138}$$

which admits solutions of the form $\mathcal{M}(x) = x^s$. Substituting this in we find that:

$$s = \frac{1}{2}\left(-1 \pm \sqrt{1-\frac{\alpha}{\alpha_c}}\right) \,, \tag{2.139}$$

with $\alpha_c = \pi/3$ representing some critical point of the behaviour of the solution, above which dynamical mass generation occurs. We show typical solutions for two gauge choices in Fig. 2.7. In Fig. 2.8 we see the Euclidean mass, defined as $\mathcal{M}^2(p^2 = M_E^2) = M_E^2$, as a function of the coupling for Landau, Feynman and Yennie [53] gauges, where the unphysical dependence of the critical coupling on the gauge is clearly evident.

This mass-function exhibits an infinite order phase transition as $\alpha \to \alpha_c$ and so obeys the Miransky scaling law [52]:

$$\frac{\kappa}{M_E} = \exp\left(\frac{A}{\sqrt{\frac{\alpha}{\alpha_c}-1}} - B\right) \,. \tag{2.140}$$

Using this to fit against our numerical data, we obtained the critical coupling for a selection of gauges, see Table 2.6.

ξ	0	1	3	
α_c	1.0472	2.0535	2.9378	no WGTI
α_c	1.0472	1.690	2.040	WGTI

Table 2.6: Critical couplings for the quenched bare-vertex approximation, with and without the WGTI employed in the $\xi q_\mu \Gamma^\mu$ part of the vertex.

2.3.2 The Curtis–Pennington Vertex

The CP vertex was developed in an attempt to restrict the transverse part of the vertex through the requirement that multiplicative renormalisability be preserved.

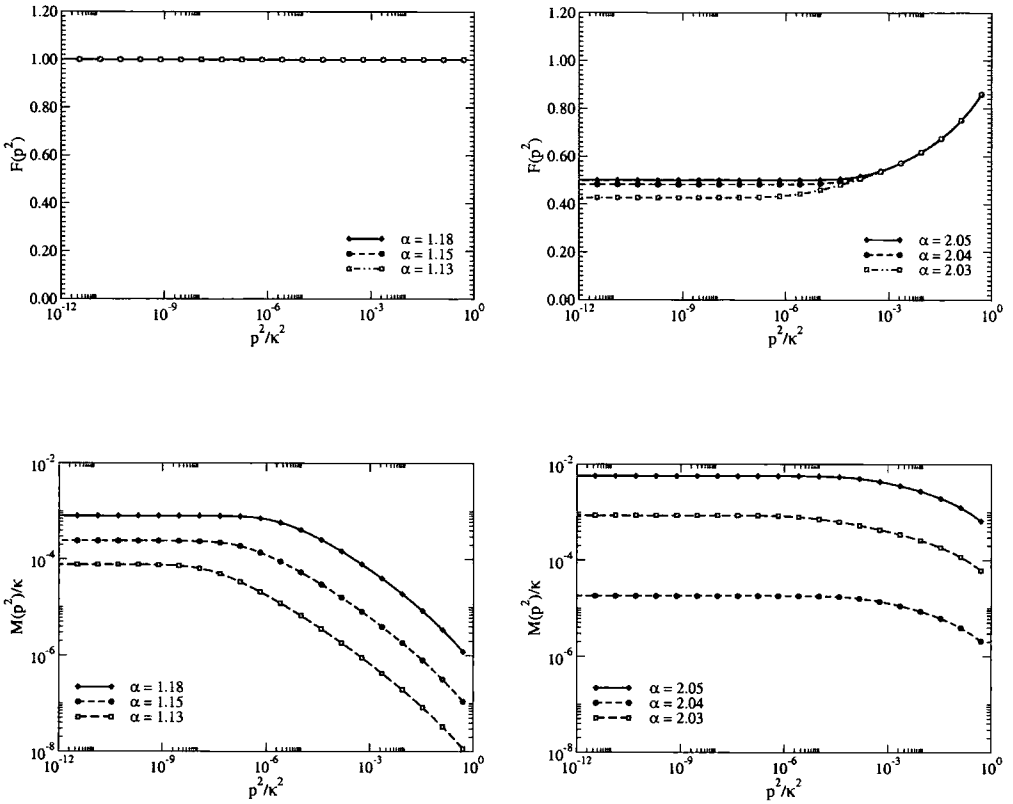

Figure 2.7: Wave-function renormalisation and mass-function in Landau Gauge (left-hand side) and Feynman gauge (right-hand side), in the quenched rainbow approximation, without WGTI.

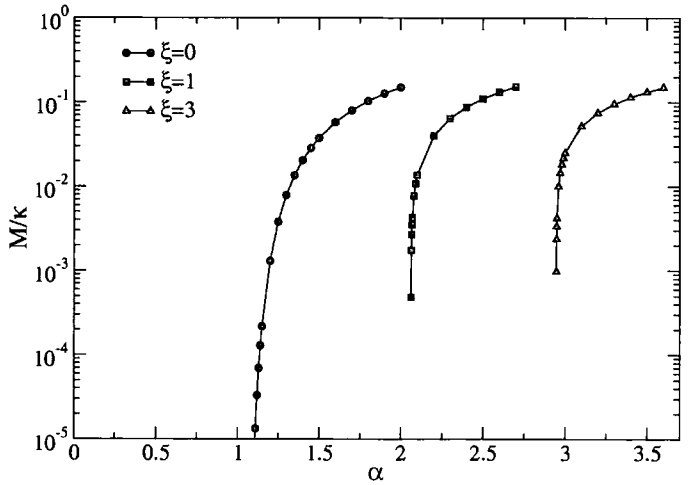

Figure 2.8: The Euclidean mass, M_E, in the quenched rainbow approximation. The explicitly gauge dependent part is derived from the vertex ansatz and is in violation of the Ward-Green-Takahashi identity.

The details of this vertex may be found in Sect. 2.2.1. In summary we employ the following in Eqs. (2.29, 2.34):

$$\begin{aligned}
\lambda_1(k,p) &= \frac{1}{2}\left(\mathcal{A}(k^2)+\mathcal{A}(p^2)\right) , \\
\lambda_2(k,p) &= \frac{1}{2}\frac{1}{k^2-p^2}\left(\mathcal{A}(k^2)-\mathcal{A}(p^2)\right) , \\
\lambda_3(k,p) &= -\frac{1}{k^2-p^2}\left(\mathcal{B}(k^2)-\mathcal{A}(B^2)\right) , \\
\tau_6(k,p) &= \lambda_2(k,p)\frac{(k^2+p^2)\,(k^2-p^2)}{(k^2-p^2)^2+\left(\mathcal{M}^2(k^2)+\mathcal{M}^2(p^2)\right)^2} ,
\end{aligned} \tag{2.141}$$

with the remaining transverse components unconstrained and set to zero. Since our longitudinal and transverse coefficients do not depend upon the loop momentum q^2, and the photon equation is quenched, the angular integrals can be performed analytically (Appendix B.2) to yield:

$$\begin{aligned}
\mathcal{A}(p^2) &= 1-\frac{3\alpha}{8\pi p^2}\int_0^{\kappa^2} dk^2 \frac{p^2\mathcal{A}(k^2)}{\mathcal{A}^2(k^2)k^2+\mathcal{B}^2(k^2)}\left[\frac{k^2}{p^2}\Theta_- + \frac{p^2}{k^2}\Theta_+\right] \\
&\quad\times\left[\lambda_2(k,p)\left(k^2+p^2\right)-\lambda_3(k,p)\frac{\mathcal{B}(k^2)}{\mathcal{A}(p^2)}-\tau_6(k,p)\left(k^2-p^2\right)\right] \\
&\quad -\frac{\alpha\xi}{4\pi}\int_0^{\kappa^2} dk^2 \frac{\mathcal{A}(k^2)\mathcal{A}(p^2)}{\mathcal{A}^2(k^2)k^2+\mathcal{B}^2(k^2)}\left[\frac{k^2}{(p^2)^2}\frac{\mathcal{B}(k^2)\mathcal{B}(p^2)}{\mathcal{A}(k^2)\mathcal{A}(p^2)}\Theta_- - \Theta_+\right] ,
\end{aligned} \tag{2.142}$$

$$\begin{aligned}
\mathcal{B}(p^2) &= \frac{3\alpha}{8\pi}\int dk^2 \frac{p^2}{\mathcal{A}^2(k^2)k^2+\mathcal{B}^2(k^2)} \\
&\quad\times\Big\{2\left(\lambda_1(k,p)+\tau_6(k,p)\left(k^2-p^2\right)\right)\mathcal{B}(k^2)\left[\frac{\Theta_-}{p^2}+\frac{\Theta_+}{k^2}\right] \\
&\qquad +\left(2\lambda_2(k,p)\mathcal{B}(k^2)+\mathcal{A}(k^2)\lambda_3(k,p)\right)\left[\frac{k^2}{p^2}\Theta_- + \frac{p^2}{k^2}\Theta_+\right]\Big\} \\
&\quad +\frac{\alpha\xi}{4\pi}\int dk^2 \frac{\mathcal{A}(k^2)\mathcal{A}(p^2)}{\mathcal{A}^2(k^2)k^2+\mathcal{B}^2(k^2)}\left[\frac{k^2}{p^2}\frac{\mathcal{B}(k^2)}{\mathcal{A}(k^2)}\Theta_- + \frac{\mathcal{B}(p^2)}{\mathcal{A}(p^2)}\Theta_+\right] .
\end{aligned} \tag{2.143}$$

For notational brevity, we use $\Theta_+ = \Theta(k^2-p^2)$ and $\Theta_- = \Theta(p^2-k^2)$ where Θ is the Heaviside step-function. We are able to investigate the critical behaviour of this ansatz through two methods. The first is a brute force numerical determination of the critical coupling strength by directly solving the coupled integral equations for $\mathcal{A}$ and $\mathcal{B}$. Results for this are presented in Fig. 2.10(a), where we note α_c is almost constant *cf.* Fig. 2.8. We determine the critical coupling α_c by fitting the Miransky scaling law of Eq. (2.140). The results are presented in Table 2.7.

The second method we can employ is a bifurcation analysis of the mass equation.

ξ	α_c	ξ	α_c
0	0.9339	4	0.8124
1	0.8909	5	0.7953
2	0.8584	6	0.7807
3	0.8329		

Table 2.7: Critical couplings with the CP vertex in the quenched approximation.

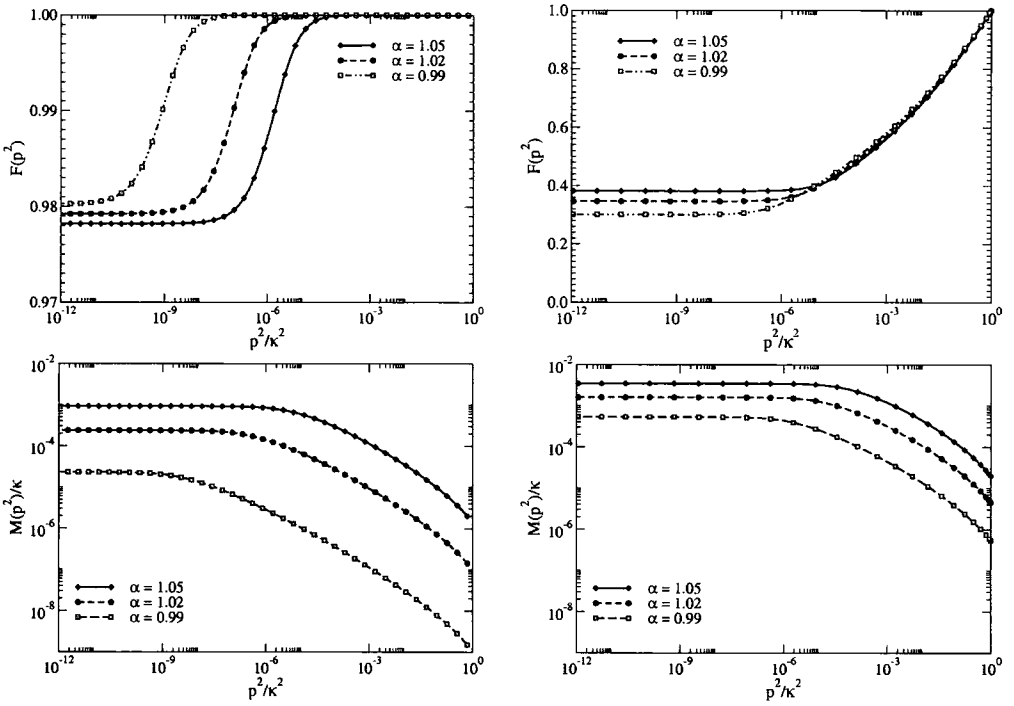

Figure 2.9: Wave-function renormalisation and mass-function in Landau Gauge (left-hand side) and Feynman gauge (right-hand side), with the quenched Curtis–Pennington vertex.

This was presented in [54] with the unfortunate inclusion of a piece that should vanish due to translational invariance; the corrected analysis can be found in [55]. The method essentially requires us to linearise the equations with respect to the mass function $\mathcal{B}$. The $\mathcal{A}$ equation is then simply:

$$\mathcal{A}(p^2) = 1 + \frac{\alpha\xi}{4\pi}\int_0^{\kappa^2} \frac{dk^2}{k^2}\frac{\mathcal{A}(p^2)}{\mathcal{A}(k^2)}\Theta_+ = 1 + \frac{\alpha\xi}{4\pi}\int_{p^2}^{\kappa^2} \frac{dk^2}{k^2}\frac{\mathcal{A}(p^2)}{\mathcal{A}(k^2)}\,, \tag{2.144}$$

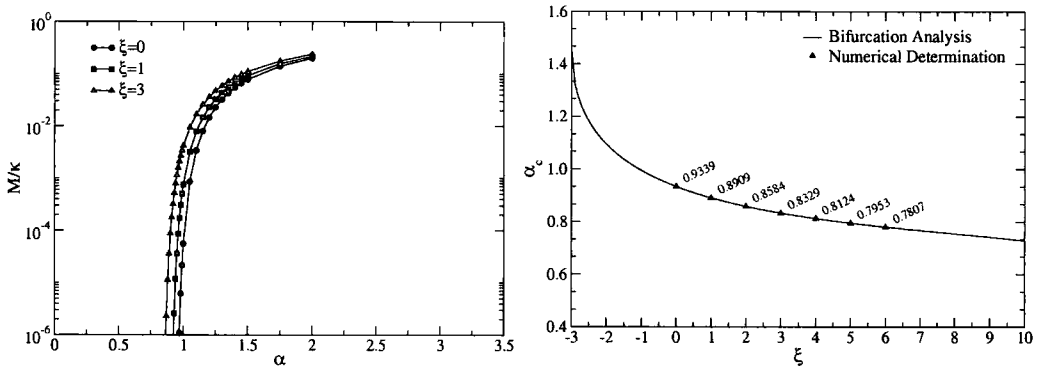

(a) (b)

Figure 2.10: For the quenched Curtis–Pennington vertex, we show (a) the dynamically generated Euclidean mass as a function of the gauge parameter, while (b) shows the critical coupling α_c as calculated through a bifurcation analysis.

which has the solution

$$\frac{1}{\mathcal{F}(p^2)} \equiv \mathcal{A}(p^2) = \left(\frac{p^2}{\kappa^2}\right)^{-\alpha\xi/4\pi} , \tag{2.145}$$

due to the CP-vertex respecting multiplicative renormalisability. The exponent of this is denoted by $\nu = \alpha\xi/4\pi$ and this solution is inserted into the linearised form of $\mathcal{B}$. At the critical point the equation is scale invariant and so is solved by:

$$\mathcal{B}(p^2) = \left(p^2\right)^{-s}\left(\frac{p^2}{\kappa^2}\right)^{\nu} , \tag{2.146}$$

with the factor in parenthesis coming from the $\mathcal{A}(p^2)$ function. Following the method contained within [54, 55] we are left to solve a pair of coupled transcendental functions:

$$\begin{aligned} f(\xi,\nu,s) \;\equiv\; & \frac{3\nu}{2\xi}\Big[2\pi\cot s\pi - \pi\cot\nu\pi + 3\pi\cot(\nu-s)\pi \\ & + \frac{2}{1-s} + \frac{1}{\nu+1} + \frac{1}{\nu} - \frac{3}{\nu-s} - \frac{1}{\nu-s+1}\Big] - \frac{1-s}{\nu-s+1} = 0 \\ g(\xi,\nu,s) \;=\; & \frac{\partial f(\xi,\nu,s)}{\partial s} = 0 \,. \end{aligned} \tag{2.147}$$

These two equations are solved using an iterative method, giving ν_c and s_c for a given ξ. This allows us to compute the critical coupling α_c from the relation $\nu = \alpha\xi/4\pi$. The results are given in Fig. 2.10(b) in agreement with our direct numerical approach.

2.3.3 Kızılersü–Pennington Vertex

Although not designed for quenched QED, nor specifically for the ($\mathcal{F}$, $\mathcal{M}$)-system, we may employ this ansatz and examine the gauge dependence of the critical coupling. Our coupled system of equations are given by Eqs. (2.29, 2.34) with the longitudinal components of Eq. (2.12), and transverse part specified by Eq. (2.76).

Examining the chirally symmetric phase, we should obtain results for the fermion wave-function renormalisation similar to the CP-vertex, see Eq. (2.145). This is indeed the case, and we may see this comparison in Fig. 2.11(a). The logarithmic scale of Fig. 2.11(b) clearly indicates the scaling behaviour is well approximated by $(p^2/\kappa^2)^\gamma$. Thus, we indeed see that multiplicative renormalisability is preserved for fermion wave-function, in the absence of dynamical mass generation and for $N_f = 0$.

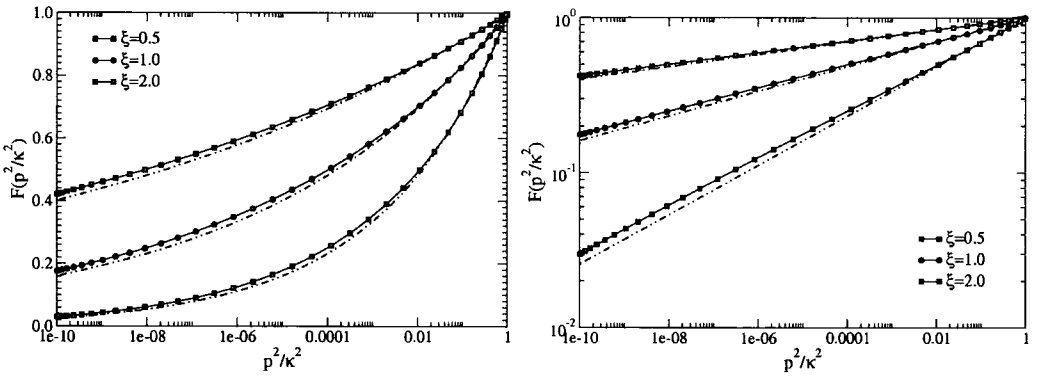

Figure 2.11: Dressing functions (a) $\mathcal{F}$ and (b) $\log\mathcal{F}$ for the quenched KP vertex in a variety of gauges, without dynamical mass generation. Dashed lines show the solution for the CP vertex, Eq. (2.145), for comparison

Now, we consider solutions in which $\mathcal{M}$ realises a non-trivial solution, and determine values for the critical coupling as a function of the gauge parameter. The results are in Table 2.8, with the approximate result for $\xi = 3$ indicating a breakdown of the Miransky scaling law here for large values of the gauge parameter. In

ξ	0	1	3
α_c	0.9351	0.7222	$\simeq 0.5$

Table 2.8: Critical couplings for KP-vertex in the quenched approximation.

Fig. 2.12 we show the Euclidean mass as a function of the coupling for three choices of gauge. Surprisingly, despite this vertex's failure to preserve multiplicative renormalisability of the mass function, the situation is much improved when compared

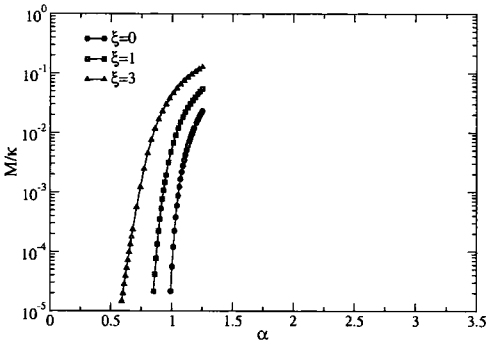

Figure 2.12: For the quenched Kızılersü–Pennington vertex, we show the dynamically generated Euclidean mass as a function of the gauge parameter.

to the bare-vertex. However, it is not competitive for the quenched approximation where the Curtis–Pennington vertex performs better. This shortcoming is likely to be evident in the unquenched studies which follow. However, we feel that the KP-vertices ability to cope with MR of the photon equation will compensate for the lack of consideration for fermion masses.

2.4 Unquenched QED

Now that we have made some progress with solving the SDEs for quenched QED, we move on to the more interesting unquenched case. Here we will investigate the residual gauge dependence of the critical coupling by direct numerical calculation in a variety of gauges for a selection of vertex ansätze. This time we include the SDE for the photon in our coupled system of integral equations. By doing this, we introduce a further dimensionless parameter into the theory, that of the number of active fermions N_f, in addition to the already present coupling α. A first step towards including the running of the coupling can be accomplished by introducing the one-loop running from perturbation theory as an ansatz:

$$\alpha(p^2) = \alpha_0 \left[1 + \frac{\alpha N_f}{3\pi} \log\left(\frac{\kappa^2}{p^2+\mu^2}\right)\right]^{-1} , \tag{2.148}$$

with $[\cdots]^{-1}$ the photon-renormalisation function, $\mathcal{G}(p^2)$. This has formed the basis of several studies [56–60] where it has been suggested the infinite order phase transition in the quenched case becomes second order, with the mass-function described now by the scaling law:

$$\mathcal{B}(0) \sim \kappa\,(\alpha - \alpha_c)^{1/2} , \tag{2.149}$$

in contrast to Eq. (2.140). In these studies, we don't wish to simply employ the one-loop approximation. Instead, we choose to couple in the equation for the photon propagator and solve for the system of three equations simultaneously. We assume that Eq. (2.149) will still approximately apply in the vicinity of the critical point.

On coupling in the photon equation, Fig. 2.13, we find that there are several choices for the momentum partition η. Most studies to date have employed the asymmetric choice, $\eta = 0, 1$ in the photon SDE. While this is easier to implement numerically, it is believed that the unequal footing of the two fermion lines can introduce spurious dependences upon the cut-off momentum, due to the breaking of translational invariance of our regulation scheme. It is believed that the symmetric choice $\eta = 1/2$ will reduce the contribution from these terms with the symmetry allowing cancellations to take place. Despite this, we will continue to use the asymmetric photon equation until the final section, where we renormalise the theory and introduce new results with the Kızılersü–Pennington vertex.

We should make a further comment on the momentum inside the fermion loop. For the fermion with momentum $l^\mu = (k + \eta q)$, we see that while both k and q are restricted to the range $[\varepsilon, \kappa]$, the composite momentum is $l \in [0, 2\kappa]$ for $\eta = 0, 1$ and $\left[0, \frac{3}{2}\kappa\right]$ for a symmetric partition. This requires extrapolation on the part of our functions beyond their own range of definition, $[\varepsilon, \kappa]$. How this is implemented, whether by:

$$\begin{aligned} \mathcal{G}(q^2 > \kappa^2) &= \mathcal{G}(\kappa^2) \,, \\ \mathcal{M}(p^2 > \kappa^2) &= \mathcal{M}(\kappa^2)\, \kappa^2/p^2 \,, \end{aligned} \tag{2.150}$$

or through a logarithmic fit as expected from one-loop perturbation theory, will affect the result. Until we impose renormalisation conditions upon the theory, we will simply use Eq. (2.150) with $\kappa^2 = 10^{10}$ to make contact with the work of Bloch [55]. Through the rest of the section we will consider one active flavour of fermion to be present, and so $N_f = 1$.

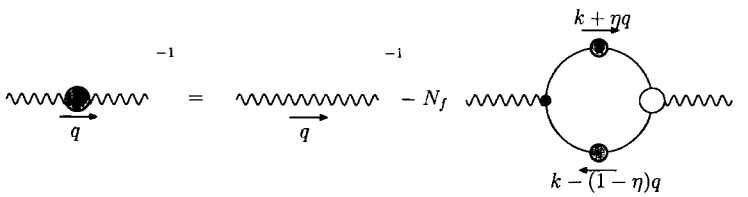

Figure 2.13: The unquenched photon SDE. Filled dots indicate full propagators and vertices.

2.4.1 Bare-vertex Approximation

The bare-vertex approximation is the simplest starting point for coupling in a third non-linear integral equation. Our SDEs in this case employ $\Gamma^\mu(k,p;q) = \gamma^\mu$ and are:

$$\begin{aligned}
\mathcal{A}(x) &= 1 - \frac{\alpha}{2\pi^2 x}\int_0^{\kappa^2} dy \frac{y\mathcal{A}(y)}{\mathcal{A}^2(y)y + \mathcal{B}^2(y)} \\
&\quad \times \int_0^\pi d\psi \sin^2\psi \frac{\mathcal{G}(z)}{z}\left[\frac{2xy\sin^2\psi}{z} - 3\sqrt{xy}\cos\psi\right] \qquad (2.151) \\
&\quad - \frac{\alpha\xi}{4\pi}\int_0^{\kappa^2} dy \frac{1}{\mathcal{A}^2(y)y + \mathcal{B}^2(y)}\left[\frac{y}{x^2}\mathcal{B}(y)\mathcal{B}(x)\Theta(x-y) - \mathcal{A}(y)\mathcal{A}(x)\Theta(y-x)\right] \\
\mathcal{B}(x) &= m_0 + \frac{3\alpha}{2\pi^2}\int_0^{\kappa^2} dy \frac{y\mathcal{B}(y)}{\mathcal{A}^2(y)y^2 + \mathcal{B}^2(y)}\int_0^\pi d\psi \sin^2\psi \frac{\mathcal{G}(z)}{z} \qquad (2.152) \\
&\quad + \frac{\alpha\xi}{4\pi}\int_0^{\kappa^2} dy \frac{1}{\mathcal{A}^2(y)y + \mathcal{B}^2(y)}\left[\frac{y}{x}\mathcal{B}(y)\mathcal{A}(x)\Theta(x-y) + \mathcal{B}(x)\mathcal{A}(y)\Theta(y-x)\right] \\
\frac{1}{\mathcal{G}(x)} &= 1 + \frac{4N_f\alpha}{3\pi^2 x}\int_0^{\kappa^2} dy \frac{y\mathcal{A}(y)}{\mathcal{A}^2(y)y + \mathcal{B}^2(y)} \\
&\quad \times \int_0^\pi \sin^2\psi \frac{\mathcal{A}(z)}{\mathcal{A}^2(z)z^2 + \mathcal{B}^2(z)}\left[y\left(1 - 4\cos^2\psi\right) + 3\sqrt{xy}\cos\psi\right], \qquad (2.153)
\end{aligned}$$

with $z = x + y - 2\sqrt{xy}\cos\psi$. Rather than solve all three simultaneously, it is only necessary to solve for the $\mathcal{A}$ and $\mathcal{B}$ equations together, updating $\mathcal{G}$ outside the main iterator. This procedure is looped until we obtain convergence, which is achieved in only a few steps. The bare-vertex does not respect the WGTI, though we have used this identity directly to fix the explicitly gauge dependent part.
We solve equations Eqs. (2.151, 2.152, 2.153) as a function of the coupling, for the gauge parameter $\xi \in [0,1]$. Using the second order scaling law Eq. (2.149) we obtain α_c, the results of which are displayed in Table 2.9.

ξ	α_c	ξ	α_c
0.0	1.72613	0.6	1.88649
0.2	1.77469	0.8	1.94249
0.4	1.82997	1.0	1.99704

Table 2.9: Critical couplings for the unquenched bare-vertex approximation with the WGTI employed in the $\xi q_\mu \Gamma^\mu$ part of the vertex.

Representative solutions close to the critical point are shown in Fig. 2.14. A plot of the Euclidean mass as a function of the coupling $\alpha(\kappa)$ is shown for a selection of gauges in Fig. 2.15.

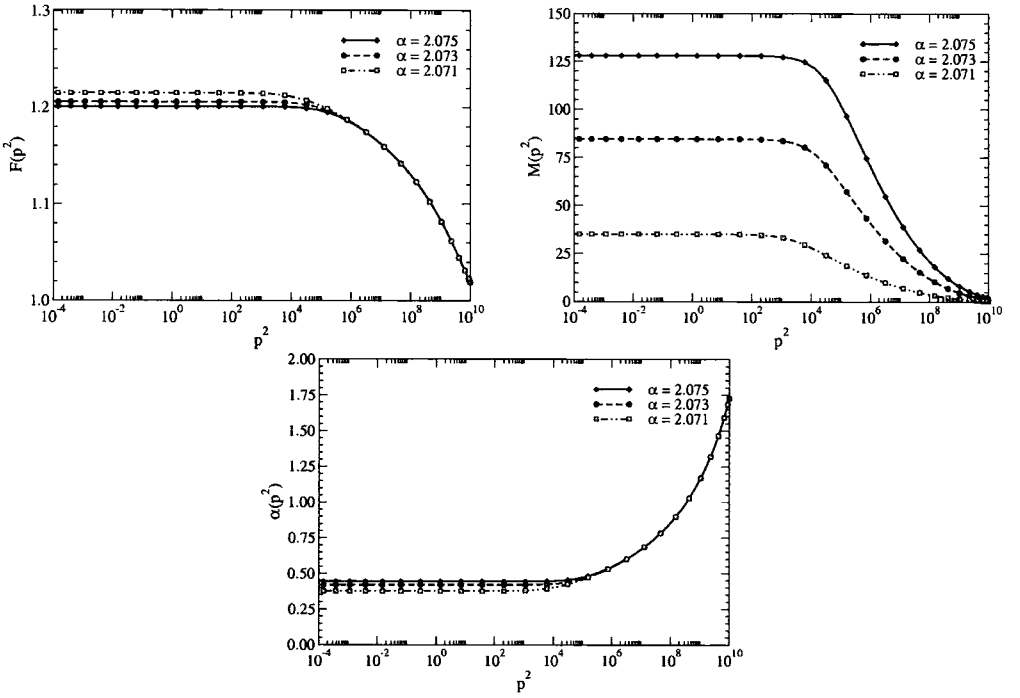

Figure 2.14: Wave-function renormalisation, mass-function and running coupling for the unquenched bare-vertex in Landau gauge.

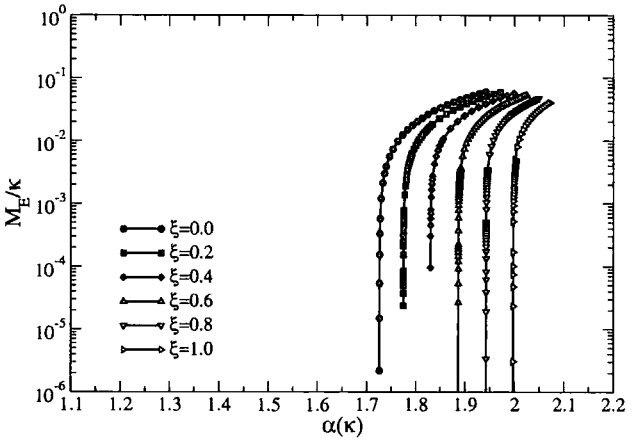

Figure 2.15: Dynamically Generated Euclidean Mass in the unquenched rainbow approximation. The WGTI is enforced in the ξq_μ part of the vertex.

2.4.2 Minimal Ball–Chiu Vertex

We can make a small modification to the model by introducing a minimal dressing of the bare-vertex; that is, we include just the first term of the Ball–Chiu construction. This eliminates the need to evaluate the terms $\lambda_2(k,p)$ and $\lambda_3(k,p)$ numerically,

whose limit as $k \to p$ must be carefully evaluated, particularly in the photon equation. Thus we are solving Eqs. (2.151, 2.152) with an extra factor of $\lambda_1(y,x)$, and Eq. (2.153) with an extra $\lambda_1(y,z)$ in the kernels.

$$\begin{aligned}
\mathcal{A}(x) &= 1 - \frac{\alpha}{2\pi^2 x}\int_0^{\kappa^2} dy \frac{y\mathcal{A}(y)}{\mathcal{A}^2(y)y + \mathcal{B}^2(y)}\lambda_1(y,x) \\
&\quad \times \int_0^{\pi} d\psi \sin^2\psi \mathcal{G}(z)\left[\frac{2xy\sin^2\psi}{z^2} - \frac{3\sqrt{xy}\cos\psi}{z}\right] \\
&\quad -\frac{\alpha\xi}{4\pi}\int_0^{\kappa^2} dy \frac{1}{\mathcal{A}^2(y)y + \mathcal{B}^2(y)}\left[\frac{y}{x^2}\mathcal{B}(y)\mathcal{B}(x)\Theta_- - \mathcal{A}(y)\mathcal{A}(x)\Theta_+\right] , \\
\mathcal{B}(x) &= m_0 + \frac{3\alpha}{2\pi^2}\int_0^{\kappa^2} dy \frac{y\mathcal{B}(y)}{\mathcal{A}^2(y)y^2 + \mathcal{B}^2(y)}\lambda_1(y,x)\int_0^{\pi} d\psi \sin^2\psi \frac{\mathcal{G}(z)}{z} \\
&\quad +\frac{\alpha\xi}{4\pi}\int_0^{\kappa^2} dy \frac{1}{\mathcal{A}^2(y)y + \mathcal{B}^2(y)}\left[\frac{y}{x}\mathcal{B}(y)\mathcal{A}(x)\Theta_- + \mathcal{B}(x)\mathcal{A}(y)\Theta_+\right] , \\
\frac{1}{\mathcal{G}(x)} &= 1 + \frac{4N_f\alpha}{3\pi^2 x}\int_0^{\kappa^2} dy \frac{y\mathcal{A}(y)}{\mathcal{A}^2(y)y + \mathcal{B}^2(y)} \\
&\quad \times \int_0^{\pi} \sin^2\psi \frac{\mathcal{A}(z)}{\mathcal{A}^2(z)z^2 + \mathcal{B}^2(z)}\lambda_1(y,z)\left[y\left(1 - 4\cos^2\psi\right) + 3\sqrt{xy}\cos\psi\right] .
\end{aligned}$$

In Fig. 2.17 we show the dynamically generated mass as a function of $\alpha(\kappa^2)$ for a variety of gauges, with the WGTI employed. Comparing this with its counterpart in the rainbow approximation, Fig. 2.15, we see that the gauge dependence is in fact more severe. Clearly simply dressing the first basis component is insufficient; one must consider the whole longitudinal part of the vertex, most likely with some specification for the transverse part. We present solutions close to the critical point in Fig. 2.16.

ξ	α_c	ξ	α_c
0.0	1.89785	0.6	1.43815
0.2	1.70233	0.8	1.34002
0.4	1.55606	1.0	1.25067

Table 2.10: Critical couplings for the unquenched Minimal Ball–Chiu vertex with the WGTI employed in the $\xi q_\mu \Gamma^\mu$ part.

We solve the SDE numerically as a function of the coupling α for a variety of gauges so as to determine the critical point α_c. For the Minimal Ball–Chiu vertex we used the second-order scaling law to fit α_c, the results of which are in Table 2.10.

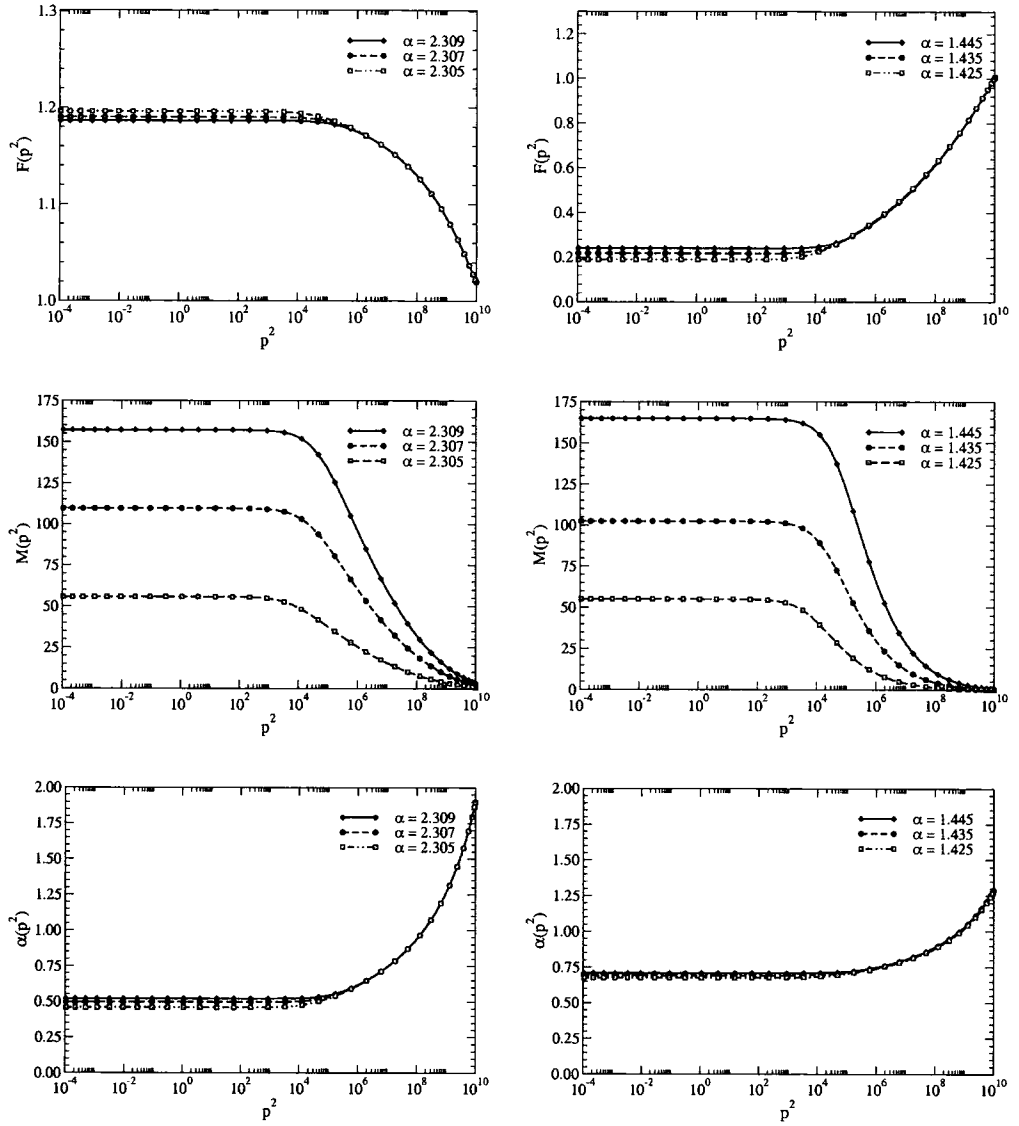

Figure 2.16: Wave-function renormalisation, mass-function and running coupling in Landau Gauge (left-hand side) and Feynman gauge (right-hand side), with the unquenched Minimal Ball–Chiu vertex.

2.4.3 Full Ball–Chiu Vertex

The Ball–Chiu vertex poses a small challenge to solve numerically, particularly in the photon equation. Here, we must ensure a smooth interpolation is employed, for there are delicate cancellations in the angular integrals that will blow-up if not treated properly. One must correctly integrate over the derivative-like pieces of the BC–vertex in order to cancel a potential numerical singularity. These problems have been dealt with in [55] by employing the Chebyshev expansion – the details

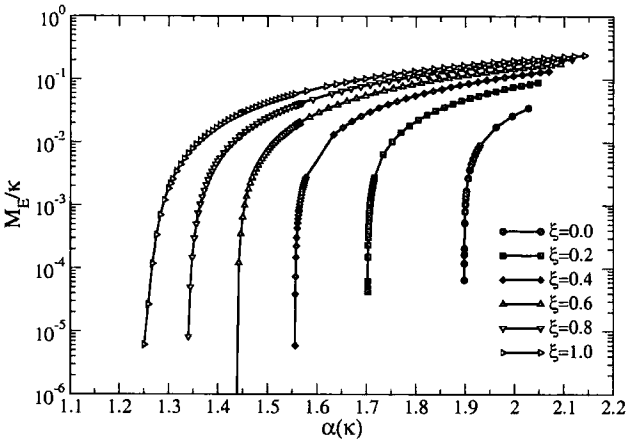

Figure 2.17: Dynamically Generated Euclidean Mass in the unquenched Minimal Ball–Chiu approximation. The WGTI is enforced in the ξ-part of the SDE.

of which can be found there, or in Appendix A. Away from Landau gauge, as with all solutions given thus far, we must appropriately approximate the missing infrared part of the integral. This may be done analytically since the behaviour of the functions is generally known, or at least easily approximated, for small momenta.

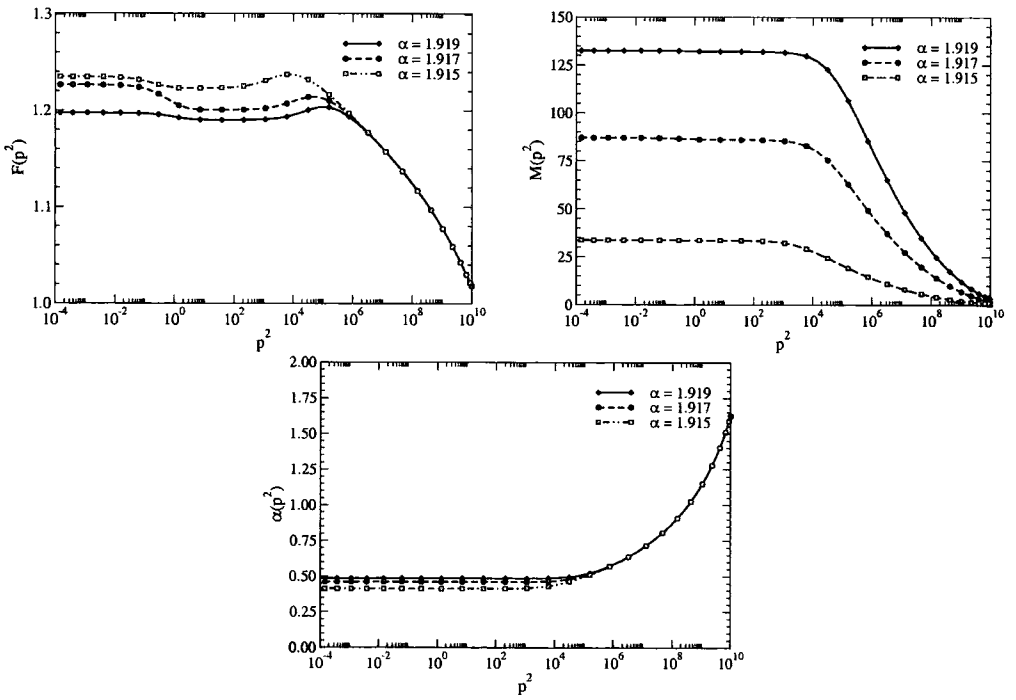

Figure 2.18: Wave-function renormalisation, mass-function and running coupling for the unquenched full Ball–Chiu in Landau gauge.

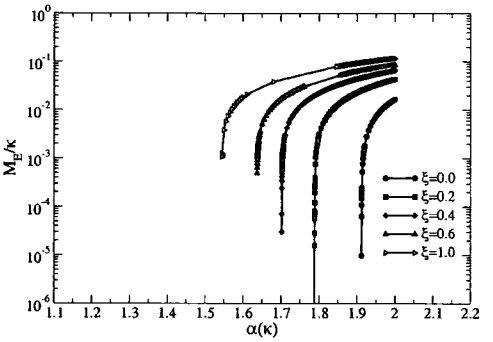

Figure 2.19: Dynamically generated Euclidean mass in the unquenched Ball–Chiu approximation.

In Fig. 2.18 we show solutions in the Landau gauge for couplings close to the critical point $\alpha_c(\xi = 0)$. It is evident that there exist some numerical instabilities in the fermion wave-function. These manifest themselves here due to the difficulty in accurately evaluating the differences of the function for small momenta, and are also partly due to extrapolations employed for the mass-function in the UV, Eq. (2.150). Removing the kink inherent at $p = \kappa$, and introducing suitable extrapolations for $\mathcal{F}$ reduces the presence of the bumps in the infrared.

We solve the $\mathcal{A}$, $\mathcal{B}$, $\mathcal{G}$-system for a selection of gauges, determining the critical coupling α_c. A plot of this is shown in Fig. 2.19, with extracted values listed in Table 2.11.

ξ	α_c	ξ	α_c
0.0	1.91220	0.6	1.63747
0.2	1.78815	1.0	1.54439
0.4	1.70200		

Table 2.11: Critical couplings for the unquenched Ball–Chiu vertex with the WGTI employed in the $\xi q_\mu \Gamma^\mu$ part.

2.4.4 Curtis–Pennington Vertex

The Curtis–Pennington vertex was designed for use in quenched QED, in which it was successful at significantly reducing the gauge dependence of the critical coupling α_c. One is therefore tempted to employ it directly in the unquenched system in the hope that it proves equally successful. The ansatz in this case requires:

$$\begin{aligned}
\lambda_1(k,p) &= \frac{1}{2}\left(\mathcal{A}(k^2)+\mathcal{A}(p^2)\right) , \\
\lambda_2(k,p) &= \frac{1}{2}\frac{1}{k^2-p^2}\left(\mathcal{A}(k^2)-\mathcal{A}(p^2)\right) , \\
\lambda_3(k,p) &= -\frac{1}{k^2-p^2}\left(\mathcal{B}(k^2)-\mathcal{B}(p^2)\right) , \\
\tau_6(k,p) &= \lambda_2(k,p)\frac{(k^2+p^2)\,(k^2-p^2)}{(k^2-p^2)^2+\left(\mathcal{M}^2(k^2)+\mathcal{M}^2(p^2)\right)^2} .
\end{aligned} \tag{2.154}$$

Unfortunately, the transverse piece of this vertex, τ_6, causes problems in the photon equation introducing an unresolvable quadratic divergence. The tack employed in [55], and used elsewhere in other studies, is to form a *hybrid* system. The Ball–Chiu vertex alone is employed in the photon equation, with the CP–vertex used for the fermion SDE.

In Fig. 2.20 we show solutions to $\mathcal{F}$, $\mathcal{M}$ and $\mathcal{G}$ for α close to the critical coupling, in both Landau gauge and Feynman gauge. The gauge dependence of this criticality is portrayed through the Euclidean mass as a function of α for a selection of gauges in Fig. 2.21. Using the approximate scaling law of Eq. (2.149) we found the critical points, and give these in Table 2.12.

ξ	α_c	ξ	α_c
0.0	1.61435	0.6	1.41316
0.2	1.54205	0.8	1.36640
0.4	1.47570	1.0	1.29152

Table 2.12: Critical couplings for the unquenched, unrenormalised hybrid CP-vertex for a variety of gauges.

If we compare the numerical solutions for the hybrid Curtis–Pennington ansatz, Fig. 2.20, with those of the Ball–Chiu vertex, Fig. 2.18, we see that the numerical artefact present in the infrared for $\mathcal{F}(p^2)$ has disappeared. The introduction of the transverse piece of the vertex stabilises the numerical procedure, in addition to improving the convergence of our procedure due to the elimination of local minima in the vicinity of our global one. If we look at solutions in different gauges, for which

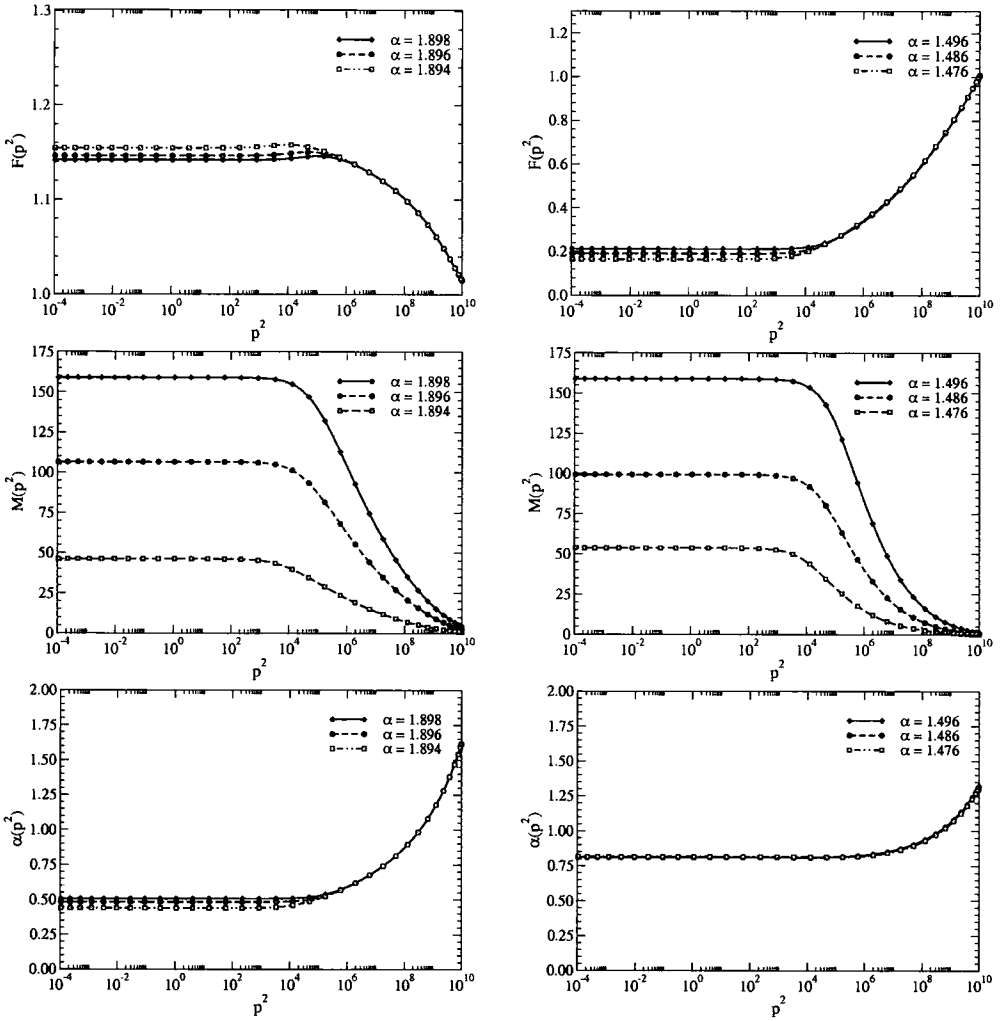

Figure 2.20: Wave-function renormalisation, mass-function and running coupling in Landau Gauge (left-hand side) and Feynman gauge (right-hand side), with the unquenched hybrid Curtis–Pennington vertex.

we compare similar masses $M(0)$, we see the structure of the mass functions are qualitatively similar. However, as with all of the unquenched solutions thus far the photon wave-function renormalisation is significantly different in both the infrared and ultraviolet, being more squat in Feynman gauge despite being a supposedly gauge invariant quantity. We thus must conclude that the violation of gauge invariance is still large for the hybrid CP vertex, despite its success for massless quenched QED.

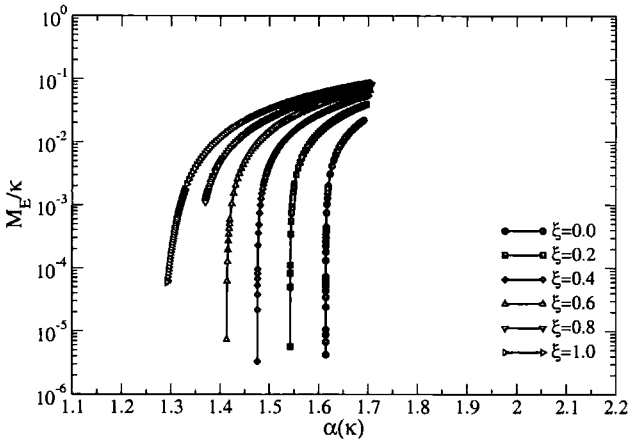

Figure 2.21: Dynamically generated Euclidean mass in the unquenched hybrid–CP approximation.

2.5 Renormalised QED

Up until this point we have not considered the renormalisation of the theory. As it stands, the Green's functions that we have calculated each depend upon the unphysical cut-off κ that we introduced to regulate the integrals. To remedy this we must define our theory at some new scale μ by employing a field renormalisation. This is most readily accomplished by introducing a finite quantity of Z-factors multiplying each of the fields, as in Eqs. (2.41–2.43).

We recall from Sect. 2.2.2 that the vertex ansatz does not trivially respect the notion of multiplicative renormalisability. Thus we may find a residual dependence upon the cut-off, in addition to that arising from the breaking of gauge invariance in part due to the regularisation scheme. Before we proceed with our vertex ansatz that purports to satisfy multiplicative renormalisability, it makes sense to explore simpler ansätze in order to have a fair comparison. In the studies that follow, we will employ a symmetric momentum partition, rather than the asymmetric choice used thus far. It is believed that this will reduce further some spurious terms arising due to the breaking of translational invariance.

In this section we examine the Kızılersü–Pennington vertex with and without dynamical mass generation, in unquenched QED renormalised at the scale $\mu = 10^8$ GeV. We compare this with the bare and hybrid-CP vertices, in addition to a CP/KP hybrid, for a variety of gauges, thus determining the residual gauge dependence of the critical coupling α_c.

2.5.1 Renormalised Bare Vertex approximation

The bare vertex approximation will manifestly break multiplicatively renormalisablity, as may be seen in Eq. (2.69). One of the consequences of this is an explicit dependence of the mass function on the renormalisation point, an artefact since this function should be strictly independent of μ. We do, however, need to gauge the violation of multiplicative renormalisability before we can claim to have improved upon the situation. Thus we make the following study:

$$\begin{aligned}
\mathcal{A}(x) &= Z_2 - Z_1\frac{\alpha_R}{2\pi^2 x}\int_0^{\kappa^2} dy \frac{y\mathcal{A}(y)}{\mathcal{A}^2(y)y+\mathcal{B}^2(y)} \\
&\quad \times \int_0^{\pi} d\psi \sin^2\psi \mathcal{G}(z)\left[\frac{2xy\sin^2\psi}{z^2} - \frac{3\sqrt{xy}\cos\psi}{z}\right] \\
&\quad -Z_1\frac{\alpha_R\xi_R}{4\pi}\int_0^{\kappa^2} dy \frac{1}{\mathcal{A}^2(y)y+\mathcal{B}^2(y)}\left[\frac{y}{x^2}\mathcal{B}(y)\mathcal{B}(x)\Theta_- - \mathcal{A}(y)\mathcal{A}(x)\Theta_+\right] , \\
\mathcal{B}(x) &= Z_2 Z_m m_R + Z_1\frac{3\alpha_R}{2\pi^2}\int_0^{\kappa^2} dy \frac{y\mathcal{B}(y)}{\mathcal{A}^2(y)y^2+\mathcal{B}^2(y)}\int_0^{\pi} d\psi \sin^2\psi\frac{\mathcal{G}(z)}{z} \\
&\quad +Z_1\frac{\alpha_R\xi_R}{4\pi}\int_0^{\kappa^2} dy \frac{1}{\mathcal{A}^2(y)y+\mathcal{B}^2(y)}\left[\frac{y}{x}\mathcal{B}(y)\mathcal{A}(x)\Theta_- + \mathcal{B}(x)\mathcal{A}(y)\Theta_+\right] , \\
\frac{1}{\mathcal{G}(x)} &= Z_3 + Z_1\frac{4N_f\alpha_R}{3\pi^2 x}\int_0^{\kappa^2} dy \frac{y\mathcal{A}(y)}{\mathcal{A}^2(y)y+\mathcal{B}^2(y)} \\
&\quad \times \int_0^{\pi} \sin^2\psi\frac{\mathcal{A}(z)}{\mathcal{A}^2(z)z^2+\mathcal{B}^2(z)}\left[y\left(1-4\cos^2\psi\right)+3\sqrt{xy}\cos\psi\right] ,
\end{aligned}$$

where $Z_1 = Z_2$ through the Ward identity, and the renormalisation procedure is given in Eqs. (2.51, 2.53, 2.56). The coupling α and the gauge ξ are defined at the renormalisation point μ, with critical couplings given in Table 2.13, and a plot of the Euclidean mass in different gauges close to the critical point is given in Fig. 2.22.

Note that here we are using the gauge parameter renormalised at μ; to compare

$\xi(\mu)$	$\alpha_c(\mu)$		$\xi(\kappa)$	$\alpha_c(\kappa)$
0.0	0.97615	$\leftrightarrow$	0.0	1.89575
0.6	0.91443	$\leftrightarrow$	0.35	1.55221
0.8	0.89251	$\leftrightarrow$	0.49	1.46485
1.0	0.87083	$\leftrightarrow$	0.63	1.38847

Table 2.13: Critical couplings for the unquenched, renormalised bare vertex for a variety of gauges.

these calculations with the unrenormalised ones, we must run the gauge from μ to κ,

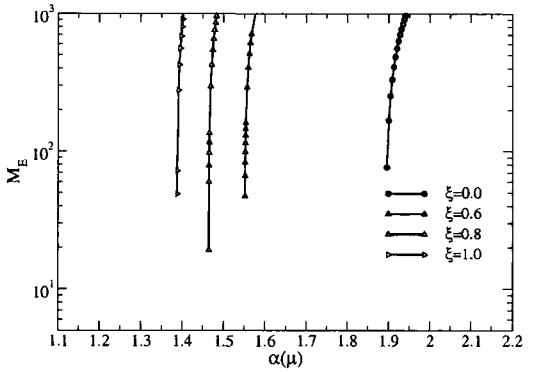

Figure 2.22: Dynamically generated Euclidean mass in the unquenched bare vertex approximation with symmetric momentum routing in the photon equation. The coupling is given at $\alpha(\kappa)$, with gauge defined at $\xi(\mu)$.

in the same manner that the coupling is run. To do this we use the renormalisation group invariant $\alpha\xi = \alpha_R\xi_R$.

2.5.2 Renormalised Curtis–Pennington Vertex

The kinematic structure of the CP vertex is such that it may not be used in the photon equation without introducing a quadratic divergence, so as before we employ the Ball–Chiu vertex in the renormalised photon equation, with the CP-vertex in the fermion SDE.

This vertex is constructed to satisfy multiplicative renormalisability of the mass function and wave-function renormalisation, up to leading and next-to-leading logarithms, for quenched QED. We saw the improvement this made to the gauge invariance of the critical coupling in Fig. 2.10. To date, the hybrid model represented the pinnacle of vertex ansätze for the unquenched theory. Unfortunately, in this case we found there still to be significant gauge dependence, Fig. 2.21.

First, let us investigate the case without mass generation and so determine the extent of gauge dependence in the $(\mathcal{F}, \mathcal{G})$ system. In Fig. 2.23 we see solutions for four different gauges with this ansatz employed. The fermion wave-function renormalisation depends upon the gauge parameter ξ, as it should. However, the photon wave-function renormalisation should be *independent* of our gauge choice due to covariance. It is clear that this is not the case, with the function depending strongly upon changes in the gauge.

Considering now solutions exhibiting mass generation, we see representative solutions in both Landau and Feynman gauge in Fig. 2.25. We determined the critical value for the coupling in a number of gauges by plotting the Euclidean mass against

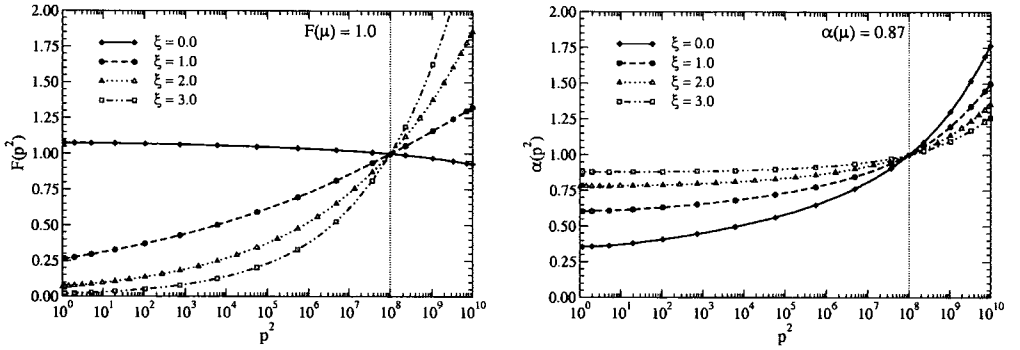

Figure 2.23: Wave-function renormalisation and running coupling in a variety of gauges for the symmetric momentum partition. We have employed the Curtis–Pennington vertex.

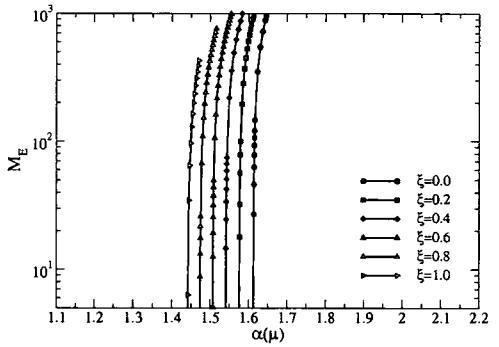

Figure 2.24: Dynamically generated Euclidean mass in the unquenched hybrid CP approximation with symmetric momentum partition in the photon equation. The coupling is given at $\alpha(\kappa)$, with gauge defined at $\xi(\mu)$.

coupling, Fig. 2.24, and using the mean-field scaling law of Eq. (2.149). We present the results for the critical coupling in Table 2.14. Comparing these renormalised

$\xi(\mu)$	$\alpha_c(\mu)$		$\xi(\kappa)$	$\alpha_c(\kappa)$
0.0	0.87127	$\leftrightarrow$	0.0	1.61346
0.2	0.88302	$\leftrightarrow$	0.11	1.57683
0.4	0.89263	$\leftrightarrow$	0.23	1.54146
0.6	0.89827	$\leftrightarrow$	0.36	1.50705
0.8	0.90348	$\leftrightarrow$	0.49	1.47357
1.0	0.90681	$\leftrightarrow$	0.63	1.44091

Table 2.14: Critical couplings for the unquenched, renormalised hybrid CP/BC vertex for a variety of gauges.

solutions with the unrenormalised ones Fig. 2.20 we see that the flattening with increasing ξ of the photon wave-function renormalisation is not so severe. One

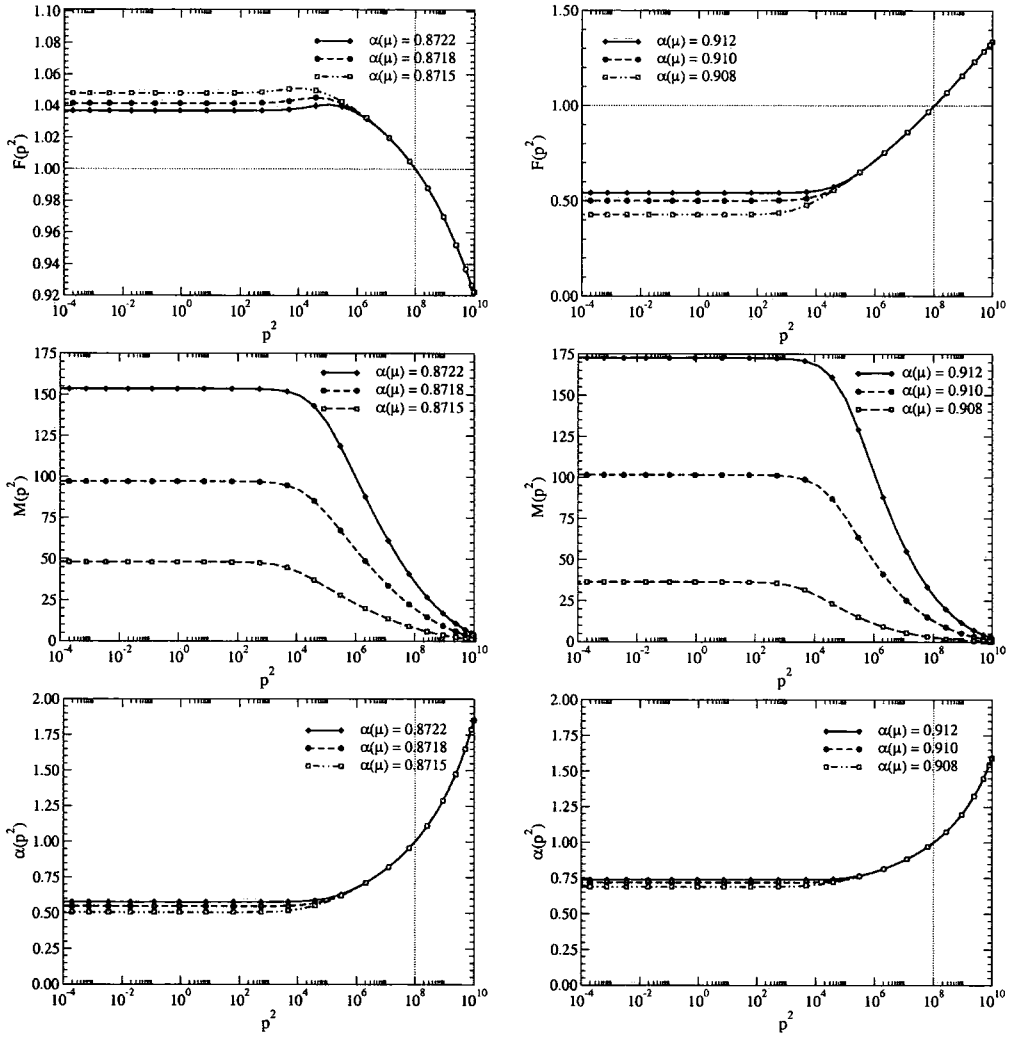

Figure 2.25: Wave-function renormalisation, mass-function and running coupling in Landau Gauge (left-hand side) and Feynman gauge (right-hand side), with the unquenched hybrid CP vertex.

concludes that the renormalisation procedure subtracts away some of the spurious dependence upon the cut-off due to the regularisation procedure, though with this vertex not satisfying MR some will remain.

2.5.3 Renormalised Kızılersü–Pennington Vertex

Our final ansatz is that of Kızılersü and Pennington, whose properties and construction we discussed in Sect. 2.2.3. It is designed primarily to satisfy multiplicative renormalisability for the fermion and photon wave-functions, in the massless limit.

Since it is built upon the Ball–Chiu vertex, it automatically satisfies the Ward-Green-Takahashi identity together with the Ward identity. In terms of our standard set of basis vectors, we employ the following coefficients in our projections of the Schwinger-Dyson equations:

$$\begin{aligned}
\tau_2\left(p^2,k^2,q^2\right) &= -\frac{4}{3}\frac{2\lambda_2\left(k^2,p^2\right)}{\left(k^2+p^2\right)} - \frac{1}{3}\frac{2\lambda_1\left(k^2,p^2\right)}{\left(k^2+p^2\right)^2}\ln\left(\frac{\mathcal{A}(k^2)\mathcal{A}(p^2)}{\mathcal{A}^2(q^2)}\right), \\
\tau_3\left(p^2,k^2,q^2\right) &= -\frac{5}{12}2\,\lambda_2\left(k^2,p^2\right) - \frac{1}{6}\frac{2\lambda_1\left(k^2,p^2\right)}{\left(k^2+p^2\right)}\ln\left(\frac{\mathcal{A}(k^2)\mathcal{A}(p^2)}{\mathcal{A}^2(q^2)}\right), \\
\tau_6\left(p^2,k^2,q^2\right) &= \frac{1}{4}\frac{\left(k^2-p^2\right)}{\left(k^2+p^2\right)}2\,\lambda_2\left(k^2,p^2\right), \\
\tau_8\left(p^2,k^2,q^2\right) &= 0\,. \qquad (2.155)
\end{aligned}$$

The functions λ_1, λ_2 and λ_3 are defined as:

$$\begin{aligned}
\lambda_1\left(k^2,p^2\right) &\equiv \frac{1}{2}\left[\mathcal{A}(k^2)+\mathcal{A}(p^2)\right], \\
\lambda_2\left(k^2,p^2\right) &\equiv \frac{1}{2}\frac{1}{k^2-p^2}\left[\mathcal{A}(k^2)-\mathcal{A}(p^2)\right], \\
\lambda_3\left(k^2,p^2\right) &\equiv -\frac{1}{k^2-p^2}\left[\mathcal{B}(k^2)-\mathcal{B}(p^2)\right]. \qquad (2.156)
\end{aligned}$$

which also play the rôle of the longitudinal coefficients.

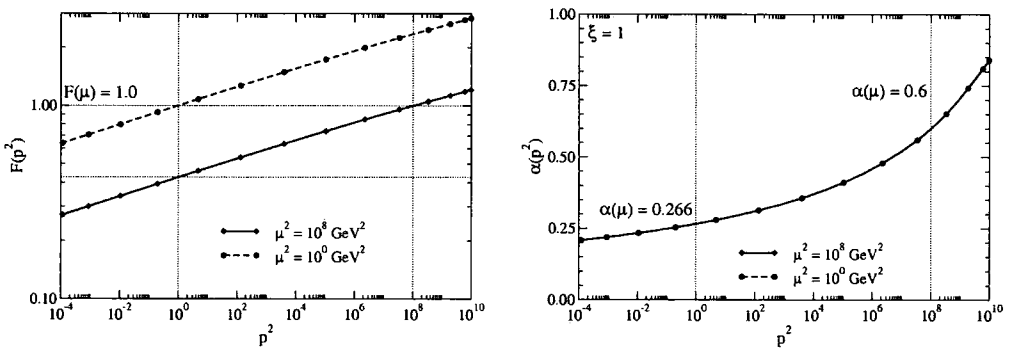

Figure 2.26: The wave-function renormalisation and running coupling calculated in Feynman gauge with the KP vertex, at two different renormalisation points $\mu^2 = 10^0$ and $\mu^2 = 10^8$ GeV^2. The coupling remains identical, with the two fermion wave-functions related by the expected scale factor, Z_2.

First, let us consider massless solutions in some gauge $\xi \neq 0$. We can solve the resulting system for $\mathcal{F}$ and $\mathcal{G}$ at a renormalisation scale, which we choose to be $s = \mu^2 = 10^8$ GeV^2. We must check that we may change to a new renormalisation point, $t = \mu'^2 = 1$ GeV^2 say, and that our functions are either invariant, or scale

correctly. In Fig. 2.26 we show this for Feynman gauge, and indeed see from the log plot that $\mathcal{F}$ scales with the expected renormalisation factor Z_2. Additionally, we find that the running coupling $\alpha(p^2) = \alpha(\mu^2)\mathcal{G}(p^2, \mu^2)$ remains invariant.

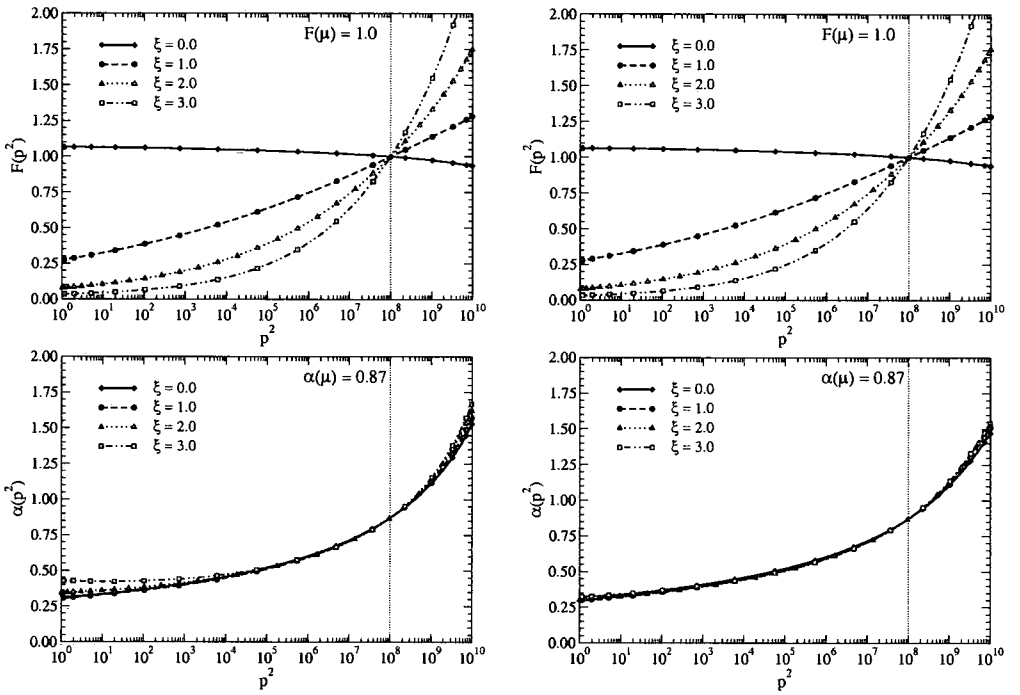

Figure 2.27: Wave-function renormalisation and running coupling in a variety of gauges for the asymmetric (left) and symmetric (right) momentum partition. We have employed the Kızılersü–Pennington vertex

The KP vertex is inspired by the requirement that multiplicative renormalisability be upheld. It is hoped that the structure required to achieve this will improve gauge invariance, in much the same way as achieved by the CP vertex. To test this, we calculate both $\mathcal{F}$ and $\mathcal{G}$ iteratively in a number of gauges for a fixed coupling, defined at renormalisation point $\mu^2 = 10^8$ GeV^2. The results can be seen in Fig. 2.27, with the left panel calculated for the asymmetric momentum partition $\eta = 0$, and the right panel for symmetric momenta $\eta = 1/2$. We can see that the dependence of the coupling α on ξ is significantly reduced, as compared to the Curtis–Pennington vertex of Fig. 2.23. One may also see that the symmetric momentum partition performs better than the asymmetric choice, with the contribution due to spurious terms in our regularisation procedure reduced.

2.5.4 KP-vertex with Mass Generation

We have demonstrated the efficacy of this ansatz for QED in the massless case, and so we now wish to investigate its properties when dynamical mass generation is realised. In Fig. 2.28 we give examples of $\mathcal{F}$, $\mathcal{M}$ and $\mathcal{G}$ for a selection of couplings close to the critical point α_c, with the left-hand side corresponding to Landau gauge, and the right for Feynman gauge.

The solutions with the KP vertex are similar to those of the CP vertex, with the spurious numerical artefacts from the BC part of the vertex removed. We do see

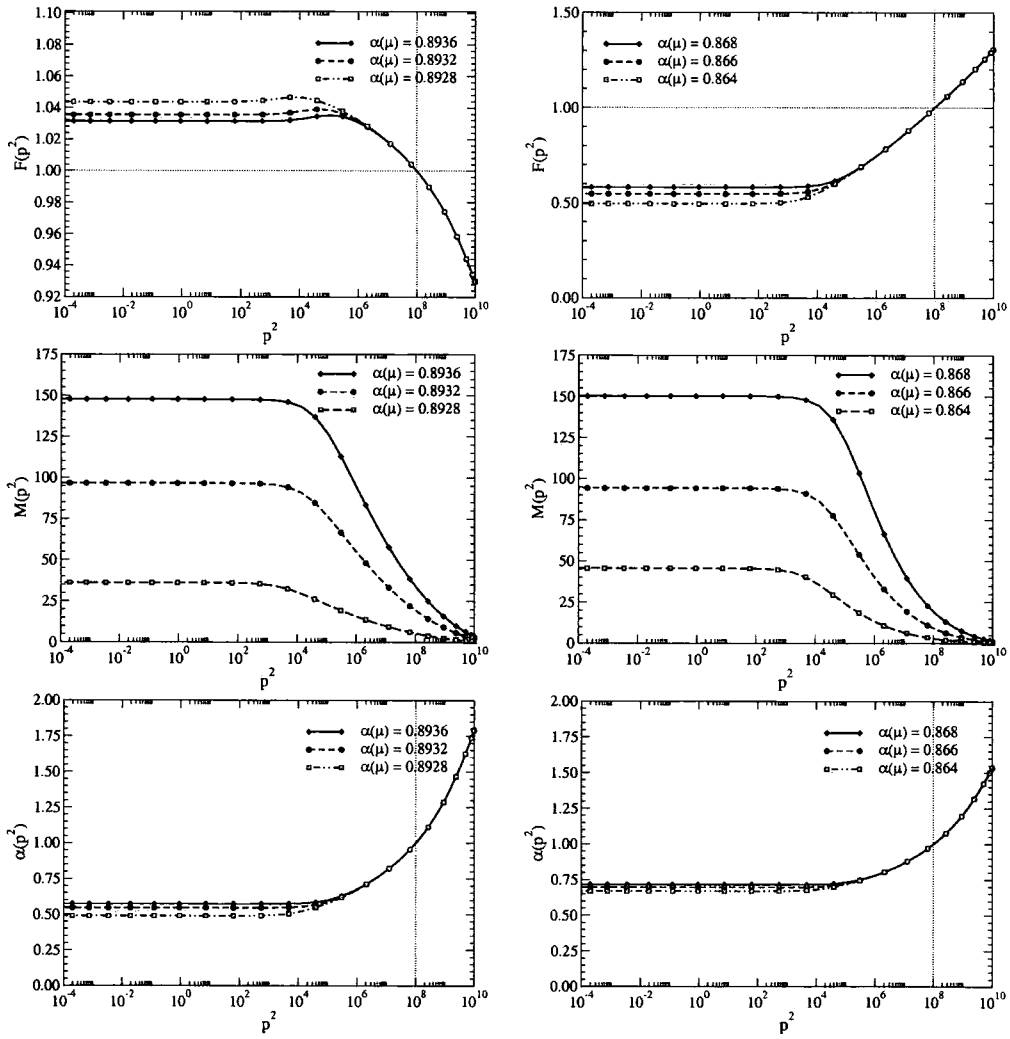

Figure 2.28: Wave-function renormalisation, mass-function and running coupling in Landau Gauge (left-hand side) and Feynman gauge (right-hand side), with the unquenched Kızılersü–Pennington vertex.

$\xi(\mu)$	$\alpha_c(\mu)$		$\xi(\kappa)$	$\alpha_c(\kappa)$
0.0	0.90567	$\leftrightarrow$	0.0	1.57830
0.2	0.89071	$\leftrightarrow$	0.12	1.54203
0.4	0.87650	$\leftrightarrow$	0.23	1.50726
0.6	0.86290	$\leftrightarrow$	0.35	1.47359
0.8	0.84950	$\leftrightarrow$	0.47	1.44023
1.0	0.83658	$\leftrightarrow$	0.59	1.40804

Table 2.15: Critical couplings for the unquenched, renormalised KP vertex for a variety of gauges, with partition $\eta = 1/2$.

$\xi(\mu)$	$\alpha_c(\mu)$		$\xi(\kappa)$	$\alpha_c(\kappa)$
0.0	0.89592	$\leftrightarrow$	0.0	1.61493
0.2	0.88206	$\leftrightarrow$	0.11	1.57685
0.4	0.86830	$\leftrightarrow$	0.23	1.53707
0.6	0.85500	$\leftrightarrow$	0.34	1.50534
0.8	0.84200	$\leftrightarrow$	0.46	1.47228
1.0	0.82914	$\leftrightarrow$	0.58	1.43966

Table 2.16: Critical couplings for the unquenched, renormalised KP vertex for a variety of gauges, with partition $\eta = 0$.

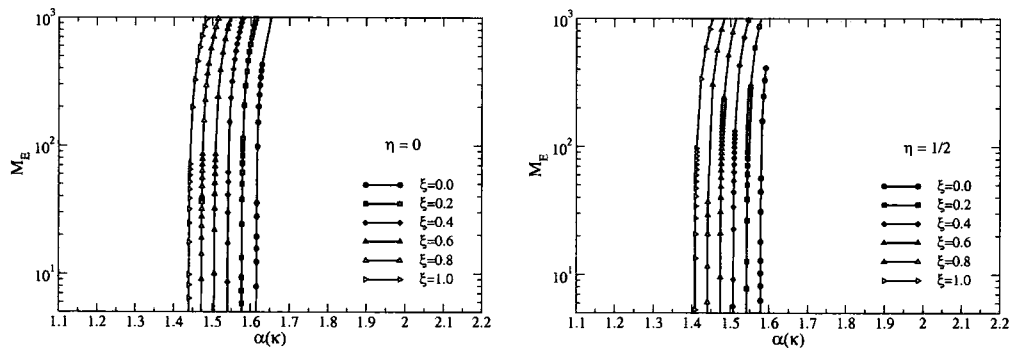

Figure 2.29: Dynamically generated Euclidean mass in the unquenched KP approximation with asymmetric (left) and symmetric (right) momentum partition in the photon equation. All couplings are given at $\alpha(\kappa)$, with the gauge defined at $\xi(\mu)$ – see Tables 2.15 and 2.16.

with like-for-like masses generated, that the photon wave-function renormalisation is different for these two gauges, with this reflected in the value of the critical coupling in Table 2.15. The dependence of the Euclidean mass on the coupling is shown in Fig. 2.29 for symmetric momentum partition (right) and asymmetric momentum partition (left). Consequently, the critical couplings for the asymmetric partition are given in Table 2.16.

2.5.5 Hybrid CP/KP vertex

The KP vertex appears to be somewhat lacking is preserving gauge invariance where dynamical mass generation is concerned. We thus form a hybrid system, in which the CP vertex is used in the fermion SDE, with the KP vertex utilized in the photon SDE, with $\eta = 1/2$. It is hoped that, since both these ansätze are formulated in different momentum regimes appropriate to their particular SDE, that this hybrid system will prove a useful combination.

In Fig. 2.30 we show solutions close to the critical coupling α_c for both Landau

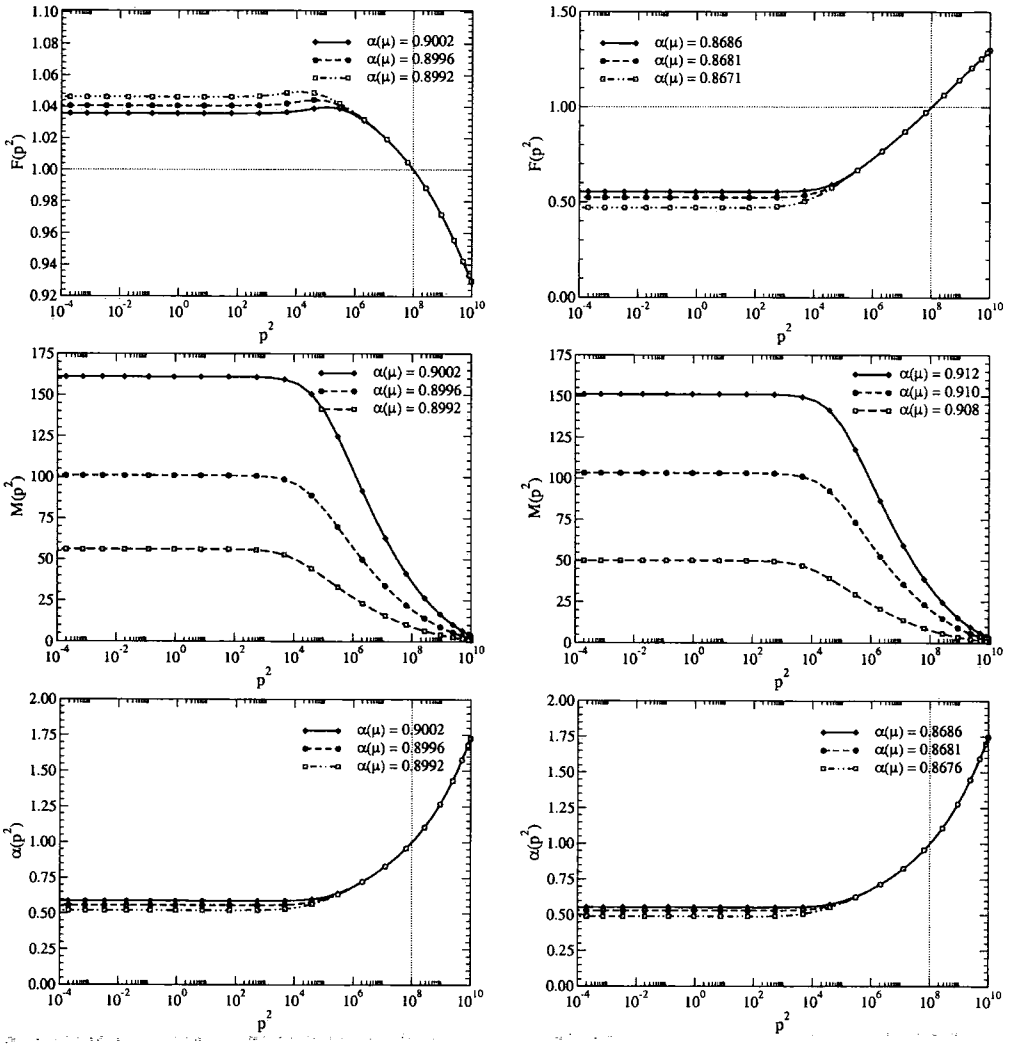

Figure 2.30: Wave-function renormalisation, mass-function and running coupling in Landau Gauge (left-hand side) and Feynman gauge (right-hand side), with the unquenched CP/KP hybrid vertex.

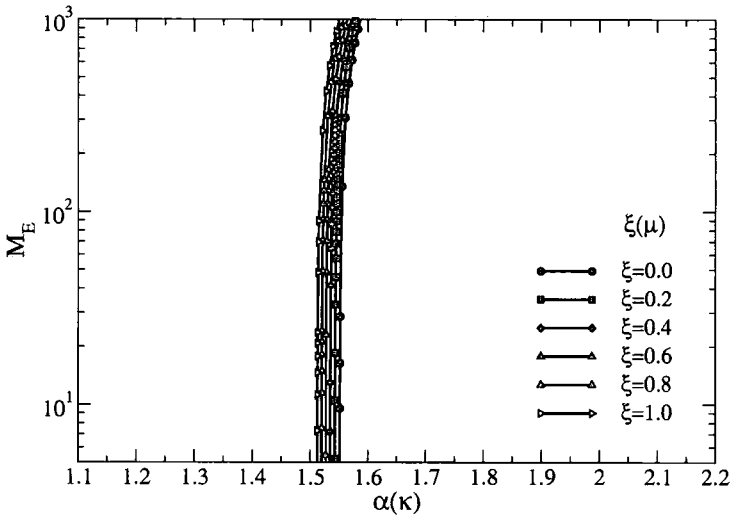

Figure 2.31: Dynamically generated Euclidean mass in the unquenched hybrid CP/KP approximation with symmetric momentum partition in the photon equation. The coupling is given at $\alpha(\kappa)$, with gauge defined at $\xi(\mu)$.

$\xi(\mu)$	$\alpha_c(\mu)$		$\xi(\kappa)$	$\alpha_c(\kappa)$
0.0	0.89860	$\leftrightarrow$	0.0	1.55043
0.2	0.89130	$\leftrightarrow$	0.12	1.54214
0.4	0.88450	$\leftrightarrow$	0.23	1.53399
0.6	0.88720	$\leftrightarrow$	0.35	1.52618
0.8	0.87268	$\leftrightarrow$	0.46	1.51972
1.0	0.86726	$\leftrightarrow$	0.57	1.51260

Table 2.17: Critical couplings for the unquenched, renormalised hybrid CP/KP vertex for a variety of gauges, with partition $\eta = 1/2$.

and Feynman gauge. We see that this choice of hybrid vertex exhibits the same qualitative features as our other ansätze. The real difference lies in the residual gauge dependence of the critical coupling. Crucially, we now see strong similarity between the photon wave-function renormalisation in different gauges, in contrast with results of our other vertices. We plot the Euclidean mass as a function of the coupling for a selection of gauges in Fig. 2.31, and give numerical values in Table 2.17. We clearly see that this combination significantly reduces the gauge variance of the critical coupling, *cf.* Figs. 2.22, 2.24 and 2.29, though the actual magnitude depends on the scale at which α_c is measured.

It appears that, even in the unquenched theory, it is the CP-vertex is most apposite for the fermion SDE. Though it does not know anything about the photon and its renormalisation, it is its ability to preserve MR of the fermion mass-function

that appears to be most important. For the photon SDE, it is the KP-vertex's ability to preserve MR for the photon and fermion wave-function renormalisations that is key, with knowledge of the mass-function less relevant. Learning lessons from the construction of both vertices – to produce a consistent ansatz respecting multiplicative renormalisability of all three scalar functions $\mathcal{A}, \mathcal{B}, \mathcal{G}$ – is the obvious next step in future studies.

2.6 Summary

We presented the fermion-boson vertex of QED in detail, giving a summary of the construction of non-perturbative ansätze that are most commonly used in the literature. To this we added the Kızılersü–Pennington vertex whose form is such that it preserves the multiplicative renormalisability of $\mathcal{F}$ and $\mathcal{G}$ in the massless limit.

We investigated this novel truncation scheme, in addition to a selection of vertex ansätze, in both quenched and unquenched QED. Our analysis concentrated primarily upon the numerical solution of the Schwinger-Dyson equations for the propagators, in which we systematically changed the coupling in order to find α_c as a function of the gauge parameter. To quantify the residual dependence of α_c upon the gauge, we form the quantity:

$$\Delta = \left| \frac{\alpha_c^{(\xi_{0,R}=1)}(\kappa)}{\alpha_c^{(\xi_{0,R}=0)}(\kappa)} - 1 \right| / \delta\xi \,, \tag{2.157}$$

where $\delta\xi$ is the difference between the two ξ at momentum κ and is typically 1 when unrenormalised, or ~ 0.6 at the renormalisation point $\mu = 10^4$ GeV.

For the quenched studies, we looked at the bare-vertex approximation for which a sizeable dependence upon the gauge choice was found, which we quantify with a Δ of $61 - 96\%$ depending on our use of the WGTI. Employing the CP vertex, one could determine either through brute force numerical methods or by a bifurcation analysis, the critical coupling as a function of the gauge parameter. It was seen that the violation of gauge invariance is significantly reduced, yielding $\Delta = 4.8\%$. As a precursor to unquenched studies, we looked at the KP-vertex in the context of quenched QED. Although performing better than the simplest vertex ansatz, with $\Delta = 30\%$, we found that the logarithmic pieces of the ansatz are not well-suited to the quenched theory, though this vertex shares some favourable characteristics to the CP vertex, such as MR of the wave-function renormalisation in the chirally

symmetric phase.

We continued our investigation by reviewing calculations in unquenched and unrenormalised QED, typically restricted to the Landau gauge in the literature, and looked at the gauge dependence of the critical coupling as a function of the gauge parameter. We began with the bare-vertex approximation, and found that $\Delta = 16\%$. Introducing a minimal dressing of the first longitudinal piece worsened the situation, yielding $\Delta = 52\%$. We thus considered the full Ball–Chiu ansatz, requiring careful treatment of numerical singularities in the photon equation, for a range of ξ. The gauge dependence of α_c was quantified by $\Delta = 24\%$. Looking at the hybrid CP vertex, where the BC vertex is used in the photon equation due to quadratic divergences, we finally found $\Delta = 25\%$ with this ansatz.

To conclude our studies of unquenched QED, we chose to renormalise our theory at the point $\mu^2 = 10^8$ GeV^2. Finding solutions once again for the bare-vertex approximation, this time with symmetric momentum partition in the photon equation, yielded a deviation of 58% as determined by Eq. (2.157). This is exacerbated here by the manifest violation of multiplicative renormalisability. We then considered the hybrid CP/BC vertex, finding this time that $\Delta = 19\%$. The Kızılersü–Pennington vertex was examined for both symmetric and asymmetric momentum partition in the photon equation, yielding $\Delta = 20\%$ and $\Delta = 21\%$ respectively. Despite performing exceptionally well in the absence of dynamical mass generation, maintaining near gauge invariance of the photon wave-function renormalisation, its lack of respect for MR of massive fermions seems to indicate a shortcoming. Motivated by the hybrid CP/BC vertex, we formulated a new hybrid ansatz employing the CP vertex in the fermion SDE, for whose momentum regions it is designed, using only the KP vertex in the photon SDE. This combination resulted in a significant improvement, as quantified by a Δ of only 4.4%.

It is envisaged that improvements to the KP vertex that will respect multiplicative renormalisability of the fermion mass-function will improve the gauge invariance of the critical coupling further. We will then have a tool that (approximately) satisfies the symmetries of the underlying field theory, which will allow one to investigate in detail the phase structure and triviality of unquenched QED on the inclusion of irrelevant operators.

Chapter 3

QED in Three Dimensions

Three dimensional QED is an interesting theory for a multitude of reasons. In the study of finite temperature field theories, it has been proposed that at high temperatures the four dimensional formulation reduces to that of three dimensions [61], so long as the coupling α is small and we look at distances greater than the Debye screening length $T/\sqrt{\alpha}$. Interest in QED_3 has enjoyed a resurgence in popularity with potential applications to condensed matter physics, for example in certain cuprate superconductors where the conductivity is confined to a two-dimensional plane [62–65].

Of more pedagogical importance are the characteristics intrinsic to this theory. It is quite different to its four dimensional cousin for, despite being an Abelian gauge theory, its compact version exhibits the property of confinement [66–69] with the non-compact formulation realising dynamical symmetry breaking [70], at least for a small number of fermion flavours. Moreover, in three dimensions this theory is super-renormalisable and so avoids the additional complication of UV regularisation of the quantum field theory, as this can obscure the connection between the intrinsic scales and those that appear as a consequence of symmetry breaking. Since we have one fewer spatial dimension, the coupling becomes dimensionful, which may be useful for the study of dynamical mass generation in GUTs where we can link the natural scale of the theory to the scale of generated masses.

Here we do not consider compact QED in three dimensions. Instead, we concentrate on the non-compact version at zero temperature where the criticality of the theory is of interest. Here dynamical mass generation occurs for a small number of active fermions in the loop corrections to the photon propagator, with potential for some critical point N_f^{crit}. The degree of mass generation is measured by the correlator $\langle\bar{\psi}\psi\rangle$. This correlator may depend upon the parameter N_f, but of course should

be gauge independent since it is reasoned to be a physical observable. There have been many studies of the hierarchy of mass generation in this theory [71–76] and several lattices studies have been performed [77–79]. These have taken a number of different approaches to the problem at hand – one of identifying the existence of a second order phase transition. Each have come to different conclusions.

Extensive investigations have been employed using the SDE approach to non-perturbative phenomena. The SDE studies of [71,72] employed the $1/N_f$ expansion to leading order, when the fermion wave-function renormalisation was taken to be identically 1. Following some further simplifications and writing the SDE as a differential equation, the critical value for the number of active fermions could be determined to be $N_f^{crit} = 32/\pi^2 \simeq 3.24$. Higher order corrections were considered [80] which modified the result to $N_f^{crit} \simeq 3.28$, supporting convergence of the expansion within this approximation scheme.

However, the existence of a critical number of active fermions in non-compact QED_3 was contested in [73,81] where they argue that the $1/N_f$ expansion is a poor approximation for momenta $p \ll M(0)$, the region of importance for dynamical breaking of chiral symmetry. Indeed, it was argued that the fermion wave-function renormalisation could contribute large $\mathcal{O}(N_f)$ corrections, a possibility that could be equally true for the mass function. It was suggested that the scale of the dynamically generated mass m was related to the number of flavours via:

$$\log M(0) \sim -N_f\,, \tag{3.1}$$

that is, the mass function decreases exponentially as a function of the number of flavours. This behaviour is a numerical challenge in Schwinger-Dyson studies, for we must work with a large momentum range. The scale poses an even greater challenge for calculations performed on the lattice, necessitating huge volumes to work with such potentially small masses. It has also been suggested that finite volume effects may lead to an artificial phase transition on the lattice [82].

In the literature there have been many attempts to determine N_f^{crit} through methods other than SDE and the Lattice. A renormalisation group analysis [83] suggests that the critical number of flavours may fall in the range $3 \leq N_f^{crit} \leq 4$. If one considers the inequality $f_{IR} \leq f_{UV}$, where f is the thermodynamic free energy, one finds through counting of the number of degrees of freedom that $N_f^{crit} \leq 3/2$. However, this inequality may be inapplicable due to the system not being weakly interacting [84]. One further approach is to draw analogy between QED_3 and the Thirring model, which has the same breaking of global symmetries. Numerical

studies [85–87] suggest $4 \leq N_f^{crit} \leq 6$.

Calculations of non-compact QED_3 performed on the lattice have been performed for a number of integer values of N_f, recently for $N_f = 2$ [88] and $N_f = 1, 4$ [79]. Though evidence for dynamical symmetry breaking is found for $N_f = 1$, the condensate is too small to be determined on the lattice for $N_f = 2$, placing only an upper bound. For $N_f = 4$ it was hoped that qualitative differences would be evident, though if the condensate does drop off exponentially, as in Eq. (3.1), the computational requirements for $N_f \geq 2$ may be too demanding to say anything definitive.

In the next few sections we will first highlight the differences between compact and non-compact formulations of QED_3, thus motivating our choice of study. We present the Landau-Khalatnikov-Fradkin (LKF) transformation in momentum space, which we will use to explore the gauge covariance of our numerical solutions. We then perform extensive numerical calculations of quenched and unquenched three dimensional QED, in different gauges. We finish with a short corollary of the LKF transformation that confirms some of our numerical findings.

3.1 Compact/Non-Compact

Since our gauge theory here is still that of Quantum Electrodynamics, irrespective of the number of space-time dimensions, our Lagrangian is still written:

$$\mathcal{L}_{QED_3} = \bar{\psi}(i\gamma^\mu D_\mu)\psi - \frac{1}{4}F_{\mu\nu}F^{\mu\nu} - \frac{1}{2\xi}(\partial_\mu A^\mu)^2 \ . \tag{3.2}$$

However, as a result of having one fewer spatial dimensions, QED in three dimensions is a very different theory to that of its four dimensional counterpart. We have already touched upon some of these differences, which we will further investigate numerically, but for now discuss the composition of the three dimensional theory. It turns out that the choice of representation is very important in QED_3, for in the construction of the Dirac equation it is only necessary to have *three* γ matrices. It is thus possible to write the 2×2 representation, in terms of the Pauli sigma matrices:

$$\gamma^0 = \sigma_3 \ , \qquad \gamma^1 = i\sigma_1 \ , \qquad \gamma^2 = i\sigma_2 \tag{3.3}$$

which satisfies the Clifford algebra $\{\gamma^\mu, \gamma^\nu\} = 2g^{\mu\nu}$, with $g^{\mu\nu} = \mathrm{diag}\,(1, -1, -1)$ the metric.

However, if we restrict ourselves to the 2×2 representation, we find there are no

remaining 2×2 matrices that anti-commute will all of our γ^ν. This is significant, for it means there is no generator of the chiral symmetry that may be broken by a mass term of the form $m\bar{\psi}\psi$. Thus the massive theory in the 2×2 representation contains the same symmetries as the massless one, trivialising the phase structure.

Since our interest lies with the dynamical generation of mass, it is necessary to formulate three dimensional QED using the 4×4 representation familiar to QED. Here one could choose the Weyl representation of the γ matrices to be:

$$\gamma^0 = \begin{pmatrix} \sigma_3 & 0 \\ 0 & -\sigma_3 \end{pmatrix}, \qquad \gamma^1 = \begin{pmatrix} i\sigma_1 & 0 \\ 0 & -i\sigma_1 \end{pmatrix}, \qquad \gamma^2 = \begin{pmatrix} i\sigma_2 & 0 \\ 0 & -\sigma_2 \end{pmatrix}. \quad (3.4)$$

This time we have the choice of two 4×4 matrices that anti-commute with the γ^0, γ^1 and γ^2:

$$\gamma^3 = i\begin{pmatrix} 0 & \mathbb{I} \\ \mathbb{I} & 0 \end{pmatrix}, \qquad \gamma^5 = i\begin{pmatrix} 0 & \mathbb{I} \\ -\mathbb{I} & 0 \end{pmatrix}. \quad (3.5)$$

and so our (massless) Lagrangian is invariant under a global $U(2N_f)$ symmetry with the generators 1, γ^3, γ^5, $[\gamma^3, \gamma^5]$. We could break this with a mass term of the form:

$$m\bar{\psi}\left[\gamma^3, \gamma^5\right]\psi, \quad (3.6)$$

though this is not invariant under parity. Thus we introduce the usual mass term of the form $m\bar{\psi}\psi$ to our Lagrangian:

$$\mathcal{L}_{QED_3} = \bar{\psi}(i\gamma^\mu D_\mu - m)\psi - \frac{1}{4}F_{\mu\nu}F^{\mu\nu} - \frac{1}{2\xi}\left(\partial_\mu A^\mu\right)^2 . \quad (3.7)$$

This is of the same form as four dimensional QED in the previous section, other than having a different space-time dimension d.

3.1.1 LKFT in momentum space

It has been shown that for QED in three dimensions, where the integrals are manifestly convergent, that the LKF transformation may be applied directly in momentum space [89], so long as one makes positive shifts in the gauge parameter. If we wish to perform a negative shift in the gauge parameter, it is necessary to Fourier transform our momentum space Green's functions to coordinate space, apply the LKF transform directly, and then Fourier transform back [90].

In order to derive the momentum space LKF transformation, we start with the usual expressions for the fermion propagator, which in both coordinate and

momentum space are written:

$$\begin{aligned} S(x;\xi) &= \not{x} X(x;\xi) + Y(x;\xi) && (3.8) \\ S(p;\xi) &= \frac{\mathcal{F}(p;\xi)}{i\not{p} - \mathcal{M}(p;\xi)} \\ &= -i\not{p} K_X(p;\xi) + K_Y(p;\xi)\,, && (3.9) \end{aligned}$$

where the functions $K_{X,Y}(p;\xi)$ are related to the parameterisations $\mathcal{F}(p;\xi)$ and $\mathcal{M}(p;\xi)$ by:

$$K_X(p,\xi) = \frac{\mathcal{F}(p;\xi)}{p^2 + \mathcal{M}^2(p;\xi)}\,, \tag{3.10}$$

$$K_Y(p,\xi) = \frac{\mathcal{F}(p;\xi)\mathcal{M}(p;\xi)}{p^2 + \mathcal{M}^2(p;\xi)}\,. \tag{3.11}$$

These two representations are related via the usual Fourier transforms:

$$S(x;\xi) = \int \frac{d^3p}{(2\pi)^3} e^{-ip\cdot x} S(p;\xi)\,, \tag{3.12}$$

$$S(p;\xi) = \int d^3p\; e^{ip\cdot x} S(x;\xi)\,. \tag{3.13}$$

It is obvious that these Fourier transforms also relate the individual components of the propagator.

In coordinate space, the LKF transformation is given by:

$$S(x;\xi) = e^{-ax} S(x;0)\,, \tag{3.14}$$

where $a = \alpha\xi/8\pi$, and we assume the propagator starts in Landau gauge. If we start in a covariant gauge ξ_0 then one simply replaces ξ by $\xi - \xi_0$ in the following Eqs. (3.17–3.19). Since we have that

$$\begin{aligned} X(x;0) &= -\frac{i}{(2\pi)^3 x^2} \int d^3p\; e^{-ip\cdot x} p\cdot x K_X(p;0)\,, \\ Y(x;0) &= -\frac{1}{(2\pi)^3} \int d^3p\; e^{-ip\cdot x} K_Y(p;0)\,, \end{aligned} \tag{3.15}$$

which on performing some trivial angular integrations yields:

$$\begin{aligned} X(x;0) &= \frac{1}{2\pi^2 x^2}\int_0^\infty dp\, p^2 \left(\cos px - \frac{\sin px}{px}\right) K_X(p;0)\,, \\ Y(x;0) &= -\frac{1}{2\pi^2}\int_0^\infty dp\, p^2 \left(\frac{\sin px}{px}\right) K_Y(p;0)\,, \end{aligned} \tag{3.16}$$

we can use Eq. (3.14) to move from Landau gauge to a more general gauge:

$$\begin{aligned} X(x;\xi) &= \frac{e^{-ax}}{2\pi^2 x^2}\int_0^\infty dp\, p^2 \left(\cos px - \frac{\sin px}{px}\right) K_X(p;0) \\ Y(x;\xi) &= -\frac{e^{-ax}}{2\pi^2}\int_0^\infty dp\, p^2 \left(\frac{\sin px}{px}\right) K_Y(p;0)\,. \end{aligned} \tag{3.17}$$

Using the inverse Fourier transform of Eq. (3.12) applied to the components $K_{X,Y}$:

$$\begin{aligned} K_X(p;\xi) &= \int d^3x\, e^{ip\cdot x} X(x;\xi)\,, \\ K_Y(p;\xi) &= \int d^3x\, e^{ip\cdot x} Y(x;\xi)\,. \end{aligned} \tag{3.18}$$

So long as the LKF transformation parameter $a > 0$, the integrals are convergent and we can swap the x and p integrations:

$$\begin{aligned} K_X(p;\xi) &= \frac{a}{\pi p^2}\int_0^\infty dk k^2 K_X(k;0)\left[\frac{1}{a_+} + \frac{1}{a_-} + \frac{1}{2kp}\log\left|\frac{a_-}{a_+}\right|\right], \\ K_Y(p;\xi) &= \frac{a}{\pi p}\int_0^\infty dk k K_Y(k;0)\left[\frac{1}{a_-} - \frac{1}{a_+}\right], \end{aligned} \tag{3.19}$$

where we have employed the shorthand $a_\pm = a^2 + (k \pm p)^2$.

3.2 Numerical Review

There are extensive examples in the literature of numerical determinations of QED_3 for a variety of different vertex ansätze and approximations. As with most non-perturbative studies, we start with the simplest system and proceed to relax these restrictions or improve upon our assumptions. We thus start with the quenched theory, followed by a one-loop dressing of the photon equation and eventually building up to the unquenched system.

In the forthcoming sections it will be necessary to quantify our models by de-

termining the chiral condensate in systems where spontaneous breaking of chiral symmetry is realised. To this end, we use the standard formula:

$$\begin{aligned}\langle\overline{\psi}\psi\rangle = \lim_{x\to 0}\langle 0|\,\bar{\psi}(0)\psi(x)\,|0\rangle &= -\mathrm{Tr}_D\left[S_F(x)\right]_{x\to 0} \\ &= -4\int\frac{d^3k}{(2\pi)^3}\frac{\mathcal{B}(k^2)}{k^2\mathcal{A}^2(k^2)+\mathcal{B}^2(k^2)}\,, \end{aligned} \tag{3.20}$$

which should give the same value to that of the asymptotic formula:

$$\langle\overline{\psi}\psi\rangle \simeq -\frac{4}{2+\xi}p^2\mathcal{B}(p^2)\,, \qquad \text{for } p^2 \text{ large}\,. \tag{3.21}$$

We will find in the following that the particular choice of vertex ansatz leads to varying degrees of agreement between these two equivalent determinations of extracting the condensate. This is because descrepencies in the choice of vertex ansatz will break the delicate correlation between different momentum regions. In addition to this, the use of a vertex not embodying the correct structure will lead to an artificial gauge dependence of this physical observable. We now explore the more common vertex ansätze in both the chirally symmetric and broken phases.

3.2.1 Quenched Approximation

Quenched models are the natural starting point for any numerical study of the Schwinger-Dyson equations. In the context of QED, this approximation involves neglecting contributions from virtual fermion loops in our gauge boson propagator. Hence, we set our photon dressing function $\mathcal{G}(p^2) = 1$, or equivalently the photon polarisation scalar to be $\Pi(p^2) = 0$. Thus, our preliminary study only entails the SDE for the fermion propagator and, depending on the form of the vertex ansatz, one may often evaluate the angular integrals analytically.

It is enlightening not only to study those solutions in which we have dynamical symmetry breaking, but also to look into the properties of the vertex ansatz in the chiral symmetric phase. This latter case leads to a simpler set of equations that may also yield analytic solutions.

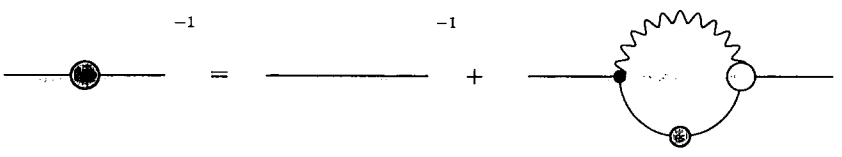

Figure 3.1: The quenched fermion SDE for QED_3. Filled dots indicate full propagators and vertices.

Bare Vertex Approximation

In studies of QED, particularly those restricted to the Landau gauge, employing the bare-vertex has long been held to be an acceptable approximation. Though in renormalisable theories it violates the notion of multiplicative renormalisability, the important caveat in three dimensional physics is the lack of consistency with the Ward-Green-Takahashi identity (WGTI), Eq. (1.56). If we choose to employ only the bare vertex throughout, including the explicitly gauge dependent part of the SDE, we have the simpler set of equations:

$$\begin{aligned}\mathcal{A}(p^2) &= 1+\frac{\alpha\xi}{2\pi p^2}\int dk^2 \frac{k\,\mathcal{A}(k^2)}{\mathcal{A}^2(k^2)k^2+\mathcal{B}^2(k^2)}\left(\frac{k^2+p^2}{2kp}\log\left|\frac{k+p}{k-p}\right|-1\right)\\ \mathcal{B}(p^2) &= \frac{\alpha}{2\pi}\int dk^2 \frac{k}{\mathcal{A}^2(k^2)k^2+\mathcal{B}^2(k^2)}\mathcal{B}(k^2)\frac{1}{kp}\log\left|\frac{k+p}{k-p}\right|(2+\xi)\ ,\end{aligned} \tag{3.22}$$

which can be solved using the methods outlined in Appendix A.

We note that in the Landau gauge, the solution to $\mathcal{A}$ is trivially one. Applying the LKF transformation to this, with $\mathcal{B}=0$, one is left with the analytic expression:

$$\frac{1}{\mathcal{A}(p^2)} = 1-\frac{\alpha\xi}{2p}\tan^{-1}\left[\frac{2p}{\alpha\xi}\right]\ , \tag{3.23}$$

which does not match solutions calculated directly from Eq. (3.22), except of course for $\xi=0$.

Turning our attention to solutions exhibiting dynamical mass generation, which we present in Fig. 3.2, we can calculate the condensate, in units of e^4, through Eqs. (3.20, 3.21). The results of this are given in Table 3.1, where we see excellent

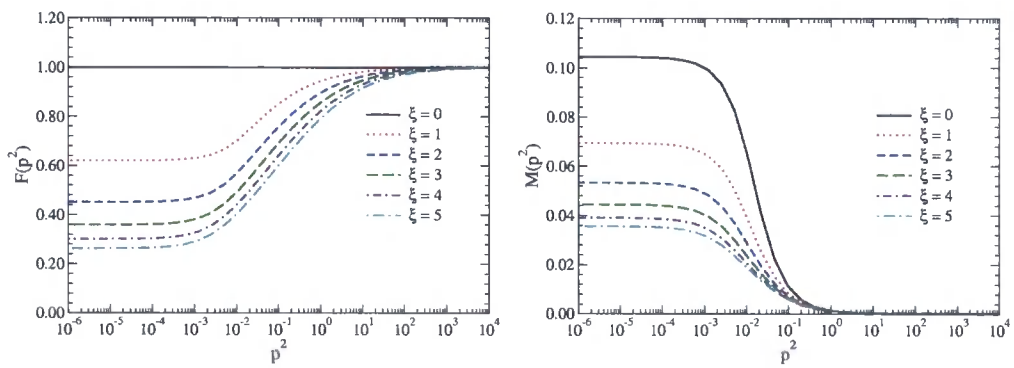

Figure 3.2: Wave-function renormalisation and mass function for the quenched SDE of Eq. (3.22), employing the bare vertex in the dynamically broken phase.

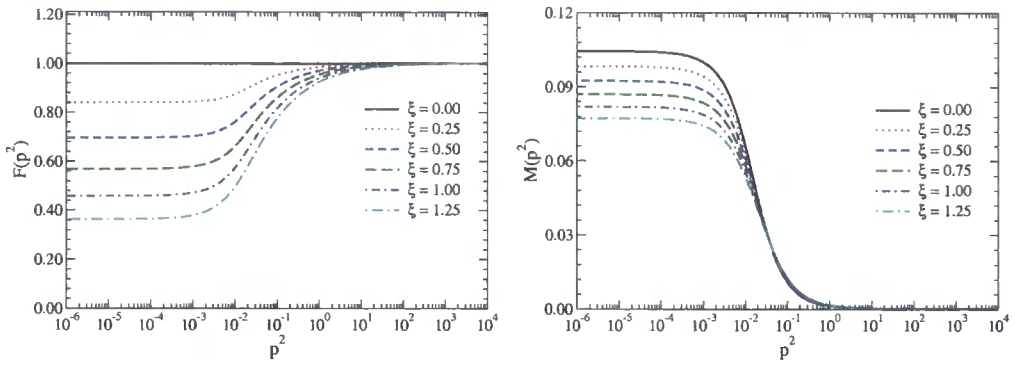

Figure 3.3: Wave-function renormalisation and mass function for the quenched SDE employing the bare vertex in the dynamically broken phase for a variety of gauges. The WGTI is satisfied in the explicitly gauge dependent part of the vertex projection.

agreement between the two determinations of the condensate. This is perhaps somewhat surprising, being as this vertex manifestly violates the Ward-Green-Takahashi identity (WGTI) in all but the Landau gauge. What we do see, however, is a marked

ξ	$-\langle\bar{\psi}\psi\rangle_{asy}$	$-\langle\bar{\psi}\psi\rangle_{int}$	ξ	$-\langle\bar{\psi}\psi\rangle_{asy}$	$-\langle\bar{\psi}\psi\rangle_{int}$
0	0.002316	0.002316	5	0.0007453	0.0007453
1	0.001448	0.001448	10	0.0006875	0.0006875
2	0.001088	0.001088	15	0.0007664	0.0007664
4	0.0008048	0.0008048	20	0.0008975	0.0008975

Table 3.1: Condensates via asymptotic and integral evaluation in the quenched bare vertex approximation, without use of the WGTI.

dependence of the condensate on the gauge parameter ξ. This is an object which we expect to be gauge invariant, and so we perform the same calculation as before, this time with the WGTI satisfied in the ξq_μ projection of the vertex, to check for improvements. Solutions for a much smaller range of gauges are given in Fig. 3.3, with values for the condensate presented in Table 3.2. Though the value of the gauge parameter we explored is rather more restrictive in this case, we do see the variation of the condensate has reduced by $\sim 14\%$ by enforcing the WGTI in at least part of the SDE. We also find good agreement between the two methods of extracting the condensate.

We now consider the LKF transformation of our solutions. If we solve the coupled system of Eq. 3.22 in Landau gauge, then transform to covariant gauges $\xi > 0$ using

ξ	$-\langle\bar{\psi}\psi\rangle_{asy}$	$-\langle\bar{\psi}\psi\rangle_{int}$	ξ	$-\langle\bar{\psi}\psi\rangle_{asy}$	$-\langle\bar{\psi}\psi\rangle_{int}$
0.00	0.002316	0.002316	1.25	0.001639	0.001639
0.25	0.002173	0.002173	1.50	0.001505	0.001504
0.50	0.002033	0.002033	1.75	0.001406	0.001406
1.00	0.001766	0.001766	2.00	0.001239	0.001239

Table 3.2: Condensates via asymptotic and integral evaluation in the quenched bare vertex approximation, with the WGTI employed in the $\xi q_\mu \Gamma^\mu$ part of the projection.

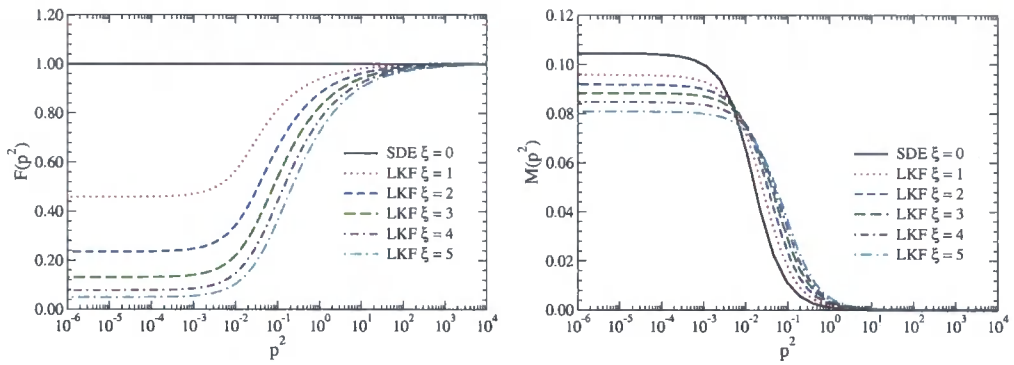

Figure 3.4: Wave-function renormalisation and mass function for the quenched SDE employing the bare vertex. The SDE are solved in Landau gauge, with LKF transformation obtaining solutions for $\xi > 0$. Compare with Fig. 3.2.

Eq. (3.19),we obtain the fermion wave-function renormalisation and mass-function of Fig. 3.4. Comparing this with Fig. 3.2, we see there is a distinct qualitative difference between the two sets of solutions, which we highlight by plotting the Euclidean mass as a function of the gauge parameter in Fig. 3.5. We have calculated the condensate for solutions obtained through the LKF transformation, and found that the condensate exhibited no dependence upon the gauge parameter. We will comment upon this in later sections. That there is a difference between these is not surprising due to the violation of gauge invariance in the SDE solutions. What we do see is, as expected, that the Euclidean mass of the LKF solutions is not invariant with the gauge parameter, for it is the *physical* pole mass that is gauge invariant by virtue of the WGTI – the Euclidean mass is more of an *indicator* one may use to measure the scale of mass generation, much like the condensate. If our vertex ansatz preserved gauge covariance, at least approximately, we would expect closer agreement between the two curves of Fig. 3.5.

Ball–Chiu Vertex

In order for the WGTI to be consistently satisfied, we should employ an appropriate vertex ansatz. One that achieves this, whilst being free of kinematic singularities, is the Ball–Chiu vertex of Eq. (2.12). We start with the projected SDE of Eq. (2.29) and Eq. (2.34) with λ_i given as:

$$\begin{aligned}
\lambda_1(k,p) &= \frac{1}{2}\left(\mathcal{A}(k^2)+\mathcal{A}(p^2)\right) , \\
\lambda_2(k,p) &= \frac{1}{2}\frac{1}{k^2-p^2}\left(\mathcal{A}(k^2)-\mathcal{A}(p^2)\right) , \\
\lambda_3(k,p) &= -\frac{1}{k^2-p^2}\left(\mathcal{B}(k^2)-\mathcal{B}(p^2)\right) ,
\end{aligned} \tag{3.24}$$

with the remaining transverse coefficients τ_i set to zero. With the WGTI satisfied we find an improved dependence of the condensate upon the gauge parameter, although the asymptotic extraction and integral methods show a sizeable disagreement. We give the numerical values in Table 3.3.

ξ	$-\langle\bar{\psi}\psi\rangle_{asy}$	$-\langle\bar{\psi}\psi\rangle_{int}$	ξ	$-\langle\bar{\psi}\psi\rangle_{asy}$	$-\langle\bar{\psi}\psi\rangle_{int}$
0.00	0.003313	0.003209	0.75	0.003566	0.003198
0.25	0.003429	0.003210	1.00	0.003588	0.003172
0.50	0.003512	0.003208	2.00	0.003981	0.003435

Table 3.3: Condensates via asymptotic and integral evaluation in the quenched Ball–Chiu approximation.

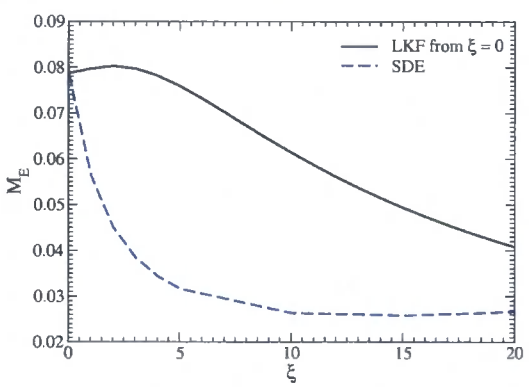

Figure 3.5: Euclidean mass for solutions calculated via the SDE and by LKF transformation of the $\xi = 0$ solution. Units are defined by setting $e^2 = 1$.

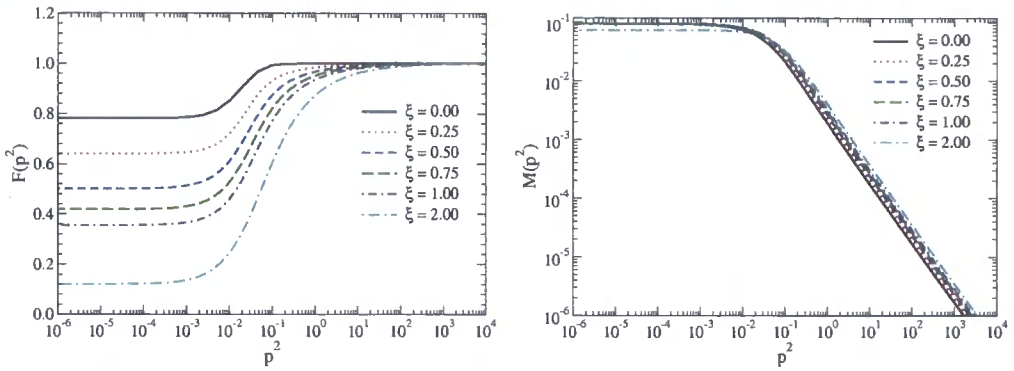

Figure 3.6: Wave-function renormalisation and mass function for the quenched SDE employing the Ball–Chiu vertex in the dynamically broken phase for a variety of gauges.

Furthermore, if we examine the chirally symmetric phase, we have to solve:

$$\begin{aligned}\mathcal{A}(p^2) \;=\; 1 - \frac{\alpha}{2\pi p^2}\int_0^\infty \frac{dk^2}{k}\frac{1}{\mathcal{A}(k^2)}\Bigg[\xi\Bigg(\frac{k^2\mathcal{A}(k^2)-p^2\mathcal{A}(p^2)}{k^2-p^2} \\ -\frac{p^2\mathcal{A}(p^2)+k^2\mathcal{A}(k^2)}{2kp}\log\left|\frac{k+p}{k-p}\right|\Bigg) \\ +\Bigg(1-\frac{k^2+p^2}{2kp}\log\left|\frac{k+p}{k-p}\right|\Bigg)\left(k^2+p^2\right)\frac{\mathcal{A}(k^2)-\mathcal{A}(p^2)}{k^2-p^2}\Bigg]\,.\end{aligned} \tag{3.25}$$

One can again show that solutions for arbitrary gauge do not match those as obtained through the LKF transformation, demonstrating a violation of gauge covariance with the Ball–Chiu vertex.

In Fig. 3.7 we plot the condensate, as extracted via the asymptotic formula, for solutions to the SDE equations for different start gauges. Overlayed on this is the result of LKF transforming the solutions to higher gauges and calculating $\langle\bar{\psi}\psi\rangle$. We clearly see numerically that the condensate remains flat for all start gauges in quenched QED_3. It turns out that this is a trivial fact which we come back to later.

Curtis–Pennington Ansatz

The CP vertex arises when one studies certain perturbative and kinematic limits of QED in four dimensions, placing upon the ansatz the requirement that multiplicative renormalisability be preserved on the level of leading and next-to-leading logarithms. It is built upon the Ball–Chiu vertex, and so the longitudinal coefficients, λ_i, are as

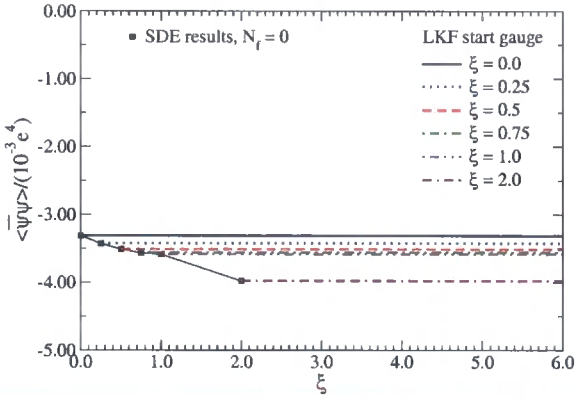

Figure 3.7: For the condensate, we show the result of LKF transforming a SDE with the Ball–Chiu vertex for different start gauges in quenched QED_3. We use the asymptotic formula Eq. (3.21), and note that it remains completely flat.

Eq. (3.24). The CP vertex brings a restriction on the form of the transverse part, requiring that:

$$\tau_6(k,p;q) = \frac{1}{2}\left(\frac{\mathcal{A}(k^2)-\mathcal{A}(p^2)}{k^2-p^2}\right)\frac{(k^2+p^2)\,(k^2-p^2)}{(k^2-p^2)^2+(M^2(k^2)+M^2(p^2))^2} \tag{3.26}$$

Before considering dynamical mass generation with this vertex, we first consider the chiral symmetric phase. Here, we have a single integral equation to solve:

$$\mathcal{A}(p^2) \;=\; 1+\frac{\alpha\xi}{2\pi}\int_0^\infty dk^2\frac{1}{k}\frac{\mathcal{A}(p^2)}{\mathcal{A}(k^2)}\left[\frac{1}{k^2-p^2}+\frac{1}{2kp}\log\left|\frac{k+p}{k-p}\right|\right], \tag{3.27}$$

due to cancellations provided by the transverse part, τ_6. This has an analytic solution [31]:

$$\frac{1}{\mathcal{A}(p^2)} = 1-\frac{\alpha\xi}{2p}\tan^{-1}\left[\frac{2p}{\alpha\xi}\right], \tag{3.28}$$

which we note is the same as the LKF transformation of the bare-vertex in Landau gauge, Eq. (3.28), in which $\mathcal{A}(p^2)=1$ for $\xi=0$.

The assumption that this is correct relies upon the transversality condition proposed by [90]:

$$\int\frac{d^3k}{(2\pi)^3}\gamma^\mu S_F(k)\Gamma^\nu(k,p)\Delta^{0}_{\mu\nu}{}^{T}(q) = 0\,. \tag{3.29}$$

While this condition holds true to one-loop order in perturbation theory, it has been shown through an explicit two-loop calculation [91] that this assumption of transversality fails.

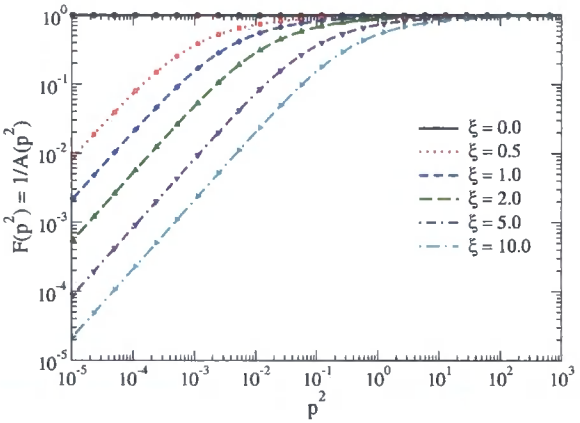

Figure 3.8: The analytic solution (lines), given by Eq. (3.23). Symbols indicate the numerical solution to Eq. (3.27), in perfect agreement.

We now couple in the mass function and consider solutions exhibiting dynamical mass generation. The condensate is again calculated through the integral method and by examining the asymptotic of the mass function, which we present in Table 3.4. The small differences between this and Ref. [92] are attributable to differences in

ξ	$-\langle\bar{\psi}\psi\rangle_{asy}$	$-\langle\bar{\psi}\psi\rangle_{int}$
0.0	0.00331	0.00330
0.5	0.00341	0.00341
1.0	0.00350	0.00349

Table 3.4: Condensates via asymptotic and integral evaluation in the quenched bare vertex approximation.

the numerical method. We do see, however, the same close agreement between the two methods of extracting the condensate, in contrast to the Ball–Chiu vertex of the previous section.

Kızılersü–Pennington Vertex

The final vertex ansatz we have at hand is that of Kızılersü and Pennington, developed for massless unquenched QED in four dimensions such that multiplicative renormalisability of the $(\mathcal{F},\mathcal{G})$ system is preserved. Our basis coefficients are as for the Ball–Chiu vertex for the longitudinal part of Eq. (3.24), with the transverse part

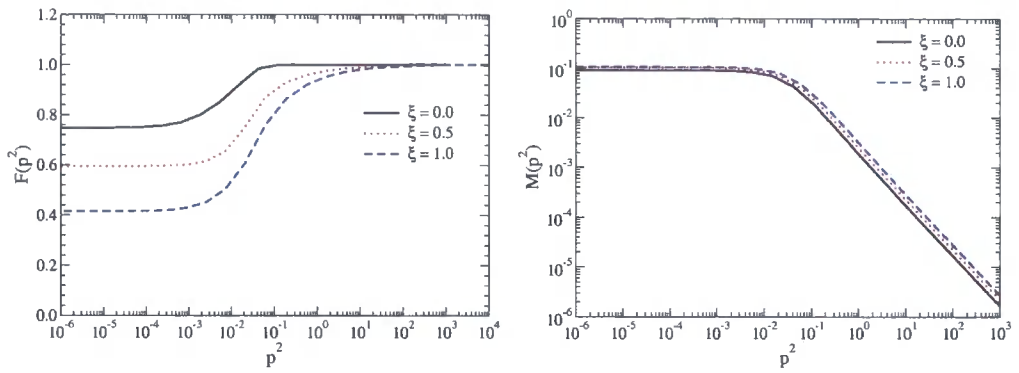

Figure 3.9: Wave-function renormalisation and mass function for the quenched SDE employing the Curtis–Pennington vertex in the dynamically broken phase.

specified by[1]:

$$\begin{aligned}
\tau_2\left(p^2,k^2,q^2\right) &= -\frac{8}{3}\frac{\lambda_2\left(k^2,p^2\right)}{\left(k^2+p^2\right)} - \frac{2}{3}\frac{\lambda_1\left(k^2,p^2\right)}{\left(k^2+p^2\right)^2}\log\left(\frac{\mathcal{A}(k^2)\mathcal{A}(p^2)}{\mathcal{A}^2(q^2)}\right) , \\
\tau_3\left(p^2,k^2,q^2\right) &= -\frac{5}{12}2\,\lambda_2\left(k^2,p^2\right) - \frac{1}{3}\frac{\lambda_1\left(k^2,p^2\right)}{\left(k^2+p^2\right)}\log\left(\frac{\mathcal{A}(k^2)\mathcal{A}(p^2)}{\mathcal{A}^2(q^2)}\right) , \\
\tau_6\left(p^2,k^2,q^2\right) &= \frac{1}{4}\frac{\left(k^2-p^2\right)}{\left(k^2+p^2\right)}2\,\lambda_2\left(k^2,p^2\right) , \\
\tau_8\left(p^2,k^2,q^2\right) &= 0 .
\end{aligned}$$

The logarithmic terms here depend upon q^2 through the function $\mathcal{A}$, rather than simply k^2 and p^2. This forces us to evaluate the angular component for this part at each iteration, instead of outside the main loop, increasing the computational requirements.

If we consider solutions exhibiting chiral symmetry breaking, Fig. 3.10, we can extract the value of the condensate through the asymptotic and integral evaluation, indicating the scale of this mass generation. The results are in Table 3.5. What we see is, compared to the Curtis–Pennington vertex, a huge disagreement between $\langle\bar{\psi}\psi\rangle_{asy}$ and $\langle\bar{\psi}\psi\rangle_{int}$.

We now consider the chirally symmetric phase with the KP vertex. We already examined the CP vertex, in which case the integral equation for $\mathcal{A}(p^2)$ simplified such that an analytic solution was found, Eq. (3.23), for all ξ. This exactly matched the analytic solution found by applying the Landau-Khalatnikov-Fradkin transformation

[1]It is of course not obvious that these forms are appropriate to QED_3, where the logarithms characteristic of four dimensional theories perhaps should become powers.

ξ	$-\langle\bar{\psi}\psi\rangle_{asy}$	$-\langle\bar{\psi}\psi\rangle_{int}$
0.0	0.00350	0.00341
1.0	0.00445	0.00353
2.0	0.00543	0.00383
3.0	0.00651	0.00426
4.0	0.00771	0.00481
5.0	0.00905	0.00546

Table 3.5: Condensates via asymptotic and integral evaluation with the quenched Kızılersü–Pennington vertex.

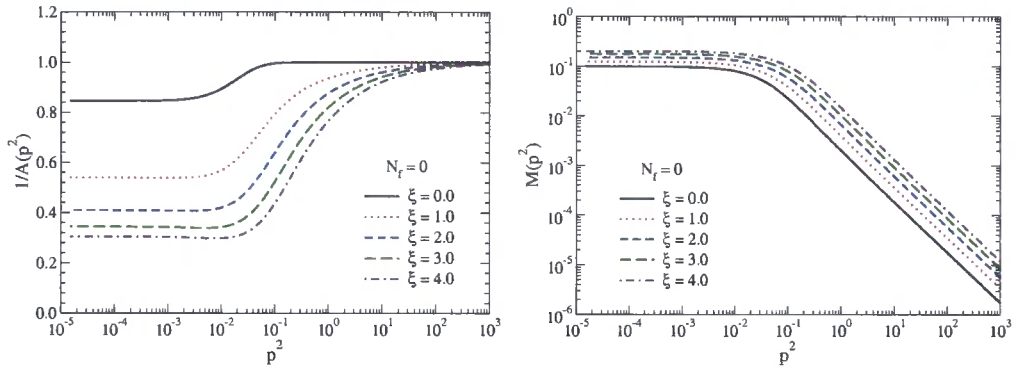

Figure 3.10: Wave-function renormalisation and mass function for the quenched SDE employing the Kızılersü–Pennington vertex in the dynamically broken phase for a variety of gauges.

to the $\xi = 0$ case, in which $\mathcal{A}(p^2) = 1$. However, if one performs a perturbative expansion of the analytic formula, Eq. (3.23), in Minkowski space:

$$\mathcal{F}(p^2) = 1 - \frac{\pi\,\alpha\xi}{4\sqrt{-p^2}} - \frac{\alpha^2\xi^2}{4p^2} + \mathcal{O}\left(\alpha^3\right)\,, \tag{3.30}$$

and compare with an explicit two-loop calculation of [91]:

$$\mathcal{F}(p^2) = 1 - \frac{\pi\,\alpha\xi}{4\sqrt{-p^2}} - \frac{\alpha^2\xi^2}{4p^2}\left(1 + \frac{\pi^2}{12}\right) - \frac{\alpha^2\xi}{2p^2}\left(1 - \frac{\pi^2}{4}\right) + \mathcal{O}(\alpha^3)\,, \tag{3.31}$$

we see the result is not the same. The three distinctive features of this have already been highlighted in [91]. To recapitulate what is said there, $\mathcal{F} \neq 1$ in Landau gauge, the transversality condition of Eq. 3.29 is violated and the analytic solution of Eq. 3.23 cannot hold in general. The LKF transformation is thus only magically satisfied with the CP ansatz, a result of all but the xi-dependent part cancelling.

Turning to the vertex of Kızılersü and Pennington, we find that no analytic solution can be found due to the now complicated angular integrals. Setting $\mathcal{B} = 0$, we solve the SDE for $\mathcal{A}(p^2)$ in the quenched approximation numerically. In Fig. 3.11 we show solutions (data points with lines) for $\mathcal{A}(p^2)$ calculated through the SDE for a selection of gauges. Overlaid in this graph are the $\mathcal{A}(p^2)$ as the result of LKF transforming from the $\xi = 1$ SDE solution to $\xi = 2, 3, 4, 5$. We find close agreement for momenta $p^2 > 10^{-2}$, with the scale set by $e^2 = 1$. However, the differences are more marked in the important infrared region, showing disagreement between the SDE generated results and the LKF transformation, and thus a violation of gauge covariance. However, this vertex is specifically designed for renormalisable theories which are characterised by the appearance of logarithms. These then become ill-behaved in the three-dimensional theory, and so a different formulation of the KP-vertex would be required.

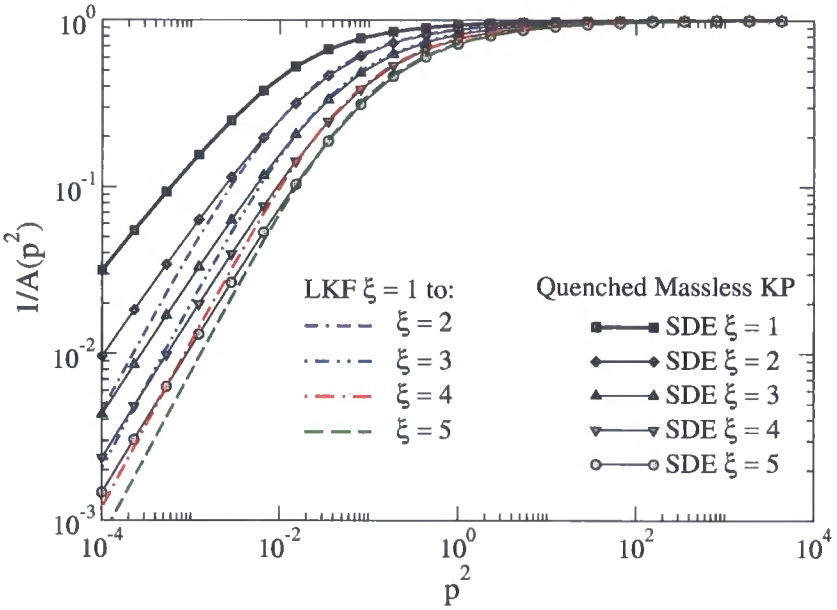

Figure 3.11: Wave-function renormalisation for the quenched SDE employing the Kızılersü–Pennington vertex in the chirally symmetric phase, showing comparison with LKF transformation.

3.2.2 Partial Unquenching

Studies of partially unquenched QED, where the $1/N_f$ expansion is employed in the photon equation, have already been undertaken for the bare vertex and the Ball-Chiu

construction [71–76,93]. These effectively sum up massless fermion loops in the photon SDE, thus softening the infrared behaviour below the natural scale $\bar{\alpha} = e^2 N_f/8$. This gives validity to the $1/N_f$ perturbative expansion in the low momentum region when applied to the photon. In Landau gauge our photon propagator is:

$$D_{\mu\nu}(q) = \frac{\mathcal{G}(q^2)}{q^2}\left(g_{\mu\nu} - \frac{q_\mu q_\nu}{q^2}\right) , \tag{3.32}$$

with

$$\mathcal{G}(q^2) = \frac{q^2}{q^2 + \bar{\alpha} q} , \tag{3.33}$$

derived from the resummation. Plots of this ansatz, which is independent of the choice of vertex function can be seen in Fig. 3.12. In our numerical calculations we have used $e^2 = 1$ to set the scale of mass generation in the theory. In Fig. 3.13 we show solutions to the SDE with the Ball–Chiu vertex [75, 93]. The equivalent solutions [76] for the Curtis–Pennington vertex are given in Fig. 3.14.

We use Eq. (3.20) and Eq. (3.21) to extract the condensate (in units of e^4) for each ansatz, displaying the numerical values in Table 3.6.

It is interesting to see that the two methods for extracting the condensate only agree to within 10% for the Ball–Chiu vertex, whilst the discrepancy for the Curtis–Pennington vertex is less than 2%.

3.2.3 Unquenched SDE in the Landau Gauge

Studies of QED_3 where the photon equation is calculated self-consistently by use of a vertex ansatz have been undertaken for the bare and minimal Ball–Chiu vertices [94,

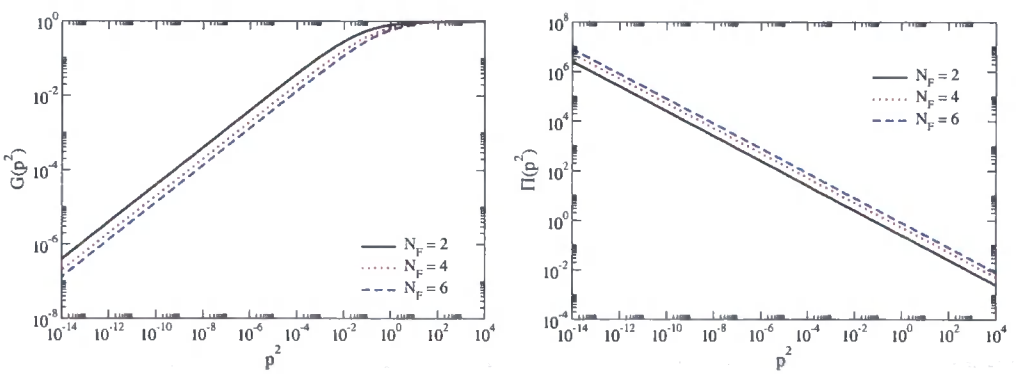

Figure 3.12: Photon wave-function G and polarisation scalar $\Pi(p^2)$ as a result of resumming massless fermion loops.

	Ball–Chiu		Curtis–Pennington	
N_f	$-\langle\bar{\psi}\psi\rangle_{asy}$	$-\langle\bar{\psi}\psi\rangle_{int}$	$-\langle\bar{\psi}\psi\rangle_{asy}$	$-\langle\bar{\psi}\psi\rangle_{int}$
2	$1.603 \cdot 10^{-4}$	$1.746 \cdot 10^{-4}$	$1.7047 \cdot 10^{-4}$	$1.7053 \cdot 10^{-4}$
4	$3.924 \cdot 10^{-7}$	$4.385 \cdot 10^{-7}$	$2.5379 \cdot 10^{-7}$	$2.5408 \cdot 10^{-7}$
6	$4.009 \cdot 10^{-11}$	$5.526 \cdot 10^{-11}$	$3.6968 \cdot 10^{-12}$	$3.7039 \cdot 10^{-12}$

Table 3.6: Condensates via asymptotic and integral evaluation in the partially unquenched approximation employing the Ball–Chiu and Curtis–Pennington vertices.

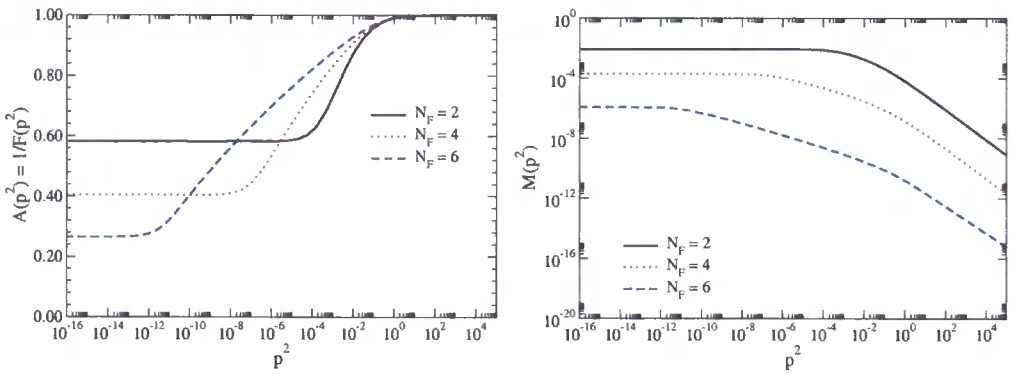

Figure 3.13: Wave-function renormalisation and mass function for SDE employing the Ball–Chiu vertex in the dynamically broken phase. The photon equation re-sums massless fermion loops.

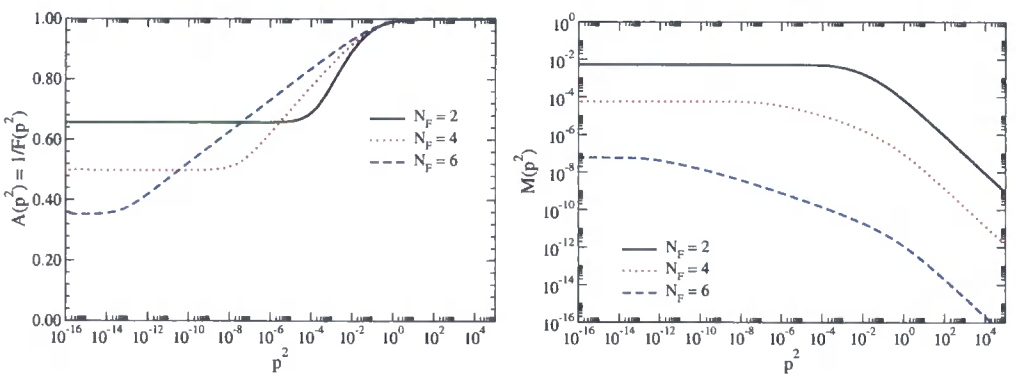

Figure 3.14: Wave-function renormalisation and mass function for SDE employing the Curtis–Pennington vertex in the dynamically broken phase. The photon equation re-sums massless fermion loops.

95] and for the hybrid-CP vertex [92]. In past studies of dynamical mass generation in fully unquenched three dimensional QED, a photon equation has been employed

using an asymmetric momentum routing. Here we will be using the symmetric one of Eq. 2.39, as seen in Fig. 2.4 with momentum partition $\eta = 1/2$.

We now look at the criticality of three-dimensional QED as a function of the number of active fermions for different gauges. This we do through numerical solution of the Schwinger-Dyson equations for a variety of vertex ansätze.

Bare Vertex Approximation

The bare-vertex is the first step in any fully-coupled unquenched study. This is equivalent to the following choice of basis coefficient in the projections of the SDE of Eqs. (2.29, 2.34):

$$\lambda_1(k,p) = 1 \,, \tag{3.34}$$

with the remaining λ_i and τ_i set to zero. In the left-hand column of Fig. 3.15 we show solutions in Landau gauge, showing a strong depedence between the scale of dynamically generated mass and the number of flavours. This feature is not seen when $\xi \neq 0$, indeed we obtained solutions in the chirally broken phase just beyond the apparent critical number of $N_f \approx 3.4$. The dependence of the condensate on the number of flavours for a selection of gauges is given in Table 3.7.

N_f	$-\langle\psi\psi\rangle_{asy}$	$-\langle\psi\psi\rangle_{int}$	N_f	$-\langle\psi\psi\rangle_{asy}$	$-\langle\psi\psi\rangle_{int}$
1.0	$8.5 \cdot 10^{-4}$	$8.5 \cdot 10^{-4}$	3.0	$9.2 \cdot 10^{-8}$	$9.3 \cdot 10^{-8}$
2.0	$8.4 \cdot 10^{-5}$	$8.5 \cdot 10^{-5}$	3.2	$5.9 \cdot 10^{-9}$	$5.9 \cdot 10^{-9}$
2.8	$7.3 \cdot 10^{-7}$	$7.3 \cdot 10^{-7}$	3.4	$9.6 \cdot 10^{-11}$	$9.7 \cdot 10^{-11}$

Table 3.7: Condensates via asymptotic and integral evaluation in the unquenched bare-vertex approximation.

Minimal Ball–Chiu Vertex

The minimal Ball-Chiu vertex entails discarding the two derivative like pieces of the full Ball–Chiu vertex and setting the transverse component to zero:

$$\lambda_1(k,p) \;=\; \frac{1}{2}\left(\mathcal{A}(k^2) + \mathcal{A}(p^2)\right) \,. \tag{3.35}$$

Whilst being a good approximation in the ultraviolet, this neglect impacts upon the behaviour in the intermediate and infrared regions. However, the numerical difficulties brought about by the full ansatz are avoided and one may at least begin a preliminary study beyond the bare vertex approximation, in which some form of

minimal dressing is employed. We show numerical results for Landau gauge in the right-hand column of Fig. 3.15, so that one may compare them with the bare-vertex.

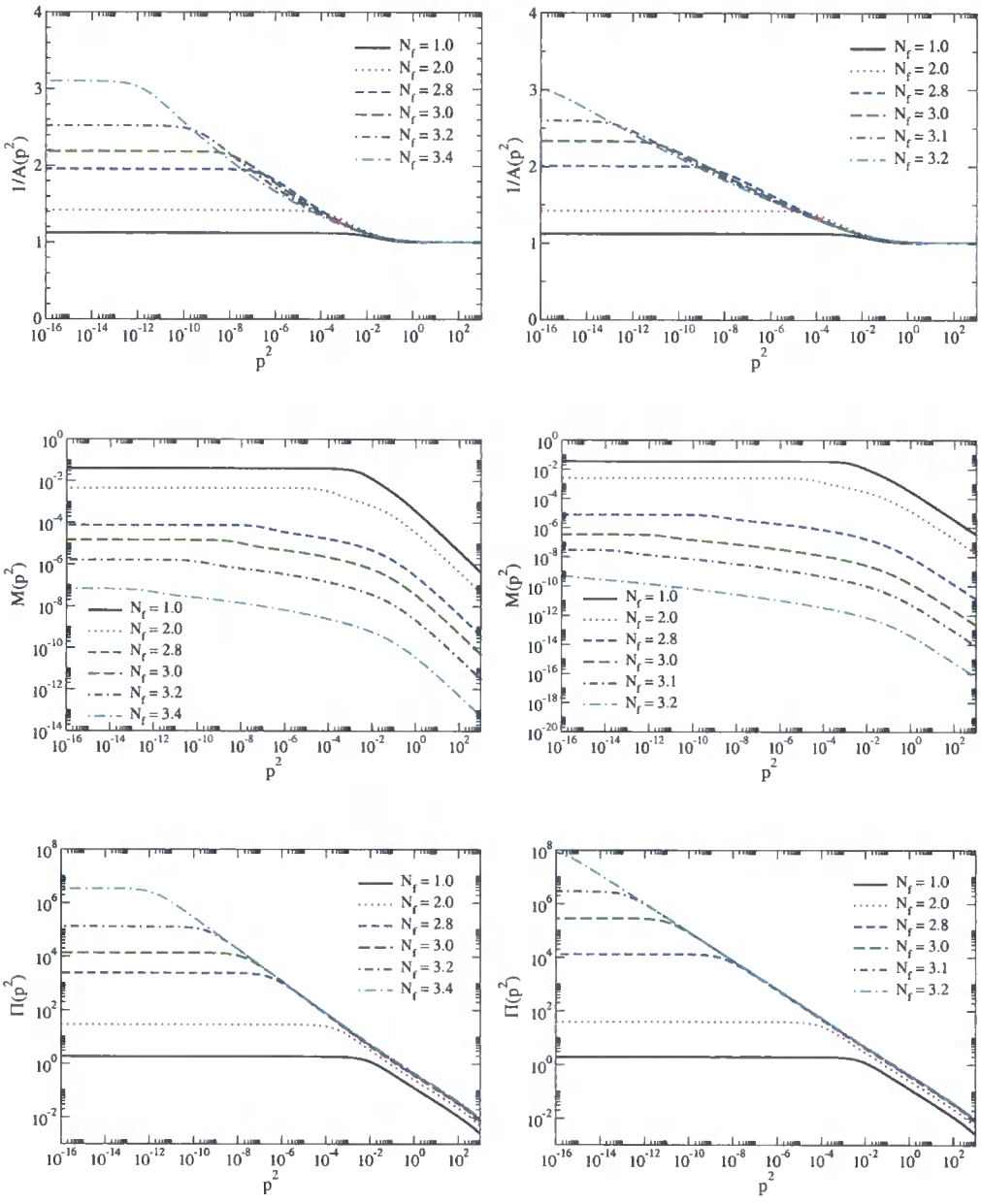

Figure 3.15: The fermion wave-function renormalisation, mass function and photon polarisation scalar for the bare vertex (left) and the minimal Ball–Chiu vertex (right). Solutions are obtained in Landau gauge for a selection of flavours, with $e^2 = 1$ setting the scale.

N_f	$-\langle\bar{\psi}\psi\rangle_{asy}$	$-\langle\bar{\psi}\psi\rangle_{int}$	N_f	$-\langle\bar{\psi}\psi\rangle_{asy}$	$-\langle\bar{\psi}\psi\rangle_{int}$
1.0	$6.9 \cdot 10^{-4}$	$7.1 \cdot 10^{-4}$	3.0	$3.6 \cdot 10^{-10}$	$4.0 \cdot 10^{-10}$
2.0	$3.4 \cdot 10^{-5}$	$3.6 \cdot 10^{-5}$	3.1	$1.4 \cdot 10^{-11}$	$1.6 \cdot 10^{-11}$
2.8	$2.3 \cdot 10^{-8}$	$2.5 \cdot 10^{-8}$	3.2	$9.5 \cdot 10^{-14}$	$1.1 \cdot 10^{-13}$

Table 3.8: Condensates via asymptotic and integral evaluation for the unquenched minimal Ball–Chiu vertex.

It can clearly be seen that the effect of this minimal dressing is to lower the value of N_f to approximately 3.2.

Ball–Chiu Construction

The next evolutionary step for the vertex is the full Ball–Chiu ansatz. This satisfies the Ward-Green-Takahashi identity together with the Ward identity, and so is consistent with our choice for the explicitly ξ-dependent part of the SDE projection. Our coefficients are given by:

$$\begin{aligned}
\lambda_1(k,p) &= \frac{1}{2}\left(\mathcal{A}(k^2)+\mathcal{A}(p^2)\right) , \\
\lambda_2(k,p) &= \frac{1}{2}\frac{1}{k^2-p^2}\left(\mathcal{A}(k^2)-\mathcal{A}(p^2)\right) , \\
\lambda_3(k,p) &= -\frac{1}{k^2-p^2}\left(\mathcal{B}(k^2)-\mathcal{B}(p^2)\right) ,
\end{aligned}$$

and set the remaining coefficients $\tau_i = 0$. We once again study the critical behaviour of this coupled set of equations with respect to the number of flavours present in the photon loop. We calculate the condensate, in units of e^4, for Landau gauge by varying the number of fermions, and give the results in Table 3.9. The critical number of flavours is slightly higher with this vertex at $N_f^{crit} \simeq 3.4$

N_f	$-\langle\bar{\psi}\psi\rangle_{asy}$	$-\langle\bar{\psi}\psi\rangle_{int}$	N_f	$-\langle\bar{\psi}\psi\rangle_{asy}$	$-\langle\bar{\psi}\psi\rangle_{int}$
1.0	$1.2 \cdot 10^{-3}$	$1.2 \cdot 10^{-3}$	3.0	$8.1 \cdot 10^{-8}$	$9.1 \cdot 10^{-8}$
2.0	$1.2 \cdot 10^{-4}$	$1.3 \cdot 10^{-4}$	3.2	$4.9 \cdot 10^{-9}$	$5.5 \cdot 10^{-9}$
2.8	$7.2 \cdot 10^{-7}$	$8.0 \cdot 10^{-7}$	3.4	$9.3 \cdot 10^{-11}$	$1.0 \cdot 10^{-10}$

Table 3.9: Condensates with the BC vertex in the unquenched theory as a function of N_f in Landau gauge.

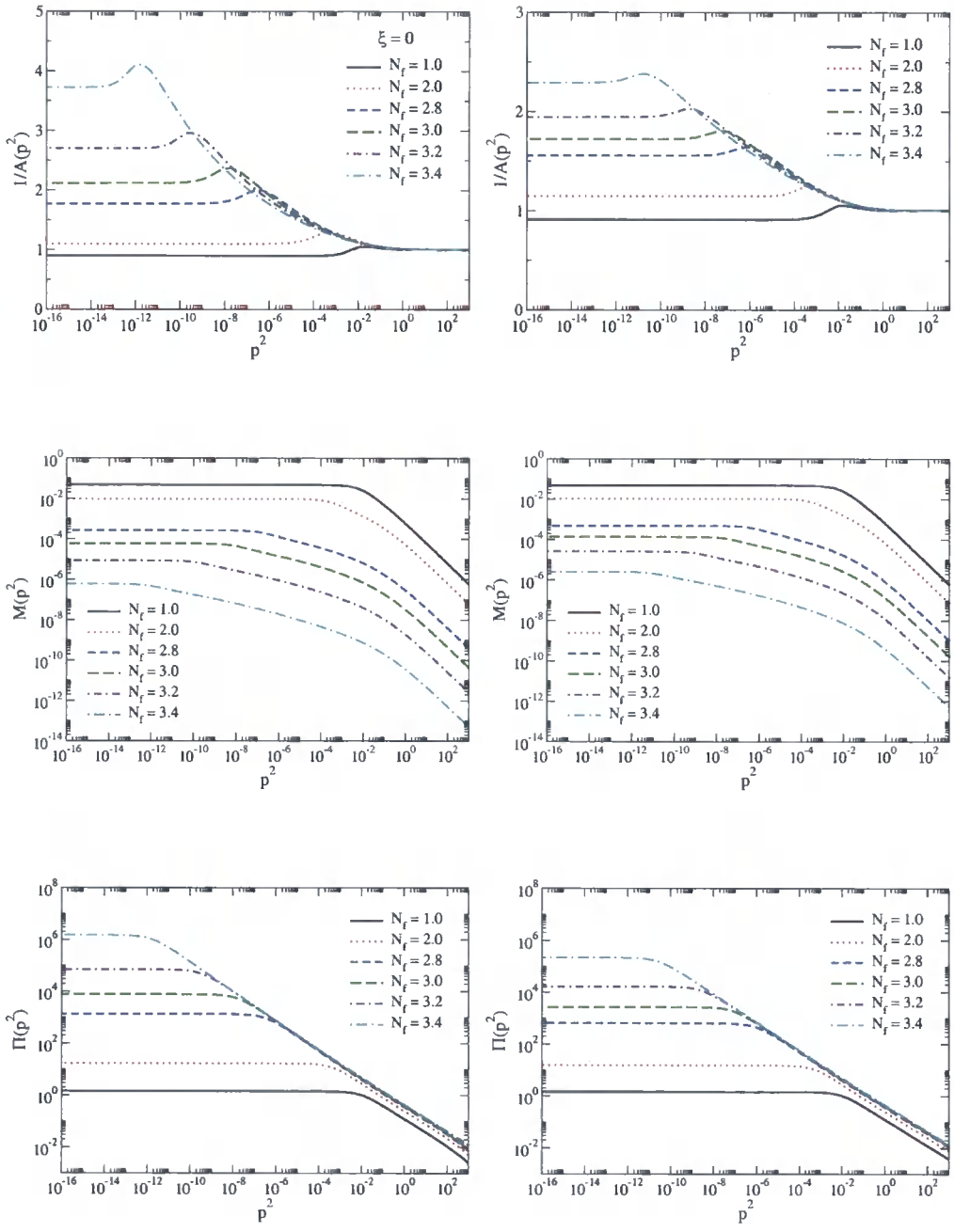

Figure 3.16: The left-hand column shows solutions for the fermion wave-function renormalisation, mass function and photon polarisation scalar for the BC, whilst the right-hand demonstrates the hybrid CP vertex for comparison. We use Landau gauge, and set $e^2 = 1$ to fix the scale.

Hybrid CP Vertex

For the hybrid CP model, where the Ball–Chiu vertex is employed in the photon equation and the Curtis–Pennington vertex used for the fermion SDE, we obtain results similar to that of the straight Ball–Chiu vertex. However, the important distinction is that the inclusion of the transverse coefficient:

$$\tau_6(k,p;q) = \frac{1}{2}\left(\frac{\mathcal{A}(k^2)-\mathcal{A}(p^2)}{k^2-p^2}\right)\frac{(k^2+p^2)(k^2-p^2)}{(k^2-p^2)^2+(M^2(k^2)+M^2(p^2))^2}\,, \tag{3.36}$$

yields a better agreement between the asymptotic and integral evaluation of the condensate, particularly for $\xi \neq 0$. The condensates in Landau gauge are given in Table 3.10.

N_f	$-\langle\bar{\psi}\psi\rangle_{asy}$	$-\langle\bar{\psi}\psi\rangle_{int}$	N_f	$-\langle\bar{\psi}\psi\rangle_{asy}$	$-\langle\bar{\psi}\psi\rangle_{int}$
1.0	$1.217\cdot10^{-3}$	$1.216\cdot10^{-3}$	3.0	$3.130\cdot10^{-7}$	$3.130\cdot10^{-7}$
2.0	$1.431\cdot10^{-4}$	$1.430\cdot10^{-4}$	3.2	$2.862\cdot10^{-8}$	$2.862\cdot10^{-8}$
2.8	$1.909\cdot10^{-6}$	$1.909\cdot10^{-6}$	3.4	$9.521\cdot10^{-10}$	$9.517\cdot10^{-10}$

Table 3.10: Condensates with the CP vertex in the unquenched theory as a function of N_f in Landau gauge.

In Fig. 3.16 we see a comparison between solutions obtained with the Ball–Chiu and Curtis–Pennington vertices, as a function of the number of active fermion flavours in Landau gauge.

Kızılersü–Pennington Vertex

The final vertex ansatz we may employ in the SDE in solutions exhibiting chiral symmetry breaking is that of Kızılersü and Pennington. A summary of the longitudinal and transverse coefficients has been given for the quenched case. Here we couple in the photon equation and work in Landau gauge, obtaining values for the condensate given in Table 3.11.

	$N_f=0$		$N_f=1$		$N_f=2$	
ξ	$-\langle\bar{\psi}\psi\rangle_{asy}$	$-\langle\bar{\psi}\psi\rangle_{int}$	$-\langle\bar{\psi}\psi\rangle_{asy}$	$-\langle\bar{\psi}\psi\rangle_{int}$	$-\langle\bar{\psi}\psi\rangle_{asy}$	$-\langle\bar{\psi}\psi\rangle_{int}$
0.0	$3.5\cdot10^{-2}$	$3.41\cdot10^{-2}$	$1.23\cdot10^{-3}$	$1.27\cdot10^{-3}$	$1.68\cdot10^{-4}$	$1.47\cdot10^{-4}$

Table 3.11: Condensates with the KP-vertex in the unquenched theory as a function of N_f in Landau gauge.

We obtain a similar trend for the scale of the condensate as a function of N_f as in the other ansätze. However, what is clear is there exists a disagreement between the two methods for extracting the value of the condensate. Comparing these results with the Ball–Chiu vertex, it is possible that the transverse pieces like $\log \mathcal{F}(p^2)$ interfere with the relationship between the infrared and ultraviolet behaviour. Indeed, the Curtis–Pennington vertex involves the mass function $\mathcal{M}$, an ingredient missing from the Kızılersü–Pennington ansatz. The regulation that this provides in the infrared may be the key linking the asymptotic and integral evaluations of the condensate, as may be replacing the logarithmic pieces of the ansatz with something more appropriate.

3.2.4 Unquenched Results for $\xi \neq 0$

We now look towards the dependence of the condensate on the number of flavours N_f away from Landau gauge. For the Ball–Chiu vertex we have calculated the condensate for $N_f = 1, 2$ in different gauges, the results of which we give in Table 3.12. The discrepancy between the two values of the condensate is more evident for $\xi \neq 0$,

	$N_f = 1$		$N_f = 2$		$N_f = 3$	
ξ	$-\langle\bar{\psi}\psi\rangle_{asy}$	$-\langle\bar{\psi}\psi\rangle_{int}$	$-\langle\bar{\psi}\psi\rangle_{asy}$	$-\langle\bar{\psi}\psi\rangle_{int}$	$-\langle\bar{\psi}\psi\rangle_{asy}$	$-\langle\bar{\psi}\psi\rangle_{int}$
0.0	$1.19 \cdot 10^{-3}$	$1.20 \cdot 10^{-3}$	$1.21 \cdot 10^{-4}$	$1.26 \cdot 10^{-4}$	$8.13 \cdot 10^{-8}$	$9.11 \cdot 10^{-8}$
1.0	$2.08 \cdot 10^{-3}$	$1.81 \cdot 10^{-3}$	$1.03 \cdot 10^{-3}$	$0.866 \cdot 10^{-3}$	$0.682 \cdot 10^{-3}$	$0.562 \cdot 10^{-3}$
2.0	$2.37 \cdot 10^{-3}$	$2.00 \cdot 10^{-3}$	$1.23 \cdot 10^{-3}$	$0.999 \cdot 10^{-3}$	$0.881 \cdot 10^{-3}$	$0.705 \cdot 10^{-3}$

Table 3.12: Condensates for the unquenched BC vertex as a function of the number of active fermions, N_f, evaluated for different gauges.

with the magnitude linked the the scale of dynamically generated mass. What we see is that, for $\xi > 0$ the condensate drops approximately by a factor of two as we move from $N_f = 1$ to $N_f = 2$, and again as we move from $N_f = 2$ to $N_f = 3$. However, in the Landau gauge this drop is of order ten, followed by a drop of 10^3.

In Fig. 3.18 we show the effect LKF transforming the solutions has on the value of the calculated condensate, for $N_f > 1$ and for different start gauges. As alluded to before, we find that the condensate remains perfectly flat. This trivial fact is discussed in the next section.

For the CP–vertex we have closer agreement between the asymptotic and integral extraction of the condensate:

We now consider the Kızılersü–Pennington vertex in different gauges with $N_f = 1$. From Table 3.14 we still see strong gauge dependence upon the condensate,

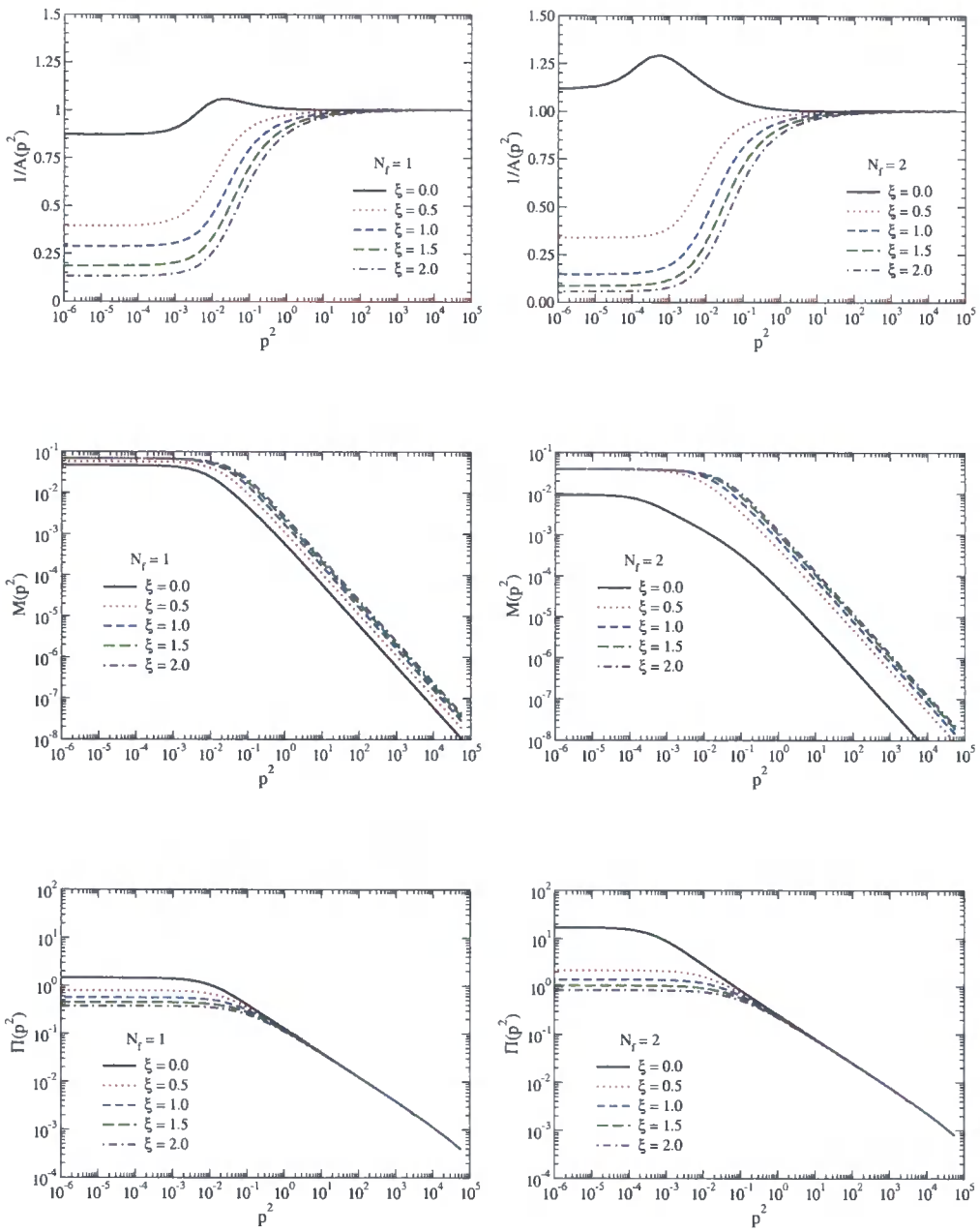

Figure 3.17: The left-hand column shows solutions for the fermion wave-function renormalisation, mass function and photon polarisation scalar for $N_f = 1$, with the right-hand side solved for $N_f = 2$. We use the Ball–Chiu vertex throughout and set the scale by $e^2 = 1$.

	$N_f = 1$		$N_f = 2$		$N_f = 3$	
ξ	$-\langle\bar{\psi}\psi\rangle_{asy}$	$-\langle\bar{\psi}\psi\rangle_{int}$	$-\langle\bar{\psi}\psi\rangle_{asy}$	$-\langle\bar{\psi}\psi\rangle_{int}$	$-\langle\bar{\psi}\psi\rangle_{asy}$	$-\langle\bar{\psi}\psi\rangle_{int}$
0.0	$1.22 \cdot 10^{-3}$	$1.22 \cdot 10^{-3}$	$1.43 \cdot 10^{-4}$	$1.43 \cdot 10^{-4}$	$3.13 \cdot 10^{-7}$	$3.13 \cdot 10^{-7}$
1.0	$2.04 \cdot 10^{-3}$	$2.03 \cdot 10^{-3}$	$1.28 \cdot 10^{-3}$	$1.28 \cdot 10^{-3}$	$0.765 \cdot 10^{-3}$	$0.765 \cdot 10^{-3}$
2.0	$2.89 \cdot 10^{-3}$	$2.89 \cdot 10^{-3}$	$2.19 \cdot 10^{-3}$	$2.19 \cdot 10^{-3}$	$1.50 \cdot 10^{-3}$	$1.50 \cdot 10^{-3}$

Table 3.13: Condensates for the unquenched CP vertex as a function of the number of active fermions, N_f, evaluated for different gauges.

with large disagreement between the two methods for extracting the condensate. Clearly the vertex, due to its explicit construction for four-dimensional theories, is inapplicable to QED_3 and adds nothing beyond the BC-vertex other than a more significantly more complicated numerical procedure.

ξ	$-\langle\psi\psi\rangle_{asy}$	$-\langle\psi\psi\rangle_{int}$
0.0	0.00123	0.00127
1.0	0.00256	0.00197
2.0	0.00372	0.00253

Table 3.14: Condensates with the KP vertex in the unquenched theory for different gauges and $N_f = 1$.

We consider the LKF transformation of some of these solutions to see qualitatively how they compare to direct self-consistent SDE solutions. We use the Ball–Chiu vertex in Landau gauge, for both $N_f = 0, 1$, and LKF transform these solutions to different gauges. The results can be seen in Fig. 3.18.

We see that the LKF transformation pushes $\mathcal{A}$ to larger values in the infrared as the gauge increases, as we expect from SDE studies. However, looking at the mass function we see the LKF transformation *pushes* the shoulder down and to the right. It is hard to say intuitively whether this is what we expect, or is merely an artefact of having the "wrong solution" in our starting gauge. What we do know is that these LKF solutions do not match those as obtained directly from the Schwinger-Dyson equations, *cf.* Figs. 3.6, 3.17. At present this tells us our ansätze do not respect gauge covariance of the solutions, a somewhat irrelevant point from the perspective of SDE studies since it tells us nothing of actually *how* to construct a better ansatz. One may choose the perspective that we don't need a vertex valid for all gauges, but one that works in one particular gauge. This is not a bad idea, but we have no way to tell if our ansatz *is* correct non-perturbatively since, for example, the condensate is always gauge invariant irrespective of the vertex employed. Other checks would

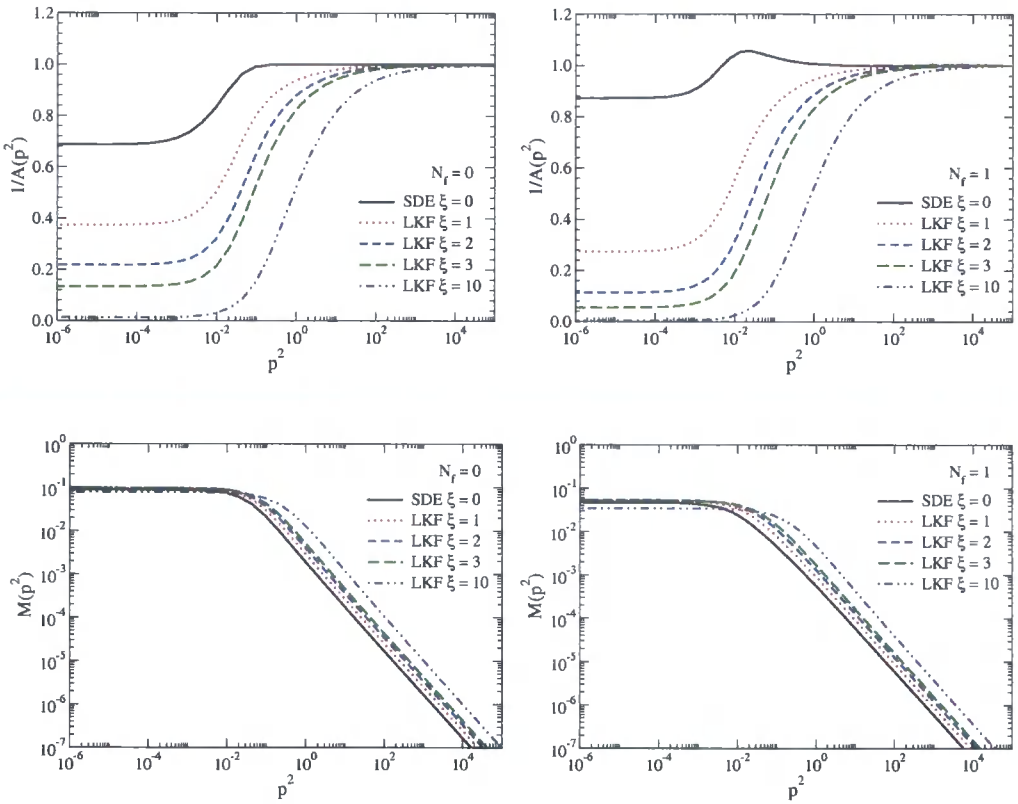

Figure 3.18: We show the result of LKF transforming a SDE with the Ball–Chiu vertex from the Landau Gauge, for $N_f = 0, 1$. These are to be compared with Figs. 3.6, 3.17.

require self-consistency of the SDE themselves, or the LKF transform of higher order Green's functions – which are far more complicated to implement.

3.2.5 Corollary of LKFT

It is in fact obvious that the chiral condensate in QED_3 is a gauge invariant object, since as an operator we write it as $\langle\bar{\psi}\psi\rangle$. The question remains of whether it is trivially invariant under the LKF transformations applied to the propagators derived in some starting gauge. In QED_3 the condensate, in coordinate space, is defined by $-\mathrm{Tr}_D S(x;\xi)$ with $x \to 0$. If we apply the LKF transformation in coordinate space to this expression, we can easily show the condensate to be gauge invariant under LKF transformations. What we present here is the momentum space version of the proof, necessarily more complicated due to the Fourier transformations that must

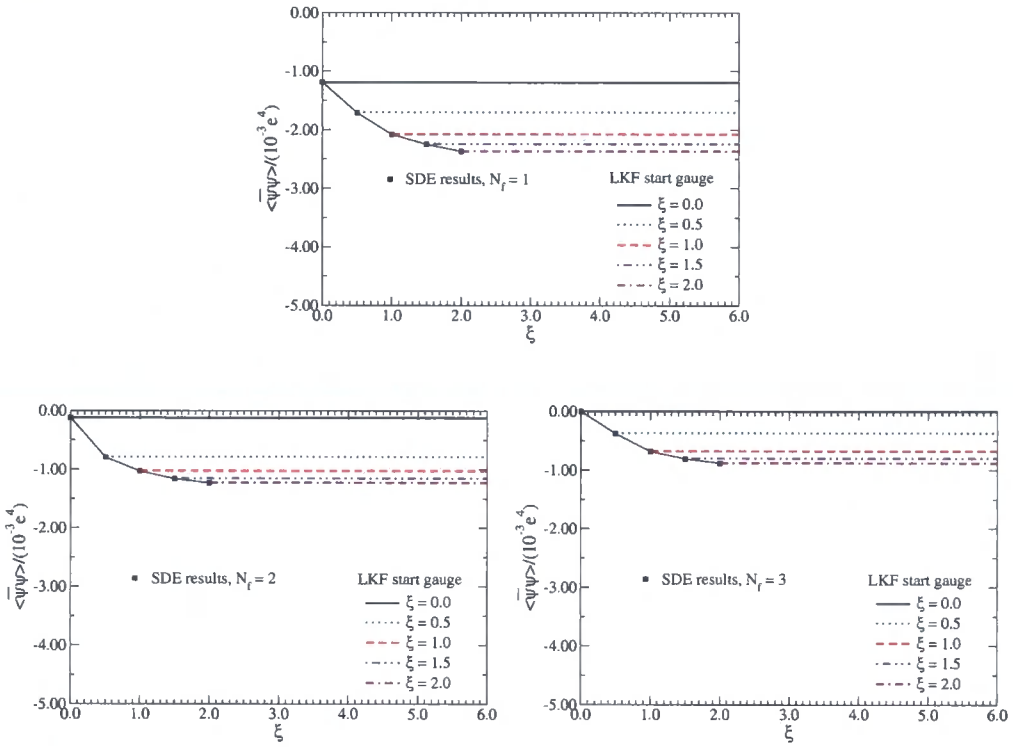

Figure 3.19: We show the result of LKF transforming a SDE with the Ball–Chiu vertex for different start gauges and active fermions. The condensate, as extracted via the asymptotic formula Eq. (3.21), remains completely flat.

take place. We start with:

$$\begin{aligned} \langle\overline{\psi}\psi\rangle_\xi &= -4\int \frac{d^3p}{(2\pi)^3}\frac{\mathcal{F}(p;\xi)\mathcal{M}(p;\xi)}{p^2+\mathcal{M}^2(p;\xi)} \\ &= -4\int \frac{d^3p}{(2\pi)^3} K_Y(p;\xi)\,, \end{aligned} \tag{3.37}$$

where the subscript ξ indicates gauge dependence of the propagator used in the trace, not of the condensate itself. We thus wish to transform $\langle\overline{\psi}\psi\rangle_0$ to $\langle\overline{\psi}\psi\rangle_\xi$ and show that it is indeed a gauge invariant object with respect to the LKF transformations.

We know from Eq. (3.19) that in momentum space the LKF transformation of the object $K_Y(p;\xi)$ is given by:

$$K_Y(p;\xi) = \frac{a}{\pi p}\int_0^\infty dk\; k\; K_Y(k;0) f(k,p)\,, \tag{3.38}$$

with

$$f(k,p) = \left[\frac{1}{a^2+(k-p)^2} - \frac{1}{a^2+(k+p)^2}\right] . \tag{3.39}$$

We can thus write the LKF transformation of Eq. (3.37) from Landau gauge as:

$$\begin{aligned} \langle\overline{\psi}\psi\rangle_\xi &= -4\int \frac{d^3p}{(2\pi)^3} K_Y(p;\xi) \\ &= -4\frac{a}{\pi}\int dk\, k\, K_Y(k;0) \int \frac{d^3p}{(2\pi)^3}\frac{f(k,p)}{p} . \end{aligned} \tag{3.40}$$

We concentrate our efforts on the integral over p

$$\begin{aligned} I \equiv \int \frac{d^3p}{(2\pi)^3}\frac{f(k,p)}{p} &= \frac{1}{2\pi^2}\int_0^\infty dp\, p f(k,p) \\ &= \frac{1}{4\pi^2}\int_{-\infty}^\infty dp\, p f(k,p) , \end{aligned} \tag{3.41}$$

where the final step is accomplished using the symmetry as $p \to -p$. Substituting in the explicit form of $f(k,p)$ from Eq. (3.39) in the above yields:

$$I = \frac{1}{4\pi^2}\int_{-\infty}^\infty dp\, p \left[\frac{1}{a^2+(k-p)^2} - \frac{1}{a^2+(k+p)^2}\right] \tag{3.42}$$

which can be written as:

$$\begin{aligned} I = \frac{1}{8i\pi^2 a}\int_{-\infty}^\infty dp\, p \Bigg[&\frac{1}{k-p-ia} + \frac{1}{k-p+ia} \\ &- \frac{1}{k-p-ia} - \frac{1}{k-p+ia}\Bigg] . \end{aligned} \tag{3.43}$$

The first two terms correspond to poles in the lower half-plane, whilst the last two terms belong to the upper half-plane since $a > 0$. Choosing to close the contour in the upper half-plane, as shown in Fig. 3.20 we have:

$$I = \frac{2\pi i}{8i\pi^2 a}\left[(k+ia) - (-k+ia)\right] = \frac{k}{2\pi a} . \tag{3.44}$$

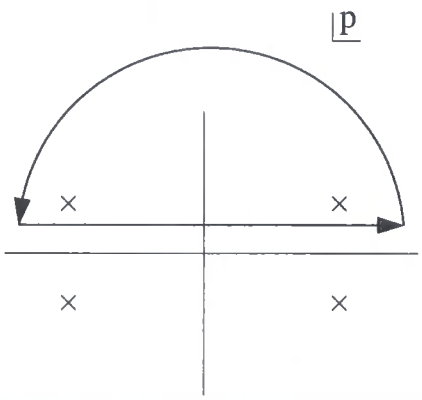

Figure 3.20: Contour of integration used in the evaluation of Eq. (3.43).

Substituting this into Eq. (3.40):

$$\begin{aligned} \langle\overline{\psi}\psi\rangle_\xi &= -4\int \frac{d^3p}{(2\pi)^3} K_Y(p;\xi) \\ &= -4\frac{1}{2\pi^2}\int dk\; k^2\; K_Y(k;0)\;, \end{aligned} \tag{3.45}$$

where crucially the right-hand side is independent of the gauge transformation parameter a. Relabelling the integration momentum of the second term to p and restoring the trivial angular integrals demonstrates that:

$$-4\int \frac{d^3p}{(2\pi)^3} K_Y(p;\xi) = -4\int \frac{d^3p}{(2\pi)^3} K_Y(p;0) \tag{3.46}$$

and so the condensate $\langle\overline{\psi}\psi\rangle$ is indeed independent of the gauge parameter ξ upon application of the LKF transformation.

This shows that the LKF transformations will give a gauge independent condensate regardless of the Green's function used as input and so cannot be used as a discriminant between vertex ansätze or any other truncation of the SDE hierarchy.

3.3 Summary

We examined numerical solutions of non-compact QED in three-dimensions by use of the truncated Schwinger-Dyson equations. This was done for the quenched case with a variety of vertex ansätze, in which we determined the gauge dependence of the condensate for solutions in the dynamically broken phase. We compared

solutions in arbitrary covariant gauge with those obtained by LKF transformations of Landau gauge SDE studies, finding that gauge covariance was violated for all but the CP vertex, which fails to match perturbative calculations. We also employed the KP vertex to complete the numerical study, finding that it was a poor ansatz in quenched QED_3.

We turned our attention to unquenched studies in multiple gauges where the criticality of the theory is of interest. The KP vertex proved to be largely inapplicable here due to its explicitly four-dimensional forms, and was hence not appropriate in furthering estimates for N_f^{crit}. Solutions with the Ball–Chiu vertex in Landau gauge were LKF transformed, for both the quenched and $N_f = 1$ case, which on comparison with the relevant SDE solutions again showed violation of gauge covariance. Qualitatively, the solutions behave quite differently with the shoulder of the LKF obtained mass-function generally moving down and to the right with increasing gauge; the SDE solutions simply move downwards.

Though the LKF transformations tell us nothing more about the validity of our solutions, there is still use for them. In order to use these as a tool for learning more about vertex construction, one must turn their attention towards the LKFT of higher order Green's functions, i.e. the three-point vertex, whose LKFT is given by Eq. (1.102). Although a difficult task even in three-dimensions, if successfully applied to even the bare-vertex in Landau gauge, it is likely to show how the structure of the vertex for arbitrary covariant gauges is built-up, highlighting inadequecies in our existing ansätze.

Chapter 4

Quantum Chromodynamics

Quantum Chromodynamics (QCD) is the accepted description of quarks and gluons at the Lagrangian level. It has enjoyed much success in studies at high-energies where its property of asymptotic freedom allows one to perform perturbative expansions. There we find remarkable agreement between theoretical calculations and their experimental measurements. These perturbative calculations rely upon the LSZ formalism, in which asymptotic states are regarded as free fields. Although this works well for gauge theories such as QED, the situation is far more complicated in QCD where asymptotic states are composite. Indeed, quarks and gluons have not been directly observed, a phenomenon known as confinement, and so these fields do not even appear in external states.

Ultimately, any study of high-energy physics requires knowledge of low-energy phenomena; bringing our interest towards studies of hadrons and confinement. We must therefore formulate alternative methods to extract the relevant information from our QCD Lagrangian. It is the understanding of how coloured objects such as quarks and gluons come together and form into the colourless hadrons, which necessitates a non-perturbative study of the infrared behaviour of QCD.

Many methods have been employed over the years to describe the physical spectrum of hadrons and their scattering processes. One of the first models, that of Nambu–Jona-Lasinio (NJL), was developed to describe nucleons in the pre-QCD era; its use as an effective field theory has persisted since its inception in 1961 with many extensions and developments. Besides effective theories, many tools have been devised with the aim of extracting information from the Lagrangian of QCD, including chiral-perturbation theory, the operator product expansion, and lattice field theory. This latter involves the studying of a large quantity of representative gauge configurations on a discretized momentum grid, whose spacing acts as reg-

ulator for the intrinsic divergences of the QFT. However, to make this simulation tractable there are severe limits placed on the volume of space-time examined, with the discretization softening any singularities that may be so essential to the confinement process. Of course, they also have the problem of keeping quarks with such small masses "inside the box".

The approach that we have chosen to follow in this thesis is that of the Schwinger-Dyson equations. In contrast to lattice methods, these can be formulated in the continuum limit thus avoiding two key caveats of the numerically intensive lattice method. However, as we have previously discussed, the infinite tower that comprises the SDEs must be truncated by introducing ansätze for some sufficiently low order n-point Green's functions – in practice this means the three- and four-point vertices of QCD. In Sect. 2.1 we showed how one may construct the fermion-boson vertex of Abelian QED, upon which we will base the quark-gluon vertex of QCD. The remaining vertices (ghost-gluon, three- and four-gluon) will be replaced by either their bare form, some suitable dressed vertex, or neglected altogether.

In the next few sections we will introduce a selection of approximations to the SDEs of QCD. We begin with an overview of the Quark sector and the phenomenology that may be derived from our solutions, without giving specifics as to the model employed. Following this we examine the Yang-Mills sector, with and without ghosts, and summarise the truncation scheme of Alkofer and Fischer [96] that will play a rôle in later studies. One may use these to garner phenomenological descriptions of the non-perturbative coupling in QCD, which we contrast with another well-established phenomenologically inspired model [97, 98]. We will end by comparing and contrasting some chiral observables, specifically the pion decay constant, quark condensate, and another quantity known as the Euclidean mass.

4.1 Yang-Mills Studies

The Yang-Mills (YM) sector of QCD comprises of the ghosts and gluons which, due to the self-interactions that arise from the non-Abelian group structure, is an interesting system in itself to study in the absence of quarks – for example, one could imagine bound states of gluons, the so-called glue-balls. From the Schwinger-Dyson equations of Eq. (1.90), we see that there is only one contribution that involves quark loops, leading us to the assumption that the main structure of the ghost and gluon propagators largely arises from just the YM part. Of course, rather than calculating these directly, we could just speculate upon their form and create phe-

nomenological models of the running coupling for use in the quark SDE. However, we need something from which to draw inspiration, and so explicit solutions to the YM sector – even if with some gross approximation – are a necessary requirement. Thankfully though, it turns out that the ultraviolet behaviour is quite well-known from perturbation theory, and that the infrared dynamics may often be calculated analytically (for a given truncation scheme) in the Schwinger-Dyson approach, leaving us the intervening momentum region open to speculation. We must remember, however, that these Green's functions are gauge dependent objects and so their exact structure will depend greatly upon the gauge-fixing prescription and the choice of gauge parameter.

As a first approximation, one may wish to neglect the quark loop contribution to the YM sector of QCD, and this has formed the basis of many studies in the literature. Initial studies were concerned with determining the infrared behaviour of the gluon propagator and worked within the Axial gauge:

$$n_\mu \cdot A^{a\mu} = 0 \,, \tag{4.1}$$

such that the gluon propagator is transverse to the gauge vector n_μ. This gauge is chosen due to the absence of ghost-fields and so that the four-gluon vertex is projected out. Hence, the gluon propagator can be written in Euclidean space as:

$$D_{\mu\nu}(p^2,\gamma) = -\frac{i}{p^2}\left(F(p^2,\gamma)M_{\mu\nu} + H(p^2,\gamma)N_{\mu\nu}\right) \,, \tag{4.2}$$

for gauge parameter $\gamma = (n\cdot p)^2/n^2p^2$, with the two tensors $M_{\mu\nu}$ and $N_{\mu\nu}$ given by:

$$M_{\mu\nu} = g_{\mu\nu} - \frac{p_\mu n_\nu + p_\nu n_\mu}{n\cdot p} + n^2\frac{p_\mu p_\nu}{(n\cdot p)^2} \,, \tag{4.3}$$

$$N_{\mu\nu} = g_{\mu\nu} - \frac{n_\mu n_\nu}{n^2} \,. \tag{4.4}$$

An ansatz for the three-gluon vertex is provided via recourse to the Slavnov-Taylor identity:

$$q_\mu \Gamma^{\mu\nu\rho}(p,q,k) = \Pi^{\mu\rho}(k) - \Pi^{\mu\rho}(p) \,, \tag{4.5}$$

where $\Pi^{\lambda\mu}(p^2,\gamma)$ is the gluon vacuum polarisation tensor, defined as:

$$\Pi^{\lambda\mu}D_{\mu\nu} = g^\lambda_\nu - \frac{n^\lambda n_\nu}{n\cdot p} \,. \tag{4.6}$$

The longitudinal component of the full-vertex may be constrained with this, yield-

ing [99]:

$$\begin{aligned}\Gamma_L^{\mu\nu\rho}(p,q,k) &= g^{\mu\nu}\left(\frac{p_\rho}{F(p^2,\gamma)}-\frac{q_\rho}{F(q^2,\gamma)}\right)\\ &+\frac{1}{p^2-q^2}\left(\frac{1}{F(p^2,\gamma)}-\frac{1}{F(q^2,\gamma)}\right)(p^\nu q^\mu - g^{\mu\nu}p\cdot q)\,(p-q)^\rho\\ &+ \quad \text{cyclic permutations}\,. \end{aligned} \tag{4.7}$$

The drawback of working in Axial gauge is the dependence of the propagator upon an unphysical gauge, the presence of gauge dependent singularities for $p\cdot n = 0$ and the loss of Lorentz invariance. Moreover, these studies [100,101] have often neglected the H term, since at leading order $F = 1$ and $H = 0$, and the possibility of cancellations in the infrared has not been ruled out. This last point can have dramatic impact upon the degree of singularity of the gluon in the deep infrared [102].

Alternative first investigations have also been performed using linear covariant gauges, especially in Landau gauge. These neglected the contribution from the Ghost degrees of freedom [36, 103–107]. The contribution from the four-gluon vertex is no longer projected out, and so here is simply ignored in the hope that consideration of the three-gluon vertex alone would be sufficient; the belief is that the two-loop like diagrams are sub-leading contributions at both infrared and ultraviolet momenta.

One of the first forays into solving the gluon SDE was performed by Mandelstam [103]. Here we ignore all but the three-point gluon vertex, with the corresponding SDE depicted in Fig. 4.1. An ansatz for the longitudinal part of the vertex is provided by the Slavnov-Taylor identity, which with ghosts neglected is:

$$p_\mu\Gamma^{\mu\nu\rho}(k,p,q) = \frac{q^2}{\mathcal{Z}(q^2)}\left(\delta^{\nu\rho}-\frac{q^\nu q^\rho}{q^2}\right) - \frac{p^2}{\mathcal{Z}(p^2)}\left(\delta^{\nu\rho}-\frac{p^\nu p^\rho}{p^2}\right)\,, \tag{4.8}$$

where all momenta are incoming, and $\mathcal{Z}$ is the gluon dressing function defined by:

Figure 4.1: The SDE for the gluon in the Mandelstam approximation. Filled dots indicate full propagators and vertices. Ghosts and four-point vertices are neglected.

$$D_{\mu\nu}(k) = \left(g_{\mu\nu} - \frac{k_\mu k_\nu}{k^2}\right)\frac{\mathcal{Z}(k^2)}{k^2} + \xi\frac{k_\mu k_\nu}{k^4}\,, \tag{4.9}$$

in covariant gauges. Following the same procedure of Ball and Chiu [33], one arrives at the ansatz for the longitudinal part of the vertex:

$$\begin{aligned}\Gamma^{\mu\nu\rho}_L(k,p,q) &= A_+(k^2,p^2)\delta^{\mu\nu}\,(k-p)^\rho + A_-(k^2,p^2)\delta^{\mu\nu}\,(k+p)^\rho \\ &\quad + C(k^2,p^2)\,(\delta^{\mu\nu}kp - k^\nu p^\mu) + \text{cyclic permutations}\,,\end{aligned} \tag{4.10}$$

where:

$$A_\pm(k^2,p^2) = \frac{1}{2}\left(\frac{1}{\mathcal{Z}(k^2)} \pm \frac{1}{\mathcal{Z}(p^2)}\right) \qquad , \qquad C(k^2,p^2) = 2\frac{A_-(k^2,p^2)}{k^2-p^2}\,. \tag{4.11}$$

One may simplify Eq. (4.10) to:

$$\Gamma^{\mu\nu\rho}_L(k,p,q) = A_+(k^2,p^2)\delta^{\mu\nu}\,(k-p)^\rho\,, \tag{4.12}$$

if one assumes $\mathcal{Z}$ to be slowly varying. This significantly reduces the complexity of the SDE we have to solve, while at the same time embodying some of the dressing provided by the Slavnov-Taylor identity. Solutions have been found [108], which are given in Fig. 4.2. We see here that, without ghosts present and with this particular vertex ansatz, that the gluon is infrared singular.

Before we discuss the inclusion of ghosts in the SDEs, we first comment upon a qualitatively similar analysis to the above in which quark loops [36] are also considered. Therein the authors found that the introduction of even one quark flavour has a de-confining effect on the gluon; that is the degree of singularity of the gluon in the infrared is softened. Thus the infrared behaviour is not necessary as given and may yet be greatly affectly by the ghost sector of the theory.

4.1.1 Including Ghosts

Various arguments have been put forward regarding the behaviour of the gluon propagator at small momentum. It has been shown by Gribov [109] that the Faddeev-Popov gauge fixing procedure leaves a residual gauge-transformation leading to *Gribov copies*. Elimination of these through the introduction of additional ghost fields [109,110] leads to the low-energy behaviour $(q^2)^\kappa$ for the gluon, with κ strictly positive. Hence, contrary to those studies in which the ghosts are neglected (and believed to be infrared finite or vanishing), it is the gluon propagator that must vanish in the infrared.

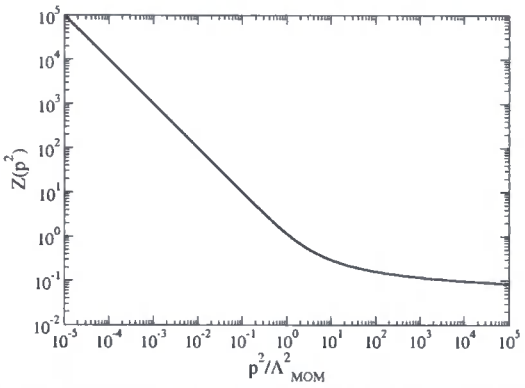

Figure 4.2: The gluon dressing function, $Z(p^2)$ in the Mandelstam approximation with ghosts neglected.

Whilst the first forays in the SDE approach to QCD were being made, studies of quenched Lattice-QCD had been rapidly advancing. Here the propagators of both ghosts and gluons were calculated, albeit for rather small lattice volumes [111]. Though these cannot yet probe deep into the infrared, it was found that an infrared enhanced ghost with vanishing gluon, as suggested by Gribov, was not inconsistent with the simulations and so further work from the Lattice community, as well as the Schwinger-Dyson community, was needed.

Returning to our SDE studies, now with the inclusion of ghosts, we have three- and four-point gluon vertices, the ghost-gluon vertex and the quark-gluon vertex, together with propagators for the ghost, gluon and quarks. These manifest themselves as tadpole like diagrams, one-loop forms and several two-loop contributions in the form of sunset and squint diagrams. Although we are now prepared to have ghosts in the picture, we still choose to neglect the four-gluon vertex, and hence two-loop diagrams; the tadpoles are safely ignored since they only contribute a UV divergent constant and are hence renormalised away.

Figure 4.3: The quenched ghost SDE. Filled dots indicate full propagators and vertices. Dashed lines indicate ghosts, whilst wiggly lines represent gluons.

The Schwinger-Dyson equation for the ghost is given by:

$$[D_G(k)]^{-1} = -\widetilde{Z}_3 + g^2 N_c \widetilde{Z}_1 \int \frac{d^4q}{(2\pi)^4} \Gamma^{(0)\mu}(k) D_{\mu\nu}(k-q) \Gamma^{\nu}(k,q) D_G(q) \,, \qquad (4.13)$$

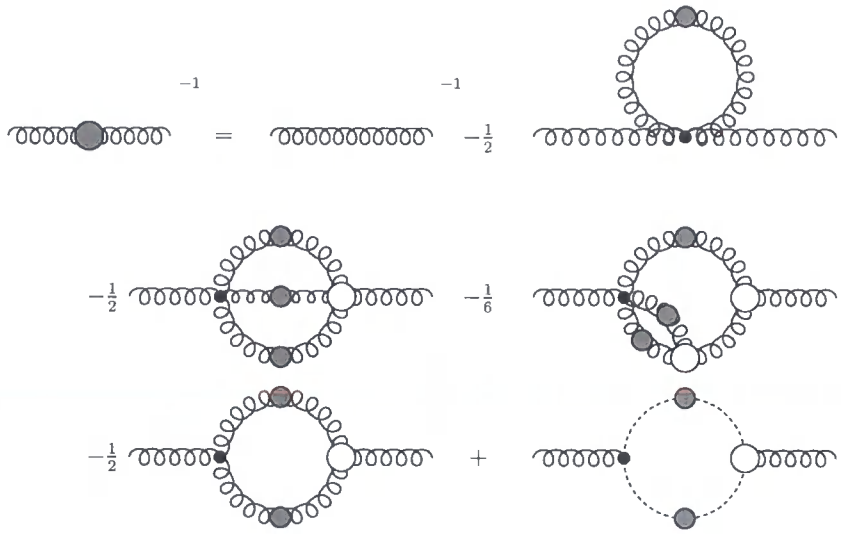

Figure 4.4: The quenched gluon SDE. Filled dots indicate full propagators and vertices. Dashed lines indicate ghosts, whilst wiggly lines represent gluons.

where we use:

$$D_G(k) = -\frac{\mathcal{G}(k^2)}{k^2} \quad , \quad D_{\mu\nu}(k) = \left(g_{\mu\nu} - \frac{k_\mu k_\nu}{k^2}\right)\frac{\mathcal{Z}(k^2)}{k^2} + \xi\frac{k_\mu k_\nu}{k^4} \, , \tag{4.14}$$

as representations of the propagators. One first step is to simply extend the Mandelstam approximation by the inclusion of ghosts, with some form for the dressing function. A first approximation scheme for ghost-gluon vertex was proposed in [112,113]:

$$\Gamma_\mu(p,q) = -q_\mu\left(\frac{\mathcal{G}(k^2)}{\mathcal{G}(q^2)}\right) - p_\mu\left(\frac{\mathcal{G}(k^2)}{\mathcal{G}(p^2)} - 1\right) \, , \tag{4.15}$$

drawing influence again from the Slavnov-Taylor identities arising from the BRS symmetry. Thus, in Euclidean space the ghost renormalisation function reads:

$$\frac{1}{\mathcal{G}(k^2)} = \widetilde{Z}_3 - g^2 N_c \int \frac{d^4q}{(2\pi)^4}\frac{\Delta^2}{p^2}\frac{\mathcal{Z}(p^2)\mathcal{G}(q^2)}{k^2p^2q^2}\left(\frac{\mathcal{G}(p^2)}{\mathcal{G}(q^2)} + \frac{\mathcal{G}(p^2)}{\mathcal{G}(k^2)} - 1\right) \, , \tag{4.16}$$

with triangle function $\Delta^2 = (k\cdot q)^2 - k^2q^2$ and $p = k - q$.

To tackle the gluon SDE, a vertex ansatz is required for the three-gluon vertex.

A suggestion following the same approximations used in determining Eq. (4.15) is:

$$\begin{aligned}\Gamma_{\mu\nu\rho}(p,q,k) &= A_+(p^2,q^2;k^2)\delta_{\mu\nu}(p-q)_\rho + A_-(p^2,q^2;k^2)\delta_{\mu\nu}(p+q)_\rho \\ &+ 2\frac{A_-(p^2,q^2;k^2)}{p^2-q^2}\left(\delta_{\mu\nu}\sqrt{p^2q^2} - p_\nu q_\mu\right)(p-q)_\rho \\ &+ \text{cyclic permutations}\,. \end{aligned} \tag{4.17}$$

where the quantity $A_\pm$ is defined as:

$$A_\pm(p^2,q^2;k^2) = \frac{1}{2}\mathcal{G}(k^2)\left(\frac{\mathcal{G}(q^2)}{\mathcal{G}(p^2)\mathcal{Z}(p^2)} \pm \frac{\mathcal{G}(p^2)}{\mathcal{G}(q^2)\mathcal{Z}(q^2)}\right)\,. \tag{4.18}$$

The SDE for the gluon reads:

$$\begin{aligned}[D_{\mu\nu}]^{-1} &= Z_3\left[D^{(0)}_{\mu\nu}\right]^{-1} - g^2N_c\widetilde{Z}_1\int\frac{d^4q}{(2\pi)^4}q_\mu D_G(p)D_G(q)\Gamma_\nu(q,p) \\ &- \frac{g^2N_cZ_1}{2}\int\frac{d^4q}{(2\pi)^4}\Gamma^{(0)}_{\mu\rho\alpha}(k,-p,q)D_{\alpha\beta}(q)D_{\rho\sigma}(p)\Gamma_{\beta\sigma\nu}(-q,p,-l)\,. \end{aligned} \tag{4.19}$$

Employing the above ansätze in Eq. (4.19) and projecting with the Brown-Pennington projector gives:

$$\begin{aligned}\frac{1}{\mathcal{Z}(k^2)} &= Z_3 - Z_1\frac{g^2N_c}{6}\int\frac{d^4q}{(2\pi)^4}\left\{N_1(p^2,q^2;k^2)\frac{\mathcal{Z}(p^2)\mathcal{G}(p^2)\mathcal{Z}(q^2)\mathcal{G}(q^2)}{\mathcal{Z}(k^2)\mathcal{G}^2(k^2)}\right. \\ &+ \left. N_2(p^2,q^2;k^2)\frac{\mathcal{Z}(p^2)\mathcal{G}(p^2)}{\mathcal{G}(q^2)} + N_2(q^2,p^2;k^2)\frac{\mathcal{Z}(q^2)\mathcal{G}(q^2)}{\mathcal{G}(p^2)}\right\}\frac{\mathcal{G}(k^2)}{k^2p^2q^2} \\ &+ \frac{g^2N_c}{3}\int\frac{d^4q}{(2\pi)^4}\left\{\left(\frac{k^2q^2-4\,(k\cdot q)^2}{k^2}\right)\left(\mathcal{G}(k^2)\mathcal{G}(p^2)-\mathcal{G}(q^2)\mathcal{G}(p^2)\right)\right. \\ &\left. -\frac{4\,(k\cdot q)^2-3k\cdot qk^2-k^2q^2}{k^2}\mathcal{G}(k^2)\mathcal{G}(q^2)\right\}\frac{1}{k^2p^2q^2} \end{aligned} \tag{4.20}$$

Explicit forms for N_i are given in the appendices of [113].

These two equations are simplified yet further by the introduction of angular approximations. For the ghost SDE, the angular replacement $\mathcal{G}(p^2) \to \mathcal{G}(k^2)$ is made for $q^2 < k^2$, whilst for $q^2 > k^2$ the substitution is $\mathcal{G}(p^2), \mathcal{G}(k^2) \to \mathcal{G}(q^2)$. Similar replacements occur for $\mathcal{Z}$. The angular approximations for the gluon SDE are detailed in [113] and necessitates the $q^2 < k^2$ contribution from the three-gluon loop to be neglected. The authors therein showed numerically that this was an acceptable approximation since we are most concerned with the infrared and ultraviolet behaviour rather than the interpolating behaviour between these regions.

The resultant equations to solve in this scheme are hence:

$$\frac{1}{\mathcal{G}(k^2)} = \widetilde{Z}_3 - \frac{g^2}{16\pi^2}\frac{3N_c}{4}\left\{\frac{1}{2}\mathcal{Z}(k^2)\mathcal{G}(k^2) + \int_{k^2}^{\Lambda^2}\frac{dq^2}{q^2}\mathcal{Z}(q^2)\mathcal{G}(q^2)\right\}, \quad (4.21)$$

and:

$$\begin{aligned}\frac{1}{\mathcal{Z}(k^2)} &= Z_3 + Z_1\frac{g^2}{16\pi^2}\frac{N_c}{3}\left\{\int_0^{k^2}\frac{dq^2}{k^2}\left(\frac{7}{2}\frac{q^4}{k^4} - \frac{17}{2}\frac{q^2}{k^2} - \frac{9}{8}\right)\mathcal{Z}(q^2)\mathcal{G}(q^2)\right. \\ &\left. + \int_{k^2}^{\Lambda^2}\frac{dq^2}{q^2}\left(\frac{7}{2}\frac{k^2}{q^2} - 7\right)\mathcal{Z}(q^2)\mathcal{G}(q^2)\right\} \\ &+ \frac{g^2}{16\pi^2}\frac{N_c}{3}\left\{\int_0^{k^2}\frac{dq^2}{k^2}\frac{3}{2}\frac{q^2}{k^2}\mathcal{G}(k^2)\mathcal{G}(q^2) - \frac{1}{3}\mathcal{G}^2(k^2) + \frac{1}{2}\int_{k^2}^{\Lambda^2}\frac{dq^2}{q^2\mathcal{G}^2(q^2)}\right\}.\end{aligned} \quad (4.22)$$

By undertaking an infrared analysis, it was found that the resulting solutions have a power-like behaviour

$$\mathcal{Z}(p^2) \propto \left(p^2\right)^{2\kappa}, \quad \mathcal{G}(p^2) \propto \left(p^2\right)^{-\kappa} \quad (4.23)$$

The calculation contained within [113] concluded that this $\kappa \simeq 0.92$. This system was solved numerically in [114].

Following this work, Atkinson and Bloch [115] found inconsistency with this ansatz and the angular approximations. They performed a similar analysis by employing a bare, rather than dressed vertex and the y–max approximation[1]. Starting from Eq. (4.20), on removing the dressing and performing the trivial angular integrals, one is left to solve:

$$\begin{aligned}\frac{1}{\mathcal{Z}(k^2)} &= Z_3 + \widetilde{Z}_1\frac{g^2N_c}{48\pi^2}\left(\int_0^{k^2}\frac{dq^2}{k^2}\mathcal{G}(k^2)\left[-\frac{q^4}{k^4} + \frac{3q^2}{2k^2}\right)\mathcal{G}(q^2) + \int_{k^2}^{\Lambda^2}\frac{dq^2}{2q^2}\mathcal{G}^2(q^2)\right] \\ &+ Z_1\frac{g^2N_c}{48\pi^2}\left[\int_0^{k^2}\frac{dq^2}{k^2}\mathcal{Z}(k^2)\left(\frac{7q^4}{2k^4} - \frac{17q^2}{2k^2} - \frac{9}{8}\right)\mathcal{Z}(q^2)\right. \\ &\left. + \int_{k^2}^{\lambda^2}\frac{dq^2}{q^2}\left(-7 + \frac{7k^2}{8q^2}\right)\mathcal{Z}^2(q^2)\right] \\ \frac{1}{\mathcal{G}(k^2)} &= \widetilde{Z}_3 - \widetilde{Z}_1\frac{9}{4}\frac{g^2N_c}{48\pi^2}\left[\int_0^{k^2}\frac{dq^2}{k^2}\frac{q^2}{k^2}\mathcal{Z}(k^2)\mathcal{G}(q^2) + \int_{k^2}^{\Lambda^2}\frac{dq^2}{q^2}\mathcal{Z}(q^2)\mathcal{G}(q^2)\right].\end{aligned} \quad (4.24)$$

At which point a further simplification was made, the omission of the term corresponding to the gluon loop (i.e. set $Z_1 = 0$). An infrared analysis of this system with

[1]In this case, this entails $\mathcal{G}(p^2) \to \mathcal{G}(\min(p^2, q^2))$ and similarly for $\mathcal{Z}(p^2)$.

the angular approximation yields a similar power-law behaviour, with $\kappa \simeq 0.77$.

So far we have seen two truncation schemes, one with a dressed vertex, that aimed to solve the coupled system of ghosts and gluons. These both came to the conclusion that, in Landau gauge, it was the ghost that is singular in the infrared, whilst the gluon vanishes. Moreover, further analysis showed that a renormalisation-group invariant was:

$$\alpha = \widetilde{Z}_1^{-2} Z_3 \widetilde{Z}_3^2 \alpha_0 \,, \tag{4.25}$$

and, noting that in Landau gauge $\widetilde{Z}_1 = 1$ [116], one could identify this with the running coupling:

$$\alpha(p^2) = \alpha(\mu^2)\mathcal{Z}(p^2)\mathcal{G}^2(p^2) \,. \tag{4.26}$$

With the definition of the non-perturbative coupling given in Eq. (4.26), together with the infrared analysis of Eq. (4.23) we have an infrared stable fixed point, $\alpha_s \simeq 9.5$ for Alkofer *et al*, while Atkinson *et al* obtain $\alpha_s \simeq 11.47$

Before considering further ansätze, or indeed removing the angular approximation, we must first consider the ultraviolet behaviour of these solutions. From an expansion in α, we expect for some perturbative renormalisation point μ:

$$\mathcal{Z}(p^2) \equiv \mathcal{Z}(\mu^2)\left(1 + \omega \log \frac{p^2}{\mu^2}\right)^{\gamma} \,, \tag{4.27}$$

$$\mathcal{G}(p^2) \equiv \mathcal{G}(\mu^2)\left(1 + \omega \log \frac{p^2}{\mu^2}\right)^{\delta} \,, \tag{4.28}$$

where the exponents γ and δ should be related via $\gamma + 2\delta = -1$. In the case of Atkinson *et al* [115], the omission of the gluon loop was expected to cause inconsistency. They find $\gamma = \frac{1}{8}$ and $\delta = -\frac{9}{16}$ which does not agree with the one-loop anomalous dimensions. Composing the running coupling, we find $\beta_0 = 4$, in stark contrast to $\beta_0 = 11$ we would expect for quenched QCD with $N_c = 3$.

4.1.2 Removing Angular Approximations

So far we have discussed some of the preliminary studies of QCD involving the Schwinger-Dyson approach to non-perturbative phenomena. It is generally believed that confinement requires some form of singularity in the Yang-Mills sector, and those studies in Axial gauge, or in which ghosts are neglected, necessarily gave this rôle to the gluons.

However, recent studies including the ghost contribution [112, 113, 115] found that in Landau gauge, that it is the ghost that becomes singular in the infrared,

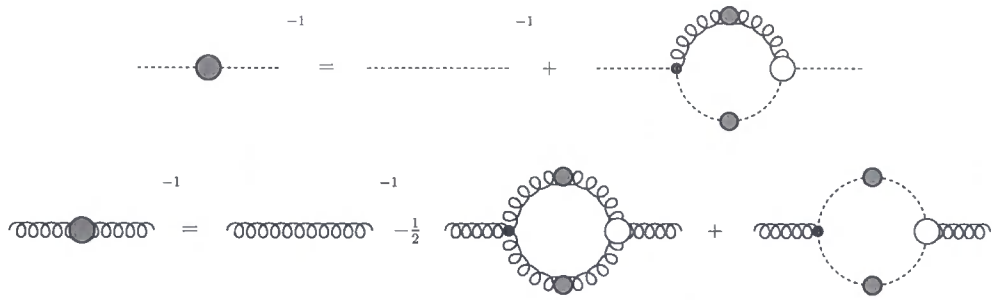

Figure 4.5: The quenched ghost and gluon SDE neglecting two-loop diagrams and tadpoles. Filled dots indicate full propagators and vertices. Dashed lines indicate ghosts, whilst springs represent gluons.

with the gluon vanishing. Further improvements to the ansätze contained there, together with the removal of the angular approximation, led to their numerical solution contained within [27], which we consider here.

The full quenched system of Schwinger-Dyson equations for the ghost and gluon propagator is shown in Fig. 4.5. For completeness we repeat the form of the ghost and gluon propagators:

$$D_G(k) = -\frac{\mathcal{G}(k^2)}{k^2} \quad , \quad D_{\mu\nu}(k) = \left(g_{\mu\nu} - \frac{k_\mu k_\nu}{k^2}\right)\frac{\mathcal{Z}(k^2)}{k^2} + \xi\frac{k_\mu k_\nu}{k^4} \, , \tag{4.29}$$

These two propagators are characterised by the two dressing functions $\mathcal{G}(k^2)$ and $\mathcal{Z}(k^2)$.

As with the ghost-gluon system of Alkofer *et al.* [112,113], in which an angular approximation was employed, we expect the ultraviolet behaviour to match one-loop resummed perturbation theory:

$$\mathcal{Z}(p^2) \equiv \mathcal{Z}(\mu^2)\left(1 + \omega \log\frac{p^2}{\mu^2}\right)^{\gamma} , \tag{4.30}$$

$$\mathcal{G}(p^2) \equiv \mathcal{G}(\mu^2)\left(1 + \omega \log\frac{p^2}{\mu^2}\right)^{\delta} , \tag{4.31}$$

where $\omega = 11N_c\alpha(\mu^2)/12\pi$ for $N_f = 0$. the exponents γ and δ are the anomalous dimensions of the gluon and ghost, related via $\gamma + 2\delta = -1$. In perturbation theory the ghost anomalous dimension takes value $-9/44$ for zero flavours, and hence for consistency we must also have $\gamma = -13/22$.

The proposed ansätze are that the ghost-gluon vertex be taken as bare:

$$\Gamma_\mu(k,p) = iq_\mu \, , \tag{4.32}$$

and the bare three-gluon vertex is dressed according to:

$$\Gamma_{\lambda\mu\nu}(k,p;q) = \frac{1}{\tilde{Z}_1(\mu,\Lambda)} \frac{G(k^2)^{-2-6\delta}}{Z(k^2)^{1+2\delta}} \frac{G(q^2)^{-2-6\delta}}{Z(q^2)^{1+2\delta}} \Gamma^{(0)}_{\lambda\mu\nu}(k,p;q) \tag{4.33}$$

with $q = k - p$. Two loop-like diagrams are ignored, as are the tadpoles that contribute an infinite constant removed by renormalisation. The SDEs for the ghost and gluon, Fig. 4.5, are therefore:

$$\frac{1}{\mathcal{G}(x)} = \tilde{Z}_3 - g^2 N_c \int \frac{d^4k}{(2\pi)^4} \frac{K(x,y,z)}{xy} \mathcal{G}(y)\mathcal{Z}(z) \,, \tag{4.34}$$

$$\begin{aligned} \frac{1}{\mathcal{Z}(x)} &= Z_3 + g^2 \frac{N_c}{3} \int \frac{d^4k}{(2\pi)^4} \frac{M(x,y,z)}{xy} \mathcal{G}(y)\mathcal{G}(z) \,, \\ &\quad + g^2 \frac{N_c}{3} \int \frac{d^4k}{(2\pi)^4} \frac{Q(x,y,z)}{xy} \frac{\mathcal{G}(y)^{-2-6\delta}}{\mathcal{Z}(y)^{3\delta}} \frac{\mathcal{G}(z)^{-2-6\delta}}{\mathcal{Z}(z)^{3\delta}} \,, \end{aligned} \tag{4.35}$$

where $x = p^2$, $y = k^2$ and $z = (k-p)^2 = q^2$. We define the general projector:

$$\mathcal{P}^{(\zeta)}_{\mu\nu} = \delta_{\mu\nu} - \zeta \frac{p_\mu p_\nu}{p^2} \,, \tag{4.36}$$

where $\zeta = 4$ is the Brown-Pennington projector, and $\zeta = 1$ the transverse projector. Applying the projector, Eq. (4.36), to the gluon SDE of Eq. (4.19), and subtracting quadratic terms in $4 - \zeta$ according to Eq. (3.32) of [27], yields the kernels:

$$\begin{aligned} K(x,y,z) &= \frac{1}{z^2}\left(-\frac{(x-y)^2}{4}\right) + \frac{1}{z}\frac{x+y}{2} - \frac{1}{4} \,, \\ M(x,y,z) &= \frac{1}{z}\left(-\frac{1}{4}x + \frac{y}{2} - \frac{1}{4}\frac{y^2}{x}\right) + \frac{1}{2} + \frac{1}{2}\frac{y}{x} - \frac{1}{4}\frac{z}{x} \,, \\ Q(x,y,z) &= \frac{1}{z^2}\left(\frac{1}{8}\frac{x^3}{y} + x^2 - \frac{9}{4}xy + y^2 + \frac{1}{8}\frac{y^3}{x}\right) \\ &\quad + \frac{1}{z}\left(\frac{x^2}{y} - 4(x+y) + \frac{y^2}{x}\right) \\ &\quad - \left(\frac{9}{4}\frac{x}{y} + \frac{1}{4} + \frac{9}{4}\frac{y}{x}\right) + z\left(\frac{1}{x} + \frac{1}{y}\right) + z^2\frac{1}{8}\frac{1}{xy} \,, \end{aligned} \tag{4.37}$$

where we have set $\zeta = 1$. The philosophy here is that both subtractions take place in the gluon loop to prevent interference with the infrared properties. An infrared analysis provides us with power-law solutions:

$$Z(x) = Ax^{2\kappa} \,, \qquad G(x) = Bx^{-\kappa} \,. \tag{4.38}$$

As in the previous section, it was noted that from the Slavnov-Taylor identity $\widetilde{Z}_1 = Z_g \widetilde{Z}_3 Z_3^{1/2}$ a renormalisation group invariant was:

$$\alpha = \widetilde{Z}_1^{-2} Z_3 \widetilde{Z}_3^2 \alpha_0 \, . \tag{4.39}$$

Combining this with the result in Landau gauge, $\widetilde{Z}_1 = 1$ [116], we arrive at the non-perturbative running of the coupling as fixed by the ghost-gluon vertex:

$$\alpha(p^2) = \alpha(\mu^2)\, \mathcal{G}^2(p^2, \mu^2)\, \mathcal{Z}(p^2, \mu^2) \, , \tag{4.40}$$

where we have used $\alpha = g^2/4\pi$. Using the power laws of Eq. (4.38) we obtain the fixed point value of the coupling in the infrared:

$$\alpha(0) = \frac{g^2}{4\pi} A B^2 \, , \tag{4.41}$$

in terms of the coefficients A and B. Infrared matching with the transversal tensor gives rise to $\kappa \simeq 0.595353$. With this value for κ, the fixed point for the coupling in the infrared is found to be:

$$\alpha(0) \simeq \frac{8.915}{N_c} \tag{4.42}$$

This entails that A and B of Eq. (4.38) are related. As a result, we cannot employ the renormalisation condition $G(\mu^2) = Z(\mu^2) = 1$ and must instead use the more relaxed condition $Z(\mu^2)G^2(\mu^2) = 1$.

Numerically, the gluon equation is subtracted at the renormalisation point $p^2 = s = 980.975$ with the ghost equation subtracted at $t = 0$. This latter choice is necessary to give numerical stability to the solution, and momentum units are left unspecified for now. We are in fact free to choose values for A or B, so long as they satisfy the relation of Eq. (4.41), and this consequently determines $Z(\mu)$ *and* μ though the requirement that our functions remain smooth at some infrared matching point. We make the arbitrary choice $A = 420$, which leads to $Z(s) = 0.26847$ to avoid discontinuities in the IR[2]. By specifying $\alpha(\mu^2) = g^2/4\pi = 0.97$ we determine the value of the renormalisation point.

The momentum scale is fixed by requiring $\alpha(M_Z^2) = 0.1176$ at the Z-mass, $M_Z = 91.187$ GeV. The two dressing functions are shown in Fig. 4.6 together with the non-perturbative running of the coupling, Eq. (4.40). The bump in the intermediate momentum region was deemed unphysical, and so fits were employed that eliminated

[2]These values were suggested by Christian Fischer, who also provided advice on the numerical procedure.

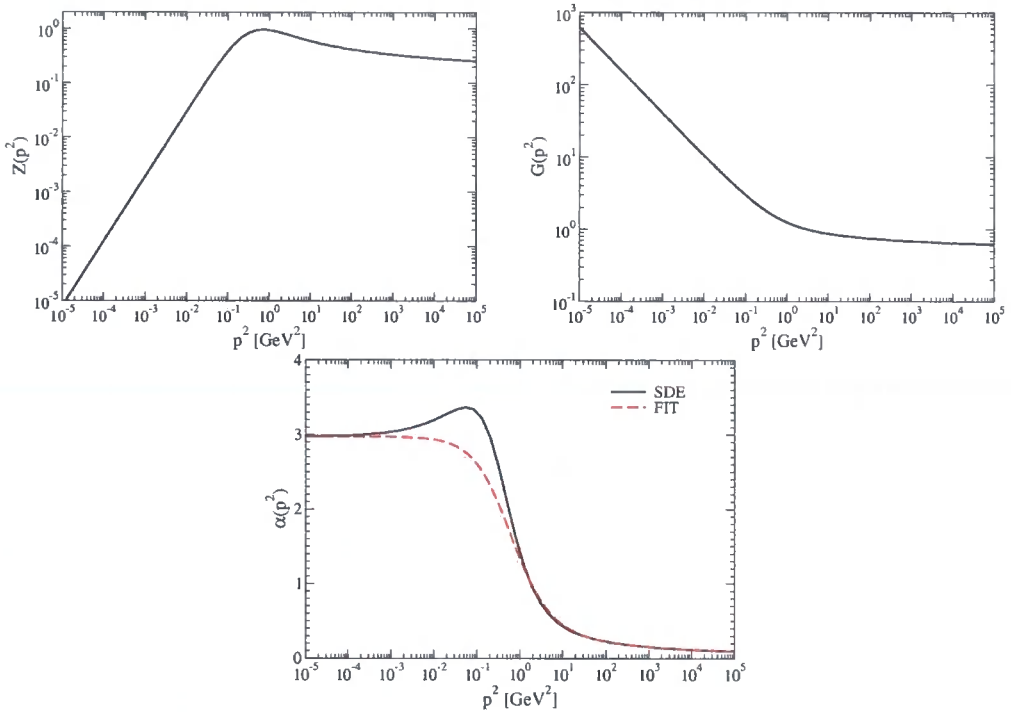

Figure 4.6: The ghost and gluon dressing functions, together with the non-perturbative running coupling as defined by the ghost-gluon vertex. The fit of Eq. (4.44) is also shown.

this feature. The difference in the shape of the fit, versus the numerical solution does not offer any qualitative difference, though the difference in the integrated strength provided means a smaller mass-gap will be generated. Since chiral observables are somewhat correlated to this scale, they will be a few percent smaller on employing the fit. However, since we are neglecting the four-gluon vertex, whose effect is envisaged to be largest in the intermediate momentum region where the bump is apparent, we choose to view the numerical solution as a guide to modelling the ghost and gluon. The actual linking between the infrared and ultraviolet regions is assumed to be unimportant. Thus, we describe the dressing functions for the ghost and gluon by:

$$\begin{aligned} R(x) &= \frac{c\left(x/\Lambda_{QCD}^2\right)^{\kappa} + d\left(x/\Lambda_{QCD}^2\right)^{2\kappa}}{1 + c\left(x/\Lambda_{QCD}^2\right)^{\kappa} + d\left(x/\Lambda_{QCD}^2\right)^{2\kappa}}\,, \\ Z(x) &= \left(\frac{\alpha(x)}{\alpha(\mu^2)}\right)^{1+2\delta} R^2(x)\,, \\ G(x) &= \left(\frac{\alpha(x)}{\alpha(\mu^2)}\right)^{-\delta} R^{-1}(x)\,, \end{aligned} \tag{4.43}$$

with $c = 1.269$, $d = 2.105$ and $\Lambda_{QCD} = 0.714$ GeV. The coupling $\alpha(x)$ is fitted by:

$$\begin{aligned}\alpha(p^2) &= \frac{1}{1+p^2/\Lambda_{QCD}^2}\left[\alpha(0) + p^2/\Lambda_{QCD}^2 \times \right. \\ &\left. \frac{4\pi}{\beta_0}\left(\frac{1}{\ln(p^2/\Lambda_{QCD}^2)} - \frac{1}{p^2/\Lambda_{QCD}^2 - 1}\right)\right] .\end{aligned} \tag{4.44}$$

The infrared fixed point, $\alpha(0)$, is determined from Eq. (4.42), and $\beta_0 = (11N_c - 2N_f)/3$ from one-loop resummed perturbation theory, where here $N_f = 0$ and $N_c = 3$.

In the forthcoming sections we will investigate solutions we find for the quark propagator with this choice for the running coupling. We also see how the choice of ansatz for the quark-gluon affects the chiral phenomenology.

4.2 Quark Sector of QCD

In order to learn about QCD, we must of course examine in detail the quarks themselves, for the propagators are the necessary inputs for any further study, such as the Bethe-Salpeter equations for bound states. In Eq. (1.91) we gave the Schwinger-Dyson equation for the quark, whose form we repeat here for completeness:

$$[S_F(p)]^{-1} = Z_2\left[S_F^{(0)}(p)\right]^{-1} - C_F\frac{Z_2\widetilde{Z}_1}{\widetilde{Z}_3}\frac{g^2}{(2\pi)^4}\int d^4k\gamma^\mu S_F(k)\Gamma_q^\nu(k,p)D_{\mu\nu}(p-k) . \tag{4.45}$$

This is shown pictorially in Fig. 4.7. The general form of the quark propagator is as for QED, *viz.*

$$S_F^{-1}(p) = \mathcal{A}(p^2)\left(\not{p} + \mathcal{M}(p^2)\right) , \tag{4.46}$$

While $\mathcal{A}$ is also a function of the renormalisation point μ and so strictly $\mathcal{A}(p^2;\mu^2)$, the quark mass function $\mathcal{M}(p^2)$ is renormalisation group invariant. These two functions are projected out by taking the appropriate traces. Of course, Eq. (4.45) involves

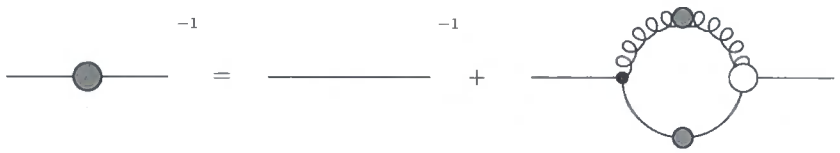

Figure 4.7: The quark SDE. Filled dots indicate full propagators and vertices. Solid lines indicate quarks, whilst wriggly lines represent gluons.

not just the quark propagator S_F, but the full quark-gluon vertex, Γ_q^ν, and the gluon propagator $D^{\mu\nu}$. Note that the ghost does not explicitly appear here, bar the renormalisation factors; its presence is implicit in both the gluon propagator and the quark-gluon vertex. In general covariant gauge the gluon propagator is:

$$D_{\mu\nu}(k) = \left(g_{\mu\nu} - \frac{k_\mu k_\nu}{k^2}\right)\frac{\mathcal{Z}(k^2)}{k^2} + \xi\frac{k_\mu k_\nu}{k^4}\,, \tag{4.47}$$

from which we derive the bare gluon propagator, $D^{(0)}_{\mu\nu}$, by taking $\mathcal{Z}(k^2) = 1$. Typically we shall work in the Landau gauge, for which $\xi = 0$, also leading to the result $\widetilde{\mathcal{Z}}_1 = 1$ [116].

We leave the proposition of suitable ansätze to the next section, instead concentrating upon what phenomenological quantities one may derive from the quark propagator. Models with sufficient integrated strength below 1 GeV provide a non-trivial vacuum such that a mass gap is created. This notion of dynamical mass generation was explored in the context of Abelian field theories for QED in both three and four dimensions: for the three-dimensional formulation chiral symmetry was broken dynamically for all values of the coupling, due to its dimensionality, though a critical phase may exist in the number of active fermions; and four-dimensional QED where it is the coupling strength that determines phase transitions.

For QCD it is the chiral limit where our interest lies. Here, the Goldstone mode associated with the breaking of chiral symmetry is the pion. Employing the Bethe-Salpeter equations to study the quark-antiquark bound state, one may calculate the neutral pion decay constant f_π. The difficulty here is how to relate the ansatz in the SDE with that present in the BSE, with little progress being made beyond the rainbow approximation. To calculate f_π we can use the Pagels-Stokar [117] equation:

$$f_\pi^2 = -\frac{N_c}{4\pi^2}\int dk^2 k^2 \frac{\mathcal{A}^{-1}(k^2;\mu^2)}{\left(k^2+\mathcal{M}^2(k^2)\right)^2}\left(\mathcal{M}^2(k^2) - \frac{k^2}{2}\mathcal{M}(k^2)\frac{d\mathcal{M}(k^2)}{dk^2}\right)\,, \tag{4.48}$$

which only embodies the leading order contribution, and is known to typically underestimate the pion decay constant by approximately 10%. A different expression for f_π^2 may be obtained by considering the residue at the pion pole of the meson propagator instead of the matrix element of the axial current. Including the fermion

dressing function $\mathcal{A}(p^2)$ in Eq. (2) of [118] gives:

$$f_\pi^{2,corr} = -\frac{N_c}{4\pi^2}\int dk^2 k^2 \frac{\mathcal{A}^{-1}(k^2;\mu^2)}{(k^2+\mathcal{M}^2(k^2))^2}\left[\left(\mathcal{M}^2(k^2) - \frac{k^2}{2}\mathcal{M}(k^2)\frac{d\mathcal{M}(k^2)}{dk^2}\right)\right. \\ \left. + \frac{k^4}{2}\left(\frac{d\mathcal{M}(k^2)}{dk^2}\right)^2 - \frac{k^2}{2}\mathcal{M}^2(k^2)\left(\frac{d\mathcal{M}(k^2)}{dk^2}\right)^2 - \frac{k^2}{2}\mathcal{M}(k^2)\frac{d\mathcal{M}(k^2)}{dk^2}\right]. \tag{4.49}$$

As with the Pagels-Stokar formula, Eq. (4.48), this involves only the mass-function and fermion wave-function renormalisation, with derivatives, and is hence calculable from our solutions to the Schwinger-Dyson equations.

The non-trivial vacuum is polarised by long range $\bar{q}q$ correlations, or condensates, whose scale determines the mass dynamically generated. The scale of this may be determined by exploring the short-distance behaviour of the quarks with the Operator Product Expansion (OPE):

$$\mathcal{M}(p^2)_{asym} = \frac{2\pi^2}{3}\gamma_m\frac{\mathcal{C}}{p^2}\left(\frac{1}{2}\log\left(p^2/\Lambda_{QCD}\right)\right)^{\gamma_m - 1}, \tag{4.50}$$

with $\mathcal{C} = -\langle\bar{q}q\rangle$, a renormalisation point (RP) independent quantity. The exponent, γ_m, is the one-loop anomalous dimension of the quark mass function; its value $12/(11N_c - 2N_f)$ is known from one-loop perturbation theory.

Alternatively, we may obtain the RP-dependent quark condensate by evaluating $-i\mathrm{Tr}\left[S_F(0)\right]$, which in momentum space is:

$$-\langle\bar{q}q\rangle_\mu = Z_2(\mu,\Lambda)Z_m(\mu,\Lambda)N_c\mathrm{Tr}_D\int\frac{d^4k}{(2\pi)^4}S_F(k^2;\mu^2)\,. \tag{4.51}$$

Here Tr_D is the Dirac trace, while Tr acts on both Dirac and colour space. The renormalisation factor $Z_m(\mu,\Lambda)$ is extracted from calculations of the mass function away from the chiral limit. The (normal-ordered) RP dependent chiral condensate can be related to the RP independent one by a one-loop running:

$$\langle\bar{q}q\rangle = \left(\frac{1}{2}\log\frac{\mu^2}{\Lambda_{QCD}^2}\right)^{-\gamma_m}\langle\bar{q}q\rangle_\mu\,. \tag{4.52}$$

These two quantities, f_π and $\langle\bar{q}q\rangle$ are determinable through experiment and thus serve as a check of the model that we employ, and stand at 92 ± 3 MeV and $-(235\mathrm{MeV} \pm 15)^3$ respectively [119,120].

4.2.1 Phenomenological Models

Before we consider solutions as obtained by pure SDE studies, we first touch upon purely phenomenological approaches. While we have an idea of the form of the running coupling at large momenta, it is the intermediate and deep infrared regions for which we have a lack of knowledge. However, it is recognised that the phenomenology of the quark sector cannot be sensitive to precise details of the coupling in this region, and so one aims to provide an ansatz that gives sufficient integrated strength in the infrared, thus generating the required mass-gap of QCD. There have been many suggestions for this in the literature [97,98] which have been extensively studied. Following the lead of Maris *et al.* [97,98], we will employ an ansatz for $g^2 D_{\mu\nu}(p-k)$ which has been shown to be consistent with studies of bound state mesons, and consider other modellings elsewhere. Since this simple model assumes a rainbow vertex truncation, the solutions are not multiplicatively renormalisable and so depend on the chosen renormalisation point. The renormalisation scheme is one of modified momentum subtraction at some point μ. This we take to be at 19 GeV to compare with earlier studies. We use:

$$\frac{g^2}{4\pi}\frac{Z_2}{\tilde{Z}_3} D_{\mu\nu}(q) \to \alpha\left(q^2\right) D^{(0)}_{\mu\nu}(q)\,, \tag{4.53}$$

where the coupling is described by [97,98]:

$$\begin{aligned}\alpha\left(q^2\right) &= \frac{\pi}{\omega^6} D\, q^4 \exp(-q^2/\omega^2) \\ &+ \frac{2\pi\gamma_m}{\log\left(\tau + \left(1 + q^2/\Lambda^2_{QCD}\right)^2\right)} \times \left[1 - \exp\left(-q^2/\left[4m_t^2\right]\right)\right]\,,\end{aligned} \tag{4.54}$$

with

$$\begin{aligned} m_t &= 0.5\,\text{GeV} \quad , \quad \tau = \mathrm{e}^2 - 1 \quad , \\ \gamma_m &= 12/(33 - 2N_f) \quad , \quad \Lambda_{QCD} = 0.234\,\text{GeV}\,. \end{aligned}$$

Note that in Eq. (4.53) a renormalisation factor, Z_2, is dropped. This gives rise to a subtractive renormalisation procedure at the cost of breaking multiplicative renormalisability; though this is already broken at the level of the bare vertex ansatz.

In past studies, Λ_{QCD} is taken to be 234 MeV, a value we too shall use. The parameters ω and D control the infrared behaviour of the coupling $\alpha(q^2)$ for momenta less than Λ_{QCD}, or strictly speaking m_t. The pion decay constant correlates

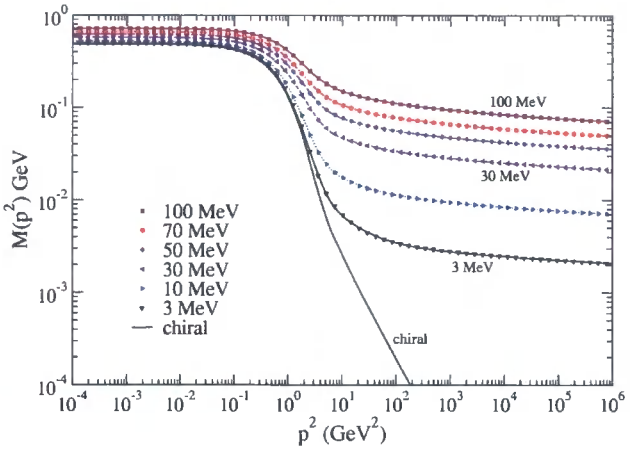

Figure 4.8: Euclidean mass functions for different current masses, specified at $\mu = 19$ GeV as labelled. The plot illustrates how on a log-log plot the behaviour dramatically changes between a current mass of 0 and 3 MeV. These results are essentially the same as found by Maris and Roberts [98].

these parameters. Typical values for this are $\omega = 0.4$ GeV, $D = 0.933$ GeV^2, as determined from $(\omega D)^{1/3} = 0.72$ [98] (see also Fig. 4.9). Solutions are obtained by solving the coupled system of fermion equations for $\mathcal{A}$ and $\mathcal{M}$ of Eq. (4.46), which we may write symbolically as:

$$\begin{aligned} \mathcal{A}(p^2;\mu) &= Z_2(\mu,\Lambda) - \Sigma_D\,(p;\Lambda)\ , \\ \mathcal{M}(p^2)\mathcal{A}(p^2;\mu) &= Z_2(\mu,\Lambda) Z_m m_R(\mu) + \Sigma_S\,(p;\Lambda)\ . \end{aligned} \tag{4.55}$$

The Σ_S and Σ_D correspond to the scalar and spinor projections of the integral in Eq. (4.45). For massive quarks we obtain the solution M by eliminating the renormalisation factors Z_2, Z_m via:

$$\begin{aligned} Z_2(\mu,\Lambda) &= 1 + \Sigma_D\,(\mu,\Lambda)\ , \\ Z_m(\mu,\Lambda) &= \frac{1}{Z_2(\mu,\Lambda)} - \frac{\Sigma_S\,(\mu,\Lambda)}{Z_2(\mu,\Lambda) m_R\,(\mu)}\ . \end{aligned} \tag{4.56}$$

The momentum dependence for different values of m_R are shown in Fig. 4.8. We can clearly see the difference in the asymptotic behaviour for chiral and massive solutions, with the former being power suppressed and the latter dominated by the logarithmic running of the current quark mass.

Being a phenomenologically derived model, the parameters are tuned so that a

suitably sized value for the condensate is obtained, together with f_π and a range of quantities associated with meson observables.

We must note that this model does not respect multiplicative renormalisability (MR), and so the mass function is dependent upon the chosen renormalisation point μ^2. There are various ways we may restore MR. The simplest is to keep the bare vertex, but replace the Z_2 of Eq. (4.53) by Z_2^{-1}. This is equivalent to dropping the subtractive renormalisation of Maris and Tandy, and choosing the vertex to be $\Gamma^\mu = Z_2\gamma^\mu$; hence we refer to this as the Z_2 vertex. This has previously been employed [27] in the quark equation, to act as a comparison for more complicated vertices. The renormalisation procedure should be changed appropriately to take into account this extra multiplicative constant. We have performed parameter scans in D and ω for the Maris–Tandy model with both the bare and Z_2 vertex, calculating the condensate $\langle\bar{q}q\rangle$, pion decay constant f_π and the Euclidean Mass $p^2 = \mathcal{M}^2(p^2)$. These are displayed as contour plots in Fig. 4.9.

For multiplicative renormalisability to be realised, the components of the vertex should behave like $\Gamma \sim \mathcal{A}$, which is the inspiration behind the $Z2$ vertex. Then all of our dressed vertices, from the Minimal Ball–Chiu to the Kızılersü–Pennington vertex, preserve MR in Landau gauge. We have similarly calculated chiral observables, and the Euclidean mass, on a parameter grid in order to compare the effect of the vertex dressing on parameter choices. All dressed vertices favour smaller values for D to obtain similarly valued observables. We can see parameter scans for the Minimal Ball–Chiu and Ball–Chiu vertices in Fig. 4.10, while the Curtis–Pennington and Kızılersü–Pennington are given in Fig. 4.11. We are working in the Abelian approximation, where we use the WGTI rather than the Slavnov-Taylor identies of QCD - our three vertices (Ball–Chiu, Curtis–Pennington, and Kızılersü–Pennington) that respect the WGTI behave similarly. We see that in order to obtain similar values for the condensate and pion decay constant, the range of viable parameters is very different between the different vertex ansätze – the additional Dirac structure clearly plays a sizeable rôle in the phenomenology of the quark SDE, even for just these basic observables.

To show the differences more clearly, we picked a particular set of parameters for the Maris-Tandy model – $\omega = 0.4$ GeV and $D = 0.933$ GeV^2 for four active flavours, N_f – and calculated the chiral observables for renormalisation point $\mu = 19$ GeV. For different vertices, we changed only the parameter D of the ansatz for the coupling in order to match the quark condensate in the Maris-Tandy model. The results are given in Table 4.1. We give the pion-decay constant as calculated through Pagels-Stokar, Eq. 4.48, and via the Barducci *et al* formula of Eq. (4.49). We see

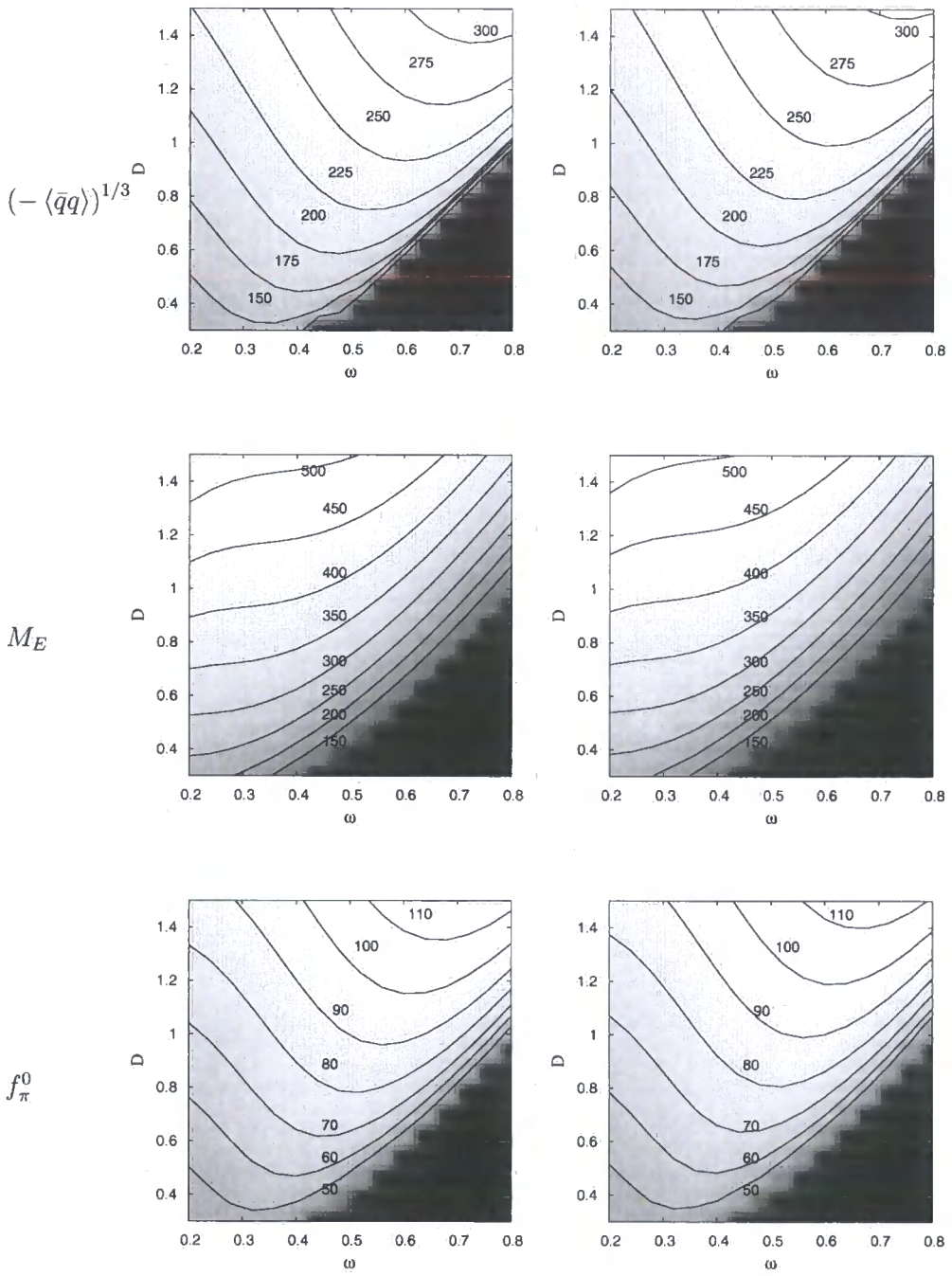

Figure 4.9: Plots showing contours of constant chiral condensate, Euclidean mass and pion decay constant for the Maris-Tandy (left) and Z2 (right) vertices. All units are in MeV.

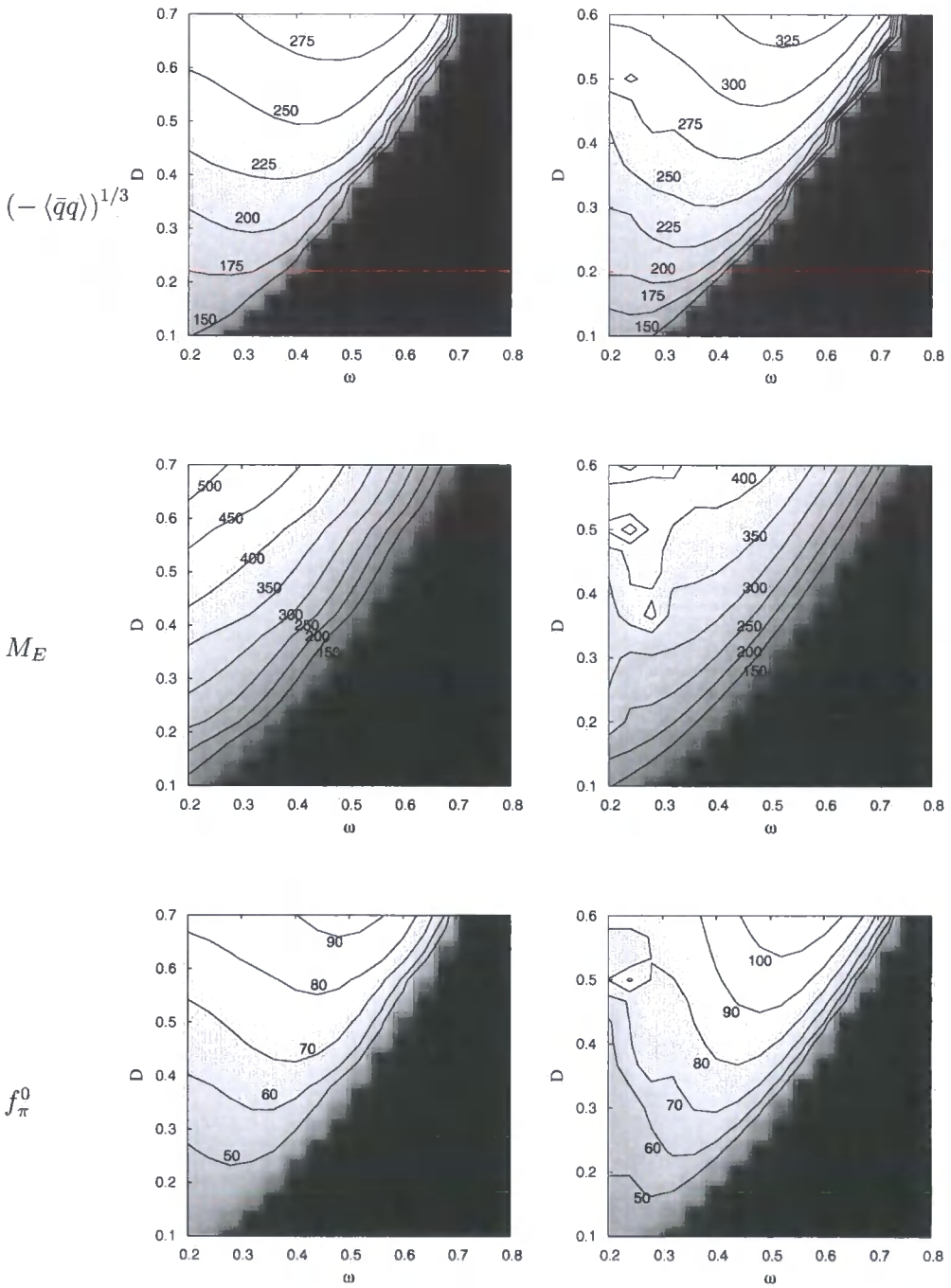

Figure 4.10: Plots showing contours of constant chiral condensate, Euclidean mass and pion decay constant for the Minimal Ball–Chiu (left) and Ball–Chiu (right) vertices. All units are in MeV.

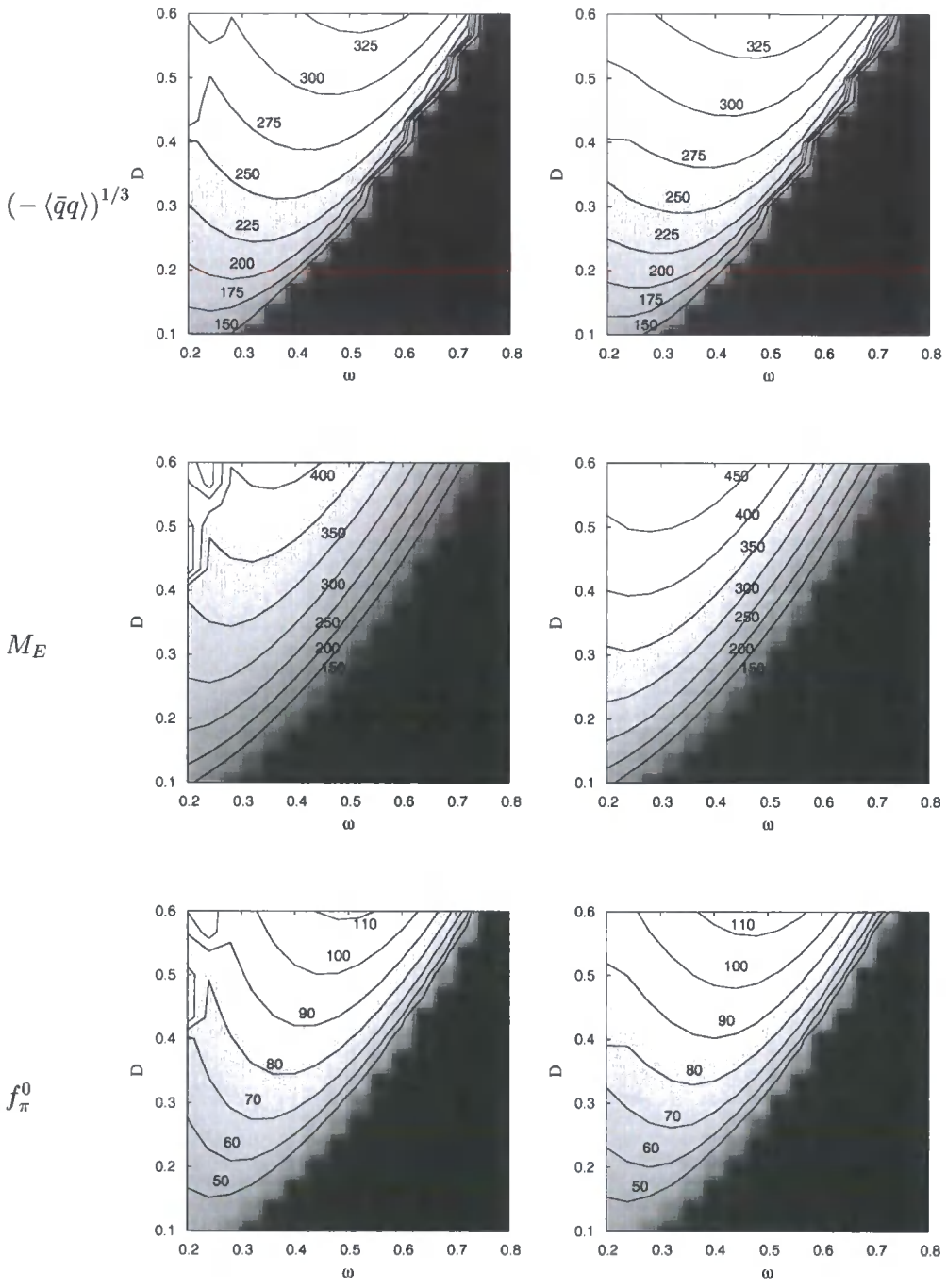

Figure 4.11: Plots showing contours of constant chiral condensate, Euclidean mass and pion decay constant for the Curtis–Pennington (left) and Kızılersü–Pennington (right) vertices. All units are in MeV.

Vertex	D [GeV^2]	$(-\langle\bar{\psi}\psi\rangle_{asy})^{1/3}$ [MeV]	f_π [MeV]	f_π^{corr} [MeV]	M_E [MeV]
bare	0.933	228.5	81.3	94.4	392.7
Z2	1.075	228.6	84.2	99.3	414.6
MBC	0.523	228.5	77.2	87.7	356.5
BC	0.331	228.6	73.1	81.9	269.0
CP	0.329	228.6	76.9	86.7	279.0
KP	0.312	228.5	75.2	84.3	264.9

Table 4.1: The condensate, pion decay constant and Euclidean mass for a range of vertex ansätze with the Maris-Tandy model coupling of Eq. (4.53). We fix $\omega = 0.4$ and vary the parameter D to maintain approximately equal values for the condensate.

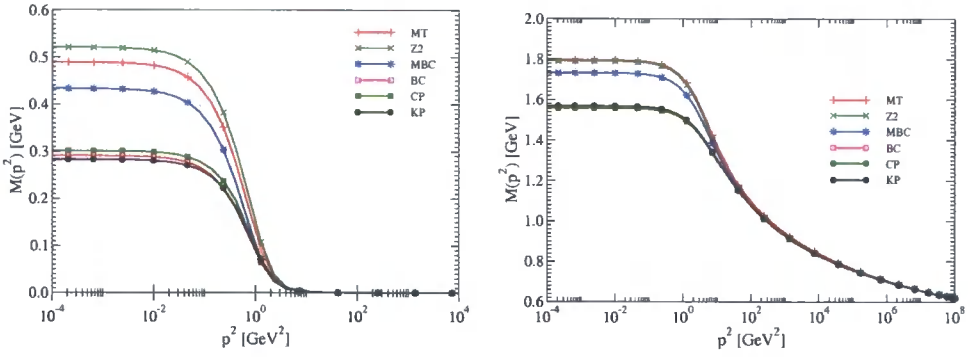

Figure 4.12: Comparison of the mass-function for different vertices in the chiral limit (left) and for an explicit quark mass (right). We fix $N_f = 4$ and $\omega = 0.4$, but tune D such that each ansatz gives the same condensate as for the MT model, $D = 0.933$.

that f_π^{corr} is typically $12 - 18\%$ larger than the Pagels-Stokar determination, which equates to $25 - 40\%$ for f_π^2, in agreement with the model estimate within [118].

4.2.2 Tübingen Model

The Tübingen model is that described in Sect. 4.1.2 where the ghost-gluon system is solved without angular approximations and for an ansatz that reproduces the one-loop anomalous dimensions of both the ghost and gluon. This provided us with fits to the non-perturbative running coupling, Eqs. (4.40, 4.44) respectively.

Returning to our Schwinger-Dyson equation for the quark, we have:

$$[S_F(p)]^{-1} = Z_2 \left[S_F^{(0)}(p)\right]^{-1} - C_F \frac{Z_2}{\widetilde{Z}_3} \frac{g^2}{(2\pi)^4} \int d^4k \gamma^\mu S_F(k) \Gamma_q^\nu(k,p) D_{\mu\nu}(p-k) \ . \quad (4.57)$$

In which we have set $\widetilde{Z}_1 = 1$. We must now specify some ansatz for the quark-gluon vertex. We assume that we can factorize this into two components:

$$\Gamma_q^\mu(k,p) = \Gamma_{\rm NA}^\mu(k,p) \Gamma_{\rm AB}^\mu(k,p) \ , \quad (4.58)$$

a non-Abelian (NA), and Abelian (AB) part respectively. For the non-Abelian part we take:

$$\Gamma_{\rm NA}(k,p;q) = \mathcal{G}^2(q^2;\mu^2) \widetilde{Z}_3(\mu^2,\Lambda^2) \quad (4.59)$$

The presence of the ghost dressing functions allows us to employ the RG invariant of Eq. (4.40). The Abelian part is taken from studies of QED, and so we have:

$$\Gamma_{\rm AB}^\mu(k,p;q) = \begin{cases} Z_2 \, \gamma^\mu & \text{Bare Vertex} \\ \Gamma_{\rm BC}^\mu(k,p;q) & \text{Ball–Chiu Vertex} \\ \Gamma_{\rm CP}^\mu(k,p;q) & \text{Curtis–Pennington Vertex} \\ \Gamma_{\rm KP}^\mu(k,p;q) & \text{Kızılersü–Pennington Vertex} \end{cases} \quad (4.60)$$

with the extra factor of Z_2 providing multiplicative renormalisability in the case of the bare vertex.

In the latter three cases, we may write:

$$\begin{aligned} \mathcal{A}(p^2;\mu) &= Z_2(\mu,\Lambda) \left(1 - \Sigma_D\left(p;\Lambda\right)\right) \ , \\ \mathcal{M}(p^2)\mathcal{A}(p^2;\mu) &= Z_2(\mu,\Lambda) \left(Z_m m_R(\mu) + \Sigma_S\left(p;\Lambda\right)\right) \ , \end{aligned} \quad (4.61)$$

with the Σ_S and Σ_D corresponding to the scalar and spinor projections of the integral in Eq. (4.57). For massive quarks we eliminate the renormalisation factors Z_2, Z_m via:

$$\begin{aligned} Z_2(\mu,\Lambda) &= 1/\left(1 - \Sigma_D\left(\mu,\Lambda\right)\right) \ , \\ Z_m(\mu,\Lambda) &= \frac{1}{Z_2(\mu,\Lambda)} - \frac{\Sigma_S\left(\mu,\Lambda\right)}{m_R\left(\mu\right)} \ . \end{aligned} \quad (4.62)$$

in which we choose conditions $\mathcal{A}(\mu^2;\mu^2) = 1$, $\mathcal{M}(\mu^2) = m_R(\mu)$.

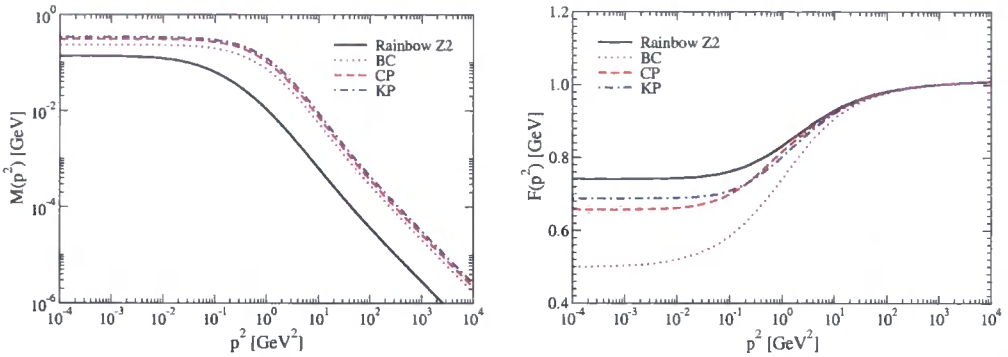

Figure 4.13: The quark mass function and wave-function renormalisation for four ansätze: bare vertex; Ball–Chiu vertex; Curtis–Pennington vertex; and the Kızılersü–Pennington vertex.

Employing the fit of Eqs. (4.43, 4.44) we obtain for the three vertices of Eq. (4.60) values for the condensate, pion decay constant and Euclidean mass, defined by $p^2 = \mathcal{M}^2(p^2)$. These we give in Table 4.2. We show the wave-function renormalisation and

Vertex	f_π [MeV]	M_E [MeV]	$(-\langle\bar{\psi}\psi\rangle_{asy})^{1/3}$ [MeV]	$(-\langle\bar{\psi}\psi\rangle_{int})^{1/3}$ [MeV]
Z2	30.0	117.1	139.3	136.3
BC	56.2	216.0	262.5	249.4
CP	74.0	277.7	286.6	278.0
KP	79.1	296.8	303.1	291.7

Table 4.2: Chiral observables and Euclidean mass for a selection of vertex ansätze employing the non-perturbative running of the Tübingen model, described by the fits of Eqs. (4.43, 4.44).

mass functions for these vertices in Fig. 4.13. We see there is a strong dependence of our chiral observables on the vertex ansatz employed.

If we employ the numerical results for the ghost and gluon propagators, in which the bump at intermediate momenta is included, the numerical values increase slightly due the additional integrated strength, as shown in Table 4.3.

4.2.3 Lattice Model

The third model we investigate has been defined in [121]. The idea is to solve the coupled system of gluon, ghost and quark Dyson-Schwinger equations on a compact manifold with periodic boundary conditions, similar to lattice QCD. For the vertices in the Yang-Mills sector the same truncation scheme as in the last section

Vertex	f_π [MeV]	M_E [MeV]	$(-\langle\bar{\psi}\psi\rangle_{asy})^{1/3}$ [MeV]	$(-\langle\bar{\psi}\psi\rangle_{int})^{1/3}$ [MeV]
Z2	39.1	159.1	162.5	159.1
BC	64.1	257.8	284.0	268.0
CP	83.0	324.3	297.8	293.0
KP	90.8	355.0	325.1	313.9

Table 4.3: Chiral observables and Euclidean mass for a selection of vertex ansätze employing non-perturbative running of the Tübingen model, without smoothing out the bump.

is employed. However, for the quark-gluon vertex an ansatz has been specified such that lattice results for the quark propagator have been reproduced on a similar manifold. Solving the system also in the infinite volume/continuum limit one can then study how finite volume affects the pattern of dynamical chiral symmetry breaking [121].

In the infinite volume/continuum limit, i.e on $\mathbb{R}^4$, the solutions for the ghost and gluon propagator are given by Fig. 4.6. The ansatz for the quark-gluon vertex is:

$$\Gamma_\nu(k,\mu^2) \;=\; \gamma_\nu\,\Gamma_1(k^2)\,\Gamma_2(k^2,\mu^2)\,\Gamma_3(k^2,\mu^2)\;, \tag{4.63}$$

with the components:

$$\Gamma_1(k^2) \;=\; \frac{\pi\gamma_m}{\ln(k^2/\Lambda^2_{QCD}+\tau)}\,, \tag{4.64}$$

$$\Gamma_2(k^2,\mu^2) \;=\; G(k^2,\mu^2)\;G(\zeta^2,\mu^2)\;\widetilde{Z}_3(\mu^2)\;h\;[\ln(k^2/\Lambda_g^2+\tau)]^{1+\delta} \tag{4.65}$$

$$\Gamma_3(k^2,\mu^2) \;=\; Z_2(\mu^2)\,\frac{a(M)+k^2/\Lambda^2_{QCD}}{1+k^2/\Lambda^2_{QCD}}\,, \tag{4.66}$$

where $\delta = -9/44$ is the (quenched) one-loop anomalous dimension of the ghost, $\gamma_m = 12/33$ the corresponding anomalous dimension of the quark and $\tau = e-1$ acts as a convenient infrared cutoff for the logarithms. The quark mass dependence of the vertex is parameterised by:

$$a(M) \;=\; \frac{a_1}{1+a_2M(\zeta^2)/\Lambda_{QCD}+a_3M^2(\zeta^2)/\Lambda^2_{QCD}}, \tag{4.67}$$

where $M(\zeta^2)$ is determined during the iteration process at $\zeta = 2.9$ GeV. The parameters have been fitted to lattice results using a staggered [122] and an overlap action [123]. Here we use only the fit to the overlap quark; the corresponding pa-

	h	Λ_g (GeV)	Λ_{QCD} (GeV)	a_1	a_2	a_3
overlap	1.31	1.50	0.35	25.58	3.44	2.23

Table 4.4: Parameters used in the vertex model, Eqs. (4.63-4.66).

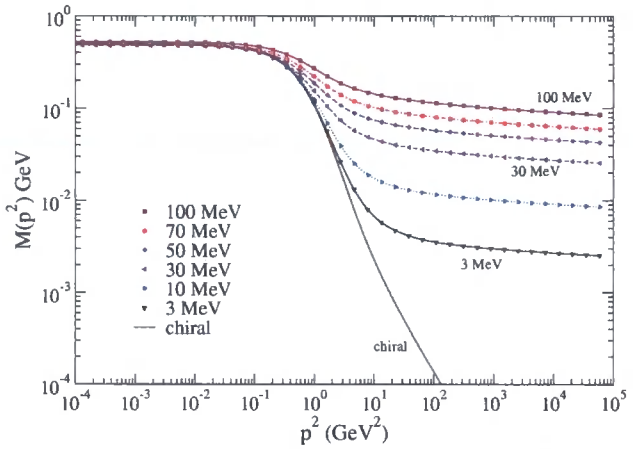

Figure 4.14: The mass function for a selection of quark masses within the lattice model. The renormalisation point is $\mu^2 = 1000$ GeV^2.

rameters are given in Table 4.4. Explicit solutions for the quark propagators are discussed in [121], and can been seen in the forthcoming chapter.

We can examine the effects of dressing the quark-gluon vertex by making comparison with the Maris-Tandy model. There we had a bare gluon vertex with an ansatz for the running coupling, Eq. (4.54). The lattice model of [121] may be similarly viewed as an effective running coupling by combining the vertex dressing functions $\Gamma_1(p^2)\Gamma_2(p^2)\Gamma_3(p^2)$ with the gluon's dressing function, $\mathcal{Z}(p^2)$.

In Fig. 4.15(a) we show the effective coupling for a selection of quark masses in the Lattice model, together with the Maris-Tandy model for $\omega = 0.4$ GeV and $D = 0.933$ GeV^2. Although the UV running differs due to the different choice of Λ_{QCD} in the two models, it is the qualitative features of the intermediate region that are of interest. These can be seen more clearly in Fig. 4.15(b) where we have compensated for the logarithmic scale and so areas are more representative of their relevance to the integrals. Both models – Maris-Tandy and that inspired from the Lattice – exhibit enhancements in the region $0.1 \leq p^2 \leq 1$ GeV, giving rise to the generation of a mass gap. It is only this integrated strength that is required for the breaking of chiral symmetry – so long as it is sufficient in size, its precise shape and form are unimportant phenomenologically. In particular, the details of the coupling

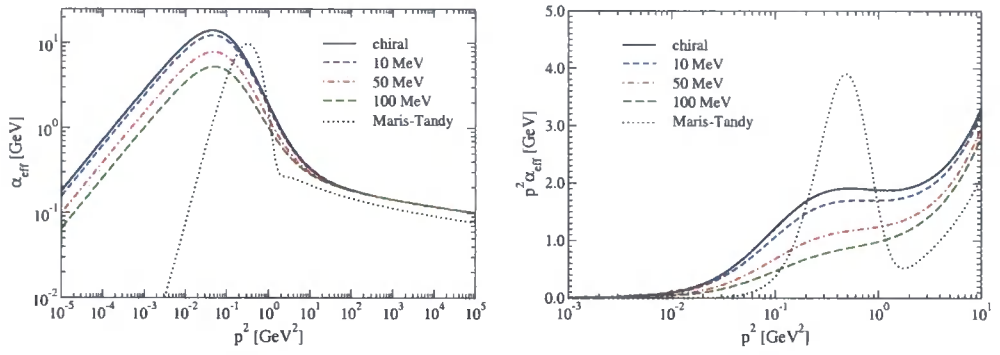

Figure 4.15: The effective coupling in the Lattice-Model for different quark masses (renormalised at $\mu^2 = 1000$), compared with the Maris-Tandy ansatz for the running coupling, as a (a) log-log plot, and (b) log-linear plot scaled by p^2 to make easier the comparison of integrated strength.

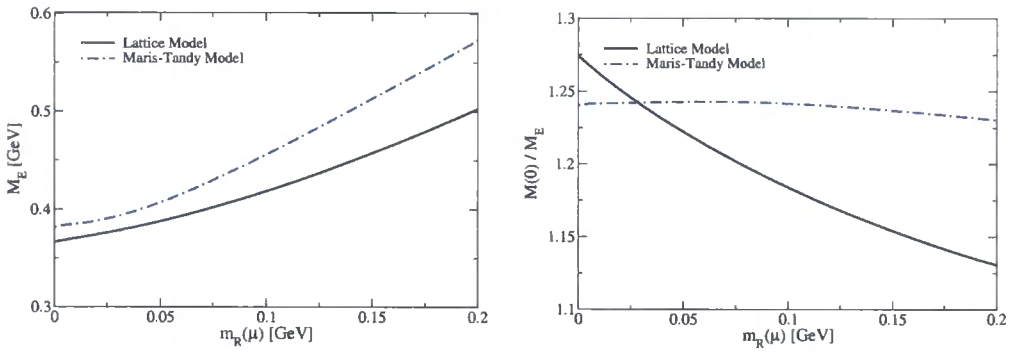

Figure 4.16: Comparison between the Euclidean mass for the Lattice model and for the Maris-Tandy model. Shown also is the ratio $M(0)/M_E$. The common renormalisation point is taken to be $\mu^2 = 1000$ GeV^2.

in the deep infrared play no rôle. Since the lattice model depends upon the quark mass, taking into account its screening properties, we see the integrated strength decreases as a function of increasing quark mass. For comparison with the other models, we find here that $f_\pi = 70.3$ MeV, $f_\pi^{corr} = 80.0$ MeV, $\left(-\langle\bar{\psi}\psi\rangle_{asy}\right)^{1/3} = 235$ MeV and $\left(-\langle\bar{\psi}\psi\rangle_{int}\right)^{1/3} = 263$ MeV.

One can also look at the evolution of the Euclidean mass (and $M(p^2)$ for $p \to 0$), as a function of the quark mass. These we show for the lattice model and Maris-Tandy model in Fig. 4.16. In the lattice model, the size of the mass-gap arising from dynamical breaking of chiral symmetry is somewhat damped, owing to the parameterised mass dependence in the vertex. This can be seen more clearly in the ratio $M(0)/M_E$, with the Maris-Tandy Model being nearly constant (i.e. the two

regions are heavily correlated), while the Lattice model decreases. This essentially describes the differences in shape of the mass function as obtained through the two models. For the Lattice-model, the ansatz provides for screening of the interaction due to massive quarks. Since this is modelled by comparison with Lattice studies, it is hoped that an interaction of this form will provide more a more realistic input for bound state studies of mesons.

4.3 Summary

We have explored the pure Yang-Mills sector of QCD, looking briefly at ghost-free gauges, covariant gauges without ghosts and finally the full ghost-gluon system. This culminated in an ansatz [96] for the non-perturbative running coupling with an infrared fixed point. Taking the same solutions to the quenched ghost-gluon system, confined to a torus to simulate finite volume effects of Lattice QCD, and using the quark-gluon vertex ansatz of Eq. (4.63) to fit to Lattice data, a model was found [121] that could be extrapolated to the continuum limit. This we compared with a phenomenologically derived model, whose parameters are tuned such that they reproduce chiral and meson observables in studies with the Bethe-Salpeter equations. In the first we examined how different vertex ansätze affect the calculable chiral observables, in particular that of the Kızılersü–Pennington vertex. We found that by tuning the condensate, the quark mass function with the Ball–Chiu, Curtis–Pennington and Kızılersü–Pennington vertex exhibited moderate variation for the pion decay constant and Euclidean mass, and so the transverse structure makes only small differences to the correlation between these variables. For the Tübingen model we found that introducing the KP vertex did produce a sizeable difference, giving rise to condensates $\sim$ 20% larger, owing to differences in the infrared and intermediate momentum regions that feed back on the solutions of the SDE.

Each of these models share qualitatively similar features, notably the agreement of the mass-functions in the UV region with perturbation theory, and the generation of dynamical mass owing to χSB. In order to further explore the differences of these models, one must move towards bound-state studies in order to see what dependence the extra vertex structure has on the predictions. However, this requires development of ansätze for the BSE and SDE that are consistent in the satisfaction of the Axial-Ward-Takahashi equation. Though there now exist such schemes as the improved rainbow-ladder approximation, in which additional subclasses of diagrams are infinitely summed, there is still little progress on the inclusion of additional

vertex structure beyond the rainbow approximation.

We will further explore solutions to these models in the next chapter, where we attempt to extract the mass dependence of the chiral condensate.

Chapter 5

Extracting the Condensate for Massive Quarks

Solving the Schwinger-Dyson Equations for QCD is an entirely non-trivial process, which we have investigated for simpler gauge theories and for QCD itself in the previous chapters. The numerical treatment is given in Appendix A, though one may see [124–127] for reviews. They comprise an infinite tower of coupled integral equations, that can be solved analytically only for specific kinematical situations and in the far infrared [128–130]. In general, some form of truncation has to be applied. To this end we require some suitable ansatz for the three-point functions in order to allow us to solve self-consistently for the ghost, gluon and quark propagators. This we discussed in the previous chapter, whereby we introduced three truncation schemes that have been tested elsewhere [97, 121, 131], within which one may solve for the fermion propagator.

The solutions of the quark propagator provide for us a great deal of phenomenology. We know that QCD is strongly coupled, and as a result the dynamics of the interaction generate a mass-gap that for light quarks is significantly larger than the scale of their masses present in the Lagrangian. Indeed, the mass gap generated far exceeds the scale of the current quark masses present in the Lagrangian. The strong coupling allows long range $\overline{q}q$ correlations to occur that polarise the vacuum. It is the scale of these condensates that determines the mass generated, and this gap persists even in the chiral limit. As long known this underpins much of QCD phenomenology.

Once a solution is known for the quark propagator, either for massless or massive quarks, one may employ the Bethe-Salpeter equations (BSE) to study bound states. From this we can determine meson masses, together with their associated decay

constants – the pion is hence well described, providing for us acceptable values for both m_π and f_π. These studies not only require knowledge of the four point Green's functions, which must be consistent with ansätze employed in the SDE, but also analytic continuation of our propagators from Euclidean p^2 to $-p^2$. Both of these steps are challenging, with no four-point kernel known that is consistent with the quark-gluon vertex ansatz beyond the bare vertex. However, a great deal of work has been done in this area, with simple models providing a number of results consistent with the experimental determinations.

Although bound state studies are of great interest, we instead wish to investigate this mass generation using the Schwinger-Dyson equations with the aim of understanding and extracting the behaviour of the $\overline{q}q$ condensate beyond the limit of vanishing quark mass.

The interest in the value of such a condensate arises in the context of QCD sum-rules. There the Operator Product Expansion (OPE) is used to approximate the short distance behaviour of QCD. In studying currents like that of $\overline{q}_i\gamma^\mu(\gamma_5)q_j$, with $q_i = s$ and $q_j = u, d$, the vacuum expectation values of $\overline{u}u$, $\overline{d}d$ and $\overline{s}s$ operators naturally arise [132–134]. The value of the $\overline{q}q$ condensate for the u and d quarks now well determined to be $-(235 \pm 15\,\mathrm{MeV})^3$ by experiment [120] is the result in the chiral limit. However, in the OPE it is the value of the condensates away from this limit that actually enters. Since the current masses of the u and d quarks are only a few MeV, the resulting condensate is expected to be close to its value in the chiral limit, but how close? For the first 20 years of QCD sum-rules their accuracy was never sufficient for it to matter whether this difference was even a 10% effect. This equally applies to the estimate by Shifman, Vainshtein and Zakharov [135,136], and also of Jamin [133], that the $\overline{s}s$ condensate was (0.8 ± 0.3) of the $\overline{u}u$ and $\overline{d}d$ values. It is the greater precision brought about by the studies of Refs. [132,137,138], for instance, that motivate the need to learn about how the $\overline{q}q$ condensate depends on the current quark mass. Our aim here is to illustrate a method for determining this dependence.

For light quarks, u, d and s, studying the Schwinger-Dyson equation for the fermion propagator in the continuum is essential, until computation with large lattice volumes become feasible. Since the continuum Schwinger-Dyson equations can be solved for any value of the quark mass, they also provide a natural way to bridge the gap between lattice data at larger masses and the chiral limit of phenomenological importance. Our primary focus is, of course, on QCD, but we shall draw on the NJL model where necessary.

5.1 Schwinger-Dyson Equations

Thus far we have demonstrated that solving the Schwinger-Dyson equations is a difficult and challenging task, with the requirement that we provide knowledge of higher order Green's functions such that our truncation is efficacious. Thus far, three models have been presented: one purely from phenomenology, though inspired in part from the Mandelstam approximation, and two others arising through attempts to solve the Yang-Mills sector of QCD and through complementary lattice studies.

Our chief aim is to calculate the mass function of the quark propagator for a range of current masses. Our starting point is the renormalized Schwinger-Dyson equation for the quark propagator:

$$S^{-1}(p) = Z_2 \left[S^{(0)}(p)\right]^{-1} - C_F \frac{Z_2 \widetilde{Z}_1}{\widetilde{Z}_3} \frac{g^2}{(2\pi)^4} \int d^4k \cdots \times \gamma_\mu S(k) \Gamma_\nu(k,p) D_{\mu\nu}(p-k) \; . \tag{5.1}$$

In Landau gauge we note that $\widetilde{Z}_1 = 1$. The inverse propagator $S^{-1}(p)$ is specified by two scalar functions $\mathcal{A}$ and $\mathcal{M}$:

$$S^{-1}(p) = \mathcal{A}(p^2) \left(\not{p} + \mathcal{M}(p^2)\right) \; . \tag{5.2}$$

Whereas $\mathcal{A}(p^2, \mu)$ is also a function of the renormalisation point μ, the quark mass function $\mathcal{M}(p^2)$ is renormalisation group invariant. Projecting out these two functions from Eq. (5.1), we have two coupled equations that are solved using a globally convergent iterator.

The operator product for the mass function has an expansion at large momenta given symbolically by:

$$\mathcal{M}(p^2) \simeq \overline{m}(p^2) + \frac{\text{const}}{p^2} \langle \bar{q}q(p^2) \rangle + \cdots \; , \tag{5.3}$$

where the first term corresponds to the explicit mass in the Lagrangian, and the second to the lowest dimension vacuum condensate. For now we just show the momentum dependence given by the canonical dimensions, and leave for later the implications of the anomalous dimensions of QCD. Having computed the mass function using the Schwinger-Dyson equations, the essential problem is how to separate these two terms in Eq. (5.3) with any accuracy if $\overline{m}$ is non-zero. We note that the mass function for a physically meaningful solution is expected to be positive definite.

Concentrating on the chiral limit, the OPE for QCD is well described by the

expression:

$$\mathcal{M}(p^2) = \frac{2\pi^2\gamma_m}{3}\frac{\mathcal{C}}{p^2}\left(\frac{1}{2}\log\left(p^2/\Lambda_{QCD}^2\right)\right)^{\gamma_m - 1} \tag{5.4}$$

on the consideration of anomalous dimensions, and valid only for large momenta, where $C = -\langle\bar{q}q\rangle$ is the chiral condensate. However, we are in fact interested in the chiral condensate for *massive* quarks. As stated in Eq. (5.3), this time showing the anomalous dimensions so necessary for QCD, we have:

$$\mathcal{M}(p^2) \simeq \overline{m}\left(\log\left(p^2/\Lambda_1^2\right)\right)^{-\gamma_m} + \frac{2\pi^2\gamma_m}{3}\frac{\mathcal{C}}{p^2}\left(\frac{1}{2}\log\left(p^2/\Lambda_2^2\right)\right)^{\gamma_m - 1}, \tag{5.5}$$

with again $\overline{m}$ taking into consideration the necessary renormalisation factors.

Separating these two functional forms proves to be a formidable task. With the expectation that the condensate is entirely inconsequential for large masses we may assume $\mathcal{C} = 0$ for very large $\overline{m}$, say of the order of the charm mass and beyond, we can attempt to fix the scale Λ_1 by consideration of large masses. From this we may expect to fix the scale Λ_1, whose value is not expected to equal Λ_{QCD} due to the effect of corrections beyond the one-loop level. However, this in itself is naïve for it precludes the contribution of higher order corrections to the OPE present for the very large quark masses where a vanishing condensate is expected.

Regardless of this, we attempted such a fit procedure by fixing Λ_2 from the chiral solution, which gave Λ_{QCD} as expected since higher order corrections to this piece of the operator product expansion are suppressed by powers of p^2. Despite this foresight, we cannot expect Λ_1 to be the equal to Λ_{QCD} since these higher order corrections are only suppressed by powers of logarithms. As a result, in this work the logarithm raised to the power of the anomalous dimension of QCD, as connected to the massive term of Eq (5.5), is in fact representative of powers of the running coupling – and thus we employ the two-loop form given by a *momentum* subtraction renormalisation scheme. Taking this on board, we fixed Λ_1 by recourse to large quark masses, with Λ_2 determined by chiral studies, and thus attempted to glean the behaviour of the condensate $\mathcal{C}$ beyond the chiral limit. While a quantitative number could be determined, it was clear that there still existed much ambiguity between the two parts of Eq. (5.5): with dependence upon the fit region indicating Λ_1 was still poorly determined, or fitted to an ambitious momentum region.

As a result, we attempted to model the whole momentum region of the quark

mass function with the fit form [139]:

$$\begin{aligned}\mathcal{M}(p^2) &= \frac{a_6}{\left(p^2/a_7^2+1\right)^4}+\frac{a_8}{\left(p^2/a_2^2+1\right)^2}+a_3\left(\log\left(p^2/a_4^2+a_5^2\right)\right)^{-\gamma_m} \\ &+\frac{\left(p^2/a_2^2\right)^2}{\left(p^2/a_2^2+1\right)^2}\frac{2\pi^2}{3}\gamma_m\frac{a_0^3}{p^2+a_2^2}\left(\frac{1}{2}\log\left(p^2/a_1^2+e\right)\right)^{\gamma_m-1}. \end{aligned} \quad (5.6)$$

This is sufficient to describe the mass function for the whole momentum region under consideration, characterised by the scales a_1, a_2, a_4 and a_7. The first two scales are fixed by the chiral dynamics, with the latter determined from the large quark mass behaviour, together with a_5 which acts like an infrared regulator. The remaining parameters a_0, a_6 and a_8 are left free, to be fitted depending on the mass function under question, with a_0 relating to the chiral condensate.

We applied this to the lattice model of the previous chapter, in an attempt to extract a_0 and so the chiral condensate for a range of quark masses. We found that the fitting the infrared region interfered too strongly with our intermediate and asymptotic momentum range, thus masking the determination of the condensate and returning artificially large values, with equally large uncertainties. This equally applied to other quark models, even when constraints on the parameters were lifted – too much slack existed between the many parameters and so accurately modelling the mass-function imposed significant errors on the chiral condensate. We thus view this as a method of obtain upper bounds on the value of the condensate, and look towards alternative methods of extracting its value.

5.1.1 Multiple Solutions

It is at this point we note that in the chiral limit, there exist three solutions for the mass function $\mathcal{M}(p^2)$. These correspond to the Wigner mode (the only solution accessible to perturbation theory), and two non-perturbative solutions of equal magnitude generated by the dynamical breaking of chiral symmetry. These we denote by:

$$M(p^2)=\begin{cases} M^W(p^2)=0 \\ \\ M^{\pm}(p^2)=\pm M^0(p^2) \end{cases}. \quad (5.7)$$

One can ask whether analogous solutions to these exist as we move away from the chiral limit and what relevance they hold. Indeed, in a recent paper [140] Chang *et al.* suggested that one could make an unambiguous definition of the massive quark condensate by taking a particular combination of these solutions. The existence of

these is restricted to the domain:

$$\mathcal{D} = \{m : 0 \leq m \leq m_{cr}\} \ , \tag{5.8}$$

where only the positive-definite solution exists beyond m_{cr}. Chang *et al.* found that inside the critical domain, the solutions for both $M^+(p^2)$ and $M^-(p^2)$ exhibit the same running current-quark mass in the ultraviolet. In terms of Eq. (5.3), this means both solutions have the same $\overline{m}$ term. Noting that in the chiral limit the $M^{\pm}(p^2)$ solutions have a condensate of opposite sign, they proposed a definition of the massive quark condensate given by:

$$\overline{\sigma}(m(\mu)) \ = \ \lim_{\Lambda\to\infty} Z_4(\mu,\Lambda)\, N_c \,\mathrm{Tr}_D \int_q^{\Lambda} \frac{1}{2}\left[S_+ \ - \ S_-\right] \ , \tag{5.9}$$

where μ denotes the renormalisation point, and $Z_4 = Z_2 Z_M$. Since both propagators $S_{\pm}$ share the same asymptotic behaviour $\mathcal{M}(p^2) \to \overline{m}(p^2)$ for large momenta, potential divergencies in the integral cancel and the expression (5.9) is well defined. The resulting condensate $\overline{\sigma}(m(\mu))$ will be equal to the one for the physical M^+ solution provided $S_{\pm}$ have condensates of equal magnitude also away from the chiral limit. However, we will show that this assumption is not correct. Morever, we find here that there is in fact an analogous solution S_W to the Wigner mode of the chiral limit. (This has been noted in the revised version of [140]). This solution has the same ultraviolet running current quark mass, *i.e.* all three, $M_{\pm}$ and M_W have the same $\overline{m}(p^2)$ in their OPE, see Eq. (5.3). Consequently, the combination:

$$S(\beta) = (2-\beta)\, S_+ - \beta S_- + 2\,(\beta - 1)\, S_W \ , \tag{5.10}$$

has its asymptotics controlled by the second term of the OPE, Eq. (5.3), for any β. Thus we can extend the definition of Chang *et al.* [140] to a family of condensates parametrised by β:

$$\overline{\sigma} \ \ (m(\mu),\beta) \ = \lim_{\Lambda\to\infty} Z_4(\mu,\Lambda)\, N_c \,\mathrm{Tr}_D \int_q^{\Lambda} \frac{1}{2} S(\beta) \tag{5.11}$$

where all S_-, S_+ and S_W are dependent upon the momentum q^2, the renormalisation point μ and the quark mass $m(\mu)$. The choice $\beta = 1$ corresponds to the definition of Eq. (5.9), with $\beta = 0$ and $\beta = 2$ corresponding to two other natural choices. In fact β could take any value from $-\infty$ to $+\infty$ and so we could have a whole range of values for the quark condensate: all agreeing in the chiral limit. Consequently,

the definition proposed by Chang *et al.* is far from unique, and does not provide a value for the condensate that corresponds to the physical M^+ solution of interest. Eq. (5.11) merely defines the value for the difference of the condensates for M^+ and M^-. However, we will show that when combined with the OPE these three solutions will pick out a precise *physical* definition of this condensate. Before investigating this in the context of models of the QCD interaction, we shall draw analogy with the NJL model, within which a natural definition of the massive quark condensate already exists.

5.2 The Nambu–Jona-Lasinio Model

Because of the complexity of QCD, it is often prudent to examine simpler systems exhibiting similar characteristics first. One such example is the Nambu-Jona-Lasinio (NJL) model. Though originally formulated to describe nucleon interactions in the pre-QCD era, the model can be reinterpreted by regarding the nucleons as quarks [141, 142]. It can be used to study bound states and so determine basic phenomenological quantities of meson interactions. The NJL model shares the same symmetry structure as QCD, and is dominated by DCSB effects at low energies too. The Lagrangian for the NJL model with just two flavours of quarks with degenerate mass $m_0 = m_u = m_d$ is:

$$\mathcal{L}_{NJL} = \overline{\psi}(x)\left(i\,\gamma^\mu\partial_\mu - m_0\right)\psi(x) + \mathcal{L}_{int}\,. \tag{5.12}$$

The interactions are given by a four-fermion contact term:

$$\mathcal{L}_{int} \;=\; \frac{G_\pi}{2}\left[\left(\overline{\psi}(x)\psi(x)\right)^2 + \left(\overline{\psi}(x)i\gamma_5\tau^a\psi(x)\right)^2\right], \tag{5.13}$$

with the two terms corresponding to the scalar and pseudoscalar channels respectively. From this can be derived the so-called gap equation:

$$m \;=\; m_0 \;+\; i\,G_\pi N_c N_f \int \frac{d^4p}{(2\pi)^4}\,\mathrm{Tr}_D S(p)\,, \tag{5.14}$$

where the trace is over spinor indices in d-dimensions. At this point one has a choice of how to regulate the integrals. Since we are dealing with a non-renormalisable effective theory, our results will depend upon the cut-off used. One may introduce a non-covariant cut-off in the Euclidean 3-momentum, or employ a variety of covariant regularisation schemes such as a four-momentum cut-off, proper time or

Pauli-Villars. The four-momentum cut-off is most closely related to the scheme we will employ in the later sections, so we choose this method. By inserting the form of the propagator into Eq. (5.14) we arrive at:

$$m = m_0 + m G_\pi N_c 8i \int^\Lambda \frac{d^4k}{(2\pi)^4} \frac{1}{k^2 - m^2} , \tag{5.15}$$

where we have introduced a cut-off Λ on the 4-momentum. Rotating to Euclidean space we obtain:

$$m = m_0 + \frac{G_\pi N_c m}{2\pi^2} \left(\Lambda^2 - m^2 \log \left(1 + \frac{\Lambda^2}{m^2} \right) \right) . \tag{5.16}$$

The coupling G_π and cut-off, Λ, are fixed by fitting to experimental data. To do this we must calculate the order parameter associated with the breaking of chiral symmetry. Thus the chiral condensate is given by:

$$\langle \bar{q}q \rangle = -i \, N_c \int \frac{d^4k}{(2\pi)^4} \, \mathrm{Tr}_D S(k;m) , \tag{5.17}$$

and for non-zero current masses we define [143]:

$$\langle \bar{q}q \rangle = -i \, N_c \int \frac{d^4k}{(2\pi)^4} \, \mathrm{Tr}_D \left[S(k;m) - S(k;m_0) \right] . \tag{5.18}$$

Working with explicitly massless quarks and employing a covariant cut-off in the Euclidean 4-momentum, the pion-decay constant is given by [144]:

$$f_\pi^2 = N_c m^2 \left[\log \left(1 + \frac{\Lambda^2}{m^2} \right) - \frac{\Lambda^2}{m^2 + \Lambda^2} \right] . \tag{5.19}$$

By solving Eq. (5.17) and Eq. (5.19) simultaneously and demanding that $f_\pi = 93$ MeV and $-\langle \bar{q}q \rangle^{1/3} = 235$ MeV, we obtain $\Lambda = 0.908$ GeV and $m = 0.265$ GeV. These can be substituted into the mass gap equation of Eq. (5.16) and thus we can solve for the effective coupling, finding $G_\pi = 10.2$ GeV^{-2}.

Our interest is to investigate the condensate's dependence on the current quark mass. In Fig. 5.1(a) we see that the behaviour of the condensate depends upon the chosen coupling. Indeed, it either increases to a maximum then decreases, or is monotonically decreasing for larger couplings as the quark mass increases. Moreover, one finds that the condensate can become vanishingly small for sufficiently large masses ($\sim$ 500 MeV).

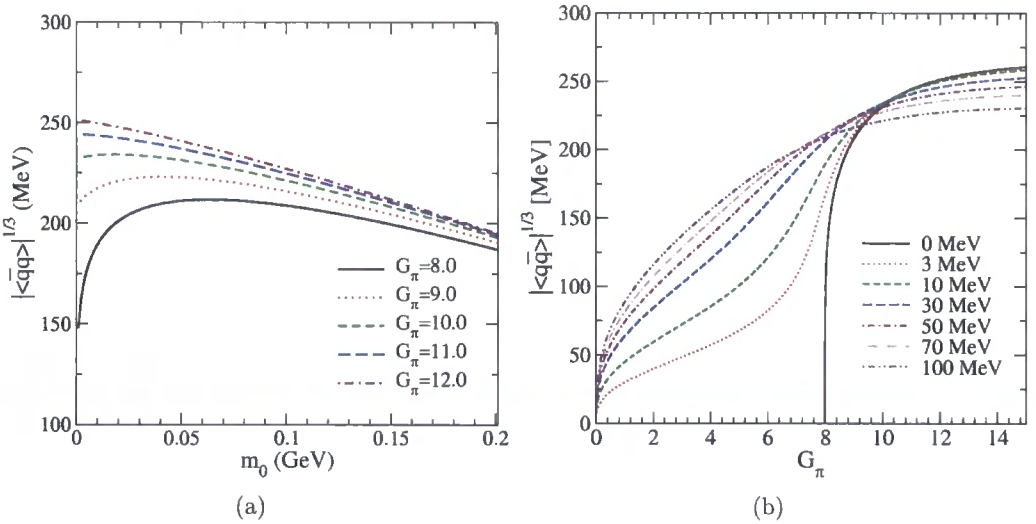

Figure 5.1: The non-perturbative condensate as: (a) a function of the current quark mass for a selection of NJL couplings G_π; and (b) a function of G_π for a selection of current quark masses.

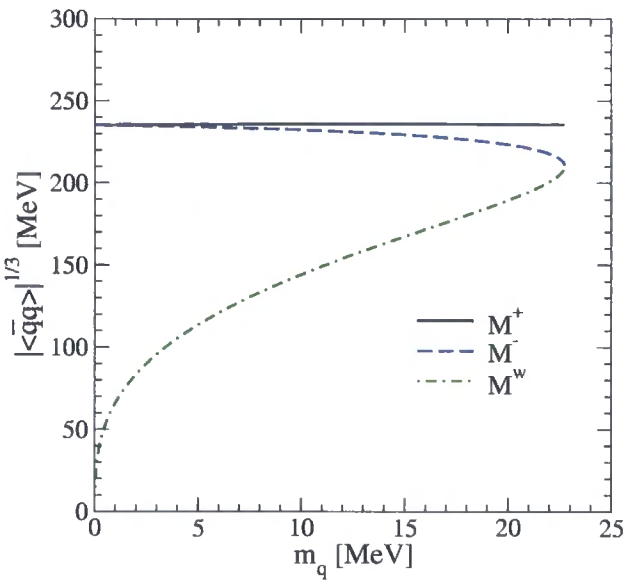

Figure 5.2: The quark condensate within the NJL model for the three solutions $M^{\pm,W}$ as functions of quark mass.

Now, within the NJL model we also find solutions corresponding to M^+, M^- and M^W away from the chiral limit within some domain. The extent of the domain depends on the parameters of the model. With those we have chosen, $m_{cr} \simeq 22.7$

MeV in Eq. (5.8). One may then use Eq. (5.18) to calculate the massive quark condensate for these solutions individually, the result of which is shown in Fig. 5.2. Furthermore, one may make an equivalent definition to Eq. (5.11), *viz*:

$$\overline{\sigma}(\beta) \;=\; -i\,N_c \int \frac{d^4k}{(2\pi)^4} \mathrm{Tr}_D \,\frac{1}{2}\Big[(2-\beta)\,S_+ - \beta S_- + 2(\beta-1)\,S_W\Big]\,. \qquad (5.20)$$

The results of this for the NJL model are given in Fig. 5.3 for $\beta = \{0, 1, 2\}$. What is clearly evident is that the condensates for the three mass functions $M^{\pm}$, M^W are not equal. Drawing analogy with the Schwinger-Dyson equations, one should therefore not expect the condensate of $M^{\pm}$ to be equal in magnitude as well as opposite in sign, as assumed by Chang *et al.* [140]. We show this to be the case in the next section.

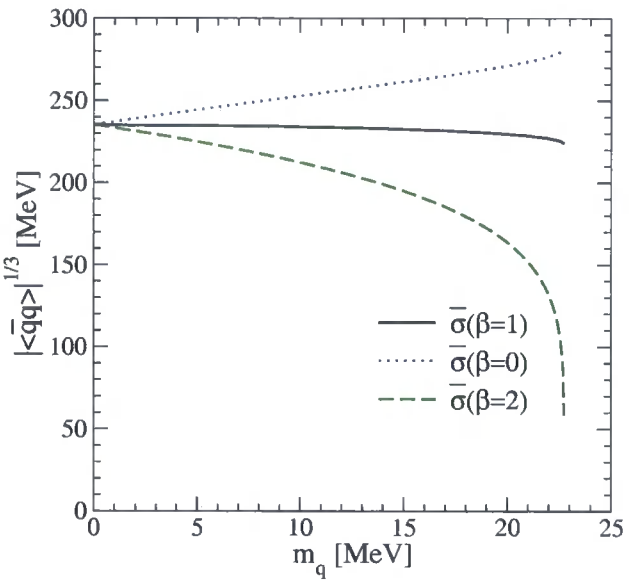

Figure 5.3: The condensate defined by $\overline{\sigma}(\beta)$ within the NJL model for values $\beta = \{0, 1, 2\}$ as a function of quark mass.

5.3 Phenomenological Model of QCD interaction

We now turn to QCD. Rather than solving for the ghost and gluon system, one may employ some suitable ansatz for the coupling which has sufficient integrated strength in the infrared so as to achieve dynamical mass generation. There have been many suggestions in the literature [97,98] which have been extensively studied. Following

the lead of Maris *et al.*, we will employ an ansatz for $g^2 D_{\mu\nu}(p-k)$ which has been shown to be consistent with studies of bound state mesons. We will consider other modellings in a later section. Since this simple model assumes a rainbow vertex truncation, the solutions are not multiplicatively renormalisable and so depend on the chosen renormalisation point. For comparison with earlier studies we take this to be $\mu = 19$ GeV. This model has been discussed in the previous chapter, for which the model requires the replacements given in Eqs. (4.53) and (4.54). Thus we use:

$$\begin{aligned} \alpha\left(q^2\right) &= \frac{\pi}{\omega^6} D\, q^4 \exp(-q^2/\omega^2) \\ &+ \frac{2\pi\gamma_m}{\log\left(\tau + \left(1 + q^2/\Lambda_{QCD}^2\right)^2\right)} \times \left[1 - \exp\left(-q^2/\left[4m_t^2\right]\right)\right] , \end{aligned} \tag{5.21}$$

with

$$\begin{aligned} m_t &= 0.5\,\text{GeV} \quad , \quad \tau = \mathrm{e}^2 - 1 \quad , \\ \gamma_m &= 12/(33 - 2N_f) \quad , \quad \Lambda_{QCD} = 0.234\,\text{GeV} . \end{aligned}$$

Note that we work in the $N_f = 0$ limit first since in Sect. 5.5 we will investigate the mass dependence of the condensate using a model derived from quenched lattice data [121]. The precise value of Λ_{QCD} is irrelevent for our current study, and we choose the parameter set $\omega = 0.4$ GeV, $D = 0.933$ GeV^2.

Solutions are obtained by solving the coupled system of fermion equations for $\mathcal{A}$ and $\mathcal{M}$ of Eq. (5.2), which we may write symbolically as:

$$\begin{aligned} \mathcal{A}(p^2,\mu) &= Z_2(\mu,\Lambda) - \Sigma_D\left(p,\Lambda\right) , \\ \mathcal{M}(p^2)\mathcal{A}(p^2,\mu) &= Z_2(\mu,\Lambda) Z_m m_R(\mu) + \Sigma_S\left(p,\Lambda\right) . \end{aligned} \tag{5.22}$$

The Σ_S and Σ_D correspond to the scalar and spinor projections of the integral in Eq. (5.1). For massive quarks we obtain the solution M^+ by eliminating the renormalisation factors Z_2, Z_m via:

$$\begin{aligned} Z_2(\mu,\Lambda) &= 1 + \Sigma_D\left(\mu,\Lambda\right) , \\ Z_m(\mu,\Lambda) &= \frac{1}{Z_2(\mu,\Lambda)} - \frac{\Sigma_S\left(\mu,\Lambda\right)}{Z_2(\mu,\Lambda) m_R\left(\mu\right)} . \end{aligned} \tag{5.23}$$

Crucially, for a given m_R we obtain the M^- and M^W solutions by inserting the same Z_2 and Z_m found for the M^+ solution. This ensures that differences in the dynamics

of the three systems do not influence the ultraviolet running of the current-quark mass. A representative example of the solutions is shown in Fig. 5.4.

The value of the critical mass is model-dependent, and is summarised in Table 5.1. Chang *et al.* [140] imbue this critical mass with some significance for the dynamics of QCD. However, criticality does not feature in the *physical* solution M^+, which exists for all values of m_q. It only occurs in the M^- and M^W solutions, which appear only in a strongly model-dependent region. Consequently, we find little evidence of criticality being important to the mass generation in QCD. We will comment again on this when we consider more sophisticated vertex structures in a later section.

As with the analogous NJL model, we clearly have an infinite set of ambiguous definitions of the quark condensate, each of which agrees with the chiral condensate in the limit $m_q \to 0$. This ambiguity seen in Fig. 5.5 arises because, although each solutions exhibits the same leading logarithmic behaviour in the ultraviolet limit, the condensates for each are not equal in magnitude, cf. Eq. (5.3). Indeed, the solutions M^- and M^W have negative condensates, but we cannot directly use combinations of these mass functions to form a well-defined and unique condensate that coincides with the true condensate contained within $M^+(p^2)$.

5.4 Extracting the Condensate

We continue our investigation of quark mass-functions with the Maris-Tandy model interaction. At very large momenta the tail of the mass function is described by the operator product expansion of Eq. (5.3). For QCD, let us introduce the appropriate

N_f	ω	0.3	0.4	0.5	[GeV]
0	$m_{cr}(\mu = 19$ GeV)	38	34	16	[MeV]
0	$m_{cr}(\mu = 2$ GeV)	49	44	21	[MeV]
4	$m_{cr}(\mu = 19$ GeV)	35	31	16	[MeV]
4	$m_{cr}(\mu = 2$ GeV)	49	44	23	[MeV]

Table 5.1: How the critical mass that defines the domain of solutions Eq. (5.8) depends on the number of quark flavours, N_f, on the gluon range parameter ω, in the Maris-Tandy model. This critical mass is listed at two different renormalization scales, 19 GeV of Ref. [140] and 2 GeV for ease of comparison with other works.

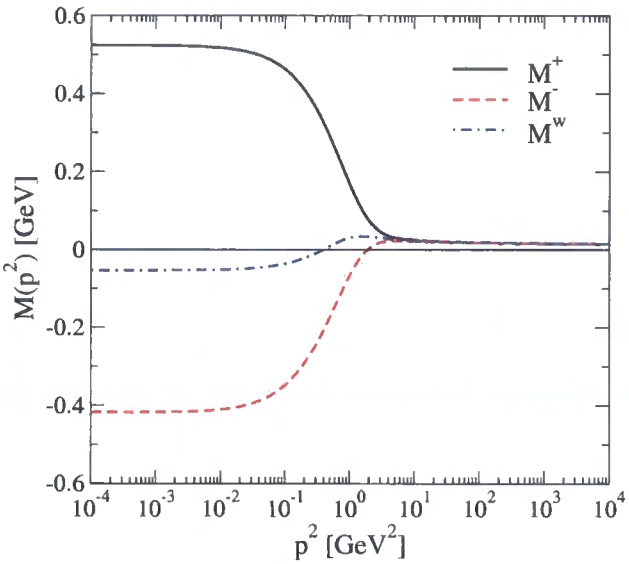

Figure 5.4: Momentum dependence of the three solutions $M^{\pm}(p^2)$ and $M^W(p^2)$ for a quark mass $m(\mu)$=16 MeV, $\mu = 19$ GeV.

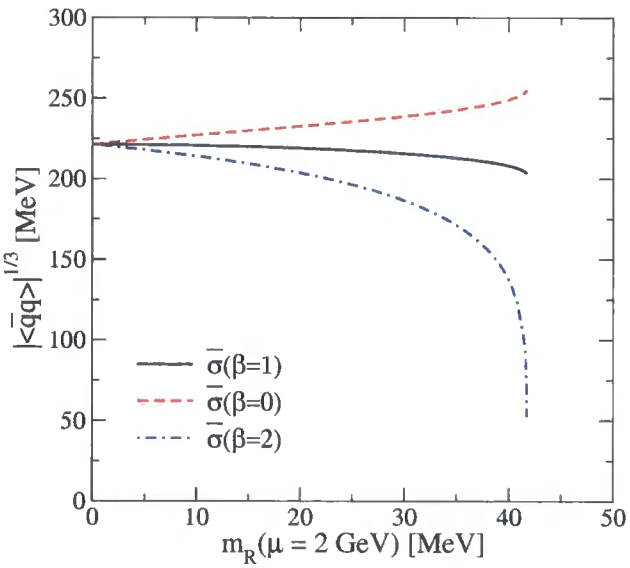

Figure 5.5: Renormalisation point independent quark condensate as a function of m_q as defined by Eq. (5.11) for three values of β, showing how they are quite different despite the solutions having the same running current-mass and being equal in the chiral limit.

anomalous dimension factors explicitly, so that:

$$M(p^2)_{asym} = \overline{m}\left(\log\frac{p^2}{\Lambda_1^2}\right)^{-\gamma_m} + \frac{2\pi^2\gamma_m}{3}\frac{\mathcal{C}}{p^2}\left(\frac{1}{2}\log\frac{p^2}{\Lambda_2^2}\right)^{\gamma_m - 1}, \qquad (5.24)$$

where $\overline{m}$ is related to the quantity $m_R(\mu)$ via some renormalisation factors. This provides an excellent representation of all our solutions. If we included the expression to all orders then the scales Λ_1, and Λ_2 would both be equal to Λ_{QCD}. However, the leading order forms in Eq. (5.24) absorb different higher order contributions into the two terms and so Λ_1 and Λ_2 are in practice different, as we will discuss below. For large masses the condensate piece, $\mathcal{C}$, is irrelevant and so it is the leading term that describes the mass function well. In contrast, in the chiral limit, $\overline{m} = 0$ and so the second term of the OPE describes the behaviour of the mass function. This then accurately determines the scale Λ_2. Indeed, its value is equal to Λ_{QCD}. We can then easily extract the renormalisation point independent condensate, $\mathcal{C} \equiv -\langle\bar{q}q\rangle$, from the asymptotics.

In this latter case, strictly in the chiral limit, we may also extract the condensate via:

$$-\langle\bar{q}q\rangle_\mu = Z_2(\mu,\Lambda)\, Z_m(\mu,\Lambda)\, N_c \,\mathrm{Tr}_D \int \frac{d^4k}{(2\pi)^4} S(k,\mu) \ , \tag{5.25}$$

where $\langle\bar{q}q\rangle_\mu$ is the renormalisation dependent quark condensate. At one-loop, this is related to the renormalisation point independent quark condensate:

$$\langle\bar{q}q\rangle_\mu = \left(\frac{1}{2}\log\frac{\mu^2}{\Lambda_{QCD}^2}\right)^{\gamma_m} \langle\bar{q}q\rangle \ . \tag{5.26}$$

which we compare with the asymptotic extraction to good agreement.

However, for small quark masses, where the condensate is believed to play a sizeable role, we cannot apply Eq. (5.25), since it acquires a quadratic divergence, cf. Eq. (5.3). Indeed, it is the elimination of this that inspired the original Eq. (5.9) and later Eq. (5.11), which we have seen lead to a wholly ambiguous definition of the physical condensate. Nevertheless, one can attempt to fit both terms of the OPE in Eq. (5.24) to the tail of the mass function, M^+ for instance. While a value for the condensate can then be extracted, this procedure is not at all reliable because of the difficulty in resolving the two functions in the OPE from one another and in fixing the appropriate scales, Λ_1 and Λ_2.

It is to this last point which we now turn. Instead of one single solution, we now have three solutions to the same model, each with identical running of the current quark mass (the first term in Eq. (5.24) in the ultraviolet region, differing only by their values of the condensate. Thus it is possible to fit Eq. (5.24) simultaneously to the three mass functions $M^\pm$, M^W and determine the condensates $\mathcal{C}^\pm$ and $\mathcal{C}^W$. The scales Λ_1 and Λ_2 are the same for any current mass within the current model

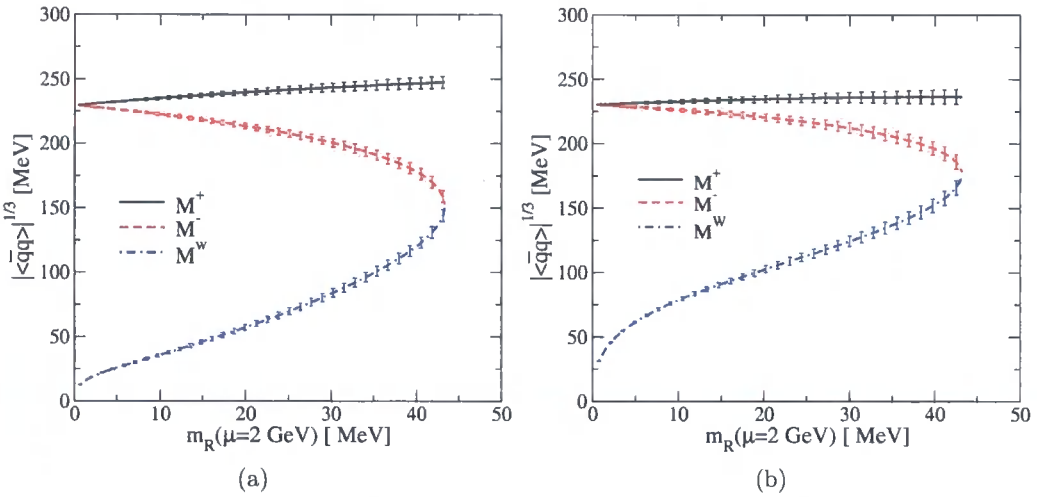

Figure 5.6: Condensate extracted through simultaneous fitting of the three solutions to the fermion mass-function in the Maris-Tandy model with $\omega = 0.4$ GeV and (a) $N_f = 0$, (b) $N_f = 4$. The functions of the current quark mass are evolved to 2 GeV in a momentum subtraction scheme.

and found to be $\sim 2\Lambda_{QCD}$ and Λ_{QCD} respectively. The condensates $\mathcal{C}^{\pm}$ and $\mathcal{C}^{W}$ are then determined in an accurate and stable way.

This fitting is performed using a modified Levenberg-Marquardt algorithm. We restrict ourselves to the momentum regions typically above 50 GeV^2, in accordance with the validity of the OPE. To perform the fit, we introduce a weight function that gives a preference of fit for larger momenta; this ensures that our asymptotics are well described, as they should be.

The results for the phenomenological model employed here are given in Fig. 5.6(a). In contrast to the condensate defined by Eq. (5.9), we find that in the limited mass range investigated the condensate increases as a function of m_q. At the critical point $m_{cr}(\mu = 1\ \text{GeV})$=44 MeV, we find the ratio for the condensate to the chiral limit to be:

$$\langle\bar{q}q\rangle_{m=44\text{MeV}} \,/\, \langle\bar{q}q\rangle_{m=0} = 1.24\ , \tag{5.27}$$

for $N_f = 0$. To estimate the errors in this determination, we can form combinations of these condensates in the same way as defined in Eq. (5.11), favourably reproducing the same results of Fig. 5.5. In Fig. 5.6(b) is a similar plot with $N_f = 4$ and $\omega = 0.4$ GeV, illustrating how m_{cr} changes compared with Fig. 5.6(a).

5.5 More sophisticated Phenomenological Models of QCD interaction

We now consider the effect of using more sophisticated vertex structure for the quark-gluon interaction in the quark Dyson-Schwinger equations. The first framework we study is a truncation scheme introduced in [27, 131]. It involves replacing the bare quark-gluon vertex with the Curtis-Pennington (CP) vertex [39], thus ensuring multiplicative renormalizability for the fermion propagator. In the Yang-Mills sector of QCD ansätze for ghost and gluon interactions have been introduced, which enable a self-consistent solution for the ghost and gluon propagators. The second scheme we investigate is an ansatz for the quark-gluon vertex, which has been fitted to lattice results, and was previously employed in Ref [121].

Both of this models are presented in some detail in Chapter 4, where we explored in some detail the positive semi-definite solutions and their phenomenological observables in the chiral limit.

Continuum studies: CP-Vertex

We have already given details of this truncation scheme. In summary, the solutions for the ghost and gluon propagators:

$$D_G(p) = -\frac{G(p^2)}{p^2}\,, \tag{5.28}$$

$$D_{\mu\nu}(p) = \left(\delta_{\mu\nu} - \frac{p_\mu p_\nu}{p^2}\right)\frac{Z(p^2)}{p^2}\,, \tag{5.29}$$

can be represented accurately by:

$$R(p^2) = \frac{c\,(p^2/\Lambda_{QCD}^2)^\kappa + d\,(p^2/\Lambda_{QCD}^2)^{2\kappa}}{1 + c\,(p^2/\Lambda_{QCD}^2)^\kappa + d\,(p^2/\Lambda_{QCD}^2)^{2\kappa}}\,, \tag{5.30}$$

$$Z(p^2) = \left(\frac{\alpha(p^2)}{\alpha(\mu)}\right)^{1+2\delta} R^2(p^2)\,, \tag{5.31}$$

$$G(p^2) = \left(\frac{\alpha(p^2)}{\alpha(\mu)}\right)^{-\delta} R^{-1}(p^2)\,, \tag{5.32}$$

with the scale $\Lambda_{QCD} = 0.714\,\text{GeV}$, the coupling $\alpha(\mu) = 0.97$ and the parameters $c = 1.269$ and $d = 2.105$ in the auxiliary function $R(p^2)$. The quenched anomalous dimension γ of the gluon is related to the anomalous dimension δ of the ghost

by $\gamma = -1 - 2\delta$ and $\delta = -9/44$ for $N_f = 0$. The infrared exponent κ is given by $\kappa = \frac{93-\sqrt{1201}}{98} \approx 0.595$. The running coupling $\alpha(p^2)$ is defined via the nonperturbative ghost-gluon vertex,

$$\alpha(p^2) = \alpha(\mu)\, G^2(p^2)\, Z(p^2) \tag{5.33}$$

and can be represented by

$$\alpha(p^2) = \frac{1}{1+p^2/\Lambda_{QCD}^2}\left[\alpha(0) + \frac{p^2}{\Lambda_{QCD}^2}\frac{4\pi}{\beta_0}\left(\frac{1}{\ln(p^2/\Lambda_{QCD}^2)} - \frac{1}{p^2/\Lambda_{QCD}^2 - 1}\right)\right] \tag{5.34}$$

The value $\alpha(0) \approx 8.915/N_c$ is known from an analytical infrared analysis [145].

In the quark SDE, Eq. (5.1), we use the solution (5.31) for the gluon propagator together with an ansatz of the form

$$\Gamma_\nu(q,k) = V_\nu^{AB}(p,q,k)\, W^{NA}(p,q,k), \tag{5.35}$$

where p and q denote the quark momenta and k the gluon momentum. The ansatz factorises into an Abelian (AB) and an non-Abelian (NA) part which are specified and discussed in detail in [131]. Here we only need to remark that the Abelian part V_ν^{AB} is identical to the Curtis-Pennington vertex [39]. This construction carries further tensor structure in addition to the γ_μ-piece, which makes it an interesting ansatz in comparison with the simple model in the last section. The corresponding numerical solutions for the quark propagator are discussed in detail in [131], and presented in chapter 4. Here we are only interested in the chiral condensate as a function of the current quark mass. The corresponding results can be found in Fig. 5.7. Regardless of the complicated tensor structure of the vertex (5.35) we find similar results for the condensate as in the previous section.

We were able to extract the condensate from all three solutions $M^{\pm}$ and M^W. The physical condensate rises for small current quark masses, with its rate of increase decreasing as we approach the critical mass. The critical value of m_{cr} is found to be 20 MeV at $\mu = 19$ GeV. This corresponds to 30 MeV at $\mu = 2$ GeV. With the parameters of [131], the condensate in the chiral limit is 270 MeV, rather than the phenomenological 235 MeV we have used. However, its dependence with the quark mass hardly depends on this exact value and so at the critical point we obtain the ratio:

$$\langle\bar{q}q\rangle_{m=30\text{MeV}} \,/\, \langle\bar{q}q\rangle_{m=0} = 1.175\,. \tag{5.36}$$

As with the phenomenological model considered in Sect. 5.3 we find a considerable increase of the chiral condensate with the current quark mass.

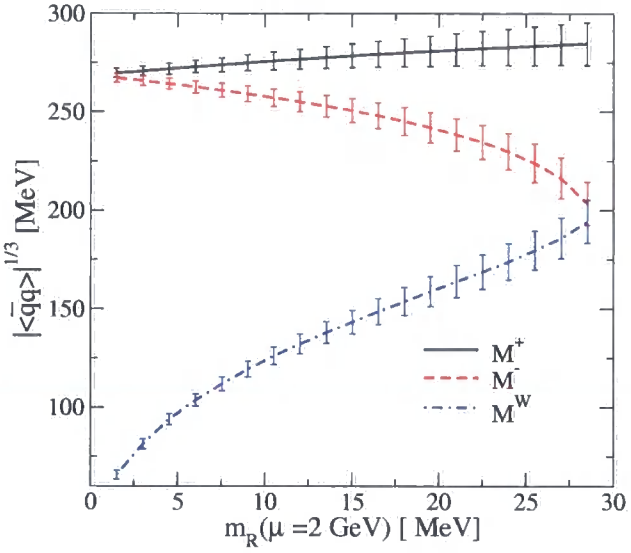

Figure 5.7: Condensate for CP-Vertex Model. $N_f = 0$

Lattice Model

We discussed the lattice model of [121] in Chapter 4. The Schwinger-Dyson equations for the coupled ghost-gluon system are solved on a compact manifold, this simulating the finite volume of lattice QCD. This was then employed in an ansatz for the quark-gluon vertex, and fitted against data from the lattice.

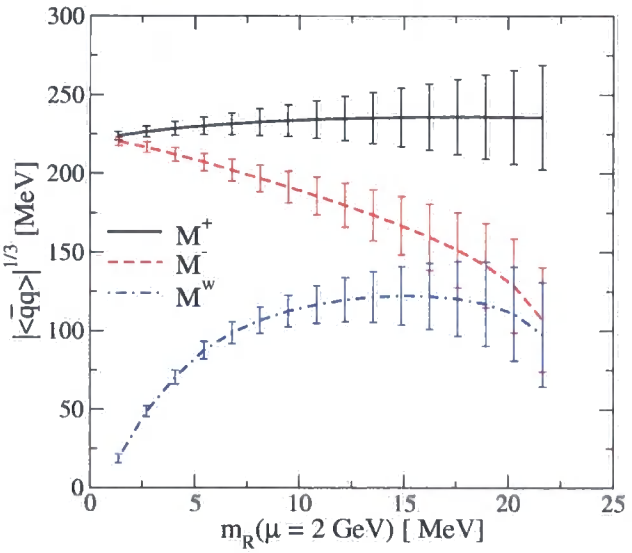

Figure 5.8: Condensate for Lattice Model. $N_f = 0$

	h	Λ_g (GeV)	Λ_{QCD} (GeV)	a_1	a_2	a_3
overlap	1.31	1.50	0.35	25.58	3.44	2.23

Table 5.2: Parameters used in the vertex model, Eqs. (5.37-5.40).

We repeat the ansatz for the quark-gluon vertex:

$$\Gamma_\nu(k,\mu^2) = \gamma_\nu \Gamma_1(k^2)\,\Gamma_2(k^2,\mu^2)\,\Gamma_3(k^2,\mu^2) \tag{5.37}$$

which has the components:

$$\Gamma_1(k^2) = \frac{\pi\gamma_m}{\ln(k^2/\Lambda_{QCD}^2+\tau)}, \tag{5.38}$$

$$\begin{aligned}\Gamma_2(k^2,\mu^2) &= G(k^2,\mu^2)\; G(\zeta^2,\mu^2)\; \widetilde{Z}_3(\mu^2) \\ &\quad \times h\;[\ln(k^2/\Lambda_g^2+\tau)]^{1+\delta}\end{aligned} \tag{5.39}$$

$$\Gamma_3(k^2,\mu^2) = Z_2(\mu^2)\,\frac{a(M)+k^2/\Lambda_{QCD}^2}{1+k^2/\Lambda_{QCD}^2}, \tag{5.40}$$

where $\delta = -9/44$ is the (quenched) one-loop anomalous dimension of the ghost, $\gamma_m = 12/33$ the corresponding anomalous dimension of the quark and $\tau = e-1$ acts as a convenient infrared cutoff for the logarithms. The quark mass dependence of the vertex is parametrised by

$$a(M) = \frac{a_1}{1+a_2 M(\zeta^2)/\Lambda_{QCD}+a_3 M^2(\zeta^2)/\Lambda_{QCD}^2}, \tag{5.41}$$

where $M(\zeta^2)$ is determined during the iteration process at $\zeta = 2.9$ GeV. The parameters have been fitted to lattice results using a staggered [122] and an overlap action [123]. Here we use only the fit to the overlap quark; the corresponding parameters are given in Table 5.2. Explicit solutions for the quark propagators are discussed in [121].

For the massive condensate we again find solutions similar to the previous sections. The condensate corresponding to the $M^\pm$ solutions are given in Fig. 5.8 and the critical value m_{cr} is in Table 5.3.

This modelling provides a link between lattice results and the continuum. The vertex function, as defined by Eqs. (5.37–5.40), which is currently fitted to the lattice

data, involves several different scales: Λ_g, Λ_{YM} and Λ_{QCD}. In the continuum this results in a failure to reproduce the perturbatively determined anomalous dimensions in the OPE, Eq. (5.24). The extraction of the tiny condensate term in the OPE is very sensitive to these anomalous dimensions. Combined with the effect the uncertainties in determining the multiple scales has on Λ_1 and Λ_2 in Eq. (5.24) leads here to much larger errors than in our previously modellings. Nevertheless, for the massive condensate we again find solutions similar to the previous sections. The condensate corresponding to the $M^{\pm}$ solutions are given in Fig. 5.8 and the critical value m_{cr} is 22 MeV, see Table 5.3. The large errors point to the need for further studies of matching lattice on a torus to the continuum, if we are to extract reliable infinite volume, continuum quantities like the quark condensate. That is for the future. The ratio of the condensates is here $\langle\overline{q}q\rangle_{m=22\,\mathrm{MeV}}$ / $\langle\overline{q}q\rangle_{m=0}$ = 1.17. This is a little lower than for the previous models of Eqs. (5.27,5.36). However, uncertainties in extraction are considerably larger. Nevertheless the ratio is still bigger than one.

Model	CP	Lattice	
$m_{cr}(\mu = 19$ GeV)	20	16	[MeV]
$m_{cr}(\mu = 2$ GeV)	30	22	[MeV]

Table 5.3: The critical mass for our quenched CP and Lattice model.

5.6 Condensate Beyond the Critical Mass Range: Noded Solutions

We see in Figs. 5.6(a), 5.6(b) that the M^- and M^W solutions bifurcate below $m_{cr} \simeq$ 43.4(44.0) MeV with $\omega = 0.4$ GeV for $N_f = 0(4)$ respectively. But what about the value of the condensate for the physical solution M^+ beyond the region where M^- and M^W exist, *i.e.* $m_R(\mu) > m_{cr}$? Having accurately determined the scales Λ_1 and Λ_2 in the OPE of Eq. (5.5) in the region where all 3 solutions exist, we could just continue to use the same values in fitting the physical M^+ solution alone and find its condensate. However, this would make it difficult to produce realistic errors as the quark mass increases.

However, as soon as one allows for solutions for the fermion mass-function that are not positive definite, one exposes a whole series of variants on the solutions M^-, M^W we have already considered. Thus there are *noded* solutions, which have also

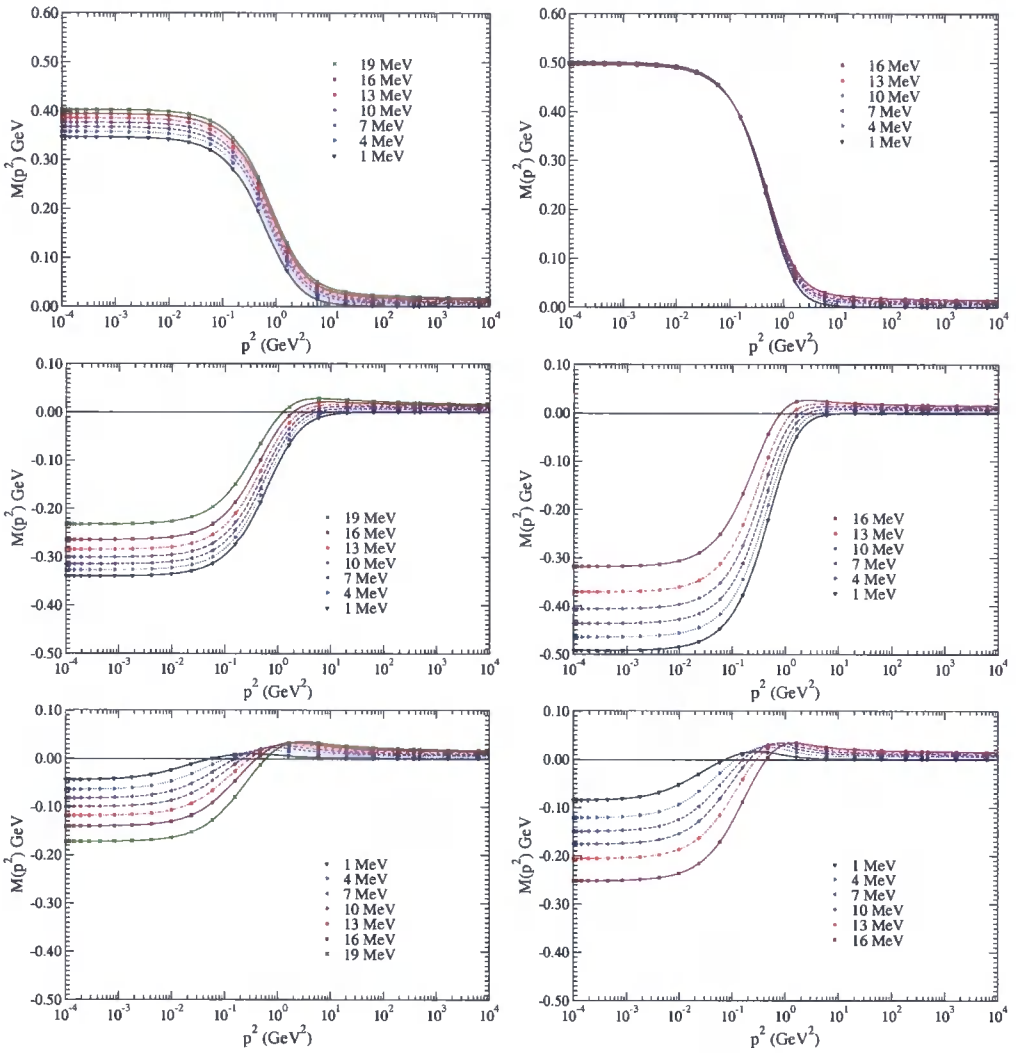

Figure 5.9: The M^+, M^- and M^W solutions as obtained for the CP-vertex (left) and the lattice model (right). Masses are renormalised at $\mu = 19$ GeV.

been discovered recently by Martin *et al* [146] in the context of a simple Yukawa theory. We illustrate this within the Maris-Tandy model, for instance with $N_f = 4$ and $\omega = 0.4$, in Fig. 5.10. There the four solutions we have found are displayed.

It is interesting to note that this noded solution is not limited to the same domain that restricts M^- and M^W. These noded solutions do develop a singularity in $M(p^2)$ beyond $m = 51.4$ MeV at $\mu = 2$ GeV. However, this is compensated for by a zero in $\mathcal{A}(p^2)$, until $m = 66.3$ MeV. Thus there exists a solution with a well-defined ultraviolet running of the quark mass exactly as the M^+ solution, as far as $m = 66.3$ MeV. While at small quark masses we have all four solutions, at larger

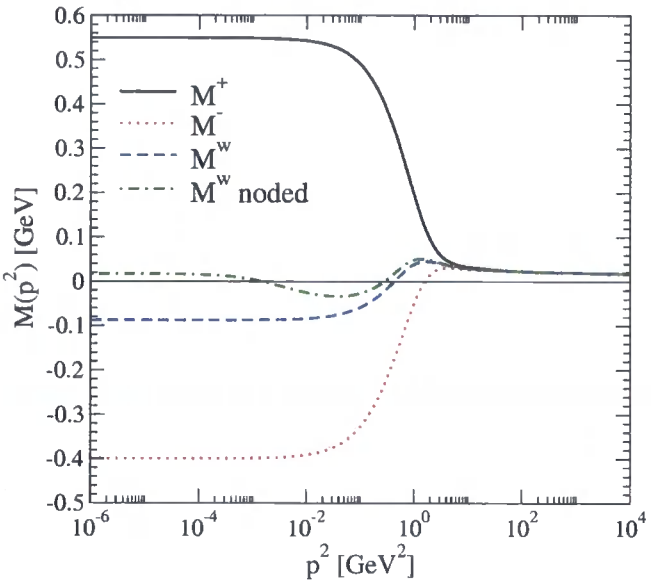

Figure 5.10: Momentum dependence of the 4 solutions for the fermion mass-function in the Maris-Tandy model with $m = 20$ MeV at $\mu = 19$ GeV, N_f=4, $\omega = 0.4$ GeV.

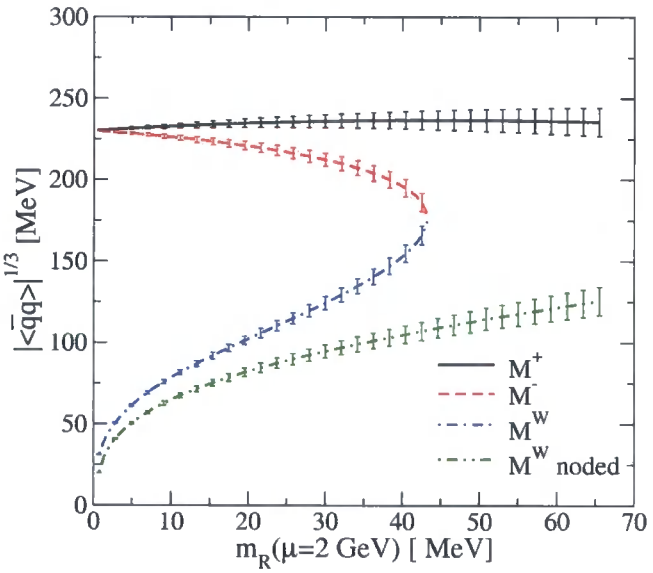

Figure 5.11: Current quark mass dependence of the condensates for Maris-Tandy model with $N_f = 4$, $\omega = 0.4$ GeV, including the noded solution of Fig. 5.10.

masses there are still two. Consequently, we confirm that the scales, Λ_1 and Λ_2, as fixed for $m < m_{cr}$ are still well-determined by our fit-procedure for $m > m_{cr}$. The results of our fitting for all four functions are shown in Fig. 5.11. Indeed, these fits confirm that Λ_1 and Λ_2 are independent of $m_R(\mu)$, at least in the Maris-Tandy

model. We can then fit the remaining M^+ solutions shown in Fig. 4.8 of the previous chapter, to give the physical condensate for acceptable values of ω as determined by [147]. In Fig. 5.11 we have in fact scaled the quark mass from $\mu = 2$ GeV in the (quark-gluon) MOM scheme by one loop running to the $\overline{MS}$ scheme at 2 GeV using the relationship between Λ_{MOM} and $\Lambda_{\overline{MS}}$ for 4 flavours deduced by Celmaster and Gonsalves [148]. We take the strange quark mass to be ~ 95 MeV [119] in the $\overline{MS}$ scheme.

Within the range of the Maris-Tandy modelling of strong coupling QCD we find that the ratio of the condensates at the strange quark mass to the chiral limit is

$$\langle\bar{q}q\rangle_{m(\overline{MS})=95\,\mathrm{MeV}} \,/\, \langle\bar{q}q\rangle_{m=0} \;=\; (1.1 \pm 0.2)^3. \tag{5.42}$$

in a world with 4 independent flavours. Moreover, here all the quarks have the same mass and there is no mixing between different hidden flavour pairs.

Of course, in the quenched case quark loops decouple and exactly replicate the results given here. Chang *et al.* have proposed that the fact that the M^- and M^W solutions only exist for some domain of quark masses, $m_q \in [0, m_{cr}]$, is directly linked to the domain of convergence of the chiral expansion [143, 149]. While the existence of multiple solutions for the fermion mass function is essential for the extraction of the condensate, we note that distinct domains exist for the different solutions and that the simplest noded solution exists in a larger domain. Though the value of m_{cr} is indeed some measure of the range of validity of the chiral expansion, the fact that m_{cr} is both strongly model and solution dependent indicates its value is no more than a guide and not likely to be the exact bound claimed by Chang *et al.*

What we have shown here is that there is a robust method of determining the value of the $\bar{q}q$ condensate beyond the chiral limit based on the Operator Product Expansion. Of course, as the quark mass increases the contribution of the condensate to the behaviour of the mass function, Fig. 4.8, becomes relatively less important and so the errors on the extraction of the physical condensate increases considerably. Nevertheless, the method is reliable up to and beyond the strange quark mass. Alternative definitions are not.

We believe that only the M^+ solution has any physical significance and the others are mathematical curiosities, which only exist on the restricted domains of Eq. 5.8. In contrast, the physical solution exists for all current quark masses, even if we cannot reliably extract the value of the corresponding condensate from the OPE. While it is clear that the radius of convergence of the chiral expansion in terms of

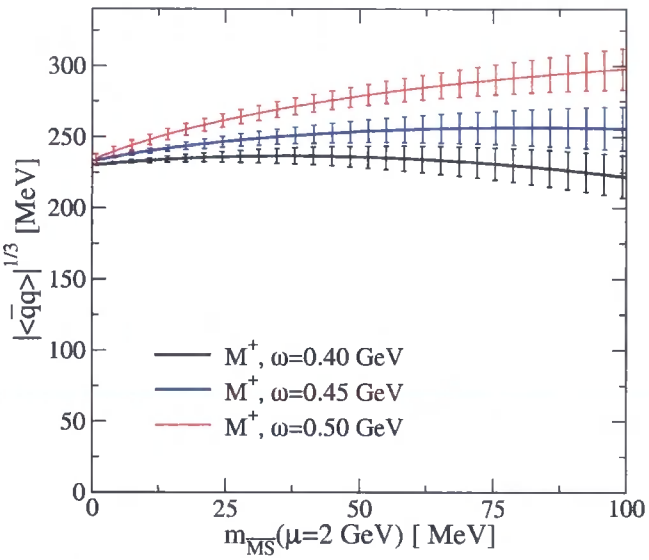

Figure 5.12: Condensate for Maris-Tandy Model with $N_f = 4$, $\omega = 0.4, 0.45, 0.5$ GeV as a function of current quark mass defined at 2 GeV in $\overline{MS}$ scheme.

the quark mass has a scale of order Λ_{QCD} or equally $(-\langle\bar{q}q\rangle)^{1/3}$, is the scale set by m_{cr}? Chang *et al.* claim it is. However, the fact that the bifurcation point for the unphysical M^- and M^W solutions differs from the region in which any *noded* solution exists (and both are highly model-dependent) makes it difficult to claim that the value of m_{cr} from the bifurcation of the M^- and M^W solutions is the key parameter in the radius of convergence of the chiral expansion.

5.7 Summary

Within the NJL model and the Schwinger-Dyson approach we investigated the three inequivalent solutions to the mass gap equation that exist within the interval $\mathcal{D}(m) = \{m : 0 \leq m \leq m_{cr}\}$. We found that by ensuring each were solved using the same renormalisation conditions that each solution exhibited the same running of the current-quark mass in the ultraviolet, differentiated solely by their infrared behaviour and value of the quark condensate.

We found that in both approaches it was not possible unambiguously to define the condensate by simply taking combinations of the three solutions. However, the increased information available on the domain $\mathcal{D}(m)$ permits a reliable extraction of the condensate through simultaneous fitting of the OPE to all three solutions.

We have investigated a number of models for the strong coupling (infrared) behaviour of the quark-gluon interaction and found in all cases that the condensate

corresponding to the solution with a positive-definite mass function increases moderately with current quark mass in the region under consideration. For the Maris-Tandy model we were able to look at masses corresponding to that of the strange quark, where we found $\langle\bar{q}q\rangle_{m(\overline{MS})=95\,\mathrm{MeV}} / \langle\bar{q}q\rangle_{m=0} = (1.1 \pm 0.2)^3$, not in disagreement with the estimate of [133,135,136] that the $\bar{s}s$ condensate was $(0.8 \pm 0.3)\,\langle\bar{u}u\rangle$. However, it is the $N_f = 3$ case that should be compared, and more specifically for $N_f = 2 + 1$ non-degenerate. This we leave for a later work.

Chapter 6

The Transverse Ward-Takahashi Identity

The Ward-Green-Takahashi identities [24–26] play an important role in the study of gauge theories, particularly in the implementation of consistent non-perturbative truncations of the corresponding Schwinger-Dyson equations [33, 39]. The Ward-Green-Takahashi identities involve contractions of vertices with external momenta and relate these to Green's functions with a lesser number of external legs. The best known of these relates the 3 point vector vertex coupling a fermion-antifermion pair to the gauge boson, $\Gamma^\mu_V(p_1, p_2)$, to the difference of fermion propagators, $S_F(p_1)$ and $S_F(p_2)$, so that with $q = p_1 - p_2$:

$$q_\mu \Gamma^\mu_V(p_1, p_2) = S_F^{-1}(p_1) - S_F^{-1}(p_2) \,. \tag{6.1}$$

Such projections constrain the so called longitudinal component of the vertices, while leaving their transverse parts unrestricted.

We have seen how the Ward-Green-Takahashi identity constrains the longitudinal part of the fermion-boson vector vertex in chapter 2. To recap, first let us recall the very first Ward identity, which is the $q \to 0$ limit of Eq. (6.1), *viz.*

$$\Gamma^\mu_V(p, p) = \frac{\partial S_F^{-1}(p)}{\partial p_\mu} \quad . \tag{6.2}$$

Let us separate the vertex into longitudinal and transverse components defined by:

$$\Gamma^\mu_V = \Gamma^\mu_L + \Gamma^\mu_T \quad , \quad \text{with} \quad q_\mu \Gamma^\mu_T = 0 \quad . \tag{6.3}$$

We can arrange for Γ^μ_L alone to satisfy the original Ward-Green-Takahashi identity,

Eq. (6.1), and for Γ^μ_T alone to contribute to the left hand side of the transverse Ward-Takahashi relation, Eq. (6.6), by writing:

$$\Gamma^\mu_L = \frac{q^\mu}{q^2}\left(S_F^{-1}(p_1) - S_F^{-1}(p_2)\right) \quad \text{, and} \quad \Gamma^\mu_T = \left(g^{\mu\nu} - \frac{q^\mu q^\nu}{q^2}\right)\Gamma^\nu_V \,. \tag{6.4}$$

This separation seemingly makes the longitudinal and transverse components unrelated. However, each component of Eq. (6.4) has a kinematic singularity at $q^2 = 0$. Consequently, the Ward identity in Eq. (6.2) requires an inter-relation between Γ^μ_L and Γ^μ_T. An alternative separation is to abandon Eq. (6.4) and ensure that each component is free of kinematic singularities. Then one can require that the longitudinal part alone not only satisfies Eq. (6.1), but its $q \to 0$ limit too, *viz.* Eq. (6.2). With this definition of the longitudinal part, whose form is given in Eq. (2.12), we arrive at the Ball–Chiu construction. Writing the massless inverse fermion propagator as $S_F^{-1}(p) = \mathcal{A}(p^2)\not{p}$, Eq. (2.12) is:

$$\Gamma^\mu_L(p_1,p_2) = \frac{1}{2}\left(\mathcal{A}(p_1^2) + \mathcal{A}(p_2^2)\right)\gamma^\mu + \frac{1}{2}\frac{\mathcal{A}(p_1^2) - \mathcal{A}(p_2^2)}{p_1^2 - p_2^2}(\not{p}_1+\not{p}_2)(p_1+p_2)^\mu \,. \tag{6.5}$$

The transverse component is then only constrained to satisfy the condition that $\Gamma^\mu_T(p,p) = 0$, which the separation of Eq. (6.4) does not.

While the Ward-Green-Takahashi identity follows from the divergence of the vector vertex, Takahashi made plausible the existence of new relations that follow from the *curl* (or wedge product) of the vertex [150]. These are referred to as transverse Ward-Takahashi relations and have the potential to restrict the transverse vertices from gauge symmetry alone. Kondo [151] re-derived these relations for the 3-point functions in coordinate space using the path integral formulation. Subsequently, He, Khanna and Takahashi [152] using canonical field theory cast these relations in momentum space. However, He [153] then showed that an essential part of the Fourier transform was overlooked and that the correct relation in QED (in the sim-

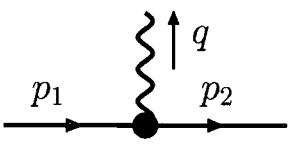

Figure 6.1: Fermion-vector boson vertex and its momenta

pler massless fermion) case is:

$$iq^\mu \Gamma_V^\nu - iq^\nu \Gamma_V^\mu = S_F^{-1}(p_1)\sigma^{\mu\nu} + \sigma^{\mu\nu} S_F^{-1}(p_2) - \frac{1}{2}(p_1+p_2)_\lambda \left\{\sigma^{\mu\nu}, \Gamma_V^\lambda\right\} + \int \frac{d^dk}{(2\pi)^d}\, k_\lambda \left\{\sigma^{\mu\nu}, \tilde{\Gamma}_V^\lambda\right\} , \tag{6.6}$$

where $\sigma^{\mu\nu} = i\left[\gamma^\mu, \gamma^\nu\right]/2$, $\Gamma_V^\mu = \Gamma_V^\mu(p_1, p_2)$ and $\tilde{\Gamma}_V^\lambda = \tilde{\Gamma}_V^\lambda(p_1, p_2; k)$. In contrast to what is written in the paper by He [153], it is the anti-commutator $\left\{\sigma^{\mu\nu}, \gamma^\lambda\right\}$ that is used in the derivation of Kondo [151]; the identification of $\left\{\sigma^{\mu\nu}, \gamma^\lambda\right\}$ with $-2\varepsilon^{\lambda\mu\nu\rho}\gamma_\rho\gamma_5$ is only valid in exactly 4 space-time dimensions and should not be used when the requisite integrals contain divergences. It is this requirement that motivates the analysis presented here.

The last two terms of Eq. (6.6) are given by the momentum transform of:

$$\lim_{x'\to x} -\frac{i}{2}\left(\partial_\lambda^x - \partial_\lambda^{x'}\right) \langle 0|\, T\bar{\psi}(x') \left\{\sigma^{\mu\nu}, \gamma^\lambda\right\} U_P(x', x)\psi(x)\psi(x_1)\bar{\psi}(x_2)\,|0\rangle \tag{6.7}$$

with

$$U_P(x', x) = \mathcal{P}\exp\left(-ig\int_x^{x'} dy^\rho A_\rho(y)\right) , \tag{6.8}$$

where ψ and A are the fermion and gauge fields respectively. $\mathcal{P}$ means the integral is path ordered, in fact a Wilson line integral. This implicitly defines the non-local vector vertex in our anti-commutator $\left\{\sigma^{\mu\nu}, \tilde{\Gamma}_V^\lambda\right\}$ of Eq. (6.6), related to the axial one $\tilde{\Gamma}_{A\rho}(p_1, p_2; k)$ in He [153]. Being non-local these involve integrals in momentum space some of which cannot be represented diagrammatically in terms of Feynman graphs. An example is the last term of Eq. (6.6), which for later we denote by $\boldsymbol{W}^{\mu\nu}$. With a textbook factor of Z_1 renormalising the vector vertices and Z_2^{-1} renormalising the fermion propagator, multiplicative renormalisability of the transverse Ward-Takahashi relation, Eq. (6.6), is ensured by the same condition $Z_1 = Z_2$ as required by the renormalisation of the longitudinal Ward-Green-Takahashi identity, Eq. (6.1).

Although the Ward-Green-Takahashi identity fixes the longitudinal part of the vertex, Γ_L^μ, it places no constraint upon the transverse part other than requiring it to be free of kinematic singularities. However, the *transverse* Ward-Takahashi relation now involves both Γ_L^μ and Γ_T^μ as well. We can illustrate the power of the transverse relation by considering the $q \to 0$ limit of this equation. We can then deduce to all orders in perturbation theory, and genuinely non-perturbatively, the

constraint $\boldsymbol{W}^{\mu\nu}(p+q,p)$ places on the transverse vertex. From Eq. (6.6) we have:

$$\begin{aligned}\boldsymbol{W}^{\mu\nu}(p_1,p_2) &\equiv \int \frac{d^dk}{(2\pi)^d}\, k_\lambda \left\{\sigma^{\mu\nu}, \tilde{\Gamma}_V^\lambda(p_1,p_2;k)\right\} \\ &= -\Big\{ S_F^{-1}(p_1)\sigma^{\mu\nu} + \sigma^{\mu\nu} S_F^{-1}(p_2) - \frac{1}{2}(p_1+p_2)_\lambda \left\{\sigma^{\mu\nu}, \Gamma_V^\lambda(p_1,p_2)\right\} \\ &\qquad - iq^\mu \Gamma_V^\nu(p_1,p_2) + iq^\nu \Gamma_V^\mu(p_1,p_2) \Big\} . \qquad (6.9)\end{aligned}$$

When $q \to 0$ then $\boldsymbol{W}^{\mu\nu}(p_1 = p_2 = p) = 0$. The general transverse vertex in the massless fermion case involves 4 vectors orthogonal to q^μ, the basis vectors T_i^μ, which are listed in Eq. (2.19) and Ref. [34], so that:

$$\Gamma_T^\mu(p+q,p) = \sum_{i=2,3,6,8} \tau_i((p+q)^2, p^2, q^2)\, T_i^\mu(p,q) \quad , \qquad (6.10)$$

where the coefficients τ_i are themselves free of kinematic singularities and are functions of the three relevant invariants, p_1^2, p_2^2 and q^2. T_2^μ and T_3^μ are quadratic in q, while T_6^μ and T_8^μ are both linear. In particular

$$T_8^\mu = i\gamma^\mu p_1^\nu p_2^\lambda \sigma_{\nu\lambda} + p_1^\mu \not{p}_2 - p_2^\mu \not{p}_1 \, . \qquad (6.11)$$

The coefficients τ_i are all symmetric under $p_1 = p+q \leftrightarrow p_2 = p$, except for τ_6, which is antisymmetric and so vanishes when $q \to 0$. We then have non-perturbatively to first order in the boson momentum q:

$$\begin{aligned}\boldsymbol{W}^{\mu\nu}(p_1 = p+q, p_2 = p) &= -i\left[(p^\mu q^\nu - p^\nu q^\mu)\not{p} + q\cdot p\,(p^\mu\gamma^\nu - p^\nu\gamma^\mu)\right] \mathcal{A}'(p^2) \\ &+ 2i\left[(p^\mu q^\nu - p^\nu q^\mu)\not{p} - q\cdot p\,(p^\mu\gamma^\nu - p^\nu\gamma^\mu)\right. \\ &\left. + p^2\,(q^\mu\gamma^\nu - q^\nu\gamma^\mu)\right] \tau_8(p,p) \, , \qquad (6.12)\end{aligned}$$

where we expect $\mathcal{A}'(p^2)$ to result from terms like $(\mathcal{A}(p_1^2) - \mathcal{A}(p_2^2))\,/\,(p_1^2 - p_2^2)$ as in Eq. (6.5). Such constraints restrict the form of the transverse coefficient τ_8, for example, and have the potential to play a critical role in constructing consistent non-perturbative Feynman rules. Consequently, it is critical to check how to evaluate the transverse Ward-Takahashi relation, which is what we do here.

It is trivial to check that the transverse Ward-Takahashi relation holds at tree

level. This follows directly from the identity:

$$iq^\mu\gamma^\nu - iq^\nu\gamma^\mu = \not{p}_1\sigma^{\mu\nu} + \sigma^{\mu\nu}\not{p}_2 - \frac{1}{2}(p_1+p_2)_\lambda \left\{\sigma^{\mu\nu},\gamma^\lambda\right\} \ . \tag{6.13}$$

when the non-local term does not appear. Note that at tree level we are in 4-dimensions so we would be permitted to use the identity $\left\{\sigma^{\mu\nu},\gamma^\lambda\right\} = -2\varepsilon^{\lambda\mu\nu\rho}\gamma_\rho\gamma_5$. He and Yu [154] have sketched a proof of the relation at one loop order. The purpose of this paper is to check this in detail in d-dimensions, where $d = 4+\epsilon$. For notational brevity we introduce the following form of the Chisholm identity:

$$-i\left\{\sigma^{\mu\nu},\gamma^\lambda\right\} \ = \ r^{\lambda\mu\nu} \ = \ \left(\gamma^\lambda\gamma^\mu\gamma^\nu - \gamma^\nu\gamma^\mu\gamma^\lambda\right) \ . \tag{6.14}$$

There has been discussion in the literature [151, 155] about the role of the Adler-Bell-Jackiw anomaly [156–158] in these relations. It has been shown [159, 160] that this plays no role in the axial-vector equivalent of Eq. (6.6). We will consider the transverse Ward-Takahashi relation in the massless fermion case for simplicity. We show that this only holds if appropriate care is taken of the integrals divergent in 4-dimensions. This allows us to complete the proof to one loop order outlined by He and Yu [154].

6.1 Perturbative Derivation of the Transverse Ward-Takahashi Relation

Following the formal derivation of the transverse Ward-Takahashi relation contained in Ref. [152], He and Yu [154] give a proof of how the relation should hold at one loop order by considering the relevant integrands, but without evaluating any of the integrals. Here we will investigate the relation in greater detail. First in this section we will reconsider the proof by deducing the integrands in d-dimensions, where $d = 4+\epsilon$. To manipulate the divergent integrals in d-dimensions we must clearly use the original object $\left\{\sigma^{\mu\nu},\gamma^\lambda\right\}$, since once again its identification with $-2\varepsilon^{\lambda\mu\nu\rho}\gamma_\rho\gamma_5$ is valid only in 4-dimensions. We will then confirm this result in the next section by explicit evaluation of each of the contributing integrals.

To derive the transverse Ward-Takahashi relation at one-loop order, we begin with the tree-level relation of Eq. (6.13):

$$iq^\mu\gamma^\nu - iq^\nu\gamma^\mu \ = \ \not{p}_1\sigma^{\mu\nu} + \sigma^{\mu\nu}\not{p}_2 - \frac{1}{2}\left[\left(\not{p}_1+\not{p}_2\right)\sigma^{\mu\nu} + \sigma^{\mu\nu}\left(\not{p}_1+\not{p}_2\right)\right] \ . \tag{6.15}$$

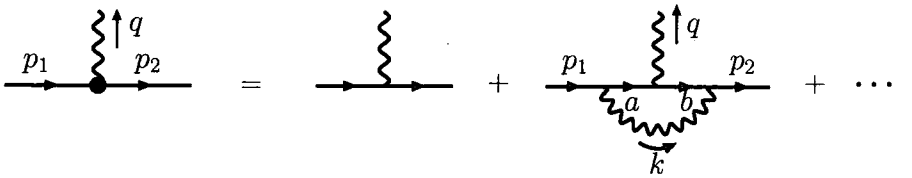

Figure 6.2: One loop corrections to the vector vertex of Fig. 6.2 with the momenta labelled as in our calculation

It is obvious that this relation is trivially satisfied at tree-level, hence we need only concentrate on the one-loop corrections to the relation. To simplify the answer we introduce the following shorthand for the integration:

$$\int \overline{dk} \equiv g^2 \int \frac{d^d k}{(2\pi)^d} \frac{-i}{k^2\, a^2\, b^2} \quad , \tag{6.16}$$

where $a = p_1 - k$ and $b = p_2 - k$ as shown in Fig. 6.2.
We use the standard Feynman rules for QED with, for example,

$$\Delta_{\alpha\beta}(k) = \frac{-i}{k^2}\left(g_{\alpha\beta} + (\xi - 1)\frac{k_\alpha k_\beta}{k^2}\right) \tag{6.17}$$

for the bare gauge boson propagator, where ξ is the usual covariant gauge parameter. If we write the full vertex to one-loop order as

$$\Gamma^\mu_V(p_1, p_2) = \gamma^\mu + \Lambda^\mu_{(2)}(p_1, p_2) \quad , \tag{6.18}$$

we can read off from Fig. 6.2 that

$$\Lambda^\mu_{(2)}(p_1, p_2) = \int \overline{dk}\, \gamma^\alpha \not{a} \gamma^\mu \not{b} \gamma_\alpha \tag{6.19}$$

in the Feynman gauge, when $\xi = 1$. We see that the left-hand side of Eq. (6.6) can be obtained by sandwiching Eq. (6.15) between $\gamma^\alpha \not{a}$ and $\not{b}\gamma_\alpha$, then integrating over the measure $\int \overline{dk}$, so that:

$$\begin{aligned} iq^\mu \Lambda^\nu_{(2)}(p_1, p_2) - iq^\nu \Lambda^\mu_{(2)}(p_1, p_2) &= \int \overline{dk} \gamma^\alpha \not{a} \left(\not{p}_1 \sigma^{\mu\nu} + \sigma^{\mu\nu} \not{p}_2\right) \not{b} \gamma_\alpha \\ &- \frac{1}{2} \int \overline{dk} \gamma^\alpha \not{a} \left[\left(\not{p}_1 + \not{p}_2\right) \sigma^{\mu\nu} + \sigma^{\mu\nu} \left(\not{p}_1 + \not{p}_2\right)\right] \not{b} \gamma_\alpha \,. \end{aligned} \tag{6.20}$$

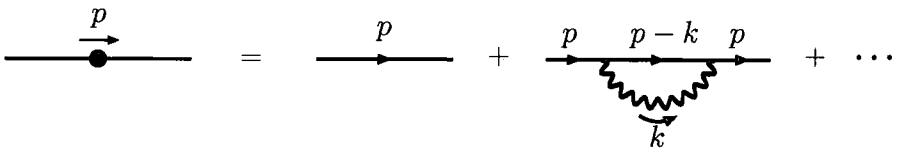

Figure 6.3: One loop correction to the fermion propagator

The second term on the right-hand side is the $-\frac{1}{2}(p_1+p_2)_\lambda \left\{\sigma^{\mu\nu}, \Lambda^\lambda_{V(2)}\right\}$ piece of the original relation and is one of the terms we wish to identify.

At the one-loop level we can write the fermion self energy parts of Fig. 6.3 as

$$\begin{aligned} S_F^{-1}(p_1) &= \not{p}_1 - \Sigma_{(2)}(p_1)\,, \qquad \text{where } \Sigma_{(2)}(p_1) = \int \overline{dk}\,\gamma^\alpha \left(\not{a} b^2\right)\gamma_\alpha \\ S_F^{-1}(p_2) &= \not{p}_2 - \Sigma_{(2)}(p_2)\,, \qquad \text{where } \Sigma_{(2)}(p_2) = \int \overline{dk}\,\gamma^\alpha \left(a^2 \not{b}\right)\gamma_\alpha\,. \end{aligned} \tag{6.21}$$

In order to extract such terms from Eq. (6.20), the unidentified term on the right hand side of this equation is re-expressed using the replacement:

$$\begin{aligned} \int \overline{dk}\,\gamma^\alpha \not{a}\left(\not{p}_1\sigma^{\mu\nu} + \sigma^{\mu\nu}\not{p}_2\right)\not{b}\gamma_\alpha &= \int \overline{dk}\,\gamma^\alpha \left(-\sigma^{\mu\nu}a^2\not{b} - \not{a}b^2\sigma^{\mu\nu}\right)\gamma_\alpha \\ &\quad + \int \overline{dk}\gamma^\alpha \not{a}\left(\not{k}\sigma^{\mu\nu} + \sigma^{\mu\nu}\not{k}\right)\not{b}\gamma_\alpha \\ &\quad + \int \overline{dk}\gamma^\alpha \not{a}\left(2\not{a}\sigma^{\mu\nu} + 2\sigma^{\mu\nu}\not{b}\right)\not{b}\gamma_\alpha\,. \end{aligned} \tag{6.22}$$

To the first line on the right-hand side of Eq. (6.22) we commute the σ-matrices to the outside of the γ^α by using $\sigma^{\mu\nu}\gamma^\alpha \to \gamma^\alpha\sigma^{\mu\nu} - 2ig^{\alpha\mu}\gamma^\nu + 2ig^{\alpha\nu}\gamma^\mu$. This gives:

$$\begin{aligned} iq^\mu\Lambda^\nu_{(2)}(p_1,p_2) - iq^\nu\Lambda^\mu_{(2)}(p_1,p_2) &= -\Sigma_{(2)}(p_1)\,\sigma^{\mu\nu} - \sigma^{\mu\nu}\,\Sigma_{(2)}(p_2) \\ &\quad - \frac{1}{2}(p_1+p_2)_\lambda\left\{\sigma^{\mu\nu}, \Lambda^\lambda_{V(2)}\right\} \\ &\quad + \int \overline{dk}\gamma^\alpha \not{a}\left(\not{k}\sigma^{\mu\nu} + \sigma^{\mu\nu}\not{k}\right)\not{b}\gamma_\alpha \\ &\quad + 2\int \overline{dk}\left\{\gamma^\alpha \not{a}\left(\not{a}\sigma^{\mu\nu} + \sigma^{\mu\nu}\not{b}\right)\not{b}\gamma_\alpha\right. \\ &\quad \left. - \left(\left(a^2\not{b} + \not{a}b^2\right)\sigma^{\mu\nu} + \sigma^{\mu\nu}\left(a^2\not{b} + \not{a}b^2\right)\right)\right\}\,. \end{aligned} \tag{6.23}$$

To be able to express this in terms of the Wilson line integral in the transverse

Ward-Takahashi relation, we need to introduce a factor of γ^α and γ_α either side of the last term in Eq. (6.23). On rearranging this becomes:

$$\begin{aligned} iq^\mu \Lambda^\nu_{(2)}(p_1,p_2) - iq^\nu \Lambda^\mu_{(2)}(p_1,p_2) &= -\Sigma_{(2)}(p_1)\,\sigma^{\mu\nu} - \sigma^{\mu\nu}\,\Sigma_{(2)}(p_2) \\ &\quad - \frac{1}{2}(p_1+p_2)_\lambda \left\{\sigma^{\mu\nu}, \Lambda^\lambda_{V(2)}\right\} \\ &\quad + \int \overline{dk}\,\gamma^\alpha \not{a}\,(\not{k}\sigma^{\mu\nu} + \sigma^{\mu\nu}\not{k})\,\not{b}\gamma_\alpha \\ &\quad - \int \overline{dk}\,(\gamma^\alpha\sigma^{\mu\nu} + \sigma^{\mu\nu}\gamma^\alpha)\left(a^2\not{b} - \not{a}b^2\right)\gamma_\alpha \\ &\quad -2(d-4)\int \overline{dk}\,(\not{a}\sigma^{\mu\nu} + \sigma^{\mu\nu}\not{a})\,b^2\,. \end{aligned} \tag{6.24}$$

Putting back in the tree-level result, together with the identification of the last 3 lines with the Wilson-line integration over non-local contributions allows us to write the transverse Ward-Takahashi relation, derived for the massless case of QED in d-dimensions in the Feynman gauge, as:

$$\begin{aligned} iq^\mu \Gamma^\nu_V(p_1,p_2) - iq^\nu \Gamma^\mu_V(p_1,p_2) &= S_F^{-1}(p_1)\,\sigma^{\mu\nu} + \sigma^{\mu\nu}\,S_F^{-1}(p_2) \\ &\quad - \frac{1}{2}(p_1+p_2)_\lambda \left\{\sigma^{\mu\nu}, \Gamma^\lambda_V\right\} \\ &\quad + \int \frac{d^dk}{(2\pi)^d}\,k_\lambda \left\{\sigma^{\mu\nu}, \tilde{\Gamma}^\lambda_V\right\}\,, \end{aligned} \tag{6.25}$$

which is indeed what is found by He, though written with explicitly d-dimensional objects. It is straightforward to check that this relation would hold in any covariant gauge.

6.2 The One Loop Integrals

Since the integrals are not finite and so the manipulations more subtle, we now proceed to explicit computation of the terms in the transverse Ward-Takahashi relation to one loop order. The following sections deal with the terms in Eq. (6.25) in turn:

- **Sect. 6.2.1** $i\,q^\mu\,\Gamma_V^\nu - i\,q^\nu\,\Gamma_V^\mu$
- **Sect. 6.2.2** $S_F^{-1}(p_1)\,\sigma^{\mu\nu} + \sigma^{\mu\nu}\,S_F^{-1}(p_2)$
- **Sect. 6.2.3** $\frac{1}{2}(p_1+p_2)_\lambda\,\left\{\sigma^{\mu\nu},\Gamma_V^\lambda\right\}$
- **Sect. 6.2.4** $\int d^4k\,k_\lambda\,\left\{\sigma^{\mu\nu},\tilde{\Gamma}_V^\lambda\right\}$

The $\mathcal{O}(\alpha)$ correction to each of these we denote by $(i\alpha\,\mathbf{P_i}^{\mu\nu}/4\pi)$ with $i = 1,..,4$. Then Eq. (6.25) if true would become simply:

$$\mathbf{P_1}^{\mu\nu} \;=\; [\mathbf{P_2} + \mathbf{P_3} + \mathbf{P_4}]^{\mu\nu} \quad . \tag{6.26}$$

This is what we set out to prove. The calculation is performed in full for an arbitrary covariant gauge, specified as usual by ξ, and in dimension d. We will be particularly concerned with the results with $d = 4+\varepsilon$ when $\varepsilon \to 0$.

6.2.1 Part 1

The first part of the calculation is the $(i\,q^\mu\Gamma_V^\nu - i\,q^\nu\Gamma_V^\mu)$ piece. This involves the full vertex $\Gamma_V^\mu(p_1,p_2)$, as calculated for arbitrary covariant gauge by Kızılersü *et al* [34]. Once we know all of the relevant standard integrals, which are collected in Appendix C, the calculation is straightforward. We begin by writing the vertex to one-loop order as in Eq. (6.18)

$$\Gamma_V^\mu(p_1,p_2) = \gamma^\mu + \Lambda_{(2)}^\mu(p_1,p_2)\;. \tag{6.27}$$

Defining the momentum flow from Fig. 6.2, we then have, using the standard Feynman rules, the vertex correction given by:

$$\Lambda^\mu(p_1,p_2) = -\frac{i\alpha}{4\pi^3}\int d^4\omega \frac{\gamma^\alpha\,(\not{p}_1-\not{\omega})\,\gamma^\mu\,(\not{p}_2-\not{\omega})\,\gamma^\beta}{\omega^2\,(p_1-\omega)^2\,(p_2-\omega)^2}\left(g_{\alpha\beta}+(\xi-1)\,\frac{\omega_\alpha\omega_\beta}{\omega^2}\right)\;, \tag{6.28}$$

where we have suppressed the $+i\epsilon$ prescribed to define the propagators. If we decompose this into its constituent tensor integrals,

$$\Lambda^\mu = -\frac{i\alpha}{4\pi^3}\left\{\gamma^\alpha\left(\not{p}_1\gamma^\mu\not{p}_2\right)\gamma_\alpha\,\boldsymbol{J^{(0)}} - \gamma^\alpha\left(\not{p}_1\gamma^\mu\gamma^\nu + \gamma^\nu\gamma^\mu\not{p}_2\right)\gamma_\alpha\,\boldsymbol{J^{(1)}_\nu}\right.$$
$$+\left(\gamma^\alpha\gamma^\nu\gamma^\mu\gamma^\lambda\gamma_\alpha\right)\boldsymbol{J^{(2)}_{\nu\lambda}} + (\xi-1)\left[\left(-\gamma^\nu\not{p}_1\gamma^\mu - \gamma^\mu\not{p}_2\gamma^\nu\right)\boldsymbol{J^{(1)}_\nu}\right.$$
$$\left.\left.+\gamma^\mu\boldsymbol{K^{(0)}} + \left(\gamma^\nu\not{p}_1\gamma^\mu\not{p}_2\gamma^\lambda\right)\boldsymbol{I^{(2)}_{\nu\lambda}}\right]\right\}, \qquad (6.29)$$

with each function in bold depending upon p_1, p_2. Reducing the tensor integrals to scalar integrals, and collecting terms together with common Dirac structures gives:

$$\begin{aligned}
\Gamma^\mu_V(p_1,p_2) \;=\; & \boldsymbol{\gamma^\mu} + \frac{\alpha}{4\pi}\left\{\boldsymbol{\not{p}_2 p_2^\mu}\left[2J_A - 2J_C + (\xi-1)\,I_D\,p_1^2\right]\right. \\
& + \boldsymbol{\not{p}_1 p_1^\mu}\left[2J_B - 2J_E + (\xi-1)\,I_D\,p_2^2\right] + \boldsymbol{\not{p}_1 p_2^\mu}\Big[-2J_0 + 2J_A + 2J_B - 2J_D \\
& \quad + (\xi-1)\left(-\frac{1}{2}J_0 - \frac{1}{2}I_C\,p_2^2 - I_D\,p_1\cdot p_2 + \frac{1}{2}I_E\,p_1^2 + J_A\right)\Big] \\
& + \boldsymbol{\not{p}_2 p_1^\mu}\left[-2J_D + (\xi-1)\left(I_C\,p_2^2 - J_A\right)\right] + \boldsymbol{\gamma^\mu\not{p}_2\not{p}_1}\left[J_0 - J_A - J_B\right. \\
& \quad \left.\left. + (\xi-1)\left(\frac{1}{4}J_0 + \frac{1}{4}I_C\,p_2^2 + \frac{1}{2}I_D\,p_1\cdot p_2 + \frac{1}{4}I_E\,p_1^2 - \frac{1}{2}J_A - \frac{1}{2}J_B\right)\right] \right. \\
& + \boldsymbol{\gamma^\mu}\left[-J_A\,p_2^2 - J_B\,p_1^2 + \frac{1}{2}J_C\,p_2^2 + J_D\,p_1\cdot p_2 + \frac{1}{2}J_E\,p_1^2 + \frac{1}{2}\left(1+\frac{3\varepsilon}{4}\right)K_0\right. \\
& \quad \left.\left.\left. + (\xi-1)\left(-\frac{1}{2}J_A\,p_2^2 - \frac{1}{2}J_B\,p_1^2 + \frac{1}{2}K_0\right)\right]\right\}, \qquad (6.30)
\end{aligned}$$

where each of the functions $I_A, \cdots, J_E, K_0$ depend on p_1, p_2 and are given in Appendix Eqs. (C.16, C.17) as well as Eqs. (6.32, 6.33, 6.34) below. Collecting the terms together with common Lorentz and Dirac structure at one loop we obtain:

$$\begin{aligned}
\boldsymbol{P_1}^{\mu\nu} \;=\; & \not{p}_1\left(p_2^\mu p_1^\nu - p_1^\mu p_2^\nu\right)\left[\left(-I_E\,p_1^2 - I_D\,p_2^2 + J_B\right)(\xi-1) - 2(J_B - J_D - J_E)\right] \\
& + \not{p}_2\left(p_2^\mu p_1^\nu - p_1^\mu p_2^\nu\right)\left[2(J_0 - 2J_A - J_B + J_C + J_D)\right. \\
& \quad \left. + \frac{1}{2}(\xi-1)\left(-2I_D\,p_1^2 + I_E\,p_1^2 - I_C\,p_2^2 + J_0 - 2J_B + 2I_D\,p_1\cdot p_2\right)\right] \\
& + \not{p}_1\not{p}_2\left(\gamma^\nu p_2^\mu + \gamma^\mu p_1^\nu - \gamma^\mu p_2^\nu - \gamma^\nu p_1^\mu\right)\left[J_0 - J_A - J_B\right. \\
& \quad \left. + \frac{1}{4}(\xi-1)\left(I_E\,p_1^2 + I_C\,p_2^2 + J_0 - 2J_A - 2J_B + 2I_D\,p_1\cdot p_2\right)\right]
\end{aligned}$$

$$
\begin{aligned}
+ \quad & (\gamma^\nu p_2^\mu + \gamma^\mu p_1^\nu - \gamma^\nu p_1^\mu - \gamma^\mu p_2^\nu) \left[\frac{1}{2} \left(2J_B\, p_1^2 - J_E\, p_1^2 + 2J_A\, p_2^2 - J_C\, p_2^2 \right.\right. \\
& \qquad \left. - K_0 - 2(2J_0 - 2J_A - 2J_B + J_D)\, p_1 \cdot p_2 + 3 \right) \\
& - \frac{1}{2}(\xi - 1) \left(-J_B\, p_1^2 - J_A\, p_2^2 + 2I_D\, (p_1 \cdot p_2)^2 \right. \\
& \qquad \left.\left. + K_0 + \left(I_E\, p_1^2 + I_C\, p_2^2 + J_0 - 2J_A - 2J_B \right) p_1 \cdot p_2 \right) \right] \ .
\end{aligned}
\tag{6.31}
$$

Except where explicitly stated otherwise, $K_0, \cdots, J_E$ are functions of p_1, p_2 as given in the Appendix, Eqs. (C.16, C.17) as well as Eqs. (6.32, 6.33, 6.34) below. This answer, Eq. (6.31), can then be substituted into the first part of the transverse Ward-Takahashi relation, Eqs. (6.6, 6.25), *i.e.* in Eq. (6.26).

6.2.2 Part 2

It is useful here to note that the many integrals appearing in evaluation of the loop graphs are expressible in terms of a set of basis functions J_0, L, L', $\mathcal{C}$ and S given by:

$$
\begin{aligned}
J_0 \ = \ & \frac{2}{\Delta} \left[Sp\left(\frac{p_1^2 - p_1 \cdot p_2 + \Delta}{p_1^2} \right) - Sp\left(\frac{p_1^2 - p_1 \cdot p_2 - \Delta}{p_1^2} \right) \right. \\
& \left. + \frac{1}{2} \ln\left(\frac{p_1 \cdot p_2 - \Delta}{p_1 \cdot p_2 + \Delta} \right) \ln\left(\frac{(p_2 - p_1)^2}{p_1^2} \right) \right]
\end{aligned}
\tag{6.32}
$$

$$
\text{with} \quad \Delta = \sqrt{(p_1 \cdot p_2)^2 - p_1^2 p_2^2} \quad , \qquad \text{and}
$$

$$
\begin{aligned}
L \ = \ & \ln\left(-\frac{p_1^2}{\mu^2} \right) \quad ; \qquad L' = \ln\left(-\frac{p_2^2}{\mu^2} \right) \quad ; \qquad S = \frac{1}{2} \ln\left(-\frac{(p_1 - p_2)^2}{\mu^2} \right) \\
& \mathcal{C} = -\frac{2}{\varepsilon} - \gamma - \ln(\pi) \quad .
\end{aligned}
\tag{6.33}
$$

In terms of these the K-scalar integrals which are about to appear are given simply by:

$$
\begin{aligned}
K_0(p_1, p_2) \ &= \ 2\,(\mathcal{C} + 2 - 2S) \quad , \\
K_0(0, p_2) \ &= \ 2\,(\mathcal{C} + 2 - L') \quad , \\
K_0(p_1, 0) \ &= \ 2\,(\mathcal{C} + 2 - L) \quad .
\end{aligned}
\tag{6.34}
$$

With these definitions the $\left(S_F^{-1}(p_1)\sigma^{\mu\nu} + \sigma^{\mu\nu}S_F^{-1}(p_2)\right)$ piece of Eq. (6.25) requires the evaluation of the inverse fermion propagator to one-loop. We note that the inverse propagator can be written as $S_F^{-1}(p_1) = \not{p}_1 - \Sigma_{(2)}(p_1)$, where

$$\begin{aligned}
\Sigma_{(2)}(p_1) &= -\frac{i\alpha}{4\pi^3}\int d^dk \frac{\gamma^\alpha\left(\not{p}_1 - \not{k}\right)\gamma^\beta}{k^2\left(p_1-k\right)^2}\left(g_{\alpha\beta} + (\xi-1)\frac{k_\alpha k_\beta}{k^2}\right) \\
&= -\frac{i\alpha}{4\pi^3}(-2-\varepsilon)\left[\not{p}_1 \boldsymbol{K^{(0)}}(p_1,0) - \gamma^\lambda \boldsymbol{K^{(1)}_\lambda}(p_1,0)\right] \\
&\quad -\frac{i\alpha}{4\pi^3}(\xi-1)\left[\gamma^\lambda \not{p}_1 \gamma^\nu \boldsymbol{J^{(2)}_{\lambda\nu}}(p_1,0) + \gamma^\lambda \boldsymbol{K^{(1)}_\lambda}(p_1,0)\right] . \qquad (6.35)
\end{aligned}$$

Once the tensor integrals have been substituted, the inverse propagator is

$$S_F^{-1}(p_1) = \not{p}_1\left(1 + \frac{\alpha\xi}{4\pi}(C+1-L)\right) , \qquad (6.36)$$

with a similar expression for $S_F^{-1}(p_2)$ with the replacement $p_1 \longrightarrow p_2$ in Eq. (6.36). From these we deduce that

$$\begin{aligned}
\boldsymbol{P_2}^{\mu\nu} &= \not{p}_1\left(\gamma^\mu\gamma^\nu - \gamma^\nu\gamma^\mu\right)\frac{\xi}{4}\left(K_0(p_1,0) - 2\right) \\
&+ \left(\not{p}_2\left(\gamma^\mu\gamma^\nu - \gamma^\nu\gamma^\mu\right) + 4\gamma^\mu p_2^\nu - 4\gamma^\nu p_2^\mu\right)\frac{\xi}{4}\left(K_0(0,p_2) - 2\right) . \qquad (6.37)
\end{aligned}$$

Substituting for these in the transverse Ward-Takahashi relation, Eqs. (6.6, 6.25), will give us the second piece.

6.2.3 Part 3

The third part we wish to compute involves the anti-commutator of $\sigma^{\mu\nu}$ with the vector vertex with momentum routing as defined in Fig. 6.2. In the work of He [153] the anti-commutator is replaced by its 4-dimensional identity, hence the appearance of the axial vector therein. We choose not to follow this path for obvious reasons — the integrals must be evaluated in $d = 4 + \varepsilon$ dimensions.
Thus we begin with:

$$-\frac{1}{2}(p_1+p_2)_\lambda \left\{\sigma^{\mu\nu},\Gamma_V^\lambda\right\} = \frac{1}{2}\frac{i\alpha}{4\pi^3}\int d^4k \frac{\gamma^\alpha(\not{p}_1-\not{k})\left\{\sigma^{\mu\nu},\gamma^\lambda\right\}(\not{p}_2-\not{k})\gamma^\beta}{k^2(p_1-k)^2(p_2-k)^2} \times\left(g_{\alpha\beta}+(\xi-1)\frac{k_\alpha k_\beta}{k^2}\right). \tag{6.38}$$

After extensive use of Dirac algebra identities and noting the definition of $r^{\lambda\mu\nu}$ in Eq. (6.14), we deduce

$$\begin{aligned}
&-\frac{1}{2}(p_1+p_2)_\lambda\left\{\sigma^{\mu\nu},\Gamma_V^\lambda\right\}\\
=\;& -\frac{i}{2}(p_1+p_2)_\lambda\, r^{\lambda\mu\nu}+\frac{\alpha}{4\pi^3}(p_1+p_2)_\lambda\Bigg\{\\
&\left(\gamma^\beta r^{\lambda\mu\nu}\gamma^\delta\right)\left(p_{1\delta}p_{2\beta}\boldsymbol{J}^{(0)}(p_1,p_2)-p_{1\delta}\boldsymbol{J}^{(1)}_\beta(p_1,p_2)-p_{2\beta}\boldsymbol{J}^{(1)}_\delta(p_1,p_2)\right)\\
&-\frac{1}{2}\gamma^\alpha\gamma^\beta r^{\lambda\mu\nu}\gamma^\delta\gamma_\alpha\boldsymbol{J}^{(2)}_{\beta\delta}(p_1,p_2)\\
&+(\xi-1)\Bigg[\frac{1}{2}\gamma^\beta\not{p}_1 r^{\lambda\mu\nu}\left(\boldsymbol{J}^{(1)}_\beta(p_1,p_2)-\not{p}_2\gamma^\delta\boldsymbol{I}^{(2)}_{\beta\delta}(p_1,p_2)\right)\\
&+\frac{1}{2}r^{\lambda\mu\nu}\left(\not{p}_2\gamma^\beta\boldsymbol{J}^{(1)}_\beta(p_1,p_2)-\boldsymbol{K}^{(0)}(p_1,p_2)\right)\Bigg]\Bigg\}.
\end{aligned} \tag{6.39}$$

Substituting the forms of the integrals from the Appendix, we again collect the terms according to their Lorentz and Dirac structures:

$$
\begin{aligned}
\boldsymbol{P_3}^{\mu\nu} \;=\; & \not{p}_1 \left[\left(I_E\, p_1^2 - I_D\, p_2^2 - J_B\right) (\xi - 1) \left(p_2^\mu p_1^\nu - p_1^\mu p_2^\nu\right) \right. \\
& \qquad \left. -2(J_B + J_D - J_E) \left(p_2^\mu p_1^\nu - p_1^\mu p_2^\nu\right) \right] \\
& + \not{p}_1 \not{p}_2 \left(\gamma^\nu p_2^\mu - \gamma^\mu p_2^\nu\right) \left[J_0 + J_A - J_B - 2J_C + 2J_D \right. \\
& \qquad \left. + \frac{1}{4}(\xi - 1) \left(4I_D\, p_1^2 + I_E\, p_1^2 - 3I_C\, p_2^2 + J_0 + 2J_A - 2J_B + 2I_D\, p_1 \cdot p_2\right) \right] \\
& + \not{p}_2 \left(p_2^\mu p_1^\nu - p_1^\mu p_2^\nu\right) \left[2(J_0 - J_B - J_C + J_D) \right. \\
& \qquad \left. + \frac{1}{2}(\xi - 1) \left(2I_D\, p_1^2 + I_E\, p_1^2 - I_C\, p_2^2 + J_0 - 2J_B + 2I_D\, p_1 \cdot p_2\right) \right] \\
& + \not{p}_1 \not{p}_2 \left(\gamma^\mu p_1^\nu - \gamma^\nu p_1^\mu\right) \left[J_0 - J_A + J_B + 2J_D - 2J_E \right. \\
& \qquad \left. + \frac{1}{4}(\xi - 1) \left(-3I_E\, p_1^2 + I_C\, p_2^2 + 4I_D\, p_2^2 + J_0 - 2J_A + 2J_B + 2I_D\, p_1 \cdot p_2\right) \right] \\
& + \frac{1}{2} \not{p}_2 \left(\gamma^\mu \gamma^\nu - \gamma^\nu \gamma^\mu\right) \left[\frac{1}{2} \left(-2J_0\, p_1^2 + 2J_A\, p_1^2 - 4J_D\, p_1^2 + 3J_E\, p_1^2 + 2J_A\, p_2^2 - J_C\, p_2^2 \right. \right. \\
& \qquad \left. -K_0 + 2(2J_A - 2J_C + J_D) p_1 \cdot p_2 - 5) + \frac{1}{4}(1 - \xi) \left(-3I_E\, p_1^4 + I_C\, p_2^2 p_1^2 + 4I_D\, p_2^2 p_1^2 \right. \right. \\
& \qquad\qquad \left. \left. + J_0\, p_1^2 - 2J_A\, p_1^2 - 2J_A\, p_2^2 + 2K_0 - 2\left(I_D\, p_1^2 - 2I_C\, p_2^2 + 2J_A\right) p_1 \cdot p_2) \right] \\
& + \frac{1}{2} \not{p}_1 \left(\gamma^\mu \gamma^\nu - \gamma^\nu \gamma^\mu\right) \left[\frac{1}{2} \left(2J_B\, p_1^2 - J_E\, p_1^2 - 2J_0\, p_2^2 + 2J_B\, p_2^2 + 3J_C\, p_2^2 - 4J_D\, p_2^2 - K_0 \right. \right. \\
& \qquad \left. +2(2J_B + J_D - 2J_E) p_1 \cdot p_2 - 5) + \frac{1}{4}(1 - \xi) \left(-3I_C\, p_2^4 + 4I_D\, p_1^2 p_2^2 + I_E\, p_1^2 p_2^2 \right. \right. \\
& \qquad \left. \left. +J_0\, p_2^2 - 2J_B\, p_2^2 - 2J_B\, p_1^2 + 2K_0 - 2\left(-2I_E\, p_1^2 + I_D\, p_2^2 + 2J_B\right) p_1 \cdot p_2) \right) \\
& + \left(\gamma^\mu p_2^\nu - \gamma^\nu p_2^\mu\right) \left[\frac{1}{2} \left(-2J_B\, p_1^2 - 4J_D\, p_1^2 + 3J_E\, p_1^2 + 2J_A\, p_2^2 - J_C\, p_2^2 - K_0 \right. \right. \\
& \qquad \left. +(4J_0 + 4J_A - 4J_B - 8J_C + 6J_D) p_1 \cdot p_2 - 5) \right. \\
& \qquad \left. + \frac{1}{2}(1 - \xi) \left(-2I_E\, p_1^4 + 2I_D\, p_2^2 p_1^2 + J_B\, p_1^2 - J_A\, p_2^2 - 2I_D\, (p_1 \cdot p_2)^2 + K_0 \right. \right. \\
& \qquad\qquad \left. \left. - \left(4I_D\, p_1^2 + I_E\, p_1^2 - 3I_C\, p_2^2 + J_0 + 2J_A - 2J_B\right) p_1 \cdot p_2) \right] \\
& + \left(\gamma^\mu p_1^\nu - \gamma^\nu p_1^\mu\right) \left[\frac{1}{2} \left(2J_B\, p_1^2 - J_E\, p_1^2 - 4J_0\, p_2^2 + 2J_A\, p_2^2 + 4J_B\, p_2^2 + 3J_C\, p_2^2 - 4J_D\, p_2^2 \right. \right. \\
& \qquad \left. -K_0 - 2(2J_0 - 2J_A - 2J_B + J_D) p_1 \cdot p_2 - 5) + \frac{1}{2}(1 - \xi) \left(-I_C\, p_2^4 + 2I_D\, p_1^2 p_2^2 \right. \right. \\
& \qquad\qquad \left. \left. +I_E\, p_1^2 p_2^2 + J_0\, p_2^2 - J_A\, p_2^2 - 2J_B\, p_2^2 - J_B\, p_1^2 + 2I_D\, (p_1 \cdot p_2)^2 + K_0 \right. \right. \\
& \qquad \left. \left. + \left(I_E\, p_1^2 + I_C\, p_2^2 + 2I_D\, p_2^2 + J_0 - 2J_A - 2J_B\right) p_1 \cdot p_2) \right] \qquad . \qquad (6.40)
\end{aligned}
$$

6.2.4 Part 4

The Wilson-line contribution comprises integration over several non-local diagrams in order to retain gauge invariance. To one-loop order these contributions are explicitly:

$$\begin{aligned}
&\int \frac{d^dk}{(2\pi)^d}\, k_\lambda \left\{\sigma^{\mu\nu}, \tilde{\Gamma}^\lambda_V\right\} \\
&= -\frac{i\alpha}{4\pi^3}\int d^dk\, k_\lambda \frac{\gamma^\alpha \left(\not{p}_1 - \not{k}\right)\left\{\sigma^{\mu\nu}, \gamma^\lambda\right\}\left(\not{p}_2 - \not{k}\right)\gamma^\beta}{k^2\left(p_1-k\right)^2\left(p_2-k\right)^2}\left(g_{\alpha\beta} + (\xi-1)\frac{k_\alpha k_\beta}{k^2}\right) \\
&- \frac{i\alpha}{4\pi^3}\int d^dk \left[\frac{\gamma^\beta\left(\not{p}_1 - \not{k}\right)\left\{\sigma^{\mu\nu}, \gamma^\alpha\right\}}{k^2\left(p_1-k\right)^2} + \frac{\left\{\sigma^{\mu\nu}, \gamma^\alpha\right\}\left(\not{p}_2 - \not{k}\right)\gamma^\beta}{k^2\left(p_2-k\right)^2}\right] \\
&\qquad \times \left(g_{\alpha\beta} + (\xi-1)\frac{k_\alpha k_\beta}{k^2}\right). \qquad (6.41)
\end{aligned}$$

Computing these two pieces separately, we find the first to be:

$$\begin{aligned}
&-\frac{\alpha}{4\pi^3}\int d^dk\, k_\lambda \frac{\gamma^\alpha\left(\not{p}_1 - \not{k}\right)\left\{\sigma^{\mu\nu}, \tilde{\Gamma}^\lambda_V\right\}\left(\not{p}_2 - \not{k}\right)\gamma^\beta}{k^2\left(p_1-k\right)^2\left(p_2-k\right)^2}\left(g_{\alpha\beta} + (\xi-1)\frac{k_\alpha k_\beta}{k^2}\right) \\
&= -\frac{\alpha}{2\pi^3}\left\{-\frac{1}{2}\boldsymbol{J}^{(1)}_{\boldsymbol{\lambda}}(p_1,p_2)\,\gamma^\alpha \not{p}_1\, r^{\lambda\mu\nu}\,\not{p}_2\gamma_\alpha - \frac{1}{2}\boldsymbol{K}^{(1)}_{\boldsymbol{\lambda}}(p_1,p_2)\,\gamma^\alpha\, r^{\lambda\mu\nu}\,\gamma_\alpha\right. \\
&\qquad \left. + \frac{1}{2}\boldsymbol{J}^{(2)}_{\boldsymbol{\lambda\delta}}(p_1,p_2)\gamma^\alpha\left(\not{p}_1\, r^{\lambda\mu\nu}\,\gamma^\delta + \gamma^\delta\, r^{\lambda\mu\nu}\,\not{p}_2\right)\gamma_\alpha\right\} \\
&+ \frac{\alpha}{4\pi^3}(\xi-1)\left\{\boldsymbol{K}^{(1)}_{\boldsymbol{\lambda}}(p_1,p_2)\left(r^{\lambda\mu\nu}\right) + \boldsymbol{J}^{(1)}_{\boldsymbol{\lambda}}(p_1,p_2)\left(-\not{p}_1\gamma^\mu\gamma^\nu\not{p}_2\gamma^\lambda + \gamma^\lambda\not{p}_1\gamma^\nu\gamma^\mu\not{p}_2\right)\right. \\
&\qquad + \boldsymbol{J}^{(2)}_{\boldsymbol{\lambda\alpha}}(p_1,p_2)\left(-\gamma^\alpha\not{p}_1 r^{\lambda\mu\nu} - r^{\lambda\mu\nu}\not{p}_2\gamma^\alpha + \gamma^\alpha\gamma^\mu\gamma^\nu\not{p}_2\gamma^\lambda - \gamma^\alpha\not{p}_1\gamma^\nu\gamma^\mu\gamma^\lambda\right) \\
&\qquad + \boldsymbol{I}^{(2)}_{\boldsymbol{\lambda\alpha}}(p_1,p_2)\left(p_1^2\gamma^\alpha\gamma^\mu\gamma^\nu\not{p}_2\gamma^\lambda - \gamma^\alpha\not{p}_1\gamma^\nu\gamma^\mu\gamma^\lambda p_2^2\right) \\
&\qquad \left. + \boldsymbol{J}^{(2)}_{\boldsymbol{\lambda\alpha}}(p_1,0)\left(\gamma^\lambda\not{p}_1\gamma^\nu\gamma^\mu\gamma^\alpha\right) + \boldsymbol{J}^{(2)}_{\boldsymbol{\lambda\alpha}}(0,p_2)\left(-\gamma^\alpha\gamma^\mu\gamma^\nu\not{p}_2\gamma^\lambda\right)\right\}. \qquad (6.42)
\end{aligned}$$

The second set of contributions to the Wilson-line at one-loop is:

$$
\begin{aligned}
&-\frac{i\alpha}{4\pi^3}\int d^dk\,\left[\frac{\gamma^\beta\left(\not{p}_1-\not{k}\right)\{\sigma^{\mu\nu},\gamma^\alpha\}}{k^2\left(p_1-k\right)^2}+\frac{\{\sigma^{\mu\nu},\gamma^\alpha\}\left(\not{p}_2-\not{k}\right)\gamma^\beta}{k^2\left(p_2-k\right)^2}\right]\\
&\qquad\qquad\times\left(g_{\alpha\beta}+\left(\xi-1\right)\frac{k_\alpha k_\beta}{k^2}\right)\\
=\;&-\frac{\alpha}{2\pi^3}\left\{\left(p_{2\lambda}\boldsymbol{K}^{(0)}(0,p_2)-p_{1\lambda}\boldsymbol{K}^{(0)}(p_1,0)+\boldsymbol{K}^{(1)}_{\boldsymbol{\lambda}}(p_1,0)-\boldsymbol{K}^{(1)}_{\boldsymbol{\lambda}}(0,p_2)\right)\right.\\
&\qquad\qquad\times\left(2\gamma^\mu g^{\lambda\nu}-2\gamma^\nu g^{\lambda\mu}+\varepsilon\left(\gamma^\mu\gamma^\nu-g^{\mu\nu}\right)\gamma^\lambda\right)\\
&\qquad\qquad\left.+\varepsilon\left(p_{1\lambda}\boldsymbol{K}^{(0)}(p_1,0)-\boldsymbol{K}^{(1)}_{\boldsymbol{\lambda}}(p_1,0)\right)r^{\lambda\mu\nu}\right\}\\
&+\frac{\alpha}{4\pi^3}\left(\xi-1\right)\left\{\boldsymbol{J}^{(2)}_{\boldsymbol{\lambda\alpha}}(p_1,0)\gamma^\alpha\not{p}_1\,r^{\lambda\mu\nu}+\boldsymbol{J}^{(2)}_{\boldsymbol{\lambda\alpha}}(0,p_2)\,r^{\lambda\mu\nu}\not{p}_2\gamma^\alpha\right.\\
&\qquad\qquad\left.-\left(\boldsymbol{K}^{(1)}_{\boldsymbol{\lambda}}(p_1,0)+\boldsymbol{K}^{(1)}_{\boldsymbol{\lambda}}(0,p_2)\right)r^{\lambda\mu\nu}\right\}\,. \qquad (6.43)
\end{aligned}
$$

Collecting these together and again ordering the terms according to their Lorentz

and Dirac structure, we have:

$$
\begin{aligned}
\boldsymbol{P_4}^{\mu\nu} \;=\; & (\not{p}_1\not{p}_2\gamma^\nu p_1^\mu - \not{p}_1\not{p}_2\gamma^\mu p_1^\nu)\left[2(J_B + J_D - J_E) + \left(-I_E\, p_1^2 + I_D\, p_2^2 + J_B\right)(\xi - 1)\right] \\
& + (\not{p}_1\not{p}_2\gamma^\mu p_2^\nu - \not{p}_1\not{p}_2\gamma^\nu p_2^\mu)\left[2(J_A - J_C + J_D) + \left(I_D\, p_1^2 - I_C\, p_2^2 + J_A\right)(\xi - 1)\right] \\
& + \not{p}_2\left[-2I_D\,(\xi - 1)\,(p_2^\mu p_1^\nu - p_1^\mu p_2^\nu)\,p_1^2 - 4(J_A - J_C)\,(p_2^\mu p_1^\nu - p_1^\mu p_2^\nu)\right] \\
& + \not{p}_1\left[4J_D\,(p_2^\mu p_1^\nu - p_1^\mu p_2^\nu) + 2\left(J_B - I_E\, p_1^2\right)(\xi - 1)\,(p_2^\mu p_1^\nu - p_1^\mu p_2^\nu)\right] \\
& + (\gamma^\nu p_2^\mu - \gamma^\mu p_2^\nu)\left[-2J_D\, p_1^2 + 2J_C\, p_2^2 - K_0 + 4(J_A - J_C + J_D)\, p_1 \cdot p_2\right. \\
& \quad + \frac{1}{2}(1 - \xi)\left(-2I_E\, p_1^4 + 2I_D\, p_2^2 p_1^2 + J_E\, p_1^2 - 3J_C\, p_2^2 + 2K_0\right. \\
& \qquad \left.\left. -2\left(2I_D\, p_1^2 - 2I_C\, p_2^2 + 2J_A + J_D\right) p_1 \cdot p_2 - 3\right) + 2\right] \\
& - \frac{1}{2}\not{p}_1\,(\gamma^\mu\gamma^\nu - \gamma^\nu\gamma^\mu)\left[J_E\, p_1^2 - 2J_A\, p_2^2 + J_C\, p_2^2 + 2J_D\, p_1 \cdot p_2 - 4\right. \\
& \quad \left. + \frac{1}{2}(1 - \xi)\left(-2I_C\, p_2^4 + 2I_E\, p_1^2 p_2^2 + 2J_A\, p_2^2 - 4J_D\, p_2^2 + K_0 - 4J_E\, p_1 \cdot p_2 - 4\right) - 1\right] \\
& + \frac{1}{2}\not{p}_2\,(\gamma^\mu\gamma^\nu - \gamma^\nu\gamma^\mu)\left[2J_B\, p_1^2 - J_E\, p_1^2 - J_C\, p_2^2 - 2J_D\, p_1 \cdot p_2\right. \\
& \quad + \frac{1}{4}(\xi - 1)\left(-3I_E\, p_1^4 + I_C\, p_2^2 p_1^2 + 4I_D\, p_2^2 p_1^2 + J_0\, p_1^2 - 4J_D\, p_1^2 + J_E\, p_1^2 - 3J_C\, p_2^2\right. \\
& \qquad \left.\left. +3K_0 - K_0(0, p_2) - 2\left(I_D\, p_1^2 - 2I_C\, p_2^2 + 2J_A + 2J_C + J_D\right) p_1 \cdot p_2 - 5\right) + 1\right] \\
& + (\gamma^\mu p_1^\nu - \gamma^\nu p_1^\mu)\left[4J_A\, p_2^2 - 2J_C\, p_2^2 - 2J_D\, p_2^2 - K_0 + 4(J_B - J_E) p_1 \cdot p_2 + 4\right. \\
& \quad + \frac{1}{2}(\xi - 1)\left(-I_C\, p_2^4 + 2I_D\, p_1^2 p_2^2 + I_E\, p_1^2 p_2^2 + J_0\, p_2^2 - 4J_D\, p_2^2 + K_0\right. \\
& \qquad \left.\left. -K_0(p_1, 0) + \left(2I_D\, p_2^2 - 4J_E\right) p_1 \cdot p_2 - 2\right) + 4\right] \\
& + \frac{1}{2}\not{p}_1\,(\gamma^\mu\gamma^\nu - \gamma^\nu\gamma^\mu)\left[\frac{1}{2}\left(4 - K_0(p_1, 0)\right)(\xi - 1) - 2\right] \\
& + \frac{1}{2}\not{p}_2\,(\gamma^\mu\gamma^\nu - \gamma^\nu\gamma^\mu)\left[\frac{1}{2}\left(4 - K_0(0, p_2)\right)(\xi - 1) + 2\right] \\
& + (\gamma^\mu p_1^\nu - \gamma^\nu p_1^\mu)\left[K_0(p_1, 0) + \xi - 5\right] \\
& + (\gamma^\nu p_2^\mu - \gamma^\mu p_2^\nu)\left[1 + \xi K_0(0, p_2)\right] \quad . \qquad (6.44)
\end{aligned}
$$

6.3 Summing terms gives the result

We now collect together the terms from Eqs. (6.31, 6.37, 6.40, 6.44) to form

$$\boldsymbol{Q}^{\mu\nu} \;=\; [\boldsymbol{P_1} - \boldsymbol{P_2} - \boldsymbol{P_3} - \boldsymbol{P_4}]^{\mu\nu} \;. \tag{6.45}$$

The fact that each term is individually antisymmetric in μ and ν assists the checking. Rather than report every term of this somewhat tedious exercise, we illustrate that the answer for $\boldsymbol{Q}^{\mu\nu}$ is indeed zero by considering two structures. First those proportional to $\mathcal{C}$ of Eq. (6.33), which are individually singular in $1/\varepsilon$, then we will consider those proportional to unity.

6.3.1 Equating $\mathcal{C}$'s

We denote the singular term in $\boldsymbol{Q}^{\mu\nu}$ by $\boldsymbol{Q}_{\boldsymbol{\varepsilon}}{}^{\mu\nu}$. Collecting these parts we have:

$$\begin{aligned}
\boldsymbol{Q}_{\boldsymbol{\varepsilon}}{}^{\mu\nu} \;\equiv\;& \gamma^\mu\,(p_2^\nu - p_1^\nu)\;\mathcal{C} \;+\; (\xi-1)\,\gamma^\mu\,(p_2^\nu - p_1^\nu)\;\mathcal{C} && (+\boldsymbol{P_1}{}^{\mu\nu})\\
&-\xi\left[\frac{1}{2}\,(\not{p}_1 + \not{p}_2)\;\gamma^\mu\gamma^\nu \;+\; 2\gamma^\mu p_2^\nu\right]\mathcal{C} && (-\boldsymbol{P_2}{}^{\mu\nu})\\
&+\xi\left[\frac{1}{2}\,(\not{p}_1 + \not{p}_2)\;\gamma^\mu\gamma^\nu \;+\; \gamma^\mu\,(p_1^\nu + p_2^\nu)\right]\mathcal{C} && (-\boldsymbol{P_3}{}^{\mu\nu})\\
&+2\,\gamma^\mu\,(p_2^\nu - p_1^\nu)\;\mathcal{C} \;+\; 2\gamma^\mu\,(p_1^\nu - p_2^\nu)\;\mathcal{C}\\
&+(\xi-1)\left[\frac{1}{2}\,(\not{p}_1 + \not{p}_2)\;\gamma^\mu\gamma^\nu \;+\; 2\gamma^\mu p_2^\nu\right]\mathcal{C}\\
&-(\xi-1)\left[\frac{1}{2}\,(\not{p}_1 + \not{p}_2)\;\gamma^\mu\gamma^\nu \;+\; 2\,\gamma^\mu p_2^\nu\right]\mathcal{C} && (-\boldsymbol{P_4}{}^{\mu\nu})\\
&-\qquad (\mu \leftrightarrow \nu)\\
=\;& \mathbf{0} \qquad .
\end{aligned} \tag{6.46}$$

The $\boldsymbol{P_i}{}^{\mu\nu}$ in brackets indicate from which part the terms originate.

6.3.2 Equating 1's

We next collect together the terms proportional to unity. We denote this collection by $Q_{(1)}{}^{\mu\nu}$:

$$
\begin{aligned}
Q_{(1)}{}^{\mu\nu} \;=\; & \frac{1}{\Delta^2}\Bigg\{ (2-\xi)\left(-p_1^\mu p_2^\nu\right)\left[\not{p}_2\left(p_1^2 - p_1\cdot p_2\right) + \not{p}_1\left(p_2^2 - p_1\cdot p_2\right)\right] \\
& +2\left(\xi-1\right)\gamma^\mu\left(p_2^\nu - p_1^\nu\right)\Delta^2 \qquad\qquad (+\boldsymbol{P_1}{}^{\mu\nu}) \\
& -\xi\left[\frac{1}{2}\left(\not{p}_1+\not{p}_2\right)\gamma^\mu\gamma^\nu + 2\gamma^\mu p_2^\nu\right]\Delta^2 \qquad\qquad (-\boldsymbol{P_2}{}^{\mu\nu}) \\
& +\frac{(4+\xi)}{2}\left(\not{p}_1+\not{p}_2\right)\gamma^\mu\gamma^\nu\,\Delta^2 + 6\gamma^\mu\left(p_1^\nu + p_2^\nu\right)\Delta^2 \\
& -(2-\xi)\left\{\gamma^\mu p_1^\nu\left[p_2^2\left(p_1\cdot p_2 + p_1^2\right) + 2\Delta^2\right] - \gamma^\mu p_2^\nu p_1^2\left(p_2^2 + p_1\cdot p_2\right)\right. \\
& \qquad +\not{p}_1\not{p}_2\gamma^\mu\left[p_2^\nu\left(p_1^2 + p_1\cdot p_2\right) - p_1^\nu\left(p_2 + p_1\cdot p_2\right)\right] \\
& \qquad \left. + p_1^\mu p_2^\nu\left[\not{p}_2\left(p_1^2 + p_1\cdot p_2\right) - \not{p}_1\left(p_2^2 + p_1\cdot p_2\right)\right]\right\} \quad (-\boldsymbol{P_3}{}^{\mu\nu}) \\
& -\left(2\not{p}_1\gamma^\mu\gamma^\nu + 4\gamma^\mu p_1^\nu\right)\Delta^2 - \left(2\not{p}_2\gamma^\mu\gamma^\nu + 4\gamma^\mu p_2^\nu\right)\Delta^2 \\
& +(2-\xi)\left\{\gamma^\mu p_1^\nu p_2^2\left(p_1^2 + p_1\cdot p_2\right) - \gamma^\mu p_2^\nu p_1^2\left(p_2^2 + p_1\cdot p_2\right)\right. \\
& \qquad +\not{p}_1\not{p}_2\gamma^\mu\left[p_2^\nu\left(p_1^2 + p_1\cdot p_2\right) - p_1^\nu\left(p_2^2 + p_1\cdot p_2\right)\right] \\
& \qquad \left. + p_1^\mu p_2^\nu\left(2\not{p}_2 p_1^2 - 2\not{p}_1 p_1\cdot p_2\right)\right\} \qquad\qquad (-\boldsymbol{P_4}{}^{\mu\nu}) \\
& \qquad -\qquad (\mu\leftrightarrow\nu) \qquad\Bigg\} \\
=\; & \mathbf{0} \quad . \qquad\qquad (6.47)
\end{aligned}
$$

6.3.3 The Result

We can similarly check for all the terms in $\boldsymbol{Q}^{\mu\nu}$, *i.e.* for the combination of $\boldsymbol{P_i}^{\mu\nu}$ $(i = 1, 4)$ of Eq. (6.45), that the result is indeed zero. This confirms that the transverse Ward-Takahashi identity to one loop order in d close to 4 dimensions is indeed given by Eq. (6.25):

$$\begin{aligned} iq^{\mu}\Gamma_V^{\nu}(p_1,p_2) - iq^{\nu}\Gamma_V^{\mu}(p_1,p_2) &= S_F^{-1}(p_1)\,\sigma^{\mu\nu} + \sigma^{\mu\nu}\,S_F^{-1}(p_2) \\ &\quad - \frac{1}{2}(p_1+p_2)_{\lambda}\left\{\sigma^{\mu\nu},\Gamma_V^{\lambda}\right\} \\ &\quad + \int \frac{d^dk}{(2\pi)^d}\,k_{\lambda}\left\{\sigma^{\mu\nu},\tilde{\Gamma}_V^{\lambda}\right\}\,. \end{aligned} \tag{6.48}$$

6.4 Summary

We have shown that the transverse Ward-Takahashi identity of Eq. (6.25) is indeed satisfied to one-loop order. This is a critical step in developing non-perturbative Feynman rules for the key fermion-boson interaction so central to Abelian and non-Abelian gauge theories in the strong coupling regime. From this relation, we have determined a constraint for one of the transverse pieces of the fermion-boson vertex. The examination of different momentum regions, combined with knowledge of the perturbative form of the wilson-line may give similar constraints, allowing the construction of non-perturbative vertex ansätze.

Chapter 7

Conclusions and Outlook

In this thesis we have considered the numerical and analytical, where appropriate, study of non-perturbative phenomena within the Schwinger-Dyson approach to field theory. Starting with QED as the prototype field theory, we have shown how one may construct non-perturbative ansätze for the vertices so necessary in applying an appropriate truncation. We showed that one obtains powerful constraints on the structure of the fermion-boson vertex by imposing the condition that our theory observed multiplicative renormalisability.

Extensive numerical studies were performed in which we explored the critical phase structure of strongly-coupled QED and the residual gauge dependence present as a result of the truncation scheme. We found that, though the novel KP vertex performed exceptionally well in the absence of dynamical mass generation, this was not so when we entered the critical phase. Oddly enough, the CP vertex, as created for the quenched theory, in fact performs better here in combination with the BC vertex in the photon propagator. Motivated by this hybrid system, we utilised the KP vertex in the photon Schwinger-Dyson equation while keeping the CP vertex in the fermion, since each are derived for the specific momentum limits important to each. The result of this was a dramatic improvement in the preservation of gauge invariance in the critical coupling, in which our photon wave-function renormalisation was near gauge independent.

After exhausting all the possible calculations of QED in four dimensions, we turned our attention towards the three dimensional non-compact formulation. Being as when the four dimensionally derived CP-vertex was tried in QED, it was surprisingly found that in the chirally symmetric phase solutions were consistent with the LKF transformations, we investigated the KP vertex in the same context. This was perhaps a little naive, being as the logarithmic factors of the ansatz are spe-

cific to renormalisable theories, rather than super-renormalisable. We hence found that the KP vertex was a poor performer in both quenched and unquenched studies. It was recently found that one may apply the LKF transformation directly in momentum space; proposals that the slope of the chiral condensate as a function of the gauge parameter could help determine the efficacy of vertex ansätze were explored. Instead, we found that the observed slope was simply the result of the numerical methods employed and was in fact an artefact. A corollary of the momentum space LKF transformation showed that was trivially true, which if looked at in coordinate space was even more apparent.

For QCD we investigated the basic chiral observables for severally widely-used models. For the Maris-Tandy model coupling we explored the parameter dependence of the chiral observables for different vertex ansätze. We also investigated the Tübingen model with the KP vertex to see how it compared with previous calculations. Once satisfied with the modelling, we examined the dependence of the chiral condensate on the quark mass and investigated whether it was possible to extract this value with any degree of accuracy. By considering a class of solutions that exist one some critical domain, we indeed managed to obtain values for the condensate within certain models of QCD. This is important in the context of QCD sum rules where it is the condensate in the presence of non-zero quark masses that arises. We obtained values that were not inconsistent with the guestimate of Shifman *et al.*

Finally, in an effort to find more methods for constraining the non-perturbative form of the vertex, we examined the Transverse Ward-Takahashi relation. It is hoped that once we have more understanding of the forms present here we will be able to obtain suitable constraints on the vertex thus improving ansätze for the fermion-boson vertex.

In this thesis we have examined only the lowest order Schwinger-Dyson studies that describe the propagators of our theory – the two-point Green's functions. Though these are important building blocks, which contain in themselves some of the underlying phenomenology, they are not the only system that one should study. In QCD, for example, we do not in fact observe the quarks and gluons present in our Lagrangian description; in experiments, we see bound states of quarks and gluons – the Hadrons. Though the lowest order SDEs exhibit the phenomena of dynamical mass generation, they do not allow us to study bound states; for these we must turn to SDEs of at least one order higher. One Schwinger-Dyson equation that allows the study of mesonic bound states is the homogenous Bethe-Salpeter equation (BSE). This constitutes an eigenvalue problem in P^2 which is the square of the bound state mass, with the eigenvector giving the amplitude of the bound

state. The main difficulty arises when one considers the symmetries that must be preserved. For example, the axial-vector Ward-Takashashi identity (in the chiral limit):

$$-P_\mu \Gamma^H_{5\mu}(k;P) = \mathcal{S}^{-1}(k_+)\gamma_5 \frac{T^H}{2} + \gamma_5 \frac{T^H}{2} \mathcal{S}^{-1}(k_-) \,, \tag{7.1}$$

where we note that the $\Gamma^H_{5\mu}$ on the left-hand side satisfies the BSE, whilst the $\mathcal{S}^{-1}$ on the right-hand side must satisfy the SDE. Thus there is a non-trivial constraint that must be satisfied by the truncation employed in our vertex ansätze. It is the last point which is the problem – only one consistent scheme is known in which the bare-vertex is employed in the SDE with the ladder approximation in the BSE. However, in combination with the phenomenological ansatz we discussed in Chapter 4, this procedure has provided a wide variety of observables [161] in good agreement with the experimental data for pseudoscalar and vector mesons – a testiment to the philosophy that only the provision of a mass gap of the right size is what dominates phenomenological predictions.

Clearly finding improved truncation schemes for the lowest order SDEs is an important goal, but we should look to SDEs of higher order and so form consistent truncation schemes that will aid us in bound state studies. However, one should not discount results with the simplest of truncation schemes, where there has been considerable success [97, 161–165]. Attempts have been made to extend this truncation and so improve the applicability to axial-vector mesons and exotic mesons [166–170], but these are still in their early stages.

Appendix A

Numerical Techniques

In the main body of this thesis we discussed solutions of the Schwinger-Dyson equations. What remains is to develop a framework within which to solve these coupled integral equations.

A computer is inherently finite and hence it is necessary for us to introduce several cut-offs in representation of the functions, in addition to those necessary in computation and regularisation of the integrals. We wish to look at a large region of momenta, therefore it is appropriate to use a logarithmic scale $t = \log(p^2)$ for the parametrisation of the external momentum. Thus we have both an infrared and ultraviolet cut-off:

$$\varepsilon^2 \leq p^2 \leq \kappa^2 \,, \tag{A.1}$$

where the range is chosen such that we adequately capture an interesting physical region. We are similarly forced to introduce cut-offs into the integration momenta. Here we must either evaluate analytically or estimate numerically that part of the integral corresponding to $\int_0^{\varepsilon^2}$, were we to take the same ε^2 as the IR cut-off of our function.

Generally, we have dealt with the two-point correlation functions herein. This necessitates solving the fermion SDE, described by two scalar functions due to its spinor structure, and either the photon or gluon and ghost equations depending on the gauge theory. Thus we have at most four unknown functions to solve simultaneously, coupled together through non-linear integral equations. In the case of QED, we solve for the two functions fermion SDE simultaneously for an input photon polarisation scalar, calculate the updated photon equation and iterate until convergence is achieved. For QCD, we have not considered quarks in the ghost/gluon Schwinger-Dyson equations and solve for these two simultaneously. The results are then fed as input into the quark SDE and the two functions therein solved for together.

A.1 Root Finding

The procedure of solving non-linear integral equations can be generalised into one of solving for the root of some function. For example, imagine we have some one-dimensional function $f(x)$ which possesses a root, $f(x) = 0$ for some unknown value x. This can be solved by employing a natural-iterative approach:

$$x_{n+1} = x_n - f(x_n) \tag{A.2}$$

where we iterate over i until convergence is achieved. More sophisticated methods exist in this case, such as bisection and Newton's method:

$$x_{n+1} = x_n - \frac{f(x_n)}{f'(x_n)} \,. \tag{A.3}$$

Our integral equation is not one-dimensional since it is discretised in the external momentum, and so in the case of the naturally-iterative method we simply form the vectorial equation:

$$\mathbf{x}_{n+1} = \mathbf{x}_n - \mathbf{F}(\mathbf{x}_n) \tag{A.4}$$

where the residual $\mathbf{F}(\mathbf{x}) = \mathbf{0}$ is the function whose roots we wish to find.

Although this is a good starting point for any numerical study it has several drawbacks. The convergence is linear and thus slow, and to find a solution we must be close to a root. There are, however, more psychological disadvantages to using such a basic method; we are tempted to simplify our whole approach to the problem. For example, implementing linear interpolation between points destroys the functions smoothness which may have an impact upon delicate cancellations in the angular integrals.

An improvement upon the natural-iterative procedure is to employ a multidimensional form of Newton's method, stemming from a generalisation of Eq. (A.3). We expand the vector of equations we wish to solve, $\mathbf{F}(\mathbf{x}) = 0$ as a Taylor series:

$$F_i(\mathbf{x} + \delta\mathbf{x}) = F_i(\mathbf{x}) + \sum_{j=1}^{N} \frac{\partial F_i}{\partial x_j} \delta x_j + \mathcal{O}(\delta x^2) \tag{A.5}$$

where $J_{ij} = \partial F_i / \partial x_j$ is the Jacobian matrix. This can be written in matrix form:

$$\mathbf{F}(\mathbf{x} + \delta\mathbf{x}) = \mathbf{F}(\mathbf{x}) + \mathbf{J} \cdot \delta\mathbf{x} + \mathcal{O}(\delta x^2) \tag{A.6}$$

Neglecting higher order corrections and setting the equation equal to zero, we have:

$$\mathbf{J} \cdot \delta\mathbf{x} = -\mathbf{F} \tag{A.7}$$

which is a matrix equation that one may solve using LU-decomposition to find $\delta\mathbf{x}$. It is this $\delta\mathbf{x}$, the Newton step, that brings the vector $\mathbf{F}$ closer to zero for all vectorial components simultaneously. We need only iterate the procedure:

$$\mathbf{x}_{\text{new}} = \mathbf{x}_{\text{old}} + \delta\mathbf{x} \tag{A.8}$$

and recalculate the Jacobian at each step until the desired convergence is met.

This approach is not infallable, however, since it is possible to get stuck inside local minima, or to overstep the root entirely and end up oscillating towards the solution. This is particularly dangerous for multidimensional root finders. To improve this, we introduce the notion of try to ensure the global convergence of the function. This is achieved by asking for subsequent iterations to minimise the function:

$$f = \mathbf{F} \cdot \mathbf{F} \,, \tag{A.9}$$

that is we always move towards a root. We can see that our Newton step $\delta\mathbf{x}$ describes a descent direction of the function f from the following:

$$\nabla f \cdot \delta\mathbf{x} = (\mathbf{F} \cdot \mathbf{J}) \,.\, \left(-\mathbf{J}^{-1} \cdot \mathbf{F}\right) = -\mathbf{F} \cdot \mathbf{F} < 0 \,, \tag{A.10}$$

and replace Eq. (A.8) with:

$$\mathbf{x}_{\text{new}} = \mathbf{x}_{\text{old}} + \lambda \cdot \delta\mathbf{x} \,, \tag{A.11}$$

where λ is chosen such that the magnitude of Eq. (A.9) is reduced with each iteration. The calculation of an optimal λ depends upon the implementation, though one suggestion is:

$$\lambda_{i+1} = \frac{\sqrt{1+6r}-1}{3r} \qquad \text{with} \qquad r = \frac{f(\mathbf{x}+\lambda_i \cdot \delta\mathbf{x})}{f(\mathbf{x})} \tag{A.12}$$

where f is the Euclidean norm of Eq. (A.9).

This requirement to calculate the Jacobian at every iteration is time consuming. Thankfully, there exist algorithms for calculating a Rank-1 approximation to the Jacobian which then may be used for subsequent steps. These iterations, where the

Jacobian is used in combination with the gradient, are referred to as dogleg steps. They can often dramatically improve the rate of convergence in multidimensional problems. One example is a modification of Powell's Hybrid method whereby the dogleg step is:

$$\delta\mathbf{x} = -\alpha\mathbf{J}^{-1}\mathbf{f}(\mathbf{x}) - \beta\nabla\left|\mathbf{f}(\mathbf{x})\right|^2 \tag{A.13}$$

One may find routines for Newton-Raphson, with or without the global condition Eq. (A.9), as part of Numerical Recipes [171] or contained within the GNU Scientific Library [172]. Similarly, routines for hybrid methods can be found in these references.

A.2 Chebyshev Polynomials

Before we implement the numerical solver we must first decide on some way of representing the functions $\mathcal{A}$, $\mathcal{B}$, $\mathcal{G}$ and $\mathcal{Z}$. To this end we represent the functions as a sum of Chebyshev polynomials, which we will proceed to introduce. The functions are necessarily defined on a logarithmic momentum scale by $t = \log p^2 \in [\log\varepsilon^2, \log\Lambda^2]$. These t are then discretized, t_i, and ultimately located at the zero's of the Chebyshev series. Since this particular choice of polynomial is defined on $[-1, 1]$, and so we must employ a mapping $t \mapsto s$.

A Chebyshev polynomial of degree n is given by:

$$T_n(x) = \cos\left(n\cos^{-1}(x)\right) \tag{A.14}$$

Obviously the parameter x is defined in the range $[-1, 1]$. Despite the appearance of trigonometric functions in it's definition, these indeed form a polynomial series:

$$\begin{aligned} T_0(x) &= 1 \\ T_0(x) &= x \\ T_0(x) &= 2x^2 - 1 \\ &\vdots \\ T_{n+1}(x) &= 2xT_n(x) - T_{n-1} \end{aligned} \tag{A.15}$$

where the final line indicates the recurrence relation that one may use for the successive determination of higher order polynomials. There are well defined minima

and maxima, and more importantly zeros located at:

$$x_k = \cos\left(\left(k+\frac{1}{2}\right)\frac{\pi}{n}\right) \qquad k = 0..n-1 \tag{A.16}$$

These polynomials also obey two orthogonality conditions: one continuous and one discrete. Here we only need the discrete form for the main result:

$$\sum_{k=0}^{n-1} T_i(x_k)T_j(x_k) = \begin{cases} 0 & i \neq j \\ n/2 & i = j \neq 0 \\ n & i = j = 0 \end{cases} \tag{A.17}$$

The continuous orthogonality allows us to write any continuous function of $x \in [-1, 1]$ as a sum of Chebyshev polynomials:

$$f(x) = \sum_{j=0}^{\infty} c_j T_j(x) - \frac{c_0}{2} \tag{A.18}$$

The difference in normalisation accounts for the factor of $1/2$ in the c_0-term.

We now truncate this series such that the approximation is exact at the N-zeros of the Chebyshev series, x_k:

$$f(x_k) = \sum_{k=0}^{N-1} c_j T_j(x_k) - \frac{c_0}{2} \tag{A.19}$$

Multiplying this through by $T_i(x_k)$ and summing over the zeros gives us:

$$\begin{aligned} \sum_{k=0}^{N-1} f(x_k) &= \sum_{j=0}^{N-1}\sum_{k=0}^{N-1} c_j T_i(x_k)T_j(x_k) - \sum_{k=0}^{N-1}\frac{c_0}{2}T_i(x_k) \\ &= \frac{N}{2}c_i \\ \Rightarrow c_i &= \frac{2}{N}\sum_{k=0}^{N-1} T_i(x_k)f(x_k) \end{aligned} \tag{A.20}$$

With this we can fit a Chebyshev series to any known function.

A.2.1 Clenshaw's Recurrence relation

In order to evaluate our approximation to the function we can calculate each and every $T_i(x)$, multiply by its respective coefficient, and sum. This is needlessly ineffi-

cient and prone to numerical inaccuracies due to the delicate cancellations that take place. A more sensible approach is to exploit the recurrent relation of the Chebyshev series and employ Clenshaw's recurrence formula.
In general we write a polynomial series as:

$$f(x) = \sum_{j=0}^{N-1} c_j F_j(x) \tag{A.21}$$

for which there is a recurrence relation of the form:

$$F_{n+1}(x) = \alpha(n,x)F_n(x) + \beta(n,x)F_{n-1}(x) \tag{A.22}$$

We then define the recurrence relation:

$$y_j = \alpha(j,x)y_{j+1} + \beta(j+1,x)y_{j+2} + c_j \qquad j = N..1 \tag{A.23}$$

with initial values $y_{N+1} = y_{N+2} = 0$. Clenshaw's formula then comes from recognising that when the c_j in Eq. (A.23) are substituted into Eq. (A.21) many of the terms cancel and leave us with:

$$f(x) = \beta(1,x)F_0(x)y_2 + F_1(x)y_1 + F_0(x)c_0 \tag{A.24}$$

All we need to do is determine the quantities y_2 and y_1.

Applying this directly to the Chebyshev polynomials we have $\alpha(n,x) = 2x$, $\beta(n,x) = -1$, thus:

$$\begin{aligned} y_{N+1} &= y_N = 0 \\ y_j &= 2xy_{j+1} - y_{j+2} + c_j \qquad j = N-1..1 \\ f(x) &= xy_1 - y_2 + c_0/2 \end{aligned} \tag{A.25}$$

NB. The last step is different because of the $c_0/2$ in Eq. (A.21) for Chebyshev polynomials.

There remain a few more definitions to make. This first lies with the range over which our polynomial series is defined, since we need to map our function from $t \in [a,b]$ to $s \in [-1,1]$. This is achieved with:

$$s = \frac{t - \frac{1}{2}(a+b)}{\frac{1}{2}(b-a)} \tag{A.26}$$

For our purposes $t = \log p^2 \in [\log \varepsilon^2, \log \Lambda^2]$, hence:

$$s = \frac{\log(p^2/\Lambda^2\varepsilon^2)}{\log(\Lambda^2/\varepsilon^2)} \tag{A.27}$$

Our unknown functions $\mathcal{F}$, $\mathcal{M}$ and $\mathcal{G}$ will then be written as:

$$\begin{aligned}
\mathcal{F}(t_i) &= \sum_{j=0}^{N-1} a_j T_j(s_i) - a_0/2 \\
\mathcal{M}(t_i) &= \sum_{j=0}^{N-1} b_j T_j(s_i) - b_0/2 \\
\mathcal{G}(t_i) &= \sum_{j=0}^{N-1} c_j T_j(s_i) - c_0/2
\end{aligned} \tag{A.28}$$

When calculating the Jacobian we will need to take derivatives of these w.r.t. the coefficients a_j, b_j and c_j. This is simply:

$$\partial a_j \mathcal{F}(t_i) = T_j(s_i) - \frac{1}{2}\delta_{0j} \quad ; \quad \partial b_j \mathcal{F}(t_i) = 0 \quad \text{etc.} \tag{A.29}$$

A.3 Gaussian Quadrature

Since we have a smooth representation of the functions to be integrated we are free to use whichever integration method we prefer. One of the more powerful methods is that of Gaussian Quadrature. Here, not only do we calculate the weights of the function at different integration nodes, but we also distribute these points optimally to maximise the precision.

Gaussian quadrature is defined as the evaluation of the integral:

$$\int_a^b \omega(x) f(x) dx \approx \sum_{j=1}^{N} \omega_j f(x_j) \tag{A.30}$$

The precise form of the quadrature depends upon the weight function chosen. In order to find the set of orthogonal polynomials we define the inner product by:

$$\langle f|g\rangle \equiv \int_a^b \omega(x) f(x) g(x) dx \tag{A.31}$$

To generate the set of orthogonal polynomials we can use the procedure of Gram-Schmidt orthonormalisation. This procedure is begun by defining the first two

polynomials of the series as:

$$\begin{aligned} p_0(x) &= 1 \qquad\qquad\qquad\qquad \text{(thus the series is } \textit{monic}\text{)} \\ p_1(x) &= \left[x - \frac{\langle xp_0|p_0\rangle}{\langle p_0|p_0\rangle}\right] p_0 \end{aligned} \tag{A.32}$$

Here p_0 and p_1 are obviously orthogonal since $\langle p_0|p_1\rangle = 0$. The remaining polynomials are found from the recurrence relation:

$$p_{i+1} = \left[x - \frac{\langle xp_i|p_i\rangle}{\langle p_i|p_i\rangle}\right] p_i - \left[\frac{\langle p_{i-1}|xp_i\rangle}{\langle p_{i-1}|p_{i-1}\rangle}\right] p_{i-1} \tag{A.33}$$

The weights for each root are given by:

$$\omega_j = \frac{\langle p_{N-1}|p_{N-1}\rangle}{p_{N-1}(x_j)p'_N(x_j)} \tag{A.34}$$

where N is the number of orthogonal polynomials.

A.3.1 Gauss-Legendre Polynomials

This class of polynomial occurs when we choose the weight function $\omega(x) = 1$. The resulting polynomials are the Legendre Polynomials $P_j(x)$, and are defined on the interval $[-1, 1]$, and obey the recurrence relation:

$$(j+1)P_{j+1}(x) = (2j+1)xP_j(x) - jP_{j-1}(x) \tag{A.35}$$

In this special case we can write Eq. (A.34) as:

$$\omega_j = \frac{2}{\left(1 - x_j^2\right)\left[P'_N(x_j)\right]^2} \tag{A.36}$$

Integration on a logarithmic scale is then achieved by:

$$\begin{aligned} \int_a^b f(y)dy &= \int_{\log a}^{\log b} tf(t)dt \qquad\qquad t = \log y \\ &\approx \frac{1}{2}\log b/a \sum_{j=1}^{N} \omega_j t_j f\left(\frac{1}{2}\log(ab) + \frac{1}{2}\log(b/a)t_j\right) . \end{aligned} \tag{A.37}$$

A.4 Numerical Singularities

On calculating the integral equations we observe numerical singularities. These arise due to coefficient functions $\lambda_2(k^2, p^2)$ and $\lambda_3(k^2, p^2)$, which behave like

$$\lambda_2(y, x) = \frac{1}{2}(f(y) - f(x))\frac{1}{y - x} \to -\frac{1}{2}f'(y)\,, \tag{A.38}$$

in the limit $q \to 0$. Despite being well-defined analytically, we must treat these carefully numerically by explicitly cancelling the divergence when q is small.

Our functions are represented by a series of Chebyshev polynomials. By exploiting Clenshaw's recurrence formula one more time, we may factor out a part proportional to $x - y$ in the limit $q \to 0$. This we explore in the next two subsections.

A.4.1 Difference of Chebyshev Expansions

The method for summing the difference of a Chebyshev series has been presented in [55]. We proceed in the same manner, by exploiting Clenshaw's recurrence formula for the difference of two functions.

Suppose we are evaluating the difference between $\Delta f \equiv f(x_1) - f(x_2)$, where $f(x_1)$ is some Chebyshev expansion. Then, since the coefficients of the expansion are the same, we can write this as:

$$\Delta f \equiv \sum_{j=0}^{N-1} c_j \left(T_j(x_1) - T_j(x_2)\right) \tag{A.39}$$

Into this expression we can substitute the original Clenshaw's recurrence formula Eq. (A.25) to give us:

$$\Delta f = x_1 y_1(x_1) - x_2 y_1(x_2) - (y_2(x_1) - y_2(x_2)) \tag{A.40}$$

We also arrive a recurrence formula for the Δy_j:

$$y_j(x_1) - y_j(x_2) = 2\left(x_1 y_{j+1}(x_1) - x_2 y_{j+1}(x_1)\right) - (y_{j+2}(x_2) - y_{j+2}(x_2)) \tag{A.41}$$

This recurrence formula allows us to find the second set of terms in Eq. (A.40), so we should look for a recurrence formula for the first set. Again, we substitute in

from Eq. (A.25):

$$\begin{aligned} x_1 y_j(x_1) - x_2 y_j(x_2) &= 2\Big[(x_1+x_2)\left(x_1 y_{j+1}(x_1) - x_2 y_{j+1}(x_2)\right) \\ &\quad -x_1 x_2 \left(y_{j+1}(x_1) - y_{j+1}(x_2)\right)\Big] \\ &\quad -\left(x_1 y_{j+2}(x_1) - x_2 y_{j+2}(x_2)\right) + (x_1 - x_2)c_j \end{aligned} \tag{A.42}$$

For simplicity we define two recurrence variables $\alpha_j(x_1, x_2)$ and $\beta_j(x_1, x_2)$ to be:

$$\begin{aligned} \alpha_j(x_1, x_2) &\equiv \frac{y_j(x_1) - y_j(x_2)}{x_1 - x_2} \\ \beta_j(x_1, x_2) &\equiv \frac{x_1 y_j(x_1) - x_2 y_j(x_2)}{x_1 - x_2} \end{aligned} \tag{A.43}$$

and rewrite the recurrence formula Eq. (A.40) and recurrence relations Eqs. (A.41, A.42) as:

$$\begin{aligned} \Delta f &\equiv f(x_1) - f(x_2) = (x_1 - x_2)\left(\beta_1(x_1, x_2) - \alpha_2(x_1, x_2)\right) \\ \alpha_j(x_1, x_2) &= 2\beta_{j+1}(x_1, x_2) - \alpha_{j+2}(x_1, x_2) \\ \beta_j(x_1, x_2) &= c_j + 2(x_1 + x_2)\beta_{j+1}(x_1, x_2) - 2x_1\alpha_{j+1}(x_1, x_2) \\ &\quad -\beta_{j+2}(x_1, x_2) \end{aligned} \tag{A.44}$$

where once again the sum runs from $j = N - 1..1$, and the initial conditions for the recurrence variables are $\beta_{N+1} = \beta_N = \alpha_{N+1} = \alpha_N = 0$.

This is only half the story. We required a mapping $s(x_1)$ from $[\varepsilon^2, \Lambda^2]$ to $[-1, 1]$, and so for the $\Lambda_2(y, z)$ coefficient for the Ball–Chiu vertex, with $f(x) = \mathcal{A}(x)$:

$$\frac{f(s(z)) - f(s(y))}{z - y} = \frac{s(z) - s(y)}{z - y}\left(\beta_1(s(z), s(y)) - \alpha_2(s(z), s(y))\right) \tag{A.45}$$

In the limit $z \to y$ we have analytically that:

$$\frac{s(z) - s(y)}{z - y} \to s'(y)\,. \tag{A.46}$$

Numerically we must cancel this explicitly, which we do so in the next subsection.

A.4.2 Cancelling the Divergence

In the case of the Chebyshev Expansion, we want to eliminate a divergence in the term:

$$\frac{s(z) - s(y)}{z - y} \tag{A.47}$$

where the mapping function s is given by Eq. (A.27):

$$s = \frac{\log(p^2/\Lambda^2\varepsilon^2)}{\log(\Lambda^2/\varepsilon^2)} \tag{A.48}$$

Substituting this into Eq. (A.47) gives:

$$\frac{s(z) - s(y)}{z - y} = \frac{\log(z/y)}{z - y} \frac{2}{\log(\Lambda^2/\varepsilon^2)} \,. \tag{A.49}$$

If we write

$$\frac{z}{y} = \frac{1+u}{1-u} \qquad \text{where } u \equiv \frac{z-y}{z+y} \tag{A.50}$$

Then the Taylor expansion is readily computable:

$$\log\left(\frac{z}{y}\right) = \log\left(\frac{1+u}{1-u}\right) = 2\left(u + \frac{u^3}{3} + \frac{u^5}{5} + \frac{u^7}{7} + \cdots\right) \tag{A.51}$$

Finally, when we are in the neighbourhood of $z \longrightarrow$ which we will choose to be when $|u| < 10^{-3}$, we evaluate:

$$\frac{t(z) - t(y)}{z - y} = \frac{\log(z/y)}{z - y} \approx \frac{2}{z+y}\left(1 + \frac{u^2}{3} + \frac{u^4}{5} + \frac{u^6}{7} + \cdots\right) \tag{A.52}$$

and our divergence is cancelled.

Appendix B

Angular Integrals

B.1 QED in 3 Dimensions

In the course of studying QED in three dimensions, we are left with a selection of angular integrals in the SDEs. For the quenched case these, and in the explicitly gauge dependent part of the projection, these can usually be analytically. Thus we need to evaluate integrals of the form:

$$I_{(\alpha,\beta)}(k,p) = \int d\psi \sin\psi \frac{(k\cdot p)^{\alpha}}{(q^2)^{\beta}} \,, \tag{B.1}$$

which can be rewritten using the substitution:

$$\frac{k^2+p^2-q^2}{2} = k\cdot p \,. \tag{B.2}$$

We expand and collect in powers of q^2, using the following angular integrals:

$$\int_0^{\pi} d\psi \sin\psi q^4 = 2\left(k^4+p^4+\frac{10}{3}k^2p^2\right) \tag{B.3}$$

$$\int_0^{\pi} d\psi \sin\psi q^2 = 2\left(k^2+p^2\right) \tag{B.4}$$

$$\int_0^{\pi} d\psi \sin\psi = 2 \tag{B.5}$$

$$\int_0^{\pi} d\psi \frac{\sin\psi}{q^2} = \frac{1}{k\,p}\ln\left|\frac{k+p}{k-p}\right| \tag{B.6}$$

$$\int_0^{\pi} d\psi \frac{\sin\psi}{q^4} = \frac{2}{\left(k^2-p^2\right)^2} \tag{B.7}$$

$$\tag{B.8}$$

which are easily evaluated.

B.2 QED in 4 Dimensions

For QED in 4 dimensions (also appropriate for QCD) we will need the angular integrals as appropriate for the fermion propagator, and additionally in section 2.2.3 we need specific integrals evaluated for the photon propagator with symmetric momentum routing.

Integrals for the Fermion Propagator

The angular integrals we encounter for the fermion propagator, with asymmetric momentum routing, can be generally written in the form:

$$I_{\alpha,\beta}(k,p) = \int d\psi \sin^2\psi \frac{(k\cdot p)^\alpha}{(q^2)^\beta} \,. \tag{B.9}$$

Since we have that $q = k - p$, we may use recast this integral with the following substitution:

$$\frac{k^2+p^2-q^2}{2} = k\cdot p \,, \tag{B.10}$$

and hence we can recursively define the $I_{\alpha,\beta}$ in terms of $I_{0,\beta}$.

Calculation of $I_{0,\,\beta}$ for $\beta \leq 0$

Integrals of the form $I_{0,\,\beta}\,(k,p)$, given by Eq. (B.9), are trivially evaluated when β is either zero or negative, and so we obtain the following results:

$$I_{0,0} = \int_0^\pi d\psi\ \sin^2\psi = \frac{\pi}{2} \tag{B.11}$$

$$I_{0,-1} = \int_0^\pi d\psi\ \sin^2\psi q^2 = \frac{\pi}{2}\left(k^2+p^2\right) \tag{B.12}$$

$$I_{0,-2} = \int_0^\pi d\psi\ \sin^2\psi q^4 = \frac{\pi}{2}\left(k^4+3p^2k^2+p^4\right) \tag{B.13}$$

$$I_{0,-3} = \int_0^\pi d\psi\ \sin^2\psi q^6 = \frac{\pi}{2}\left(k^2+p^2\right)\left(k^4+5p^2k^2+p^4\right) \tag{B.14}$$

$$I_{0,-4} = \int_0^\pi d\psi\ \sin^2\psi q^8 = \frac{\pi}{2}\left(k^8+10p^2k^6+20p^4k^4+10p^6k^2+p^8\right) \tag{B.15}$$

Calculation of $I_{0,1}$

The first such equation that we wish to evaluate is:

$$I_{0,1} = \int_0^\pi d\psi \, \frac{\sin^2\psi}{q^2} \tag{B.16}$$

which may be rewritten as:

$$I_{0,1} = \frac{\theta\left(p^2-k^2\right)}{p^2}\int_0^\pi d\psi \, \frac{\sin^2\psi}{1-2\frac{|k|}{|p|}\cos\psi+\frac{k^2}{p^2}} + \left(k^2 \leftrightarrow p^2\right) . \tag{B.17}$$

One may now use the identity:

$$\int_0^\pi \frac{\sin^2\psi}{\left(1+2a\cos\psi+a^2\right)^n} = B\left(\frac{3}{2},\frac{1}{2}\right) F\left(n,n-1;2;a^2\right) \tag{B.18}$$

where the beta-function is evaluated to be:

$$B\left(\frac{3}{2},\frac{1}{2}\right) = \frac{\Gamma\left(\frac{3}{2}\right)\Gamma\left(\frac{1}{2}\right)}{\Gamma\left(2\right)} = \frac{\pi}{2} , \tag{B.19}$$

on knowledge that $\Gamma\left(\frac{1}{2}\right) = \sqrt{\pi}$. The hypergeometric function $F(\alpha,\beta;\gamma;z)$ can be written in terms of a series expansion for $|z|<1$:

$$F(\alpha,\beta;\gamma;z) = \frac{\Gamma(\gamma)}{\Gamma(\alpha)\Gamma(\beta)}\sum_{n=0}^{\infty}\frac{\Gamma(\alpha+n)\Gamma(\beta+n)}{\Gamma(\gamma+n)n!}z^n \tag{B.20}$$

which terminates on the condition that α or β is negative. For $I_{0,1}$ we have that:

$$F(1,0;2;z) = 1 , \tag{B.21}$$

and so we find that Eq. (B.16) evaluates to be:

$$I_{0,1} = \frac{\pi}{2}\left[\frac{\theta\left(p^2-k^2\right)}{p^2}+\frac{\theta\left(k^2-p^2\right)}{k^2}\right] \tag{B.22}$$

Calculation of $I_{0,2}$

We now wish to evaluate the angular integral:

$$I_{0,1} = \int_0^\pi d\psi \, \frac{\sin^2\psi}{q^4} = \frac{\theta\left(p^2-k^2\right)}{p^4}\int_0^\pi d\psi \, \frac{\sin^2\psi}{\left(1-2\frac{|k|}{|p|}\cos\psi+\frac{k^2}{p^2}\right)^2} + \left(k^2 \leftrightarrow p^2\right) \tag{B.23}$$

which is once again written in terms of the beta-function B and hypergeometric function F:

$$\int_0^\pi d\psi \frac{\sin^2\psi}{q^4} = B\left(\frac{3}{2},\frac{1}{2}\right)\left[\frac{\theta\left(p^2-k^2\right)}{p^4}F\left(2,1;2;\frac{k^2}{p^2}\right)+\left(k^2\leftrightarrow p^2\right)\right] \tag{B.24}$$

The beta-function gives the same value of $\pi/2$, but on application of Eq. (B.20) the hypergeometric function is:

$$F(2,1;2;z) = 1+z+z^2+z^3+\cdots = \frac{1}{1-z}\,. \tag{B.25}$$

Putting this together the integral yields:

$$I_{0,2} = \frac{\pi}{2}\left[\frac{\theta\left(p^2-k^2\right)}{p^2\left(p^2-k^2\right)}+\frac{\theta\left(k^2-p^2\right)}{k^2\left(k^2-p^2\right)}\right] \tag{B.26}$$

Calculation of $I_{\alpha,\beta}$

For angular integrals with $\alpha \geq 1$ we may use Eq. (B.10) to reduce our integral to those already calculated above. Generally, we have that:

$$I_{\alpha,\beta}(k,p) = \frac{k^2+p^2}{2}I_{\alpha-1,\,\beta}(k,p) - \frac{1}{2}I_{\alpha-1,\,\beta-1}(k,p) \tag{B.27}$$

Employing this we find the following integrals for $\alpha = 1$:

$$I_{1,-4} = -\pi k^2p^2(k^2+p^2)\left(p^4+4k^2p^2+k^4\right) \tag{B.28}$$

$$I_{1,-3} = -\frac{\pi}{4}k^2p^2\left(3p^4+8k^2p^2+3k^4\right) \tag{B.29}$$

$$I_{1,-2} = -\frac{\pi}{2}k^2p^2\left(k^2+p^2\right) \tag{B.30}$$

$$I_{1,-1} = -\frac{\pi}{4}k^2p^2 \tag{B.31}$$

$$I_{1,0} = 0 \tag{B.32}$$

$$I_{1,1} = \frac{\pi}{4}\left[\frac{k^2}{p^2}\theta\left(p^2-k^2\right)+\frac{p^2}{k^2}\theta\left(k^2-p^2\right)\right] \tag{B.33}$$

$$I_{1,2} = \frac{\pi}{2}\left[\frac{k^2}{p^2\left(p^2-k^2\right)}\theta\left(p^2-k^2\right)+\frac{p^2}{k^2\left(k^2-p^2\right)}\theta\left(k^2-p^2\right)\right] \tag{B.34}$$

Following the same recursive procedure, for $\alpha = 2$ we obtain:

$$I_{2,-3} = \frac{\pi}{8}p^2k^2\left(p^6 + 9k^2p^4 + 9k^4p^2 + k^6\right) \tag{B.35}$$

$$I_{2,-2} = \frac{\pi}{8}p^2k^2\left(p^4 + 4k^2p^2 + k^4\right) \tag{B.36}$$

$$I_{2,-1} = \frac{\pi}{8}k^2p^2\left(k^2 + p^2\right) \tag{B.37}$$

$$I_{2,0} = \frac{\pi}{8}k^2p^2 \tag{B.38}$$

$$I_{2,1} = \frac{\pi}{8}\left(k^2 + p^2\right)\left[\frac{k^2}{p^2}\theta\left(p^2 - k^2\right) + \frac{p^2}{k^2}\theta\left(k^2 - p^2\right)\right] \tag{B.39}$$

$$I_{2,2} = \frac{\pi}{8}\left[\frac{k^2}{p^2}\left(\frac{3k^2 + p^2}{p^2 - k^2}\right)\theta\left(p^2 - k^2\right) + \frac{p^2}{k^2}\left(\frac{3p^2 + k^2}{k^2 - p^2}\right)\theta\left(k^2 - p^2\right)\right] \tag{B.40}$$

For integrals of the form $I_{3,\beta}$ we have:

$$I_{3,-2} = -\frac{\pi}{4}p^4k^4(p^2 + k^2) \tag{B.41}$$

$$I_{3,-1} = -\frac{\pi}{8}p^4k^4 \tag{B.42}$$

$$I_{3,0} = 0 \tag{B.43}$$

$$I_{3,1} = \frac{\pi}{16}\left[\frac{k^4\left(2p^2 + k^2\right)}{p^2}\theta\left(p^2 - k^2\right) + \left(k^2 \leftrightarrow p^2\right)\right] \tag{B.44}$$

$$I_{3,2} = \frac{\pi}{4}\left[\frac{k^4\left(p^2 + k^2\right)}{p^2\left(p^2 - k^2\right)}\theta\left(p^2 - k^2\right) + \left(k^2 \leftrightarrow p^2\right)\right] \tag{B.45}$$

Finally, we look at the integrals with $\alpha = 4$:

$$I_{4,-1} = \frac{\pi}{16}\left(k^2 + p^2\right)p^4k^4 \tag{B.46}$$

$$I_{4,0} = \frac{\pi}{16}k^4p^4 \tag{B.47}$$

$$I_{4,1} = \frac{\pi}{32}\left[\frac{k^4\left(k^2 + p^2\right)\left(2p^2 + k^2\right)}{p^2}\theta\left(p^2 - k^2\right) + \left(k^2 \leftrightarrow p^2\right)\right] \tag{B.48}$$

$$I_{4,2} = \frac{\pi}{32}\left[\frac{k^4\left(5k^4 + 2p^4 + 9k^2p^2\right)}{p^2\left(p^2 - k^2\right)}\theta\left(p^2 - k^2\right) + \left(p^2 \leftrightarrow k^2\right)\right] \tag{B.49}$$

Integrals for the Photon Propagator

The standard integral that appears in the angular part of the photon propagator, necessary for the calculation of Sect. 2.2.3, is written as:

$$K_{\alpha,1} = \int_0^\pi d\psi \sin^2\psi \frac{(l\cdot q)^\alpha}{(l^2 + q^2/4) - (l\cdot q)^2}\,. \tag{B.50}$$

By making the substitutions $a = l^2 + q^2/4$ and $b = |l|\,|q|$, we can write this using partial fractions:

$$\begin{aligned} K_{\alpha,1} &= \int_0^\pi d\psi \sin^2\psi \frac{1}{2a}\left(\frac{1}{a - b\cos\psi} + \frac{1}{a + b\cos\psi}\right)(b\cos\psi)^\alpha \ . \\ &= \frac{1}{2a}\bar{I}_{\alpha,1} + \frac{1}{2a}\tilde{I}_{\alpha,1} \ , \end{aligned} \tag{B.51}$$

where the integrals

$$\bar{I}_{\alpha,1} = \int_0^\pi \sin^2\psi \frac{(l\cdot q)^\alpha}{a - b\cos\psi}, \qquad \tilde{I}_{\alpha,1} = \bar{I}_{\alpha,1}\Big|_{b\to -b} \tag{B.52}$$

are related to those calculated in the previous section. Indeed, we find for the simplest case of $\alpha = 0$ that:

$$\bar{I}_{0,1} = \tilde{I}_{0,1} \ \equiv \ I_{0,1} = \frac{\pi}{2}\left[\frac{4}{q^2}\theta\left(q^2/4 - l^2\right) + \frac{1}{l^2}\theta\left(l^2 - q^2/4\right)\right] \tag{B.53}$$

From Eq. (B.51) we have:

$$K_{0,1} = \frac{\pi}{2}\frac{1}{l^2 + q^2/4}\left[\frac{4}{q^2}\theta\left(q^2/4 - l^2\right) + \frac{1}{l^2}\theta\left(l^2 - q^2/4\right)\right] \tag{B.54}$$

To calculate the integrals for $\alpha > 0$ we may use:

$$-l_-^2 + (l^2 + q^2/4) = l\cdot q \qquad , \qquad l_+^2 - (l^2 + q^2/4) = l\cdot q \ ,$$

to form the recurrence relations:

$$\bar{I}_{\alpha,1} = \left(l^2 + \frac{q^2}{4}\right)\bar{I}_{\alpha-1,1} - \bar{I}_{\alpha-1,0} \tag{B.55}$$

$$\tilde{I}_{\alpha,1} = -\left(l^2 + \frac{q^2}{4}\right)\tilde{I}_{\alpha-1,1} + \tilde{I}_{\alpha-1,0} \ . \tag{B.56}$$

As a starting point we need to know the integral of Eq. (B.53) together with:

$$\bar{I}_{0,0} = \tilde{I}_{0,0} \equiv I_{0,0} = \frac{\pi}{2} \tag{B.57}$$

$$\bar{I}_{2,0} = \tilde{I}_{2,0} \equiv I_{2,0} = \frac{\pi}{8}l^2q^2 \tag{B.58}$$

$$\bar{I}_{4,0} = \tilde{I}_{4,0} \equiv I_{4,0} = \frac{\pi}{16}l^4q^4 \tag{B.59}$$

Thus for the case $\alpha = 1$ we have from Eq. (B.55):

$$\bar{I}_{1,1} = \left(l^2 + q^2/4\right) \bar{I}_{0,1} - \bar{I}_{0,0} \tag{B.60}$$

$$\tilde{I}_{1,1} = -\left(l^2 + q^2/4\right) \tilde{I}_{0,1} + \tilde{I}_{0,0} \tag{B.61}$$

Since $\bar{I}_{1,1} = -\tilde{I}_{1,1}$, it is obvious from Eq. (B.51) that:

$$K_{1,1} = 0 \,, \tag{B.62}$$

and we find this to be the case for all α odd.
The next non-trivial integral to evaluate is for $K_{2,1}$ which necessitates evaluation of $\bar{I}_{2,1}$ and $\tilde{I}_{2,1}$:

$$\bar{I}_{2,1} = \left(l^2 + q^2/4\right) \bar{I}_{1,1} - \bar{I}_{1,0} \tag{B.63}$$

$$\tilde{I}_{2,1} = -\left(l^2 + q^2/4\right) \tilde{I}_{1,1} - \tilde{I}_{1,0} \tag{B.64}$$

We hence find $\bar{I}_{2,1} = \tilde{I}_{2,1} = (l^2 + q^2/4)\, I_{1,1}$, yielding:

$$K_{2,1} = \frac{\pi}{2}\left[\frac{4l^2}{q^2}\theta\left(q^2/4 - l^2\right) + \frac{q^2}{l^2}\theta\left(l^2 - q^2/4\right)\right] . \tag{B.65}$$

Finally we need the integral $K_{4,1}$ whose evaluation procedes in a similar fashion:

$$K_{4,1} = \frac{\pi}{16}\left[\frac{4l^4\left(q^2/2 + l^2\right)}{q^2}\theta\left(q^2/4 - l^2\right) + \frac{q^4\left(2l^2 + q^2\right)}{l^2}\theta\left(l^2 - q^2/4\right)\right] \tag{B.66}$$

Appendix C

Integrals for Transverse Ward-Takahashi Relation

Note that in the text these functions will be assumed to depend upon p_1 and p_2 unless explicitly indicated.

$$\boldsymbol{K^{(0)}}(p_1,p_2) = \int d^4\omega \frac{1}{(p_1-\omega)^2(p_2-\omega)^2} = \frac{i\pi^2}{2}K_0(p_1,p_2)\ , \tag{C.1}$$

$$\boldsymbol{K^{(0)}}(0,p_2) = \int d^4\omega \frac{1}{\omega^2(p_2-\omega)^2} = \frac{i\pi^2}{2}K_0(0,p_2)\ , \tag{C.2}$$

$$\boldsymbol{K^{(0)}}(p_1,0) = \int d^4\omega \frac{1}{(p_1-\omega)^2\omega^2} = \frac{i\pi^2}{2}K_0(p_1,0)\ , \tag{C.3}$$

$$\boldsymbol{K^{(1)}_\mu}(p_1,p_2) = \int d^4\omega \frac{\omega_\mu}{(p_1-\omega)^2(p_2-\omega)^2} = \frac{i\pi^2}{4}(p_1+p_2)_\mu K_0(p_1,p_2)\ , \tag{C.4}$$

$$\boldsymbol{K^{(1)}_\mu}(0,p_2) = \int d^4\omega \frac{\omega_\mu}{\omega^2(p_2-\omega)^2} = \frac{i\pi^2}{4}p_{2\mu}K_0(0,p_2)\ , \tag{C.5}$$

$$\boldsymbol{K^{(1)}_\mu}(p_1,0) = \int d^4\omega \frac{\omega_\mu}{(p_1-\omega)^2\omega^2} = \frac{i\pi^2}{4}p_{1\mu}K_0(p_1,0)\ , \tag{C.6}$$

$$\boldsymbol{J^{(0)}}(p_1,p_2) = \int d^4\omega \frac{1}{\omega^2(p_1-\omega)^2(p_2-\omega)^2} = \frac{i\pi^2}{2}J_0\ , \tag{C.7}$$

$$\boldsymbol{J^{(1)}_\mu}(p_1,p_2) = \int d^4\omega \frac{\omega_\mu}{\omega^2(p_1-\omega)^2(p_2-\omega)} = \frac{i\pi^2}{2}\left[p_{2\mu}J_A + p_{1\mu}J_B\right]\ , \tag{C.8}$$

$$\boldsymbol{J^{(1)}_\mu}(0,p_2) = \int d^4\omega \frac{\omega_\mu}{\omega^4(p_2-\omega)^2} = \frac{i\pi^2 p_{2\mu}}{p_2^2}\ , \tag{C.9}$$

$$\boldsymbol{J^{(1)}_\mu}(p_1,0) = \int d^4\omega \frac{\omega_\mu}{\omega^4(p_1-\omega)^2} = \frac{i\pi^2 p_{1\mu}}{p_1^2}\ , \tag{C.10}$$

$$
\begin{aligned}
\boldsymbol{J}^{(2)}_{\mu\nu}(p_1,p_2) &= \int d^4\omega \, \frac{\omega_\mu \omega_\nu}{\omega^2 (p_1-\omega)^2 (p_2-\omega)^2} \\
&= \frac{i\pi^2}{2}\left\{ \frac{g_{\mu\nu}}{d} K_0 + \left(p_{2\mu}p_{2\nu} - g_{\mu\nu}\frac{p_2^2}{4} \right) J_C + \left(p_{1\mu}p_{1\nu} - g_{\mu\nu}\frac{p_1^2}{4} \right) J_E \right. \\
&\quad \left. + \left(p_{1\mu}p_{2\nu} + p_{2\mu}p_{1\nu} - g_{\mu\nu}\frac{p_1\cdot p_2}{2} \right) J_D \right\} , \qquad \text{(C.11)} \\
\boldsymbol{J}^{(2)}_{\mu\nu}(0,p_2) &= \int d^4\omega \, \frac{\omega_\mu \omega_\nu}{\omega^4 (p_2-\omega)^2} \\
&= \frac{i\pi^2}{2}\left(\frac{g_{\mu\nu}}{4} K_0(0,p_2) + \frac{p_{2\mu}p_{2\nu}}{p_2^2} \right) , \qquad \text{(C.12)} \\
\boldsymbol{J}^{(2)}_{\mu\nu}(p_1,0) &= \int d^4\omega \, \frac{\omega_\mu \omega_\nu}{\omega^4 (p_1-\omega)^2} \\
&= \frac{i\pi^2}{2}\left(\frac{g_{\mu\nu}}{4} K_0(p_1,0) + \frac{p_{1\mu}p_{1\nu}}{p_1^2} \right) , \qquad \text{(C.13)} \\
\boldsymbol{I}^{(1)}_{\mu}(p_1,p_2) &= \int d^4\omega \, \frac{\omega_\mu}{\omega^4 (p_1-\omega)^2 (p_2-\omega)^2} \\
&= \frac{i\pi^2}{2}\left[p_{2\mu} I_A + p_{1\mu} I_B \right] , \qquad \text{(C.14)} \\
\boldsymbol{I}^{(2)}_{\mu\nu}(p_1,p_2) &= \int d^4\omega \, \frac{\omega_\mu \omega_\nu}{\omega^4 (p_1-\omega)^2 (p_2-\omega)^2} \\
&= \frac{i\pi^2}{2}\left\{ \frac{g_{\mu\nu}}{4} J_0 + \left(p_{2\mu}p_{2\nu} - g_{\mu\nu}\frac{p_2^2}{4} \right) I_C + \left(p_{1\mu}p_{1\nu} - g_{\mu\nu}\frac{p_1^2}{4} \right) I_E \right. \\
&\quad \left. + \left(p_{1\mu}p_{2\nu} + p_{2\mu}p_{1\nu} - g_{\mu\nu}\frac{p_1\cdot p_2}{2} \right) I_D \right\} . \qquad \text{(C.15)}
\end{aligned}
$$

C.1 J-scalar functions

$$
\begin{aligned}
J_A &= \frac{1}{\Delta^2}\left\{\frac{J_0}{2}\left(-p_1^2\left(p_2^2-p_1\cdot p_2\right)\right)+p_1\cdot p_2\,L'-p_1^2L-2\left(p_1\cdot p_2-p_1^2\right)S\right\}\\
J_B &= \frac{1}{\Delta^2}\left\{\frac{J_0}{2}\left(-p_2^2\left(p_1^2-p_1\cdot p_2\right)\right)+p_1\cdot p_2\,L-p_2^2L'-2\left(p_1\cdot p_2-p_2^2\right)S\right\}\\
J_C &= \frac{1}{4\Delta^2}\left\{2p_1^2-4p_1\cdot p_2\,S+2p_1\cdot p_2\,L'+\left(2p_1\cdot p_2\,p_1^2-3p_1^2p_2^2\right)J_A-p_1^4J_B\right\}\\
J_D &= \frac{1}{4\Delta^2}\left\{2p_1\cdot p_2\,p_2^2J_A+2p_1\cdot p_2\,p_1^2J_B-2p_1\cdot p_2+2p_2^2S-p_2^2L'-p_1^2p_2^2J_A\right.\\
&\qquad\left.+2p_1^2S-p_1^2L-p_1^2p_2^2J_B\right\}\\
J_E &= \frac{1}{4\Delta^2}\left\{2p_2^2-4p_1\cdot p_2\,S+2p_1\cdot p_2\,L+\left(2p_1\cdot p_2\,p_2^2-3p_1^2p_2^2\right)J_B-p_2^4J_A\right\}
\end{aligned}
\tag{C.16}
$$

C.2 I-scalar functions

$$
\begin{aligned}
I_A &= \frac{1}{\Delta^2}\left\{-\frac{\left(p_1^2-p_1\cdot p_2\right)}{2}J_0+2\left(1-\frac{p_1\cdot p_2}{p_2^2}\right)S-L'+\frac{p_1\cdot p_2}{p_2^2}L\right\}\\
I_B &= \frac{1}{\Delta^2}\left\{-\frac{\left(p_2^2-p_1\cdot p_2\right)}{2}J_0+2\left(1-\frac{p_1\cdot p_2}{p_1^2}\right)S-L+\frac{p_1\cdot p_2}{p_1^2}L'\right\}\\
I_C &= \frac{1}{4\Delta^2}\left\{2p_1^2J_0-4\frac{p_1\cdot p_2}{p_2^2}+\left(2p_1\cdot p_2\,-3p_1^2\right)J_A-p_1^2J_B\right.\\
&\qquad\left.+\left(2p_1\cdot p_2\,p_1^2-3p_1^2p_2^2\right)I_A-p_1^4\,I_B\right\}\\
I_D &= \frac{1}{4\Delta^2}\left\{-2p_1\cdot p_2\,J_0+4+\left(2p_1\cdot p_2\,-p_2^2\right)J_A+\left(2p_1\cdot p_2\,-p_1^2\right)J_B\right.\\
&\qquad\left.+\left(2p_1\cdot p_2\,p_2^2-p_1^2p_2^2\right)I_A+\left(2p_1\cdot p_2\,p_1^2-p_1^2p_2^2\right)I_B\right\}\\
I_E &= \frac{1}{4\Delta^2}\left\{2p_2^2J_0-4\frac{p_1\cdot p_2}{p_1^2}+\left(2p_1\cdot p_2\,-3p_2^2\right)J_B-p_2^2J_A\right.\\
&\qquad\left.+\left(2p_1\cdot p_2\,p_2^2-3p_1^2p_2^2\right)I_B\,-p_2^4\,I_A\right\}
\end{aligned}
\tag{C.17}
$$

References

[1] P. Maris and C. D. Roberts, "Pseudovector components of the pion, $\pi^0 \to \gamma\gamma$, and $F_\pi(q^2)$," *Phys. Rev.* **C58** (1998) 3659–3665, nucl-th/9804062.

[2] L. Chang, Y.-X. Liu, M. S. Bhagwat, C. D. Roberts, and S. V. Wright, "Dynamical chiral symmetry breaking and a critical mass," nucl-th/0605058.

[3] S. Weinberg, "Implications of dynamical symmetry breaking: An addendum," *Phys. Rev. D* **19** (Feb, 1979) 1277–1280.

[4] L. Susskind, "Dynamics of Spontaneous Symmetry Breaking in the Weinberg-Salam Theory," *Phys. Rev.* **D20** (1979) 2619–2625.

[5] V. A. Miransky, M. Tanabashi, and K. Yamawaki, "Is the t quark responsible for the mass of W and Z bosons?," *Mod. Phys. Lett.* **A4** (1989) 1043.

[6] M. E. Peskin and D. V. Schroeder, *An Introduction to Quantum Field Theory.* Westview Press, 1995.

[7] C. Itzykson and J. B. Zuber, *Quantum Field Thoery.* McGraw Hill, 1980.

[8] L. H. Ryder, *Quantum Field Theory.* Cambridge University Press, 1996.

[9] D. Bailin and A. Love, *Introduction to Gauge Field Theory.* IOP Pub., 1993.

[10] T. Muta, *Foundations of Quantum Chromodynamics.* World Scientific, 1987.

[11] V. A. Miransky, *Dynamical Symmetry Breaking in Quantum Field Theories.* World Scientific, 1993.

[12] M. Gell-Mann, "Symmetries of baryons and mesons," *Phys. Rev.* **125** (1962) 1067–1084.

[13] W. Heisenberg and W. Pauli, "On quantum field theory. (in German)," *Z. Phys.* **56** (1929) 1–61.

[14] W. Heisenberg and W. Pauli, "On quantum field theory. 2. (in German)," *Z. Phys.* **59** (1930) 168–190.

[15] T. Kugo and I. Ojima, "Manifestly covariant canonical formulation of Yang-Mills field theories: Physical state subsidiary conditions and physical S matrix unitarity," *Phys. Lett.* **B73** (1978) 459.

[16] T. Kugo and I. Ojima, "Manifestly covariant canonical formulation of Yang-Mills field theories. 1. the case of Yang-Mills fields of Higgs- Kibble type in Landau gauge," *Prog. Theor. Phys.* **60** (1978) 1869.

[17] T. Kugo and I. Ojima, "Local covariant operator formalism of non-Abelian gauge theories and quark confinement problem," *Prog. Theor. Phys. Suppl.* **66** (1979) 1.

[18] R. P. Feynman, "Space-time approach to nonrelativistic quantum mechanics," *Rev. Mod. Phys.* **20** (1948) 367–387.

[19] G. Parisi and Y. Wu, "Perturbation theory without gauge fixing," *Sci. Sin.* **24** (1981) 483.

[20] J. S. Schwinger, "On the Green's functions of quantized fields. 1," *Proc. Nat. Acad. Sci.* **37** (1951) 452–455.

[21] J. S. Schwinger, "On the Green's functions of quantized fields. 2," *Proc. Nat. Acad. Sci.* **37** (1951) 455–459.

[22] L. D. Faddeev and V. N. Popov, "Feynman diagrams for the Yang-Mills field," *Phys. Lett.* **B25** (1967) 29–30.

[23] C. Becchi, A. Rouet, and R. Stora, "Renormalization of gauge theories," *Annals Phys.* **98** (1976) 287–321.

[24] M. Z. Iofa and I. V. Tyutin, "Gauge invariance of spontaneously broken non-Abelian theories in the Bogolyubov-Parasiuk-Hepp-Zimmerman method. (in Russian)," *Teor. Mat. Fiz.* **27** (1976) 38–47.

[25] L. Baulieu and J. Thierry-Mieg, "The principle of BRS symmetry: an alternative approach to Yang-Mills theories," *Nucl. Phys.* **B197** (1982) 477.

[26] J. C. Ward, "An Identity in Quantum Electrodynamics," *Phys. Rev.* **78** (1950) 182.

[27] H. S. Green, "A Pre-renormalized quantum electrodynamics," *Proc. Phys. Soc.* **A66** (1953) 873–880.

[28] Y. Takahashi, "On the generalized Ward identity," *Nuovo Cim.* **6** (1957) 371.

[29] C. S. Fischer, "Non-perturbative propagators, running coupling and dynamical mass generation in ghost-antighost symmetric gauges in QCD," *PhD Thesis* (2003) `hep-ph/0304233`.

[30] E. Eichten and F. Feinberg, "Dynamical symmetry breaking of non-Abelian gauge symmetries," *Phys. Rev.* **D10** (1974) 3254–3279.

[31] L. Landau and K. I. K., "Gradient transformation of the Green function of charged particles," *Sov. Phys. JETP* **2** (1956) 69–72.

[32] E. S. Fradkin, "Concerning some general relations of quantum electrodynamics," *Zh. Eksp. Teor. Fiz.* **29** (1955) 258–261.

[33] C. J. Burden and C. D. Roberts, "Gauge covariance and the fermion-photon vertex in three-dimensional and four-dimensional, massless quantum electrodynamics," *Phys. Rev.* **D47** (1993) 5581–5588, `hep-th/9303098`.

[34] J. Bernstein, *Elementary Particles and Their Currents.* Freeman, 1968.

[35] J. S. Ball and T.-W. Chiu, "Analytic properties of the vertex function in gauge theories. 1," *Phys. Rev.* **D22** (1980) 2542.

[36] A. Kizilersu, M. Reenders, and M. R. Pennington, "One loop QED vertex in any covariant gauge: Its complete analytic form," *Phys. Rev.* **D52** (1995) 1242–1259, `hep-ph/9503238`.

[37] A. I. Davydychev, P. Osland, and L. Saks, "Quark gluon vertex in arbitrary gauge and dimension," *Phys. Rev.* **D63** (2001) 014022, `hep-ph/0008171`.

[38] N. Brown and M. R. Pennington, "Studies of confinement: How quarks and gluons propagate," *Phys. Rev.* **D38** (1988) 2266.

[39] A. W. Schreiber, T. Sizer, and A. G. Williams, "Dimensionally regularized study of nonperturbative quenched QED," `hep-ph/9807202`.

[40] A. W. Schreiber, T. Sizer, and A. G. Williams, "Dimensionally regularized study of nonperturbative quenched QED," *Phys. Rev.* **D58** (1998) 125014, `hep-ph/9804385`.

[41] D. C. Curtis and M. R. Pennington, "Truncating the Schwinger-Dyson equations: How multiplicative renormalizability and the Ward identity restrict the three point vertex in QED," *Phys. Rev.* **D42** (1990) 4165–4169.

[42] A. Kızılersü and M. R. Pennington, "Building the full fermion-photon vertex of QED by imposing the multiplicative renormalisability of the SDE for the fermion and photon propagators," (In preparation) .

[43] A. Kizilersu, *Gauge theory constraints on the fermion-boson vertex.* PhD thesis, University of Durham, UK, 1995.

[44] C. N. Leung, S. T. Love, and W. A. Bardeen, "Spontaneous symmetry breaking in scale invariant quantum electrodynamics," *Nucl. Phys.* **B273** (1986) 649–662.

[45] C. N. Leung, S. T. Love, and W. A. Bardeen, "Aspects of dynamical symmetry breaking in gauge field theories," *Nucl. Phys.* **B323** (1989) 493.

[46] D. Atkinson and M. P. Fry, "Should one truncate the electron selfenergy?," *Nucl. Phys.* **B156** (1979) 301.

[47] A. Kocic, S. Hands, J. B. Kogut, and E. Dagotto, "The equation of state and critical exponents in quenched strongly coupled QED," *Nucl. Phys.* **B347** (1990) 217–242.

[48] A. Kocic, J. B. Kogut, M.-P. Lombardo, and K. C. Wang, "Spectroscopy, scaling and critical indices in strongly coupled quenched QED," *Nucl. Phys.* **B397** (1993) 451–478, `hep-lat/9206018`.

[49] M.-P. Lombardo, A. Kocic, and J. B. Kogut, "More on strongly coupled quenched QED," `hep-lat/9411051`.

[50] J. B. Kogut and J. F. Lagae, "Quenched QED on a momentum space lattice," *Nucl. Phys. Proc. Suppl.* **42** (1995) 681–683, `hep-lat/9412024`.

[51] R. Fukuda and T. Kugo, "Schwinger-Dyson equation for massless vector theory and absence of fermion pole," *Nucl. Phys.* **B117** (1976) 250.

[52] P. I. Fomin, V. P. Gusynin, V. A. Miransky, and Y. A. Sitenko, "Dynamical symmetry breaking and particle mass generation in gauge field theories," *Riv. Nuovo Cim.* **6N5** (1983) 1–90.

[53] V. A. Miransky, "Phase diagram with respect to the coupling constant and the local limit in quantum electrodynamics," *Sov. Phys. JETP* **61** (1985) 905–911.

[54] V. A. Miransky, "Dynamics of spontaneous chiral symmetry breaking and continuum limit in quantum electrodynamics," *Nuovo Cim.* **A90** (1985) 149–170.

[55] H. M. Fried and D. R. Yennie, "New Techniques in the Lamb Shift Calculation," *Phys. Rev.* **112** (Nov, 1958) 1391–1404.

[56] D. Atkinson, J. C. R. Bloch, V. P. Gusynin, M. R. Pennington, and M. Reenders, "Strong QED with weak gauge dependence: Critical coupling and anomalous dimension," *Phys. Lett.* **B329** (1994) 117–122.

[57] J. C. R. Bloch, "Numerical investigation of fermion mass generation in QED," `hep-ph/0208074`.

[58] K.-I. Kondo, "Critical exponents, scaling law, universality and renormalization group flow in strong coupling QED," *Int. J. Mod. Phys.* **A6** (1991) 5447–5466.

[59] V. P. Gusynin, "Vacuum polarization and dynamical chiral symmetry breaking in quantum electrodynamics," *Mod. Phys. Lett.* **A5** (1990) 133.

[60] K.-I. Kondo, "Recovery of gauge invariance in strong coupling QED," *Int. J. Mod. Phys.* **A7** (1992) 7239–7262.

[61] K.-I. Kondo and H. Nakatani, "Strong coupling unquenched QED. 2. Numerical study," *Prog. Theor. Phys.* **88** (1992) 737–750.

[62] J. Oliensis and P. W. Johnson, "Possible second order phase transition in strongly coupled unquenched planar four-dimensional QED," *Phys. Rev.* **D42** (1990) 656–664.

[63] T. Appelquist and R. D. Pisarski, "High-temperature Yang-Mills theories and three-dimensional quantum chromodynamics," *Phys. Rev.* **D23** (1981) 2305.

[64] N. Dorey and N. E. Mavromatos, "QED in three-dimension and two-dimensional superconductivity without parity violation," *Nucl. Phys.* **B386** (1992) 614–682.

[65] M. Franz, Z. Tesanovic, and O. Vafek, "QED_3 theory of pairing pseudogap in cuprates I: From d-wave superconductor to antiferromagnet via algebraic Fermi liquid," *Phys. Rev.* **B66** (2002) 054535, `cond-mat/0203333`.

[66] O. Vafek, Z. Tesanovic, and M. Franz, "Relativity Restored: Dirac Anisotropy in QED_3," *Phys. Rev. Lett.* **89** (2002) 157003, `cond-mat/0203047`.

[67] M. Franz, Z. Tesanovic, and O. Vafek, "Gauge invariant fermion propagator in QED_3," `cond-mat/0204536`.

[68] A. M. Polyakov, "Compact gauge fields and the infrared catastrophe," *Phys. Lett.* **B59** (1975) 82–84.

[69] A. M. Polyakov, "Quark confinement and topology of gauge groups," *Nucl. Phys.* **B120** (1977) 429–458.

[70] T. Banks, R. Myerson, and J. B. Kogut, "Phase transitions in abelian lattice gauge theories," *Nucl. Phys.* **B129** (1977) 493.

[71] M. Gopfert and G. Mack, "Proof of confinement of static quarks in three-dimensional U(1) lattice gauge theory for all values of the coupling constant," *Commun. Math. Phys.* **82** (1981) 545.

[72] R. D. Pisarski, "Chiral symmetry breaking in three-dimensional electrodynamics," *Phys. Rev.* **D29** (1984) 2423.

[73] T. W. Appelquist, M. J. Bowick, D. Karabali, and L. C. R. Wijewardhana, "Spontaneous chiral symmetry breaking in three-dimensional QED," *Phys. Rev.* **D33** (1986) 3704.

[74] T. Appelquist, D. Nash, and L. C. R. Wijewardhana, "Critical behavior in (2+1)-dimensional QED," *Phys. Rev. Lett.* **60** (1988) 2575.

[75] M. R. Pennington and S. P. Webb, "Hierarchy of scales in three-dimensional QED,". BNL-40886.

[76] D. Atkinson, P. W. Johnson, and P. Maris, "Dynamical mass generation in QED in three-dimensions: Improved vertex function," *Phys. Rev.* **D42** (1990) 602–609.

[77] M. R. Pennington and D. Walsh, "Masses from nothing: A Nonperturbative study of QED in three-dimensions," *Phys. Lett.* **B253** (1991) 246–251.

[78] D. C. Curtis, M. R. Pennington, and D. Walsh, "Dynamical mass generation in QED in three-dimensions and the $1/N_f$ expansion," *Phys. Lett.* **B295** (1992) 313–319.

[79] E. Dagotto, A. Kocic, and J. B. Kogut, "Chiral symmetry breaking in three-dimensional QED with n_f flavors," *Nucl. Phys.* **B334** (1990) 279.

[80] S. Hands and J. B. Kogut, "Finite size effects and chiral symmetry breaking in quenched three-dimensional QED," *Nucl. Phys.* **B335** (1990) 455.

[81] S. J. Hands, J. B. Kogut, L. Scorzato, and C. G. Strouthos, "Non-compact QED_3 with $n_f = 1$ and $n_f = 4$," *Phys. Rev.* **B70** (2004) 104501, `hep-lat/0404013`.

[82] D. Nash, "Higher order corrections in (2+1)-dimensional QED," *Phys. Rev. Lett.* **62** (1989) 3024.

[83] D. Atkinson, P. W. Johnson, and M. R. Pennington, "Dynamical mass generation in three-dimensional QED,". Print-88-0616 (BNL).

[84] K.-I. Kondo and H. Nakatani, "Cutoff dependence of selfconsistent solutions in unquenched QED in three-dimensions," *Prog. Theor. Phys.* **87** (1992) 193–206.

[85] K.-I. Kubota and H. Terao, "Dynamical symmetry breaking in QED_3 from the Wilson RG point of view," *Prog. Theor. Phys.* **105** (2001) 809–825, `hep-ph/0101073`.

[86] N. E. Mavromatos and J. Papavassiliou, "Novel Phases and Old Puzzles in QED_3 and related models," `cond-mat/0311421`.

[87] **UKQCD** Collaboration, L. Del Debbio, S. J. Hands, and J. C. Mehegan, "Three-dimensional Thirring model for small N_f," *Nucl. Phys.* **B502** (1997) 269–308, `hep-lat/9701016`.

[88] L. Del Debbio and S. J. Hands, "The three dimensional Thirring model for $N_f = 4$ and $N_f = 6$," *Nucl. Phys.* **B552** (1999) 339–362, `hep-lat/9902014`.

[89] S. Hands and B. Lucini, "The phase diagram of the three dimensional Thirring model," *Phys. Lett.* **B461** (1999) 263–269, hep-lat/9906008.

[90] S. J. Hands, J. B. Kogut, and C. G. Strouthos, "Non-compact QED_3 with $N_f \geq 2$," *Nucl. Phys.* **B645** (2002) 321–336, hep-lat/0208030.

[91] A. Bashir and A. Raya, "On gauge independent dynamical chiral symmetry breaking," hep-ph/0511291.

[92] C. J. Burden and P. C. Tjiang, "Deconstructing the vertex ansatz in three dimensional quantum electrodynamics," *Phys. Rev.* **D58** (1998) 085019, hep-th/9804002.

[93] A. Bashir, A. Kizilersu, and M. R. Pennington, "Analytic form of the one-loop vertex and of the two-loop fermion propagator in 3-dimensional massless QED," hep-ph/9907418.

[94] C. S. Fischer, R. Alkofer, T. Dahm, and P. Maris, "Dynamical chiral symmetry breaking in unquenched QED_3," *Phys. Rev.* **D70** (2004) 073007, hep-ph/0407104.

[95] D. A. Walsh, *A nonperturbative study of three dimensional quantum electrodynamics with N flavours of fermion.* PhD thesis, University of Durham, UK, 1990.

[96] P. Maris, "Confinement and complex singularities in QED in three-dimensions," *Phys. Rev.* **D52** (1995) 6087–6097, hep-ph/9508323.

[97] P. Maris, "The influence of the full vertex and vacuum polarization on the fermion propagator in QED_3," *Phys. Rev.* **D54** (1996) 4049–4058, hep-ph/9606214.

[98] C. S. Fischer and R. Alkofer, "Infrared exponents and running coupling of SU(N) Yang-Mills theories," *Phys. Lett.* **B536** (2002) 177–184, hep-ph/0202202.

[99] P. Maris, C. D. Roberts, and P. C. Tandy, "Pion mass and decay constant," *Phys. Lett.* **B420** (1998) 267–273, nucl-th/9707003.

[100] M. Baker, J. S. Ball, and F. Zachariasen, "A nonperturbative calculation of the infrared limit of the axial gauge gluon propagator. 1," *Nucl. Phys.* **B186** (1981) 531.

[101] W. J. Schoenmaker, "Study of the gluon propagator in the axial gauge," *Nucl. Phys.* **B194** (1982) 535.

[102] K. Buttner and M. R. Pennington, "Infrared behavior of the gluon propagator: Confining of confined?," *Phys. Rev.* **D52** (1995) 5220–5228, hep-ph/9506314.

[103] G. B. West, "General infrared and ultraviolet properties of the gluon propagator in axial gauge," *Phys. Rev.* **D27** (1983) 1878.

[104] S. Mandelstam, "Approximation scheme for QCD," *Phys. Rev.* **D20** (1979) 3223.

[105] D. Atkinson, P. W. Johnson, and K. Stam, "Nonperturbative confinement in quantum chromodynamics. 2. Mandelstam's gluon propagator," *J. Math. Phys.* **23** (1982) 1917.

[106] D. Atkinson, J. K. Drohm, P. W. Johnson, and K. Stam, "Nonperturbative confinement in quantum chromodynamics. 1. Study of an approximate equation of Mandelstam," *J. Math. Phys.* **22** (1981) 2704.

[107] N. Brown and M. R. Pennington, "Preludes to confinement: Infrared properties of the gluon propagator in the Landau gauge," *Phys. Lett.* **B202** (1988) 257.

[108] N. Brown and M. R. Pennington, "Studies of confinement: How the gluon propagates," *Phys. Rev.* **D39** (1989) 2723.

[109] A. Hauck, L. von Smekal, and R. Alkofer, "Solving the gluon Dyson-Schwinger equation in the Mandelstam approximation," *Comput. Phys. Commun.* **112** (1998) 149, `hep-ph/9604430`.

[110] V. N. Gribov, "Quantization of non-Abelian gauge theories," *Nucl. Phys.* **B139** (1978) 1.

[111] D. Zwanziger, "Vanishing of zero momentum lattice gluon propagator and color confinement," *Nucl. Phys.* **B364** (1991) 127–161.

[112] F. D. R. Bonnet, P. O. Bowman, D. B. Leinweber, A. G. Williams, and J. M. Zanotti, "Infinite volume and continuum limits of the Landau-gauge gluon propagator," *Phys. Rev.* **D64** (2001) 034501, `hep-lat/0101013`.

[113] L. von Smekal, R. Alkofer, and A. Hauck, "The infrared behavior of gluon and ghost propagators in Landau gauge QCD," *Phys. Rev. Lett.* **79** (1997) 3591–3594, `hep-ph/9705242`.

[114] L. von Smekal, A. Hauck, and R. Alkofer, "A solution to coupled Dyson-Schwinger equations for gluons and ghosts in Landau gauge," *Ann. Phys.* **267** (1998) 1, `hep-ph/9707327`.

[115] A. Hauck, L. von Smekal, and R. Alkofer, "Solving a coupled set of truncated QCD Dyson-Schwinger equations," *Comput. Phys. Commun.* **112** (1998) 166, `hep-ph/9804376`.

[116] D. Atkinson and J. C. R. Bloch, "Running coupling in non-perturbative QCD. I: Bare vertices and y-max approximation," *Phys. Rev.* **D58** (1998) 094036, `hep-ph/9712459`.

[117] J. C. Taylor, "Ward identities and charge renormalization of the Yang-Mills field," *Nucl. Phys.* **B33** (1971) 436–444.

[118] H. Pagels and S. Stokar, "The pion decay constant, electromagnetic form-factor and quark electromagnetic selfenergy in QCD," *Phys. Rev.* **D20** (1979) 2947.

[119] A. Barducci, R. Casalbuoni, M. Modugno, G. Pettini, and R. Gatto, "Corrections to the Pagels-Stokar formula for f_π," *Phys. Lett.* **B405** (1997) 173–179, hep-ph/9703304.

[120] **Particle Data Group** Collaboration, W. M. Yao *et al.*, "Review of particle physics," *J. Phys.* **G33** (2006) 1–1232.

[121] G. Colangelo, J. Gasser, and H. Leutwyler, "The quark condensate from K_{e_4} decays," *Phys. Rev. Lett.* **86** (2001) 5008–5010, hep-ph/0103063.

[122] C. S. Fischer and M. R. Pennington, "Finite volume effects in a quenched lattice-QCD quark propagator," *Phys. Rev.* **D73** (2006) 034029, hep-ph/0512233.

[123] P. O. Bowman, U. M. Heller, and A. G. Williams, "Lattice quark propagator with staggered quarks in Landau and Laplacian gauges," *Phys. Rev.* **D66** (2002) 014505, hep-lat/0203001.

[124] J. B. Zhang *et al.*, "Quark propagator in Landau and Laplacian gauges with overlap fermions," *Phys. Rev.* **D71** (2005) 014501, hep-lat/0410045.

[125] C. D. Roberts and A. G. Williams, "Dyson-Schwinger equations and their application to hadronic physics," *Prog. Part. Nucl. Phys.* **33** (1994) 477–575, hep-ph/9403224.

[126] R. Alkofer and L. von Smekal, "The infrared behavior of QCD Green's functions: Confinement, dynamical symmetry breaking, and hadrons as relativistic bound states," *Phys. Rept.* **353** (2001) 281, hep-ph/0007355.

[127] P. Maris and C. D. Roberts, "Dyson-Schwinger equations: A tool for hadron physics," *Int. J. Mod. Phys.* **E12** (2003) 297–365, nucl-th/0301049.

[128] C. S. Fischer, "Infrared properties of QCD from Dyson-Schwinger equations," *J. Phys.* **G32** (2006) R253–R291, hep-ph/0605173.

[129] R. Alkofer, C. S. Fischer, and F. J. Llanes-Estrada, "Vertex functions and infrared fixed point in Landau gauge SU(N) Yang-Mills theory," *Phys. Lett.* **B611** (2005) 279–288, hep-th/0412330.

[130] R. Alkofer, C. S. Fischer, and F. J. Llanes-Estrada, "Dynamically induced scalar quark confinement," *hep-ph/0607293* (2006).

[131] C. S. Fischer and J. M. Pawlowski, "Uniqueness of infrared asymptotics in Landau gauge Yang-Mills theory," *hep-th/0609009* (2006).

[132] C. S. Fischer and R. Alkofer, "Non-perturbative propagators, running coupling and dynamical quark mass of Landau gauge QCD," *Phys. Rev.* **D67** (2003) 094020, hep-ph/0301094.

[133] M. Jamin, J. A. Oller, and A. Pich, "Scalar K π form factor and light quark masses," *Phys. Rev.* **D74** (2006) 074009, hep-ph/0605095.

[134] M. Jamin, "Flavour-symmetry breaking of the quark condensate and chiral corrections to the Gell-Mann-Oakes-Renner relation," *Phys. Lett.* **B538** (2002) 71–76, hep-ph/0201174.

[135] M. Jamin and B. O. Lange, "f(B) and f(B/s) from QCD sum rules," *Phys. Rev.* **D65** (2002) 056005, hep-ph/0108135.

[136] M. A. Shifman, A. I. Vainshtein, and V. I. Zakharov, "QCD and resonance physics. Sum rules," *Nucl. Phys.* **B147** (1979) 385–447.

[137] M. A. Shifman, A. I. Vainshtein, and V. I. Zakharov, "QCD and resonance physics: Applications," *Nucl. Phys.* **B147** (1979) 448–518.

[138] K. Maltman and J. Kambor, "Optimizing the FESR extraction of m(s) from hadronic tau decay data," *Nucl. Phys. Proc. Suppl.* **98** (2001) 314–318.

[139] K. Maltman, "Status of the QCD sum rule determinations of the light quark masses," *Nucl. Phys. Proc. Suppl.* **109A** (2002) 178–182.

[140] C. S. Fischer, *Private Communication.*

[141] T. Eguchi, "A new approach to collective phenomena in superconductivity models," *Phys. Rev.* **D14** (1976) 2755.

[142] K. Kikkawa, "Quantum corrections in superconductor models," *Prog. Theor. Phys.* **56** (1976) 947.

[143] T. Hatsuda, "Convergence radius of the chiral perturbation in the large n_c limit," *Phys. Rev. Lett.* **65** (1990) 543–546.

[144] S. P. Klevansky, "The Nambu-Jona-Lasinio model of quantum chromodynamics," *Rev. Mod. Phys.* **64** (1992) 649–708.

[145] C. Lerche and L. von Smekal, "On the infrared exponent for gluon and ghost propagation in Landau gauge QCD," *Phys. Rev.* **D65** (2002) 125006, hep-ph/0202194.

[146] A. P. Martin and F. J. Llanes-Estrada, "Fermion family recurrences in the Dyson-Schwinger formalism," hep-ph/0608340.

[147] R. Alkofer, P. Watson, and H. Weigel, "Mesons in a Poincare covariant Bethe-Salpeter approach," *Phys. Rev.* **D65** (2002) 094026, hep-ph/0202053.

[148] W. Celmaster and R. J. Gonsalves, "The renormalization prescription dependence of the QCD coupling constant," *Phys. Rev.* **D20** (1979) 1420.

[149] T. Meissner, "The convergence radius of the chiral expansion in the Dyson-Schwinger approach," *Phys. Lett.* **B340** (1994) 226–230, hep-ph/9405289.

[150] Y. Takahashi, "Canonical Quantization and Generalized Ward Relations: Foundation of Nonperturbative Approach,". Print-85-0421 (ALBERTA).

[151] K.-I. Kondo, "Transverse Ward-Takahashi identity, anomaly and Schwinger-Dyson equation," *Int. J. Mod. Phys.* **A12** (1997) 5651–5686, hep-th/9608100.

[152] H.-X. He, F. C. Khanna, and Y. Takahashi, "Transverse Ward-Takahashi identity for the fermion boson vertex in gauge theories," *Phys. Lett.* **B480** (2000) 222–228.

[153] H.-X. He, "Nonperturbative fermion boson vertex function in gauge theories," hep-th/0202013.

[154] H.-X. He and H.-W. Yu, "Perturbative correction to transverse Ward-Takahashi relation for the vector vertex," *Commun. Theor. Phys.* **39** (2003) 559–560.

[155] H.-X. He, "Quantum anomaly of the transverse Ward-Takahashi relation for the axial-vector vertex," *Phys. Lett.* **B507** (2001) 351–355, hep-th/0201217.

[156] S. L. Adler, "Axial Vector Vertex in Spinor Electrodynamics," *Phys. Rev.* **177** (1969) 2426–2438.

[157] J. S. Bell and R. Jackiw, "A PCAC puzzle: $\pi^0 \to \gamma\gamma$ in the sigma model," *Nuovo Cim.* **A60** (1969) 47–61.

[158] S. L. Adler and W. A. Bardeen, "Absence of higher order corrections in the anomalous axial vector divergence equation," *Phys. Rev.* **182** (1969) 1517–1536.

[159] W.-M. Sun, H.-S. Zong, X.-S. Chen, and F. Wang, "A note on transverse axial vector and vector anomalies in U(1) gauge theories," *Phys. Lett.* **B569** (2003) 211–218, hep-ph/0305197.

[160] W.-M. Sun, H.-S. Zong, X.-S. Chen, and F. Wang, "The Tensor Current Divergence Equation in U(1) Gauge Theories is Free of Anomalies," *Int. J. Mod. Phys.* **A19** (2004) 2705–2712, hep-ph/0308104.

[161] P. Maris and P. C. Tandy, "Bethe-Salpeter study of vector meson masses and decay constants," *Phys. Rev.* **C60** (1999) 055214, nucl-th/9905056.

[162] P. Maris and C. D. Roberts, "π and K meson Bethe-Salpeter amplitudes," *Phys. Rev.* **C56** (1997) 3369–3383, nucl-th/9708029.

[163] P. Maris and P. C. Tandy, "The quark photon vertex and the pion charge radius," *Phys. Rev.* **C61** (2000) 045202, nucl-th/9910033.

[164] P. Maris and P. C. Tandy, "The π, K^+, and K^0 electromagnetic form factors," *Phys. Rev.* **C62** (2000) 055204, nucl-th/0005015.

[165] A. Krassnigg, C. D. Roberts, and S. V. Wright, "Meson spectroscopy and properties using Dyson-Schwinger equations," *Int. J. Mod. Phys.* **A22** (2007) 424–431, nucl-th/0608039.

[166] A. Bender, C. D. Roberts, and L. Von Smekal, "Goldstone theorem and diquark confinement beyond rainbow-ladder approximation," *Phys. Lett.* **B380** (1996) 7–12, nucl-th/9602012.

[167] M. S. Bhagwat, M. A. Pichowsky, C. D. Roberts, and P. C. Tandy, "Analysis of a quenched lattice-QCD dressed-quark propagator," *Phys. Rev.* **C68** (2003) 015203, nucl-th/0304003.

[168] M. S. Bhagwat, A. Holl, A. Krassnigg, C. D. Roberts, and P. C. Tandy, "Aspects and consequences of a dressed-quark-gluon vertex," *Phys. Rev.* **C70** (2004) 035205, nucl-th/0403012.

[169] P. Watson and W. Cassing, "Unquenching the quark antiquark Green's function," *Few Body Syst.* **35** (2004) 99–115, hep-ph/0405287.

[170] C. S. Fischer, R. Alkofer, W. Cassing, F. Llanes-Estrada, and P. Watson, "Studying unquenching effects in QCD with Dyson-Schwinger equations," *Nucl. Phys. Proc. Suppl.* **153** (2006) 90–97, hep-ph/0511147.

[171] W. H. Press, B. P. Flannery, S. A. Teukolsky, and W. T. Vetterling, *Numerical Recipes in C++: The Art of Scientific Computing.* Cambridge University Press, Cambridge (UK) and New York, 2nd ed., 2002.

[172] "Gnu scientific library." http://www.gnu.org/software/gsl/.